2005

METHODS DEVELOPMENT IN BIOLOGICAL MASS SPECTROMETRY: APPLICATIONS IN SMALL MOLECULE RESEARCH AND PROTEOMICS

Taufika Islam Williams
University of Kentucky, tiwill2@uky.edu

ABSTRACT OF DISSERTATION

Taufika Islam Williams

The Graduate School
University of Kentucky
2005

METHODS DEVELOPMENT IN BIOLOGICAL MASS SPECTROMETRY: APPLICATIONS IN SMALL MOLECULE RESEARCH AND PROTEOMICS

ABSTRACT OF DISSERTATION

A dissertation submitted in partial fulfillment of the
requirements for the degree of Doctor of Philosophy in the
College of Arts and Sciences
at the University of Kentucky

By

Taufika Islam Williams

Lexington, KY

Director: Dr. Bert C. Lynn, Professor of Chemistry

Lexington, KY

2005

ABSTRACT OF DISSERTATION

METHODS DEVELOPMENT IN BIOLOGICAL MASS SPECTROMETRY: APPLICATIONS IN SMALL MOLECULE RESEARCH AND PROTEOMICS

Technological developments have enabled mass spectrometry (MS) to evolve as one of the most versatile, sensitive and widely used analytical methods. Key areas of research in biological MS include the development of analyte-selective MS methodologies, along with the design of MS compatible separation technology. Analytes of interest range from small, biologically active molecules in disease progression research, to macromolecules such as proteins, in proteomics investigations. Advances in these areas are vital to maintaining the level of sophistication that has become the benchmark for MS analyses.

Mass spectrometry has found a permanent station in disease progression studies, particularly in biomarker discovery. This is especially true for Alzheimer's disease (AD), a condition marked by widespread lipid peroxidation (LPO) in the brain. The main hypothesis of the first part of this dissertation is that LPO produces aldehydes that can potentially be exploited as AD biomarkers. Design of novel LC-MS/MS methods for brain aldehyde analysis is described. The methods were applied towards aldehyde quantification in the hippocampus, superior and middle temporal gyrus and cerebellum of subjects with early AD (EAD), mild cognitive impairment (MCI) and age-matched controls. Results obtained indicated elevation of neurotoxic aldehydes in MCI and EAD brain and suggested that LPO occurred early in AD. Understanding AD progression has become important for developing diagnostic methods and treatments.

Mass spectrometry is also the major analytical tool in proteomics, where gel electrophoresis is dominant in pre-MS separations. The main hypothesis of the latter part of this dissertation is that exposure of microbe fermenters including *Clostridium thermocellum* to an external stimulus, such as ethanol, can alter the membrane proteome. Design of novel doubled-SDS-PAGE (dSDS-PAGE) methods for membrane protein analysis is described, as these proteins are under-represented in standard 2D-PAGE. The newly developed Bicine-dSDS-PAGE offered superior separation over other methods and was applied towards analysis of wild type and ethanol-adapted *C. thermocellum* cell membranes. Significant differences in protein expression were observed. An understanding of ethanol adaptation will promote the design of more ethanol-tolerant strains. Such an outcome can have dramatic effects in the fuel industry as the trend towards more efficient fuel development gathers momentum.

KEYWORDS: Mass Spectrometry, Alzheimer's Disease, Aldehydes, Bicine-dSDS-PAGE, Membrane Proteins

Taufika Islam Williams

November 28, 2005

METHODS DEVELOPMENT IN BIOLOGICAL MASS SPECTROMETRY: APPLICATIONS IN SMALL MOLECULE RESEARCH AND PROTEOMICS

By

Taufika Islam Williams

Dr. Bert C. Lynn
Director of Dissertation

Dr. Mark Meier
Director of Graduate Studies

RULES FOR THE USE OF DISSERTATIONS

Unpublished dissertations submitted for the Doctor's degree and deposited in the University of Kentucky Library are as a rule open for inspection, but are to be used only with due regard to the rights of authors. Bibliographical references may be noted, but quotations or summaries of the parts may be published only with permission of the author, and with the usual scholarly acknowledgements.

Extensive copying or publication of the dissertation in whole or in part also requires the consent of the Dean of the Graduate School of the University of Kentucky.

A library that borrows this dissertation for use by its patrons is expected to secure the signature of each user.

Name	Date

DISSERTATION

Taufika Islam Williams

The Graduate School
University of Kentucky
2005

METHODS DEVELOPMENT IN BIOLOGICAL MASS SPECTROMETRY: APPLICATIONS IN SMALL MOLECULE RESEARCH AND PROTEOMICS

DISSERTATION

A dissertation submitted in partial fulfillment of the
requirements for the degree of Doctor of Philosophy in the
College of Arts and Sciences
at the University of Kentucky

By
Taufika Islam Williams

Lexington, KY

Director: Dr. Bert C. Lynn, Professor of Chemistry

Lexington, KY

2005

Dedicated to

my husband, best friend and soul-mate
Dr. Joseph B. Williams

and my beloved parents
Dr. T. M. Tajul Islam
Mrs. Tauhida Islam

Acknowledgements

My gratitude and sincerest thanks go to my advisor and mentor, Dr. Bert Lynn, for introducing me to the world of biological mass spectrometry, for his patience, tutelage, and willingness to challenge me as I developed and grew as a scientist. Dr. Lynn has inspired in me a true love for science and research and for this I am eternally grateful. His support and friendship will always be remembered fondly.

I also wish to acknowledge Dr. Mark Lovell, Professor of Chemistry, and Dr. Herbert Strobel, Professor of Animal Sciences. Countless conversations with these gentlemen throughout the course of my graduate work have contributed greatly to my breadth of knowledge in science. Many thanks to Dr. Jack Goodman, manager of the University of Kentucky Mass Spectrometry Facility, for being an important source of knowledge and assistance. My graduate experience has been richer and more fulfilling as a result of my interactions with all of them.

I am grateful to all my colleagues in the Lynn Laboratory for their fellowship and goodwill. I will always cherish the times we shared together as we progressed through our graduate studies. Special thanks to all the graduate students and staff of the Department of Chemistry at the University of Kentucky.

I will always be indebted to my loving husband, Dr. Joseph B. Williams, for his steadfast love, encouragement and for embracing my laughter and my tears as his own. The road to a PhD is a challenging one, and Joseph made it a little easier for me by always being there when I needed him. He is my Rock of Gibraltar, and I love him more than words could say.

My successes as a graduate student would not have come to pass without the contributions of my beloved parents. They always instilled in me the desire to learn and to better myself. My father, Dr. T. M. Tajul Islam, is a continuous source of inspiration to me for all his accomplishments as a scientist and humanitarian, despite his humble beginnings and in the face of life's many challenges and adversities. I will always admire my mother, Mrs. Tauhida Islam, for her patience, keen sense of morality and for her amazing intelligence. She taught me the virtues of taking all my responsibilities very seriously, both in my professional and personal life. My heartfelt thanks go to my

brother, Mr. Tonmoy Islam for his love, support and for always being a wonderful friend and patient listener.

Lastly, I wish to acknowledge my parents-in-law, Dr. Fred D. Williams and Mrs. Jo Ann Agee Williams for filling the void of living so far away from my own parents in Bangladesh. I thank them for making me feel not like their daughter-in-law, but like their own daughter.

I am fulfilling my academic dreams today because I was blessed to have all these wonderful people in my life.

Table of Contents

List of Tables

List of Figures

List of Files

tiwdis.pdf	1,423 KB

INTRODUCTION

Sir J. J. Thompson (1856-1940) made headlines in 1898 for discovering the electron and revolutionizing the sciences of physics and chemistry. For this, he was awarded the Nobel Prize in physics in 1906. The following year, he designed and built a parabola mass spectroscope to support his work on positive ray analysis, and as a consequence, became the father of mass spectrometry (1). Today, mass spectrometry (MS) has evolved into a microanalytical technique requiring only a few picomoles of sample to obtain molecular weight and structural information of the analyte under investigation (1). This analytical tool is being applied to a wide variety of research areas, including protein identification and structure determination (proteomics), drug metabolism, inherited metabolic diseases, the analysis of respiratory gases, viral identification, forensics, flavor and smell chemistry, organic fossils, atmospheric chemistry, petroleum and petrochemicals and many other specialized subjects (2). The ultrahigh detection sensitivity and unsurpassed molecular specificity have contributed to the prominence of mass spectrometry in analytical sciences.

Continuous innovation and improvement of instrumentation and techniques have made mass spectrometry one of the most versatile, sensitive and widely used analytical methods available today. Highly effective and novel approaches and paradigms have developed in this field that can tackle practical issues in the biochemical sciences, once beyond the scope of mass spectrometry. This has largely been brought about by overcoming the roadblocks of converting bioanalytes into gas-phase ions, concerns that have historically been the Achilles' heel of mass spectral analysis of large biological compounds. As a consequence, the applications of this analytical methodology to biochemical fields have grown in astronomical proportions. A new branch of mass spectrometry called biological mass spectrometry was born. It actively deals with the analysis of organic materials derived from biological systems. The spectrometry is different from organic mass spectrometry in that organic molecules are analyzed from the standpoint of biological function and the life sciences.

Recent developments in ionization methods, improvements in ion detection, increases in the mass range of instruments, and improved interfaces for separation

techniques are providing mass spectrometrists with the resources required to analyze a plethora of biologically active materials. Speedy advances in the biological sciences, particularly in the fields of molecular biology and biochemistry, have led to an increased demand for chemical and structural information on biologically active molecules, important areas where mass spectrometry outshines most other analytical tools. In the past 70 years, the applications of biological mass spectrometry have matured from trace analysis of species with masses below 50 Da to peptide sequencing and the analysis of 100 kDa proteins. In 2002, Koichi Tanaka and John Fenn shared the Nobel Prize in chemistry for the development of soft desorption ionization methods in the mass spectrometric analyses of biological macromolecules, an achievement that clearly highlights the ascension of mass spectrometry into prominence as part of the analytical tools and technology available to biological scientists today.

Key areas of research and investigation in biological mass spectrometry include the development of mass spectrometric methods for selective analysis of target analytes, along with the design of specialized separation technology that is amenable to interfacing, both online and offline, with mass spectrometry. Analytes of interest range from small, biologically active molecules in drug development and disease progression research to macromolecular structures, such as proteins, in proteomic studies. Continued advances in these areas are vital to maintaining and improving the level of sophisticated analyses that has become the benchmark for this important area of bioanalytical chemistry.

In the interest of target compound analysis, mass spectrometry has found a permanent station in one of the major goals of modern medicine: identification of biomarkers for the earliest possible stages of disease progression so that prompt clinical intervention can limit damage, reverse pathological change and ideally effect a complete cure. This is especially true in the case of Alzheimer's disease (AD) research. AD is a debilitating neurological condition that plagues the elderly and is marked by widespread lipid peroxidation in the brain. Key compounds generated as a result of lipid peroxidation include biogenic aldehydes, such as C_1-C_6 aliphatic aldehydes and α,β-unsaturated aldehydes, including acrolein and 4-hydroxynonenal (4-HNE). The design of an LC-ESI-

MS/MS methodology is described here that is ideally suited to identify and quantify such aldehydes in tissues.

The LC-MS method was successfully applied in the quantification of aldehyde concentrations in the hippocampus, superior and middle temporal gyrus (SMTG) and the cerebellum of subjects with early signs of AD (EAD), those with mild cognitive impairment (MCI), as well as and age-matched controls. This was the first study to report an in-depth comparison of aldehyde levels between these three types of individuals. Results obtained clearly indicated that HNE and acrolein are statistically significantly elevated in both MCI and EAD brain and suggested that oxidative stress occurs early in AD pathogenesis. Understanding the differences between MCI, EAD and normal subjects has becoming increasingly important in the interest of developing early diagnostic methods and treatments for AD.

The LC-ESI-MS/MS method for aldehyde analysis designed and described here makes use of standard LC separation science for small molecule separations. Another broad area of mass spectrometric applications is in the field of proteomics, where gel-based techniques play a dominant role in pre-MS separations. While chromatography has found a niche in proteomics in such techniques as multi-dimensional protein identification technology (MudPIT), 2-dimensional polyacrylamide gel electrophoresis (2D-PAGE) is still very much the gold standard for protein separations. Nevertheless, standard 2D-PAGE is wrought with problems, such as under-representation of hydrophobic membrane proteins due to solubility issues, along with very basic proteins. As with any separation method, manipulation of the mobile phase and stationary phase of the 2D-PAGE system can tailor the experiment to the needs of the particular protein sample at hand.

Proteomic analysis of the cell membranes has emerged as a very important area of research due to the unique position of this organelle as the site of first cellular contact with the external environment. The cell membrane is the location of important biochemical processes intimately associated with cell viability both in eukaryotes and prokaryotes. Hence, it is no surprise that a major area of research is the development of better separation methods for membrane proteins that bypass or overcome many of the disadvantages encountered in 2D-PAGE. The cell membrane is involved in cellular

defense, signal transduction, partitioning of organelles and protection of the integrity of the genome and proteome. Since the membrane is the site of initial communication of the cell with the exterior, many physiological changes within a cell can be traced back to changes that occur in the cell membrane. For instance, studies have shown that microbe fermenters can be selectively conditioned to grow in elevated levels of ethanol due to fundamental changes that occur in the membrane proteome. These changes enable the organism to become ethanol-adapted and encourage the production of cellular ethanol. *Clostridium thermocellum*, a cellulolytic, thermophilic anaerobe, is a classic example of such an organism. Understanding these changes will enable a better appreciation of the mechanism of ethanol adaptation and promote the development of more ethanol-tolerant strains of this bacterium. This could have dramatic consequences in the fuel industry as the general trend towards cleaner and more efficient fuel development gathers momentum.

In the interest of developing better separation methods for membrane proteins, doubled SDS-PAGE (dSDS-PAGE) methods were designed for the analysis of wild type and ethanol-adapted *C. thermocellum* cell membranes. This analytical methodology features the separation of fully denatured and solubilized proteins in two dimensions and circumvents problems associated with other gel-based methods. Solubility issues often encountered with isoelectric focusing (IEF, the first dimension of standard 2D-PAGE experiments) are avoided and circumvented by performing a molecular weight based PAGE separation in the first dimension. This is followed by another PAGE experiment in the second dimension. Orthogonality in the two dimensions can be achieved by varying an assortment of gel electrophoresis parameters in one dimension with respect to the other.

Optimization of membrane protein separation was achieved by exploring the parameter space of dSDS-PAGE. The mobile phase (running buffer) and gel preparation techniques were manipulated to arrive at the best possible separation conditions for membrane proteins. Tricine-dSDS-PAGE and a newly developed Bicine-dSDS-PAGE were investigated and optimized in membrane proteome analysis. It was shown that Bicine-dSDS-PAGE offered considerable advantages over Tricine-dSDS-PAGE and the

standard Laemmli experiment (Glycine-dSDS-PAGE) in terms of protein spot resolution and abundance, amongst other factors.

For the purposes of exploiting the advantages of the newly designed gel electrophoresis technique in understanding ethanol tolerance, a two-stage Bicine-dSDS-PAGE separation was performed to bring different regions of the *C. thermocellum* membrane proteome into focus. The two-stage analysis offered increased spot detection and resolution over a single stage experiment. Furthermore, the two-stage Bicine-dSDS-PAGE approach produced comparable results to a 3-stage Glycine-dSDS-PAGE analysis. The dSDS-PAGE investigations of the *C. thermocellum* proteome demonstrated significant differences in membrane protein expression patterns between the wild type and ethanol-adapted strains. No doubt, these results offered insight into the biochemical nature of ethanol adaptation.

This dissertation focuses on experimental design and the development of better separation-based mass spectrometric experiments to selectively analyze target compounds. Combining the power of separation science and mass spectrometry offers considerable sophistication to the arsenal of analytical methods available to clinicians and scientists. Tailoring separation and the mass spectrometric experiment to the compounds of interest can dramatically improve analysis. Analytical chemistry is a very diverse field and considerable research and development is focused on methods development for target analytes. A solid understanding of the chemistry of target species can enable the design of elegant methodologies, producing optimum analytical results, as clearly demonstrated in the experiments described in this dissertation.

References

1. Watson, J. T. (*1997*) *Introduction to Mass Spectrometry*, Lippincott-Raven Publishers, Philadelphia, PA.
2. http://masspec.scripps.edu/information/intro/chapter5.html, Scripps Center for Mass Spectrometry, La Jolla, CA.

PART ONE

LIPID PEROXIDATION BIOMARKER QUANTIFICATION

Chapter 1.1
Introduction

Alzheimer's Disease Background

Alzheimer's disease (AD) is a progressive neurological disorder of the elderly that gradually destroys neurons in the brain, particularly in regions critical to cognition, such as judgment and reasoning, memory, movement coordination and pattern recognition (1). Dr. Alois Alzheimer, a German psychiatrist and neuropathologist, identified the disease in 1906 (2). He noticed unusual changes in the brain tissue of a 51-year old woman who had died after a 4.5 year episode of progressive dementia. The tissue displayed abnormal clumps, now called amyloid or senile plaques (SPs), and tangled bundles of fibers, recognized as neurofibrillary tangles (NFTs). Such artifacts are not normally observed in patients suffering from other forms of dementia (2). The presence of SPs and NFTs in the hippocampus, amygdala, cerebral cortex and certain other brain regions are now considered to be the major histopathological hallmarks of AD. The illness afflicts some 4.5 million Americans today (1). As people live longer, AD is becoming a major medical and social concern. Risk factors for AD include age, Down syndrome, family history, and the ApoE genotype. The ApoE gene codes for apolipoprotein E, a macromolecule involved in processing and transport of cholesterol. The gene has three major alleles: E2, E3 (most common), and E4. Individuals who inherit copies of the E4 allele show an 80% increased risk of developing AD by the age of 60-65. Not all individuals with AD have E4, and not everyone who has this allele will develop AD. It is unknown why E4 is related to AD development. However, studies have shown that the allele is linked to an increased number of SPs (3).

The accepted clinical criteria for AD diagnosis include dementia ascertained by clinical examination and neuropsychological testing, deficiencies in two or more areas of cognition, progressive decline of memory and other cognitive functions, no disturbance in consciousness, onset of symptoms sometime between ages 40 and 90 and lack of differential diagnosis that could attest for the gradual deterioration of cognitive function

(2). AD diagnosis can only be established clearly by the post-mortem demonstration of increased numbers of NFTs and SPs as compared with appropriate age-matched controls (4). While AD has been diagnosed in younger patients, it remains overwhelmingly a disease of the elderly community. Approximately 5% of men and women between the ages of 65 to 74 have AD and nearly half of those aged 85 and older are believed to suffer from this neurological condition (1). It should be noted that AD is not a normal part of the aging process. To this day, the etiology and pathogenesis of AD remains elusive and it is resistant to many treatments.

The mechanisms responsible for AD pathology are multifaceted and comprise of several factors including mitochondrial dysfunction, abnormal protein aggregation, inflammation and excitotoxicity and eventual death of neurons (2). Autopsy examinations of the AD brain reveal abnormal fibers that appear to be tangles of brain tissue filaments (NFTs) and cores of amyloid surrounded by degenerative nerve endings (SPs). The amyloid fibrils of SPs are mainly composed of aggregated forms of the 39-43 amino acid peptide defined as amyloid β-peptide Aβ(1-42). This peptide (Figure 1.1.1) is generated by the abnormal proteolysis of an integral membrane precursor protein (amyloid precursor protein or APP), and is found in SPs surrounded by dystrophic neurites (5). By nature, SPs are extracellular formations (~8 nm filaments) that substantially impede electrical signal transmission by neurons (6, 7). In contrast, NFTs are intracellular ~20 nm cytoplasmic fibers comprised of bundles of paired helical filaments (PHF), the major component of which is the microtubule-associated protein tau (τ) (8-10). NFTs are thought to interfere with axonal transport in neurons (1).

One theory on the pathogenesis of AD suggests that neurodegeneration is the result of oxidative damage to vulnerable cerebral tissue. In a situation of oxidative stress, the antioxidant cellular mechanisms are inadequate to tackle the production of free radical oxidant species. It is thought that the molecular mechanism underlying Aβ toxicity may result from free radical generation enabled by the peptide (11). Studies have shown that Aβ(1-42) promotes oxidative injury to neuronal proteins and lipids *in vitro* and mediates oxidative damage in AD brain (12, 13). Such damage can be inhibited by addition of antioxidants (14). Butterfield and co-workers (12) postulated that small,

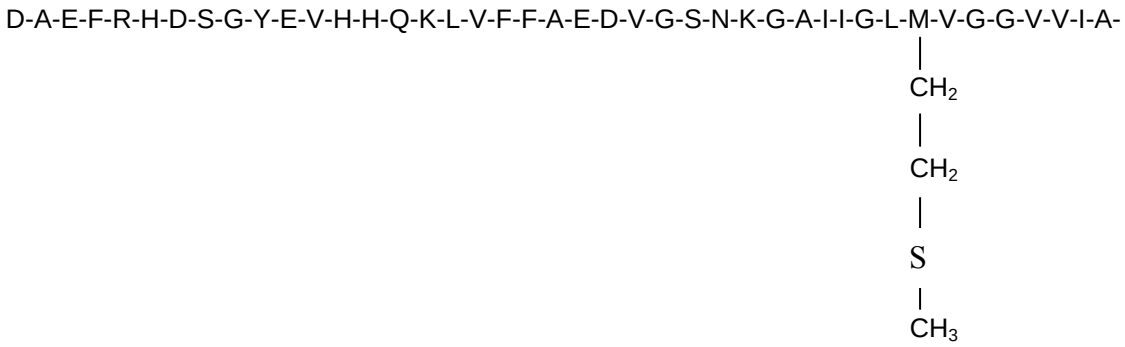

Figure 1.1.1. Sequence of Aβ(1-42) with the R group of methionine residue 35 displayed.

soluble aggregates of APP-derived amyloid β-peptide insert into the neuronal and glial membrane bilayer and produce an array of oxygen-dependent free radicals that then cause lipid peroxidation and protein oxidation. Direct membrane damage results from Aβ-associated free radicals, perhaps involving peptide-bound redox metal ions and the methionine residue at position 35. Indirect membrane damage arises by the action of lipid free radicals or various LPO products, including 4-hydroxy-2-nonenal (HNE) and 2-propenal (acrolein). In addition, Aβ contains several histidine residues (at positions 6, 13 and 14) and a tyrosine residue (at position 10) that have a remarkable ability to chelate metal ions, including iron and copper. It is thought that chelation of metals by the peptide can result in its aggregation (15, 16). These complexes, detected in SPs, have pro-oxidant properties. Furthermore, the chelation reduces transition metals to their highly active, low valency state, with a concurrent synthesis of free radicals and initiation of LPO (17).

There also appears to exist a clear mechanistic relationship between τ and oxidative stress (18-20). Compared to normal subjects, τ in the AD brain has been demonstrated to undergo a host of varied modifications. These include hyperphosphorylation (21-23), ubiquitination (24-26) and oxidation (27, 28). In addition, τ can be proteolytically processed and aggregated into filaments (23, 29, 30). Hyperphosphorylation renders τ unable to bind to microtubules and it therefore fails to promote or maintain microtubule assembly (10, 30). Studies have indicated that oxidative stress activates several kinases such as ERK, p38 and JNK, which have been shown to be activated in AD (31-33) and are capable of phosphorylating τ (34). As with τ and Aβ, data have also linked oxidative damage to AD, such as accumulation of trace elements (i.e. iron) as free radical sources, increased protein and DNA oxidation, elevated antioxidant enzymes (i.e. superoxide dismutase), *in situ* detection of carbonyls and increased LPO (35). In particular, the products of LPO have recently received considerable interest as potential biomarkers for AD.

Lipid Peroxidation Biomarkers for Alzheimer's Disease

Polyunsaturated fatty acids (PUFA), primarily of the ω-3 and ω-6 variety such as linoleic (ω-6), arachidonic (ω-6) and docosahexaenoic acid (ω-3), are the major

substrates for LPO in lipoproteins and cell membranes (17). In the process of LPO, lipid constituents of cellular membranes are attacked by free radicals, including hydroxyl, peroxynitrite and hypochlorite, that have sufficient reactivity to abstract a weakly bound hydrogen atom from a methylene carbon in their side-chains (36). As a result, a carbon-centered radical is left in the fatty acid. The radical then proceeds to bind with oxygen yielding the peroxyl radical, which can then react with other fatty acids or proteins (Figure 1.1.2). These reactions result in cell damage and a cascading increase in the production of free radicals. It has been shown that transition metal ions, such as Cu^{2+} and Fe^{3+}, are responsible in exacerbating oxidative damage by the production of highly reactive hydroxyl radicals through the Fenton reaction (17).

$$Fe^{2+} + H_2O_2 \rightarrow Fe^{3+} + OH^{\bullet} + OH^{-} \qquad (1.1.1)$$

Removal of hydrogen bonds is facilitated by the presence of higher numbers of double bonds in the PUFAs. Compared to other organ systems, the brain contains a high lipid content, high levels of transition metals, high oxygen and energy consumption rate, large stores of polyunsaturated fatty acids and relatively poor defenses against lipid peroxidation (2).

Neuronal membranes readily succumb to oxidative damage because the PUFA constituent of their phospholipids can easily react with free radicals from cell metabolism (37, 38). Normal metabolic processes generate free radicals through a variety of sources. These radicals react with the PUFA component of cell membranes, producing such compounds as hydroxylated fatty acids (HETEs), prostanoids and lipid aldehydes (37). Ordinarily, the brain is protected from this type of damage by a carefully controlled balance between pro-oxidant and antioxidant cellular mechanisms. Vitamins E and C, glutathione (GSH), albumin, bilirubin, ceruloplasmin, uric acid, along with several antioxidant enzymes, such as superoxide dismutase, glutathione peroxidase and catalase, provide protection from free radical damage. Antioxidant protection occurs through various methods within cells, including prevention of free radical formation, interception of radicals, oxidative damage repair, eradication of damaged molecules, as well as nonrepair-recognition of excessively damaged molecules to prevent mutations. A

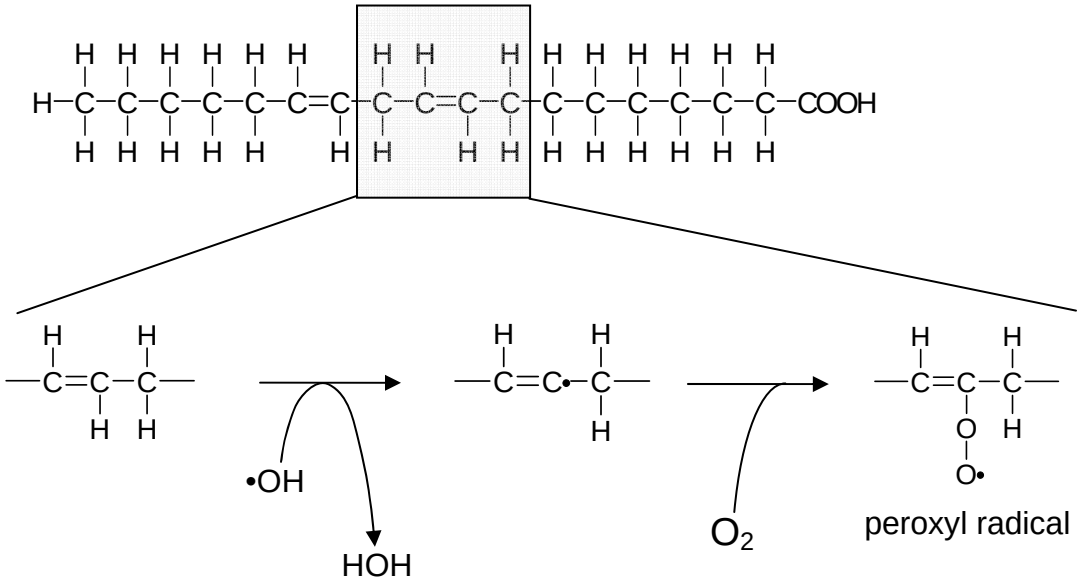

Figure 1.1.2. Peroxidation of fatty acids.

situation of oxidative stress arises from an imbalance in free radical production (particularly reactive oxygen species) and their removal by antioxidants (37).

Increasing evidence supports a role for oxidative damage in the pathogenesis of AD. Several studies demonstrated increased protein oxidation (11, 39), DNA oxidation (40-43), decreased levels of PUFAs (4, 44), and increased LPO (45-48) in AD. There have been reports of increased levels of neurotoxic markers of LPO, including HNE and acrolein, in the AD brain (49, 50) and cerebrospinal fluid (CSF) (51). Immunohistochemical studies of the AD brain also showed different markers of oxidative stress in NFTs and SPs (52-56). It is evident from the literature that an appropriate biochemical indicator or product of LPO would serve well as a biomarker for AD. Hence, it is no surprise that a considerable amount of research is currently focused on the exploration of lipid peroxidation byproducts in their suitability as biomarkers for the disease.

A major consequence of LPO is the widespread damage to membrane structure and integrity as a result of the production of fragmented fatty acyl chains, lipid-lipid cross-links, endocyclization to form a variety of fatty acid esters and lipid-protein cross-links (57). In total, these processes combine to generate significant changes in the biophysical properties of membranes that can result in profound effects on the biological activity of membrane-bound proteins. Another important outcome of LPO is the generation of secondary, more stable LPO products, which can be categorized into those formed through a host rearrangement processes and mechanisms as well as those generated by fragmentation of oxygenated lipids (57).

A small proportion of lipid hydroperoxy radicals go through internal cyclization reactions to produce endoperoxide intermediates. These species are then converted to various ringed isomers similar in structure to prostaglandins (57). Such compounds are called isoprostanes (IsoPs) when they are derived from arachidonic acid. Quantification of IsoPs rivals that of malondialdehyde, one of the most commonly used biomarkers of LP, in accuracy and precision (58). However, concern with exploiting these chemicals as indices for LP and AD stem from the lack of a thorough understanding of the link between them and oxidant stress processes (59).

Fragmentation of lipid hydroperoxides in LPO generates low molecular weight, water-soluble, electrophilic aldehydes and is commonly observed in several different types of neurodegenerative conditions, such as stroke and AD (57). Notable aldehydic products include malondialdehyde (MDA), acrolein, and HNE. MDA can be detected through the thiobarbituric acid-reactive substances (TBARS) assay. The sample to be tested is heated with TBARS at low pH. Absorbance of a pink chromogen is measured at 532 nm (60). The test is popular because it is quite simple to perform and rather inexpensive (36). However, it has the disadvantage of being an unspecific index for LPO in complex biological fluids or *in vivo*. Furthermore, the results can often be misleading as many species, including sugars, amino acids and bilirubin, can interfere with the test (36, 60, 61).

Saturated aliphatic aldehydes (C_3-C_{10}) are also generated in LPO through fragmentation mechanisms, along with the α,β-unsaturated aldehydes such as acrolein and HNE (62). Aliphatic aldehydes have no evident toxicity, but acrolein (CH_2=CH-CHO) and HNE (C_5H_{11}-CH(OH)-CH=CH-CHO) are neurotoxic and have been detected by immunohistochemistry in the AD brain, especially in NFTs and SPs (13, 63). Alkenals, such as HNE and acrolein are strong electrophiles that react in tissues by alkylating nucleophiles (Michael Addition and Schiff base formation), particularly sulfhydryl groups, amino groups (i.e., lysine), and the imidazole group of histidine (64). Such reactions can lead to the structural alteration and/or cross-linking of proteins, which in turn can cause impairment of protein function. Therefore, these LPO products are biologically very active and can cause substantial disruption of cell processes at the genetic and biochemical level. The mechanism of formation of these toxic aldehydes (Figures 1.1.3 – 1.1.5) has been described previously (38, 65). HNE, a product of ω-6 PUFA peroxidation, is a relatively stable aldehyde that can diffuse into different subcellular compartments and interact with a host of cell proteins, including τ (30, 66) and histones (67). Increased production of HNE has been shown to indicate an increased level of oxidative stress, which may not always be evident using the more common marker malondialdehyde (MDA) (68). HNE is generated in response to oxidative insults and can induce neuronal apoptosis (69, 70). HNE has been linked to a host of adverse cellular effects, including growth inhibition, alterations in glutathione levels, inhibition

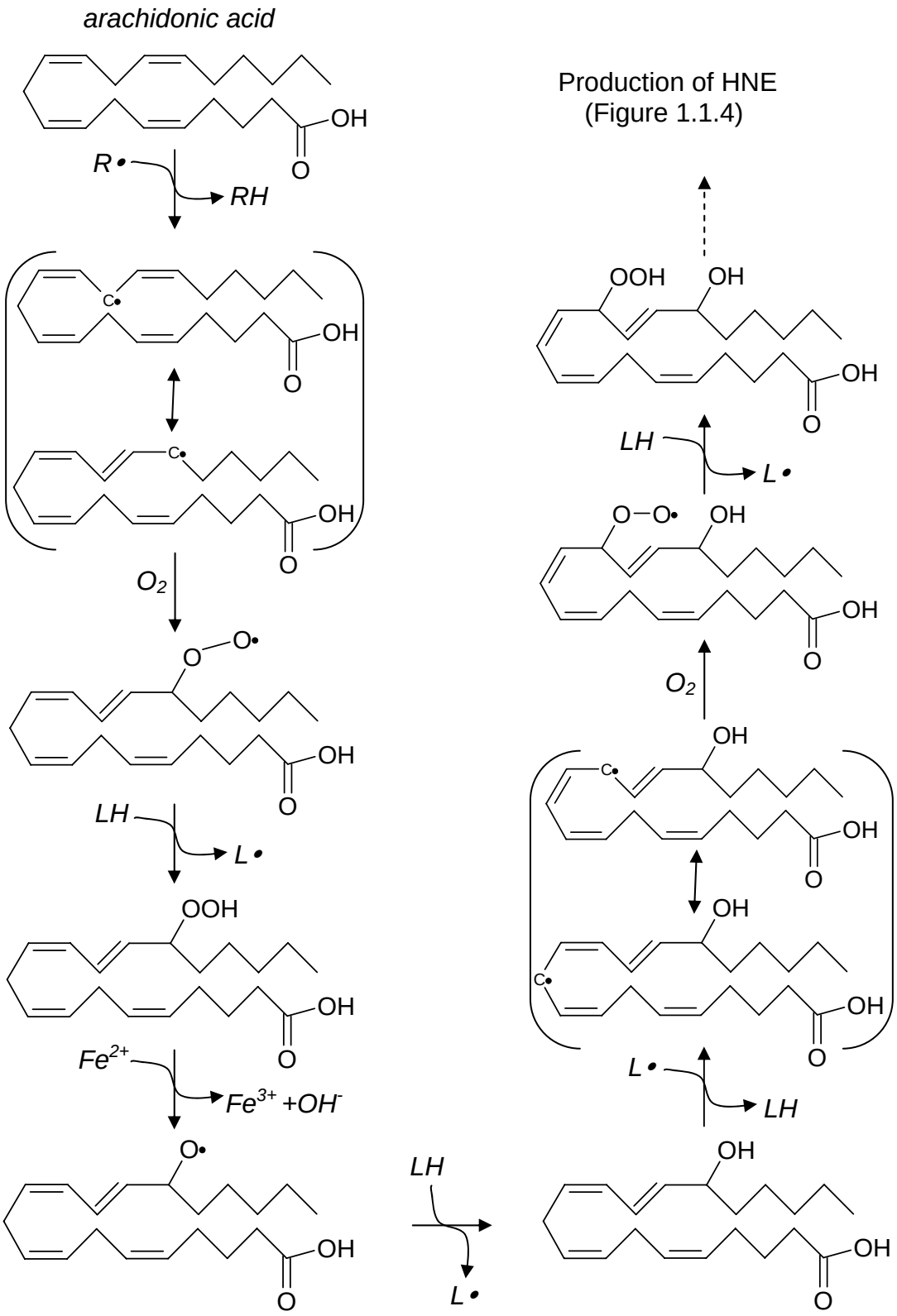

Figure 1.1.3. Initial stages of arachidonic acid peroxidation. R• represents a small free radical (such as OH•) and L• is a lipid radical.

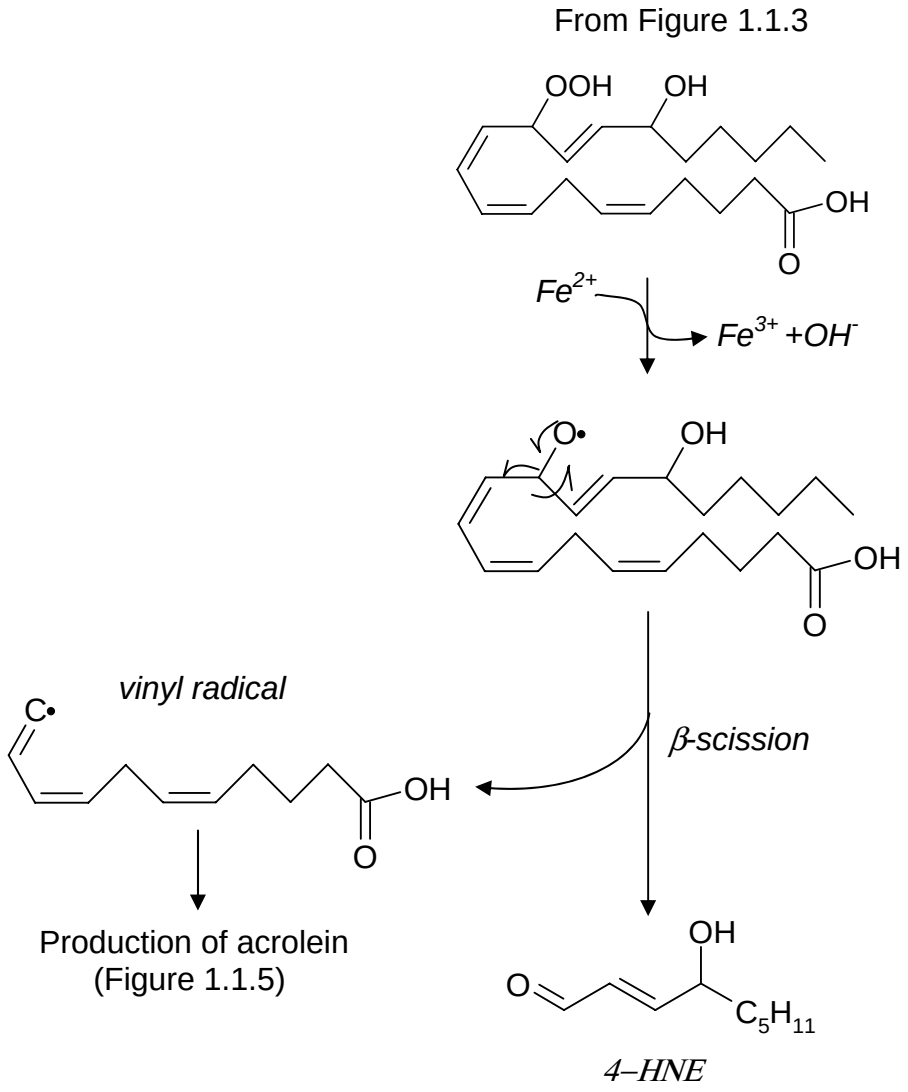

Figure 1.1.4. Peroxidation of arachidonic acid to generate 4-hydroxynonenal.

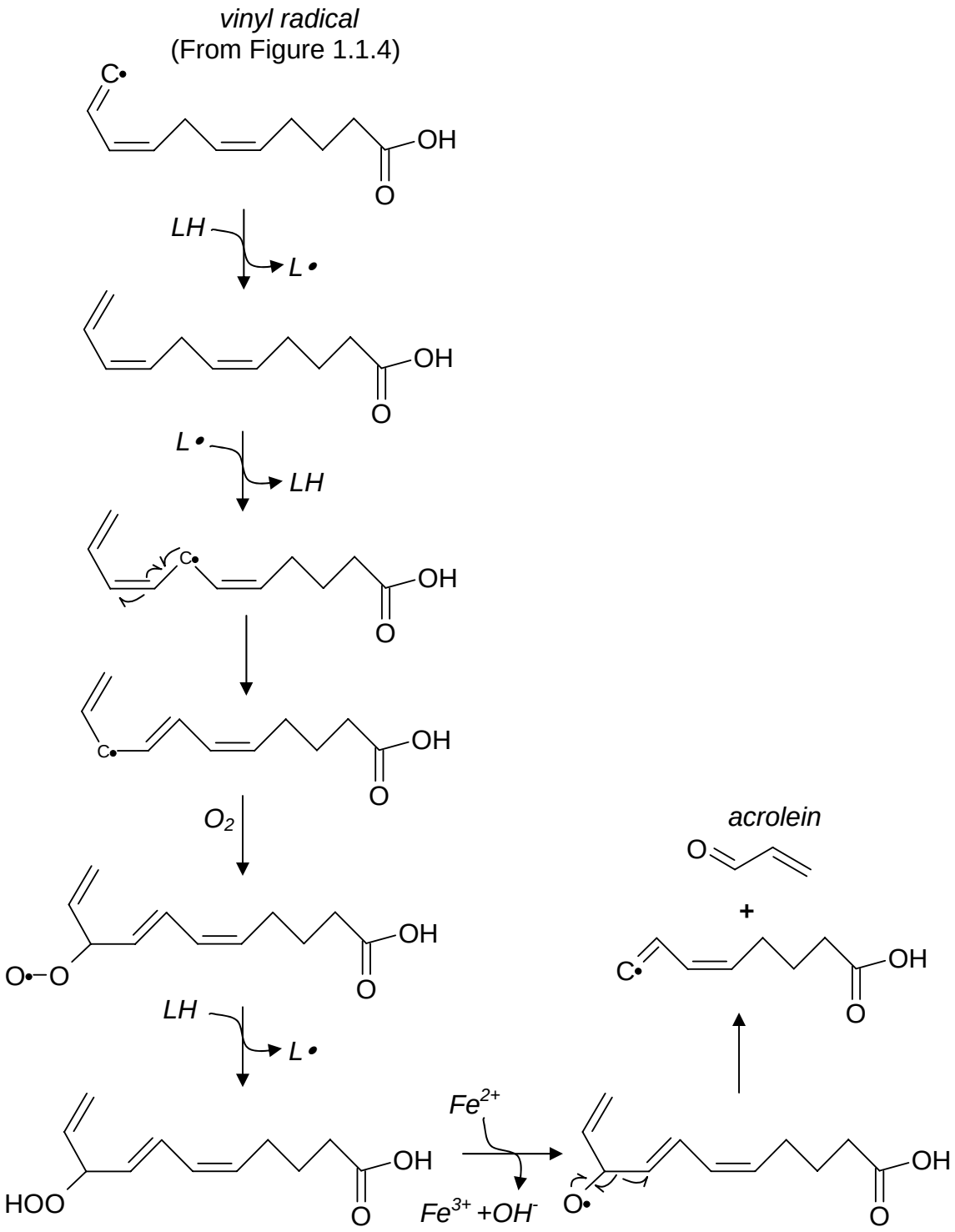

Figure 1.1.5. Peroxidation of arachidonic acid to generate acrolein. L• is a lipid radical.

of enzymes and calcium sequestration by microsomes, exhibition of chemotactic activity toward neutrophils, inhibition of protein and DNA synthesis, as well as induction of cell death (40, 71). It has been shown to play a major role in oxidative impairment of synaptic functions, leading to excitotoxic cascades (72-74) and to impair Na^+/K^+ ATPase activity (75, 76) as well as glucose and glutamate transport (76). Microtubule organization and neurite outgrowth are also vulnerable to HNE (77).

Among the α,β-unsaturated aldehydes, including HNE, acrolein shows the highest reactivity towards nucleophiles, such as lysine (40, 78, 79). This aldehyde is produced *in vivo* during the iron-catalyzed oxidation of PUFAs, such as arachidonic and docosahexaenoic acids (80). It readily reacts with proteins and phospholipids and can inhibit many enzyme systems including glucose and glutamate transport and Na^+/K^+ ATPase activity (49, 78). Acrolein is also known to modify DNA bases with the formation of exocyclic adducts, leading to chromosomal aberrations, sister chromatid exchanges and point mutations (40, 81) and has recently been linked to abnormal tau protein phosphorylation (20). It is believed that acrolein may inactivate the reductase responsible for the reduction of vitamin E radicals and, coupled with the depletion of glutathione, causes further LPO and neuronal death (13, 80).

Considering the array of cellular constituents that can react with acrolein and HNE, it is believed that a majority of these aldehydes exist in neurons bound to macromolecules, particularly proteins. *In vitro* studies have shown that α,β-unsaturated aldehydes have a high affinity for proteins (79, 82). In view of this, accurate and precise quantification of all such aldehydes in the cells can be difficult. However, previous studies have shown a direct correlation between free unsaturated aldehyde concentrations and AD progression, particularly in regions of the brain with memory function (49, 50). As such, a reliable quantification method for free aldehyde analysis (both aliphatic and unsaturated) would be a useful measure of oxidative stress, and therefore AD.

Vulnerable Regions of the AD Brain

Cortical degeneration, excluding the sensorimotor cortex, occipital poles and cerebellum, is considered as the primary basis for cognitive decline in AD (83, 84). Areas

of the brain typically affected in AD include portions of the frontal lobe associated with intelligence, judgment and social behavior, as well as areas of the temporal and parietal lobes that have memory and language function. Studies have shown a direct correlation between the prevalence of NFTs and SPs with levels of lipid peroxidation byproducts, including biogenic aldehydes, in different brain regions (11, 45, 48-50, 63, 81, 85). Cognitive deficits, particularly in memory, are associated with atrophy of the medial temporal lobe (MTL) (86). Structures comprising the MTL include the hippocampus, parahippocampal gyrus, entorhinal cortex and amygdala. Compared to age-matched controls, increased AD pathology, to varying levels, has been detected in the hippocampus, parahippocampal gyrus, superior temporal gyrus and middle temporal gyrus (Figure 1.1.6). Atrophy of the hippocampal formation is seen in AD patients with even very mild dementia. In situations of advanced dementia, atrophy extends to the parahippocampal gyrus and other structures in the temporal neocortex (87, 88).

Phylogenetically one of the oldest regions of the brain, the hippocampus is located inside the temporal lobe and is part of the limbic system, a group of structures involved in transferring information into memory. The hippocampus is intimately associated with the formation and long-term storage of associative and episodic memories, as well as an individual's ability to navigate. It is one of the first regions to succumb to AD pathology (89). Because of this, initial symptoms of AD characteristically include memory problems and disorientation. As with the hippocampus, the parahippocampal gyrus is also part of the limbic system. It is located in the most medial basal part of the temporal lobe and is also very susceptible to damage in AD. Medial temporal lobe atrophy, particularly the hippocampus and parahippocampal gyrus of the brain, can substantially impair the storage of new information and is believed to be site of initial change *preceding* the expression of AD symptoms.

Regions that show AD pathology in the temporal neocortex include the superior and middle temporal gyrus. Among other functions, the superior temporal gyrus is closely associated with an individual's ability to be insightful. The middle temporal gyrus is linked to the processing of language and semantic memory, as well as visual perception and multimodal sensory integration. Patients with damaged temporal lobes have

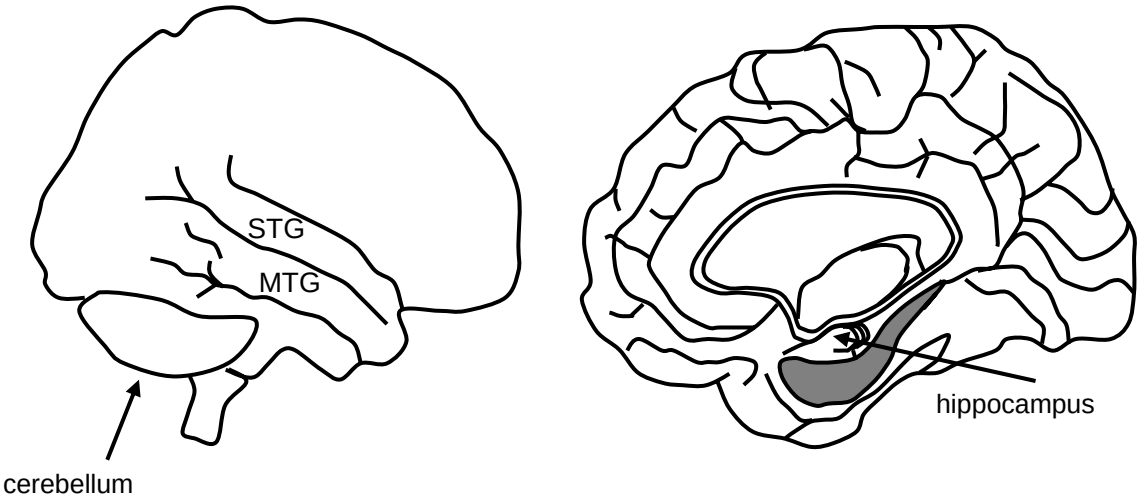

Figure 1.1.6. Regions of the human brain investigated (90, 91): hippocampus, superior temporal gyrus (STG), middle temporal gyrus (MTG), and cerebellum.

difficulty with remembering names and faces (92). Because of the association of the superior and middle temporal gyri with memory, it is not surprising that they do succumb to damage in AD. However, the pathology observed here is not as widespread and intense as that in the hippocampus and parahippocampal gyrus.

The cerebellum is an example of a part of the brain that exhibits little or no pathology in AD. It aids in the coordination of voluntary motor movement, muscle tone, balance and equilibrium. While the cerebellum has limited function in memory for reflex motor acts, it is not particularly associated with memory formation, processing or storage (93). Since the prevalence of LPO byproducts appears to be directly associated with the level of AD pathology, it is to be expected that the greatest concentrations of these species would be located in the hippocampus and parahippocampal gyrus when comparing AD brains to age-matched controls. Intermediate concentrations would be detected in such areas as the superior and middle temporal gyrus that display intermediate AD pathology while the cerebellum and other structures not predominantly involved with memory should show little, *statistically significant* elevations in the levels of these compounds. A thorough quantitative study of the distribution of biogenic aldehydes or other LPO products in the brain calls for careful methods development and analysis.

Biogenic Aldehyde Analysis

Several techniques have been explored for the analysis of biogenic aldehydes. Many of these techniques involve high performance liquid chromatographic (HPLC) separation and spectrophotometric measurements of chromophoric derivatives, such as UV absorption of dinitrophenyl hydrazones (DNP) (94-97) and fluorescence detection of cyclohexanedione (dimedone or CHD) derivatives (62, 98-101). In the absence of chromatographic separation, spectrophotometric methods fail to distinguish between specific analytes and other species capable of forming derivatives that also absorb at the selected wavelength. Coupling spectrophotometric detection with separation techniques such as HPLC adds greater selectivity, but co-eluting compounds may still interfere with quantification of aldehydes at low levels. Aldehyde quantification is further complicated by their reactivity and metabolism in tissues and biological fluids.

Methods utilizing gas chromatography/mass spectrometry (GC/MS) offer high sensitivity and the further advantage of mass specificity. This results in a much lower limit of detection for aldehydes like HNE that are present in biological samples at very low concentrations (102). Selected ion monitoring (SIM) at masses specific for target analytes considerably improves instrumental sensitivity. In addition, derivatization (such as oxime derivatives) can often be employed to direct fragmentation, further improving limits of detection (103). As such, reduced sample volumes are often needed per analysis when using GC/MS. Several types of aldehyde derivatives have been explored in conjunction with GC/MS, most popularly *o*-pentafluorobenzyl-oxime-trimethylsilyl (PFB-oxime-TMS) (102-106) and DNP (107) derivatives. PFB-oxime-TMS derivatives react quantitatively with aldehydes at room temperature within 30 minutes. Other advantages include small sample size and mild derivatization conditions (105, 106). Due to low volatility, DNP derivatives are only practical for GC separation of low molecular weight aldehydes. Also, these derivatives tend to react incompletely if the aldehydes are in low abundance, which is often the case in biological matrices. Nevertheless, they offer the benefit of little or no side-reactions (106).

GC/MS methods of aldehyde analysis are well established, however, the use of HPLC combined with tandem mass spectrometry offers several noteworthy advantages. For instance, a much greater proportion of the sample can be presented to the system, thus improving the overall sensitivity of the technique. In addition, while different classes of aldehydes can be simultaneously analyzed by HPLC/MS, multiple derivatizations are frequently necessary for the analysis of different classes by GC/MS methods (37). The temperatures applied in GC/MS for sample vaporization may not be suitable for certain analytes. Unlike GC/MS, little pre-MS sample cleanup is required in HPLC/MS methods. Furthermore, tandem mass spectrometry (MS^n) coupled with HPLC is a well-documented, specific and sensitive procedure using modern instrumentation. Scanning the precursor ions for a common product ion provides a straightforward method for aldehyde mixture analysis in biological samples, where the aldehyde composition may vary considerably. DNP (108, 109), ozonide (109) and dimedone (37, 110, 111) derivatives of aldehydes have been successfully analyzed using HPLC/MS. One report

described the detection and analysis of HNE by HPLC/MS without any form of derivatization (112).

A noteworthy advantage of CHD derivatives is that they are formed with aldehydes only. Other carbonyl compounds simply do not react in this manner. As such, this method is completely selective for these compounds. The improved selectivity afforded by HPLC/MS/MS provides significant advantages over the fluorescence detection of such derivatives, especially in the case of co-eluting compounds. This, coupled to the fact that CHD-derivatized aldehydes provide over 90% recoveries makes this procedure ideal for trace aldehyde analysis (100). It has been observed that aldehydes derivatized with CHD reagents produce analytes that display excellent electrospray response, a further advantage of exploiting this derivatization technique in conjunction with HPLC/MS (37).

Liquid Chromatography

Liquid chromatography was brought into existence by the Russian botanist M. S. Tswett (1872-1919) as a means for the separation of colored plant pigments (113). Since then, high performance liquid chromatography, a highly developed version of its predecessor, has become a well established analytical technique. This technique is used for the separation and determination of organic and inorganic solutes in a variety of settings, including biological, pharmaceutical, environmental and industrial applications. HPLC instruments consist of a reservoir of mobile phase, a pump, an injector, a separation column and a detector (113). The mobile phase reservoirs, along with associated feed lines should be inert to prevent leaching of chemicals. Solvent feed lines are typically made of non-permeable Teflon. It is important for the pumps to be able to deliver mobile phase through the system as reproducibly as possible. Typical flow rates for microbore chromatography range from 0-150 μl/min. A six-port Valco or Rheodyne injector is suitable for LC systems (113). Samples are injected by micro-syringe into a sample loop, the size of which can be chosen to meet experimental needs. The stationary phase in LC systems usually consists of small diameter (3-10 μm) uniform particles, packed into a narrow bore (0.01 inches or less) cylindrical column to minimize band

broadening. Columns are made of resilient material, such as stainless steel or plastic. They are generally 5-30 cm long with an internal diameter in the range of 0.3-9 mm. In view of the small size of HPLC column packings, pumps that are able to deliver mobile phase at high backpressures (~6000 psi) at precise flow rates (<1% variation) are a necessity (113).

In an LC separation experiment, the sample is first dissolved in the mobile phase and then passed, under pressure, through an immobile and insoluble stationary phase. The sample flows through the column by continuous addition of mobile phase, which completely permeates the stationary phase and elutes the solutes into the detector. The phases are chosen such that components of the sample have differing partitioning behavior between them. For instance, an analyte having high solubility in the stationary phase will take longer to traverse the column, compared to one that is not particularly soluble in the stationary phase but highly soluble in the mobile phase. The process of separation becomes possible because of these differences in mobilities between the analytes. Each analyte migrates through the column at a rate that is dependent on the time it spends in the mobile phase. At the detector, they each generate a signal which is recorded. Substantial benefits in the separation process can be achieved by careful consideration of chromatographic parameters.

Separation Theory

Analyte distribution between phases follows a dynamic equilibrium (113):

$$A_{mobile} \Leftrightarrow A_{stationary}\,. \tag{1.1.2}$$

The equilibrium constant, *K*, for this process is the distribution coefficient. *K* is defined as the ratio of the molar concentration of analyte in the stationary phase and the molar concentration of the analyte in the mobile phase:

$$K = \frac{C_s}{C_m}\,. \tag{1.1.3}$$

The time lapse between sample injection and a component analyte peak reaching a detector at the end of the column is the retention time (t_R). Each analyte component is characterized by a different retention time. The time for the mobile phase to pass through the column is t_M (Figure 1.1.7).

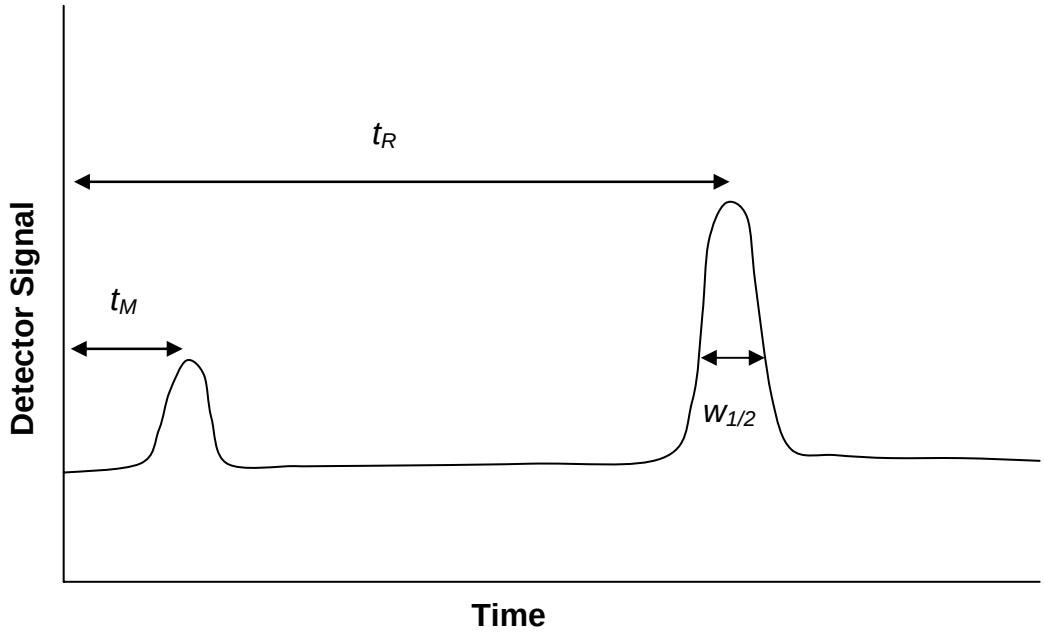

Figure 1.1.7. The separation process. The time interval between sample injection and the analyte peak reaching the detector is the retention time (t_R). The time for the mobile phase to pass through the column is t_M. The peak width at half height is $w_{1/2}$.

The capacity factor, *k'*, can be employed to define retention of an analyte on a column. For analyte$_1$, the capacity factor is:

k'_1 = (mass of analyte$_1$)$_s$ / (mass of analyte$_1$)$_m$

$$= \frac{t_R - t_M}{t_M}. \qquad (1.1.4)$$

Optimization of the chromatographic process is critical to any HPLC experiment. To this end, band separation and band broadening are of importance. Both are kinetic processes and a useful separation is only achieved when the rate of band separation is greater than the rate of band broadening. To obtain the best separations, efficiency and selectivity issues must be considered. Sharp, symmetrical chromatographic peaks can be obtained only when column efficiency is optimized.

Plate Theory

It is possible to describe column efficiency by the plate model, which assumes that the chromatographic column contains a large number of (hypothetical) separate layers, also known as theoretical plates. Furthermore, analyte equilibration between the two phases is said to occur at each plate. The analyte moves down the column as a result of transport of equilibrated mobile phase from one plate to the next. The number of theoretical plates that a real column possesses can be obtained by examining a chromatographic peak after elution (114):

$$N = 5.55\left(\frac{t_R}{w_{1/2}}\right)^2 \qquad (1.1.5)$$

where, $w_{1/2}$ = the peak width at half height.

Column efficiency increases as the number of equilibrations or theoretical plates, increases. If the length of the column is *L*, then the height equivalent to a theoretical plate (*H*) is:

$$H = \frac{L}{N}. \qquad (1.1.6)$$

The number of theoretical plates is dependent on the length of the chromatographic column. *H* is a better indicator of column efficiency as it makes inter-column comparisons more feasible (113).

Rate Theory

Chromatographic phenomena inside a column can be better understood when taking into account the time for the solute to equilibrate between the stationary and mobile phases (114). This approach is in contrast with the plate model, which postulates that equilibration is instantaneous. Rate theory highlights the kinetic factors that contribute to zone or band broadening, as represented by *H* (115). The resulting chromatographic peak shape is therefore influenced by the rate of passage of analytes through the column and by the various routes that solute molecules can take in their journey through the stationary phase. The different mechanisms that increase band broadening are described by the van Deemter equation (116):

$$H = A + \frac{B}{u} + (C_s + C_m)u \qquad (1.1.7)$$

where, u = Average velocity of mobile phase

A = Eddy diffusion

B = Longitudinal diffusion

C = Resistance to mass transfer in the stationary (C_s) and mobile (C_m) phases.

A plot of plate height versus average linear velocity gives an indication of the ideal flow rate (Figure 1.1.8). At mobile phase velocities below the optimum, the overall efficiency of the system is strongly influenced by longitudinal diffusion, or the *B* term. At velocities higher than the optimum, the efficiency decreases because resistance to mass transfer (*C* terms) becomes more important. Despite the reduced efficiency, it is generally acceptable to employ mobile phase velocities above the ideal value for the purposes of lowering analysis time (113).

For packed columns in situations of low velocity where the mobile phase random walk of solute particles is directed by longitudinal diffusion, the Eddy diffusion or *A* term, is eliminated. Eqn (1.1.7) then becomes (116):

$$H = \frac{B}{u} + C_s u + C_m u\,. \qquad (1.1.8)$$

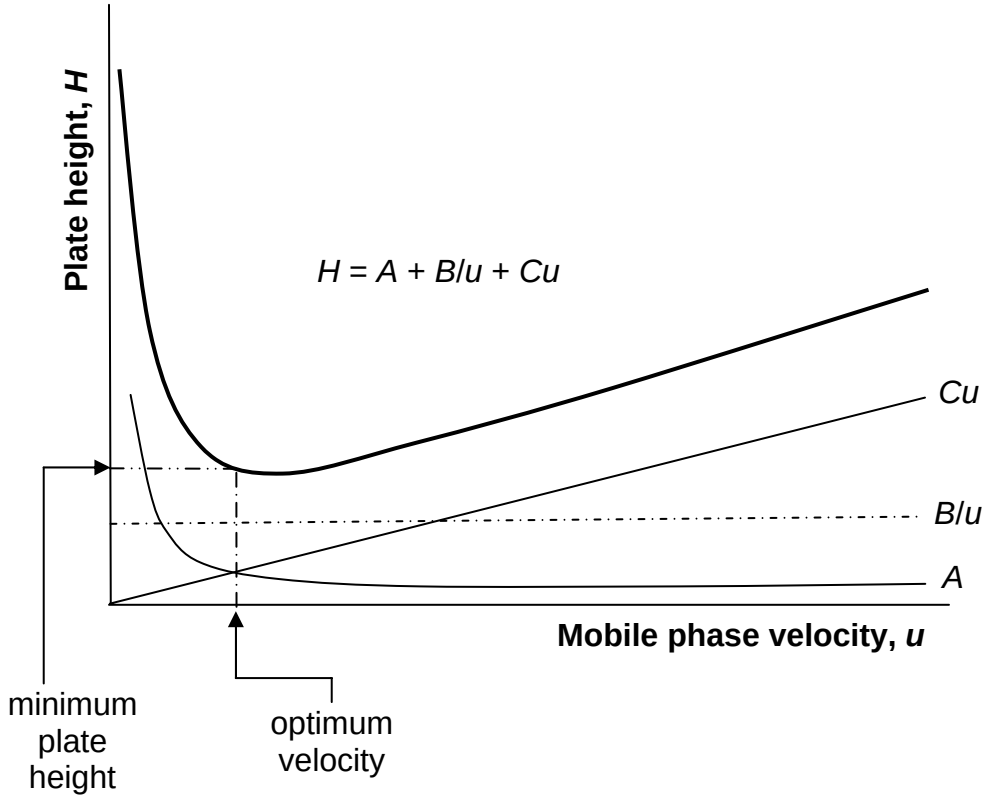

Figure 1.1.8. The van Deemter plot. *H* is the plate height, *A* is the Eddy diffusion term, *B* is the longitudinal diffusion term, *C* is the resistance to mass transfer term and *u* is the mobile phase velocity.

Sometimes, other measures of column efficiencies can prove to be more useful. Solute separation is intimately tied to selective retention by the stationary phase. This selectivity by the stationary phase can be expressed as a form of adjusted retention:

$$\alpha = \frac{k_2^{'}}{k_1^{'}} = \frac{K_2}{K_1} = \frac{t_{R2}^{'}}{t_{R1}^{'}}. \tag{1.1.9}$$

Eqn (1.1.9) clearly shows the thermodynamic basis of this type of separation, as described by the relationship of the selectivity factor to the distribution coefficient (113).

While the selectivity factor portrays the separation of solute zones, it does not take peak widths into consideration. As can be seen in Eqn (1.1.10), the resolution, R_s, is a more informative measure of separation. It considers the difference in retention, as well as column efficiency (113):

$$R_s = 2\frac{t_{R1} - t_{R2}}{w_{B1} + w_{B2}} \tag{1.1.10}$$

where, w_B = peak width at the base.

A more useful expression for resolution can describe the both the thermodynamic and kinetic aspects of the separation (117):

$$R_s = \left(\frac{N^{1/2}}{2}\right)\left(\frac{\alpha - 1}{\alpha - 2}\right)\left(\frac{k_{avg}}{1 + k_{avg}}\right) \tag{1.1.11}$$

where, k_{avg} = average k for two peaks of similar retentions.

An increase in column selectivity (α) is a powerful way of improving resolution. As such, a careful selection of both stationary and mobile phases is critical to the HPLC process.

Stationary Phase

A variety of particles are used in LC column separations, differing in type, size, shape and nature. Microparticulate (3-10 μm), porous materials (~300 Å pore diameter) offer large active surface areas for increased sample loadings, good column efficiencies and high speed of analysis (118). Silica packings are commonly used for LC columns because they can tolerate the high pressures created when 10-30 cm columns are packed with microparticulate materials. Silica is easily functionalized and the chemistry of its bonding reactions is quite well understood (113). Bonded-silica columns can be used

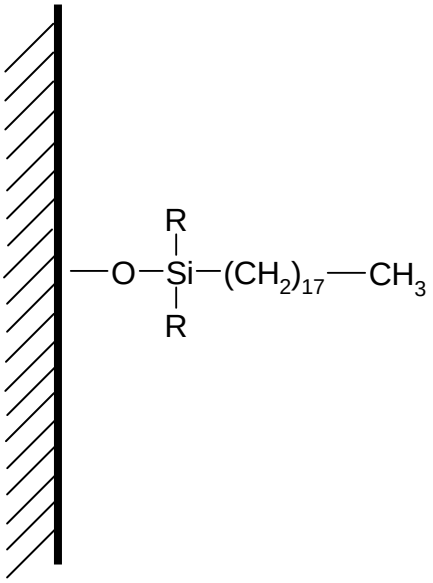

Figure 1.1.9. C_{18} stationary phase (monomeric bonding) for HPLC.

through a wide pH range (pH 1-10), although reproducibility is assured only in the range of pH 2-7.5. This is largely because of the fact that long-term exposure to pH extremes causes hydrolysis of the bonded phase (acid extremes) or degradation of the base silica (basic extremes) (119). Silica-based columns tend to offer vastly improved efficiencies, compared to non-silica materials. For the purposes of separating small, hydrophobic compounds, a carbon-chain bonded phase over microparticulate, porous silica would be useful. Longer chain bonded phases have more hydrophobic character and greater carbon loading (119). In the separation of dimedone derivatives of aldehydes, for instance, a hydrophobic C_{18} bonded phase would be suitable (Figure 1.1.9). Retention is largely based on van der Waals interactions.

Column Packing

In the wet-fill (slurry packing) method of column preparation, an appropriate solvent is used to suspend the stationary phase particles at a reasonable concentration. This suspension is then pumped under high pressure into an empty column. It is required that the solvent be able to maintain uniform particle distribution without agglomeration. The solvent must also thoroughly wet the packing material. LC packings that have low surface energy, such as C_{18} functionalized silica, can be packed in solvents of low polarity, such as a binary acetonitrile:water = 9:1 solvent mixture. To pack a column, the packing suspension is sonicated, stirred and placed in a specially designed reservoir, also known as a column bomb, which fits to the inlet end of the empty column. A porous screen (1-2 μm) or frit is placed at the outlet of the column and the packing material slurry is introduced into the column under gas pressure, producing a compact stationary phase bed (113).

Mobile Phase

Solute retention and selectivity also depend on the strength of the interaction between the solute and the mobile phase. Solvents used as the mobile phase can enhance or diminish solute ionization and can also screen active adsorption centers on the adsorbent surface. In typical LC approaches, a logical and intelligent selection of the stationary phase is made first and then the selectivity is fine-tuned by manipulating the

mobile phase. Useful solvents will have reduced viscosity, flammability and toxicity. They will also be compatible with the detection system for the LC instrument and have little or no impurities (113). Detection of solutes in HPLC occurs online, so it is imperative that the solvent be compatible with the detection system.

Solvents of low viscosity offer favorable solute diffusivity, which in turn improves column performance. It is important for solvents to be chemically inert towards the target analytes and be able to completely dissolve the analytes. In reversed-phase liquid chromatography (RP-HPLC), there is an inverse relationship between solvent strength and chromatographic elution power. For instance, pure water is a rather strong solvent but has little elution power in RP-HPLC. However, mixing water with a small quantity of an organic modifier with lesser polarity, such as acetonitrile, results in a solvent system that can elute a solute with a low capacity factor value (a solute with reduced stationary phase retention). Binary and ternary solvent mixtures provide a simple means for controlling solvent strength by varying the relative concentration of each component in the mobile phase mixture that enters the column (113).

Gradient Methods

In LC experiments, it is possible to gradually change the composition of the mobile phase during the course of a chromatographic run through a process called gradient elution. This technique is quite similar in principle to temperature programming in GC, except that changes in solvent strength rather than temperature are used to elute target analytes (113). Each experiment is begun with a weak eluting solvent, such as water, followed by steady additions of increasing amounts of a strong eluting solvent, such as acetonitrile, over the length of the chromatographic run. In high-pressure gradient formation, the high pressure mixing of the two solvents is brought about by two pumps and a microprocessor controlling device (113). A gradient is generated by careful control of the output solvent flow from each pump (Figure 1.1.10). Manipulation of solvent strength in this manner allows improved resolution of poorly retained solutes at the beginning of the separation, while the more strongly retained solutes are eluted within a shorter time. Gradient elution offers significant improvements in peak shape, resolution,

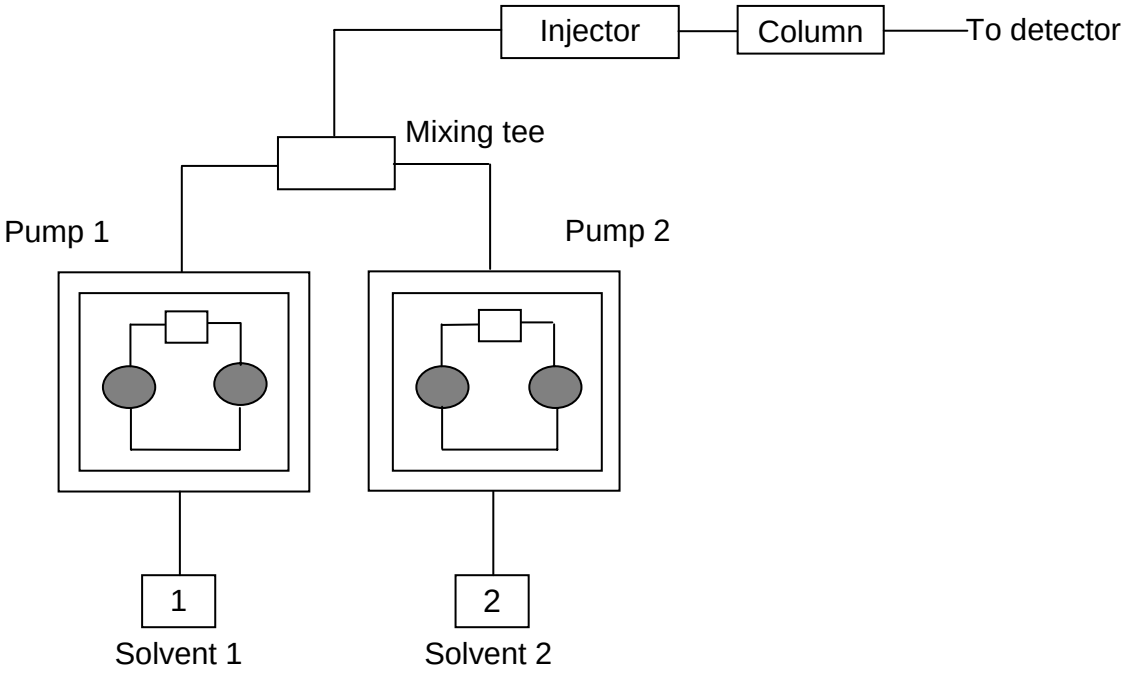

Figure 1.1.10. High-pressure gradient formation in HPLC.

detection sensitivity and analysis time. Solvent gradients are widely used with RP-HPLC since a wide range of compounds can be separated using this approach.

Reversed-Phase HPLC

RP-HPLC utilizes a non-polar stationary phase with a polar mobile phase and is very useful in separating hydrophobic analytes. Polar sample molecules interact the least with the stationary phase and are therefore eluted first. As a result, increasing the polarity of the mobile phase results in increased retention of solute. The hydrocarbon-like stationary phases have the ability to equilibrate rapidly with changes in mobile phase composition and are therefore very well suited for use with gradient elution (113). The mechanism of retention in RP-HPLC is complex and it is believed that various non-specific hydrophobic interactions between the solute and stationary phase are involved. However, these interactions alone are much too weak to account for the degree of solute retention that is characteristic of RP-HPLC. The retention mechanism can be best described as involving a combination of partition and adsorption processes. Due to the heterogeneous nature of silica-based materials, it is possible for different mechanisms to operate over different regions of the stationary phase surface. To further complicate matters, the mechanism is not always constant over the entire range of mobile phase compositions. This is largely because mobile phase composition has a significant influence on the solvation of binding sites on the stationary phase (113).

To date, the solvophobic theory provides the most likely interpretation of RP-HPLC retention. Predictions from this theory work best when using aqueous mobile phases with little organic modifier content. A basic assumption is that the stationary phase is a uniform layer of non-polar ligand. According to the solvophobic theory, the solute interacts with the stationary phase, thereby reducing the proportion of its surface area exposed to the mobile phase. This solvent effect drives the sorption of solute molecules. In other words, the solute is adsorbed because it is solvophobic. The theory assumes that aqueous mobile phases tend to be very structured because polar water molecules will self-associate by hydrogen bonding. Non-polar solutes, lacking hydrogen-bonding capabilities, cause a perturbation in this structuring (113). As a result of the very high cohesive energy of the solvent, the less polar, more hydrophobic solutes are literally

squeezed out of the mobile phase and are non-covalently bound to the hydrocarbon portion of the stationary phase.

The solvophobic theory stresses that retention occurs largely due to the strong interactions between the mobile phase and solute molecules. This implies that the mobile phase composition has a greater effect on separation selectivity than the stationary phase in RP-HPLC (113). For polar solutes, the dipolar or hydrogen bonding interaction between the solute and the mobile phase will resist the transfer of solute. It is the disparities in interactive energies between the non-polar and polar solutes with the mobile phase, along with disparities in the hydrophobic solute molecular surface areas that are the important factors associated with functional group selectivity observed in RP-HPLC techniques (113).

Electrospray Ionization – Ion Trap Mass Spectrometry

A particularly well-suited detector for LC is a mass spectrometer because it can be used in the analysis of a wide variety of compounds with diverse functional groups. Furthermore, MS offers high selectivity and sensitivity, together with considerable structural information, for the purposes of solving complex analytical problems (120). Performing LC-MS experiments online extends the well-established GC/MS methods to thermally labile compounds that are amenable to analysis through HPLC only (121). Since MS operates under a vacuum, one of the challenges of interfacing any separation system with this detector is the requirements of a suitable sample introduction method. Also, it can be difficult to completely eliminate the solvent from LC, maintain adequate vacuum levels in the mass spectrometer and generate gas phase ions. There are many reasons why electrospray (ES) is an ideal means of transferring eluent from the LC instrument into the mass spectrometer, a major one being that electrospray allows ion formation directly from solution. Also, in electrospray, ionization occurs at atmospheric pressure. These features have established ESI-MS as a convenient mass detector for liquid chromatography, as the mobile phase offers a suitable medium for analyte ionization.

Electrospray

Electrospray is an ion transport technique that enables the sensitive analysis of small, large and labile molecules, including such varied analytes as peptides, proteins, organometallics, oligosaccharides and polymers. Over 20 years ago, Fenn and co-workers demonstrated the applicability of this technique in directly coupling LC to mass spectrometry (122-124). In LC/MS, the HPLC line is attached to the electrospray probe, a metallic capillary surrounded with nitrogen gas flow, and the mobile phase is forced through the capillary. Solutes analyzed by electrospray undergo 'soft ionization' and are largely left intact in the ionization source. A major source of analyte charging is through protonation or deprotonation reactions (125). The capillary has a voltage applied to it while the sampling cone is held at low voltage. The potential difference between them can be anywhere between +500 and +4500 V. As a result of the voltage on the capillary, an aerosol of charged droplets is formed, assisted by a concentric flow of nitrogen. The droplets have both solvent and analyte molecules, and, depending upon the polarity of the applied voltage, the molecules develop a net positive or negative charge (126). Ionized molecules eventually discard the surrounding solvent and enter into the atmospheric pressure region of the mass analyzer through a low-pressure transport region (~1 torr). This part of the instrument contains a heated capillary, a skimmer and lens arrangements. The electrospray interface uses an octopole lens (Figure 1.1.11) for ion focusing into the mass analyzer of the spectrometer (121).

The aerosol droplets generated in electrospray upon nebulization decrease in size due to solvent evaporation, resulting in an increased charge density on their surface. The mutual repulsion of like charges in the droplets eventually becomes greater than the surface tension, causing ions to be ejected from the droplets. Vaporization of these charged droplets results in the production of singly- or multiply-charged gaseous analyte ions. The electrospray instrument delivers a continuous current, causing redox reactions to take place at the source. Oxidation reactions at the metal capillary remove electrons from negative ions. Likewise, reduction reactions involving the sprayed positive ions occur at the negative counter electrode (127). It is expected that the reaction having lowest electrochemical potential will generally occur at the capillary tip. In an attempt to establish the mechanism for gas-phase ion formation from charged droplets in

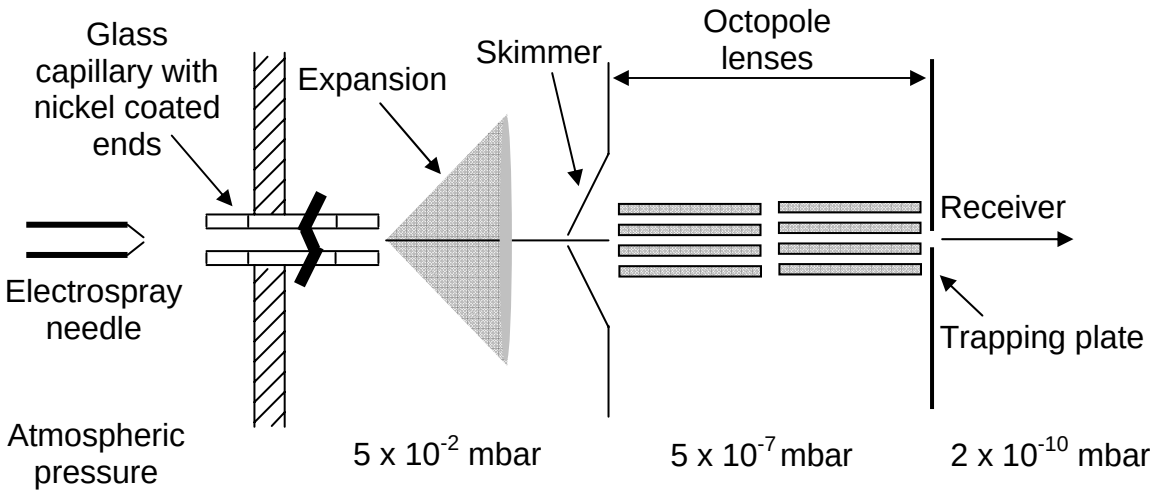

Figure 1.1.11. The electrospray source.

electrospray, the ion evaporation model (IEM) and the charged residue model (CRM) have been suggested (127). Since both models have almost equivalent support in the mass spectrometry community, both are considered when discussing electrospray mechanisms.

Ion Evaporation Model: The increased charge density on the droplet surface arising from solvent evaporation results in Coulombic repulsion becoming greater than the liquid's surface tension. This enables the release of ions from the droplet before it breaks apart, as shown in Figure 1.1.12(A).

Charged Residue Model: Evaporation of the droplets occurs continuously. The diameter of the droplet decreases while the total charge remains the same. The increased charge density, due to solvent evaporation, induces instability on the surface. This causes large droplets to divide into smaller droplets through a series of sequential fissions, eventually generating single ions, as shown in Figure 1.1.12(B).

Electrospray offers the best sensitivity with lower flow rates. The effluent flow from the LC system that enters the electrospray source can be reduced by using a splitter. Since electrospray is *not* an ionization method, it is imperative that the mobile phase have a pH such that the analytes will be ionized. Acidified mobile phase is well-suited for the analysis of basic compounds using the positive electrospray mode, while a basic pH is desirable for acidic analytes. It is best to employ volatile buffers for routine use, although non-volatile buffers, such as phosphate, can be employed as well. It should be noted that when using non-volatile buffers the salt deposit in the source will have to be periodically removed. It is important that the concentration of the buffer acid or base used to manipulate the pH be low. This is to avoid competition between the analyte and electrolyte ions for conversion into the gas-phase, as it can potentially decrease analyte response (125).

Quadrupole Ion Trap Mass Spectrometry

Ions generated through electrospray can be detected with a quadrupole ion trap (QIT), a mass analyzer invented by Wolfgang Paul and co-workers in the 1950's. Ions are guided from the source into the trap by focusing through a skimmer and two RF-only octopoles. Differential pumping with a series of mechanical and turbo pumps maintains a vacuum in the trap while the electrospray source is at atmospheric pressure. The ion trap

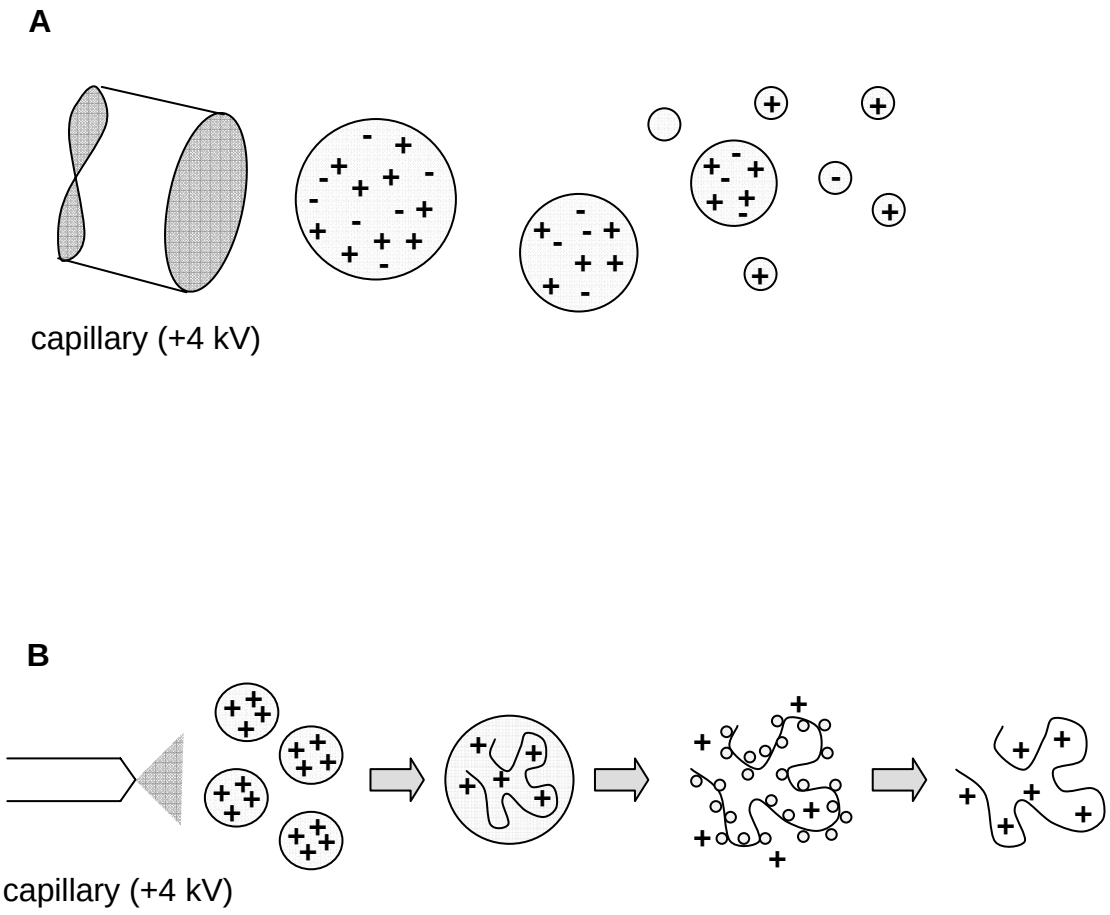

Figure 1.1.12. Electrospray mechanisms: (A) Ion evaporation model (IEM) and (B) Charge residue model (CRM).

is comprised of three electrodes of hyperboloidal geometry: a ring electrode located between an entrance end-cap and an exit end-cap electrode (Figure 1.1.13). These electrodes form a cavity within which ions can be trapped and studied. The trapping volume in a QIT has dimensions r_0 and z_0, where r_0 is the closest distance between the center of the trap and the ring electrode and z_0 is the closest distance between the center of the trap and either end-cap (128). Both end-cap electrodes have small holes in their centers through which the ions can travel. Ion entry is controlled using a gating lens that switches from positive to negative voltages to repel or attract ions toward the entrance end-cap opening. For positive ion analysis, a negative potential is applied for ion entry and for negative ion analysis, a positive potential is applied. The ionization period or time during which ions are allowed entry into the trap is adjusted to maximize signal and minimize space charge, which can arise from an excess of ions in the trap producing changes in the electrical fields and decline in trap performance. On the other hand, too few ions can result in a loss of sensitivity (129, 130).

In a quadrupole ion trap, a *rf* oscillating electrical potential on the ring electrode directs and focuses ions to the trap center. Helium gas in the instrument, at a pressure of about 1 mtorr, collides with the trapped ions and aids in the reduction of their kinetic energy and causes the contraction of trajectories toward the center of the trap. Ions within the trapping volume experience a potential described by (128, 131):

$$\Phi_{x,y,z} = \frac{(U - V\cos\Omega t)}{2}\left[\frac{x^2 + y^2 - 2z^2}{r_0^2}\right] + \frac{(U - V\cos\Omega t)}{2} \tag{1.1.12}$$

$$\text{or, } \Phi_{r,z} = \frac{(U - V\cos\Omega t)}{2}\left[\frac{r^2 - 2z^2}{r_0^2}\right] + \frac{(U - V\cos\Omega t)}{2} \tag{1.1.13}$$

where, U = *dc* amplitude on end-cap electrodes

V = *rf* amplitude on ring electrode (fundamental *rf*)

Ω = oscillating frequency of *rf* (V), typically 1.1 MHz

$r = \sqrt{x^2 + y^2}$ = radial displacement.

Each ion in this quadrupolar field experiences a force that is dictated by Newton's law (128):

$$\vec{F}_{r,z} = \vec{E}_{r,z} = -e\nabla\Phi_{r,z} = m\vec{a}_{r,z} \tag{1.1.14}$$

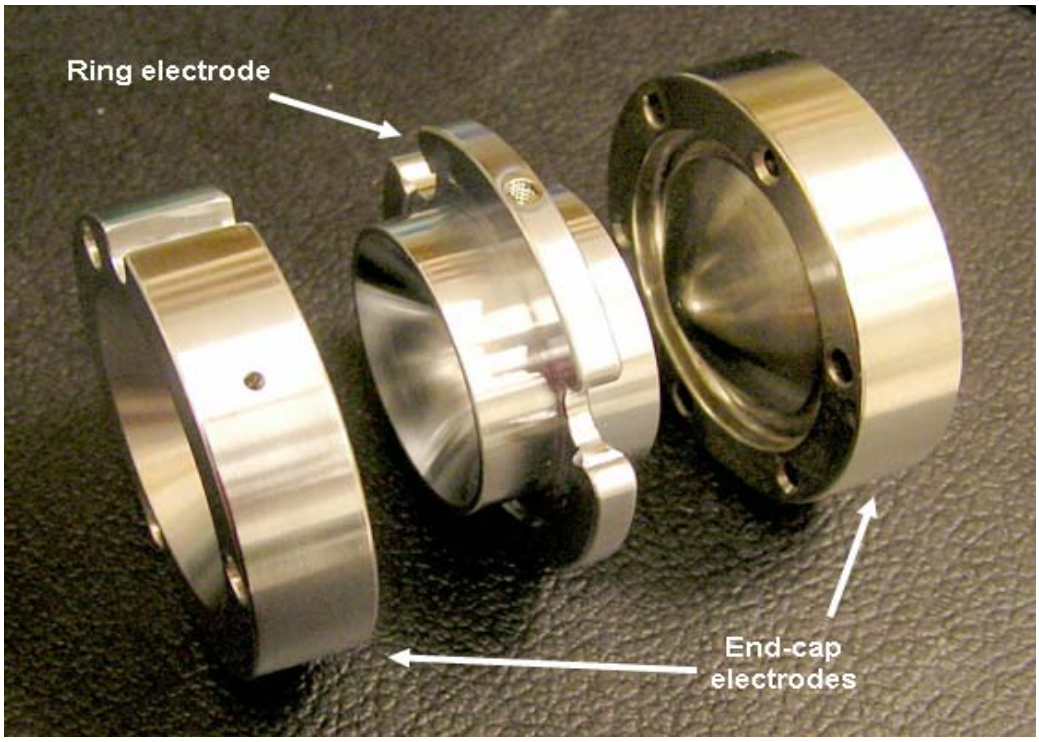

Figure 1.1.13. The quadrupole ion trap (QIT).

where, m = mass of ion

e = charge of ion

a = acceleration of ion

$E_{r,z}$ = electric field strength.

The mass (m) and charge (e) of an ion, the size of the ion trap (r_0), oscillating frequency of the applied voltage to the ring electrode (Ω) along with the amplitude of the voltages on the end-cap (U) and ring (V) electrodes all come together in a second order differential equation or *Mathieu Equation* to determine whether or not that ion will have stable motion in the trap (129, 132).

$$\frac{d^2u}{d\xi^2} + (a_u - 2q_u \cos 2\xi)u = 0 \tag{1.1.15}$$

where, u = coordinate axes x, y and z

ξ = dimensionless parameter $\Omega t/2$ (t is time)

a_u and q_u = dimensionless trapping parameters.

Solutions for the Mathieu equation that provide stable ion trajectories are described by the parameters q_z and a_z in the axial direction,

$$q_z = -\frac{4eV}{mr_0^2\Omega^2} \tag{1.1.16}$$

$$a_z = -\frac{8eU}{mr_0^2\Omega^2} \tag{1.1.17}$$

as well as a_r and q_r in the radial direction:

$$a_r = -\frac{a_z}{2} \tag{1.1.18}$$

$$q_r = -\frac{q_z}{2} \tag{1.1.19}$$

$$\xi = \frac{\Omega t}{2} \text{ (dimensionless parameter).} \tag{1.1.20}$$

In reference to ions, m/z (z is the ion charge) is synonymous with m/e.

Mathieu Stability Diagram

A plot of a_z vs q_z or Mathieu Stability Diagram describes the regions of stability in the trap for ions of different m/z values (Figure 1.1.14). Depending upon the amplitude

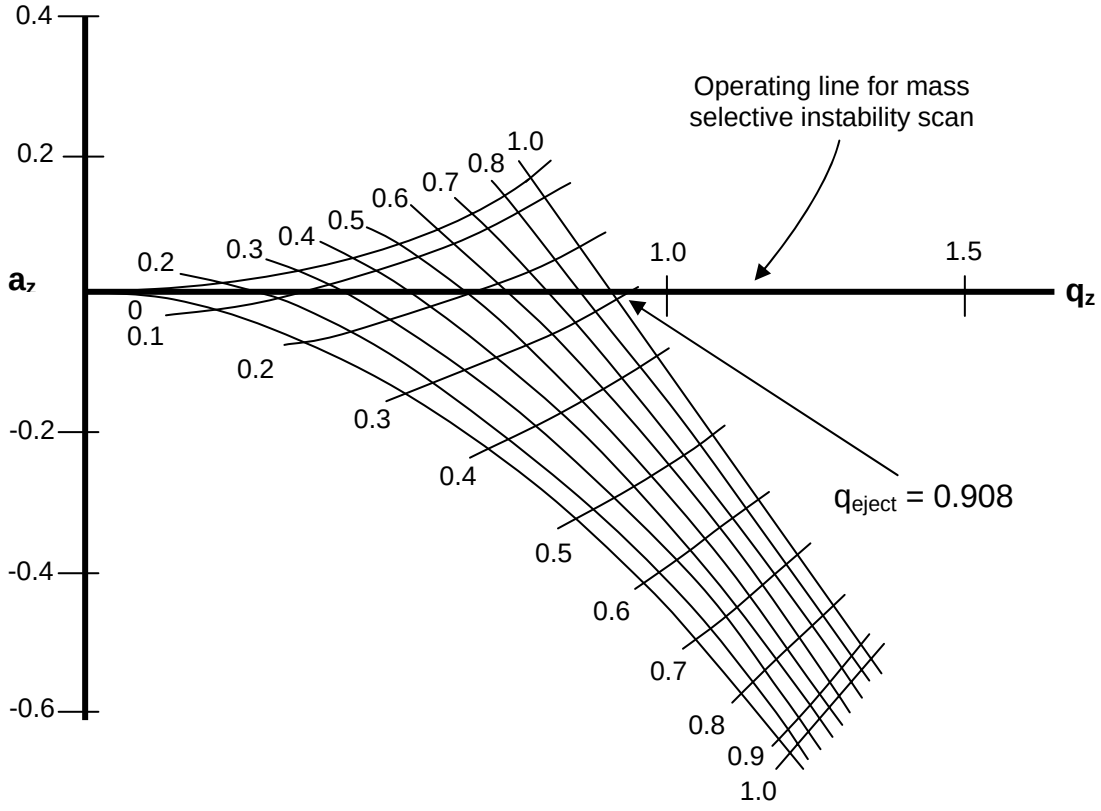

Figure 1.1.14. Mathieu stability diagram for a 3D quadrupole ion trap. The a_z parameter is proportional to *dc* and the q_z parameter is proportional to *rf*.

of *U* and *V*, an ion of a given *m/z* will have a q_z value that is located within the boundaries of the diagram. This means that the ion will have stable motion and be trapped. An ion can be maneuvered within the boundaries of the stability diagram by manipulation of *U* and *V*. In addition, the trajectory of an ion can be made unstable through careful selection of *U* and *V*, causing it to be selectively expelled from the trap. Whether or not stability exists for a particular ion within the trap depends solely on the parameters *a* and *q* and not on the initial parameters of ion motion, such as velocity. The Mathieu equation has two types of solutions (129):

1. *periodic and stable*: These solutions dictate stable ion trajectories in the trap. Ions can be stored in a trap provided that their motion is stable in both the *r*- and *z*-directions.
2. *periodic but unstable*: These solutions apply to the boundaries of unstable regions in the *aq* map, which represent points at which ion trajectories become unstable.

It should be noted that commercial ion traps generally do not offer the ability to manipulate *dc* voltages. With no *dc* potential applied, all ions are assured radial stability. Hence, in order to eject ions, they must be made unstable in the axial direction.

On the *q*-axis (*a*=0, no *dc* voltage) there is a stability region extending from $0 < q < q_{max} = 0.908$, which dictates the low-mass cutoff of the mass analyzer. As such, the lower *m/z* ions have *q* values closer to the exclusion limit, while higher *m/z* ions have *q* values closer to the origin. All masses between $\infty > m > m_{min}$ have stable orbits. Scanning *V* to higher voltages will make trapped ions move to higher *q* values and eventually, the lowest *m/z* ion reaches, and then crosses the stability boundary. In other words, the ion gains kinetic energy and its axial motion becomes increasingly larger until it is ejected from the trap through holes in the end cap aperture. A full scan mass spectrum is generated by sequentially ejecting ions from low *m/z* to high *m/z* and detecting them using a collision dynode and electron multiplier system. This is known as the *mass selective instability scan* (129).

Although the angular frequency of the applied voltage *V* on the ring electrode is Ω, ions in the trap do not oscillate at this frequency because of their own inertia. Instead, the ions oscillate with a frequency known as the secular frequency f_z that is lower than Ω

and decreases with increasing mass. This frequency is proportional to Ω by a constant of proportionality β_z that is dependent on both a_z and q_z (131):

$$f_z = \beta_z \frac{\Omega}{2}. \tag{1.1.21}$$

When $q_z < 0.4$, this constant of proportionality can be approximated in the following manner:

$$\beta_z^2 = a_z + \frac{q_z^2}{2}. \tag{1.1.22}$$

In situations where no *dc* voltages are applied to the ion trap and $a_z = 0$, the expression can be simplified to:

$$\beta_z = \frac{q_z}{\sqrt{2}}. \tag{1.1.23}$$

Since the maximum value of β_z for a stable ion trajectory is $\beta_z = 1$, the highest possible secular frequency f_z that an ion can have is half the value of Ω (130).

There is an alternate method to the mass selective instability scan that can be applied towards ion ejection. This method, termed *resonance ejection*, involves making the trajectory of a particular ion unstable through the application of a *high-amplitude ac voltage* or supplementary *rf* potential on the end-cap electrodes. The q_z value of the ion is changed until the secular frequency of the ion matches the frequency of the applied *rf* voltage. In a special case of resonance ejection, the supplementary *rf* frequency is held constant (corresponding to a q_z value less than 0.908) while the *rf* drive amplitude is ramped, a process known as *axial modulation*. In this manner, several or all ions can be ejected mass selectively. The ions absorb excess energy from the applied field, sequentially go into resonance, causing the amplitude of oscillations to linearly increase in the *z* direction. If the applied voltage is high enough, the oscillations will become so large that the ions are destabilized and finally ejected from the trap through the end-cap electrode. Axial modulation creates 'holes' in the q_z axis so that ions can be expelled at values of *V* lower than those needed to attain $q_z = 0.908$ in the standard instability scan. Furthermore, very large ions that may not be able to achieve this q_z value no matter how high the value of *V* can be easily ejected with this approach. A full scan mass spectrum may be obtained by combining resonant ejection with an *rf* (*V*) scan, thereby enabling

successively larger ions to move to the position in the stability diagram where they fall into resonance with the supplementary *rf* and are ejected. When the supplementary *rf* frequency is decreased, corresponding to a much lower value for q_z, axial modulation can enable extension the mass range of the ion trap (128).

Ion Isolation Methods

It is often desirable to study a particular ion in detail, perhaps for the purposes of doing ion-molecule reactions or tandem mass spectrometry (MS^n) experiments. Resonance ejection can be employed to isolate an ion of particular *m/z*, while ejecting all others. In this case, a *supplemental rf waveform* may be applied to the end-cap electrodes. This waveform creates unstable trajectories for all ions *except* the species that is to be trapped. Another approach to ion isolation is by a technique called *reverse-then-forward scanning*. An ejection hole is formed at low q_z by applying a supplemental *rf* to the end-cap electrodes. Scanning the *rf* amplitude on the ring electrode (*V*) in the reverse direction results in the ejection of all *m/z* values larger than that of the desired species through the ejection hole. Likewise, *m/z* values lower than that of the ion to be isolated are expelled from the trap by changing the supplemental *rf* to form an ejection hole at high q_z. The *rf* amplitude on the ring electrode (*V*) is then scanned forward, thus ejecting all ions of lower *m/z* (131). If manipulation of *dc* is an option, then a further method of ion isolation is possible. By applying an appropriate combination of *dc* and *rf* (*V*) potentials on the ring electrode, the ion of interest can be isolated at the apex of the stability diagram, while ejecting all other species (130).

Tandem Mass Spectrometry

Tandem mass spectrometry, abbreviated MS/MS or MS^2, is any general mass spectrometric method of at least two mass analysis stages, either in association with a fragmentation mechanism or a chemical reaction that modifies the mass or charge of an ion (130). In the ion trap, it is possible to perform time-dependent multistage MS^n experiments. Analysis of fragment ions generated from tandem experiments offers considerable structural information of precursor ions. While a high-amplitude supplemental *rf* applied to the end-cap electrodes can initiate resonance ejection of ions,

it is possible to induce ion fragmentation by applying a *low-amplitude supplemental rf* (a few hundred millivolts) to the same electrodes. This process is called *resonant excitation*.

Prior to resonant excitation of a particular ion, all other unwanted ions are excited and expelled from the trap by applying an appropriate supplemental *rf* waveform to the end-cap electrodes. The remaining ions are then focused collisionally to the vicinity of the center of the trap under the influence of collisions with helium atoms. The process has been described as 'ion cooling' as ion kinetic energies are reduced to ~0.1 eV. At this point, ion migrations from the center of the trap are less than 1 mm. A low-amplitude supplemental *rf* is then applied to the end-caps, causing excitation of ions. As a result, the ions start to move away from the trap center, resulting in their experiencing a greater trapping field. Since the supplemental *rf* has low amplitude, ions undergo *low-energy* collisions with helium as opposed to being ejected. Resonance excitation increases ion kinetic energy and promotes collision induced dissociation (CID) with helium, resulting in the formation of fragment ions. A mass spectrum (MS^2) is generated by successively ejecting the fragments from low *m/z* to high *m/z* by choosing supplemental *rf* amplitudes and *V* potentials that induce instability in the ion trajectories (128).

Mass Spectrometric Experiment Design

With the advent of numerous decision-making algorithms, it has become possible to perform a wide array of mass spectrometric experiments focused on the needs of the sample under analysis. Data-dependent algorithms have been used to obtain both MS and MS/MS data during the course of a single LC/MS run. The ion trap mass spectrometer is ideal for these analyses because of its high sensitivity in the full scan mode and the ease of switching from the MS to MS/MS mode. Furthermore, the ion trap employs helium for both ion collection and fragmentation, which considerably simplifies the experiment. In data-dependent experiments, the instrument automatically performs MS/MS experiments on precursor ions in previously acquired full scan mass spectra. The switch from MS mode to MS/MS mode occurs once a signal threshold is reached. As can often be the case, some samples have multiple co-eluting species. Data-dependent scanning can easily be employed to obtain MS/MS information on these species. The mass analyzer performs an MS/MS analysis on the most intense ion and then puts this ion on an exclusion list.

The ion is not analyzed further for a pre-selected time window. Then the instrument proceeds with the analysis of other ions present in the full scan.

The time for completion of one analytical full scan followed by one analytical MS/MS scan is determined by the duty cycle of the instrument. For the purposes of enhancing ion statistics, several micro-scans are averaged to produce one analytical scan. However, in doing so, the duty cycle of the mass analyzer tends to suffer, resulting in fewer full scans and MS/MS scans being acquired. This can be a substantial issue in instances of overlapping peaks produced as a result of mediocre chromatographic resolution. In such cases, fewer analytical scans per unit time are likely to preclude certain analytes from tandem mass spectrometry experiments. There is some user control on the rate of analytical scan acquisition through such parameters as the number of averaged full scans and MS/MS scans as well as the ion trap injection time. Wenner *et al*. investigated the factors that influence data-dependent scanning in ion trap MS (133).

Data-dependent scanning enables the rapid analysis of all key components present in a particular sample. However, sometimes it may be required to perform mass spectrometric investigations on certain target analytes within the sample and more focused experiments are necessary. In such situations, it is desirable to perform segmented MS/MS analyses in which the data acquisition time window is divided into discrete sections. Each time segment is devoted exclusively for the MS/MS analysis of a target analyte. Any sections of the time window not involved in the analysis of particular solutes may be used to do data-dependent scanning to obtain a full picture of the MS fingerprint of the sample. Segmented analyses have the advantage of greatly improving the signal-to-noise ratio (SNR). Furthermore, the isolation of a particular analyte in this manner for exclusive MS/MS analysis can be described as a form of ion purification. Segmented MS/MS analysis can simultaneously provide structural and quantitative information on target analytes.

Goals

This chapter has provided a background on the nature and importance of Alzheimer's disease. The clinical criteria for AD diagnosis, histopathological hallmarks,

as well as elements of the etiology that have been established to date were discussed. Numerous studies have shown the relevance of Aβ and τ in oxidative stress and AD pathogenesis. These findings have been stressed, along with the connection of Aβ and τ to the widespread lipid peroxidation and oxidative stress observed in the AD brain. The importance of LPO byproducts as viable biomarkers for AD, such as the neurotoxic aldehydic species acrolein and HNE, was explained. Exploiting these compounds as biochemical indicators of AD requires the development of sensitive, selective and reliable methodologies for their detection and quantification. The benefits of derivatizing these biogenic aldehydes with cyclohexanedione reagents for analysis by LC/MS have been detailed. Furthermore, principles of LC/MS operation as applicable to biogenic aldehyde quantification were discussed.

Chapter 1.2 describes the development of LC-ESI-MS/MS methods for the detection and accurate quantification of aliphatic and unsaturated aldehydes of biological importance, particularly in AD pathogenesis. Several LC and MS parameters were explored and a description of how their values were optimized in order to arrive at the most effective methodology is provided. Appropriate calibration curves for quantitative analysis were constructed using standard aldehyde samples and their reliability and usefulness was investigated in the analysis of real tissues.

Chapter 1.3 focuses on the application of the developed LC-ESI-MS/MS method in the analysis of aldehydic products *in vivo*. Post-mortem samples from several brain regions of individuals that had been suffering from different stages of AD were analyzed for biogenic aldehydes. These results were then compared to the analysis of brain tissues from suitable age-matched controls. Detailed statistical examination of the data is given.

Chapter 1.4 provides some concluding remarks and highlights the significance and future direction of this work.

Chapter 1.2

Development of LC-MS Methodologies for the Quantitative Analysis of Biogenic Aldehydes in Alzheimer's Disease

Introduction

Liquid chromatography (LC) separations, coupled to a variety of detection methods, have been employed in the analysis of derivatized biogenic aldehydes. These include derivatization by 2,4-dinitrophenyl hydrazines followed by UV detection as well as fluorescence detection of several derivatives (40, 94-96, 98-101, 107). In cases where analysis was carried out by gas chromatography (GC), the detection method of choice has been mass spectrometry (MS) (103, 105-107). For instance, Zhang and co-workers (104) have recently developed a simple, rapid, sensitive, solvent-free GC/MS method with solid-phase microextraction (SPME) and on-fiber derivatization for the analysis of aldehyde levels in the blood of lung cancer patients. Aldehydes in blood headspace were extracted by a SPME fiber and reacted with O-2,3,4,5,6-(pentafluorobenzyl)hydroxylamine hydrochloride (PFBHA) on-fiber. The resulting oxime derivatives were desorbed and quantitatively studied by GC/MS. The blood samples were shown to contain substantially elevated levels of hexanal and heptanal compared to controls, suggesting the potential use of these aldehydes as biomarkers for this disease.

There are some noteworthy reports that describe the use of LC in association with mass spectrometry in aldehyde analysis of tissue samples (37, 97, 108, 109, 112). Several derivatization techniques have been explored, including the Hantzsch reaction (110). Compared to the more frequently used hydrazine reagents, this mode of derivatization displays some very interesting characteristics. In this reaction, an aldehyde, two β-dicarbonyl compounds and ammonia combine to form a heterocyclic system. The resulting compound, known as a dimedone derivative, has fluorescent properties (110). Several β-dicarbonyl compounds have been studied. Acetylacetone was the first β-diketone derivatized in this manner, producing a dihydropyridine derivative (134).

Sawicki *et al*. described the use of 5,5-dimethyl-1,3-cyclohexanedione as the β-diketone (135). The products of this reaction are decahydroacridines. Several researchers have also applied the use of other β-dicarbonyl compounds, such cyclohexanedione (134, 135), in this type of aldehyde derivatization. The derivatization mechanisms are described elsewhere (136).

Mallet *et al*. (37) developed a LC-MS procedure for analyzing hexanal and larger aldehydes in blood plasma. Aldehyde derivatization using the Hantzsch reaction preceded analysis by a LC-Quattro instrument with electrospray (ES). Quantification was achieved by multiple reaction monitoring (MRM), with benzaldehyde as an internal standard. This is a non-physiological aldehyde of little structural similarity with the target compounds. The approach has the potential drawback that benzaldehyde reactivity in the derivatization may not be identical to that of the target aldehydes. However, experimental data did not suffer and indicated the applicability of LC-MS in plasma aldehyde quantification. Smaller (C_1-C_5) straight chain and unsaturated aldehydes were not studied.

Karst and co-workers (110) described LC-MS methods for the determination of aliphatic aldehydes following derivatization with acetylacetone through the Hantzsch reaction. The authors employed atmospheric pressure chemical ionization (APCI) and electrospray in the positive ion mode to ionize the dihydropyridine and decahydroacridine derivatives, protonated at their basic secondary amine groups. The oxidation products of the formaldehyde derivatives were identified as side products. The authors concluded that the combination of LC and mass spectrometry offered considerably high selectivity in comparison to the conventional detection approaches.

We extended and applied the protocols of Karst *et al.* and Mallet *et al*. in developing methodology for analyzing small aliphatic and unsaturated aldehydes of biological importance, especially in AD etiology. In contrast to other biogenic aldehyde studies, dimethyl CHD was our derivative of choice due to improved chromatographic quality. A range of aliphatic aldehydes were studied (C_1-C_6), along with acrolein and HNE. Furthermore, two internal standards were employed (heptanal and octanal) to accurately quantify low and high abundance aldehydes. Influence of several instrument parameters on the quality of mass spectral data was explored and a description of how their values were optimized is provided. We detail the development of sensitive, selective

and dependable methods for the detection and quantification of biogenic aldehydes in tissues by LC-ESI-MS/MS.

Experimental

Materials

All aliphatic aldehydes except methanal (Sigma, St. Louis, MO) and ethanal (EM Industries, Inc., Hawthorne NY) were obtained from Wako Pure Chemical Industries, Ltd. (Osaka, Japan). HNE was obtained from Cayman Chemical Co. (Ann Arbor, MI). Acrolein, 1,3-cyclohexanedione (CHD), 5-methyl-1,3-cyclohexanedione (methyl CHD) and 5,5-dimethyl-1,3-cyclohexanedione (dimethyl CHD) came from Aldrich (St. Louis, MO). HPLC grade water, acetonitrile (ACN), methanol, glacial acetic acid, PrepSep C_{18} solid phase extraction (SPE) cartridges and a PrepSep 12-port vacuum manifold were obtained from Fisher Scientific (Pittsburgh, PA). Ammonium acetate came from Sigma (St. Louis, MO). Standard solutions to generate calibration curve data for aldehyde quantification were prepared with Wiretrol disposable micro pipets from VWR Scientific Products (St. Paul, MN).

Brain Tissue

Specimens of the superior and middle temporal gyrus (SMTG) from one AD patient and one age-matched control subject were obtained from short post mortem interval (PMI) autopsies, immediately frozen in liquid nitrogen and subsequently stored at -80^{o}C until used for analysis (blind experiment, performed in triplicate).

Derivatization of Aldehydes

Aldehyde derivatization was carried out using the procedure of Lovell *et al*. (62) Figure 1.2.1. Several dimedone derivatives were explored. Similar schemes were used to derivatize standard aldehyde solutions and human brain samples. Derivatized standard aldehyde mixtures were employed in generating calibration curves for quantitative analysis.

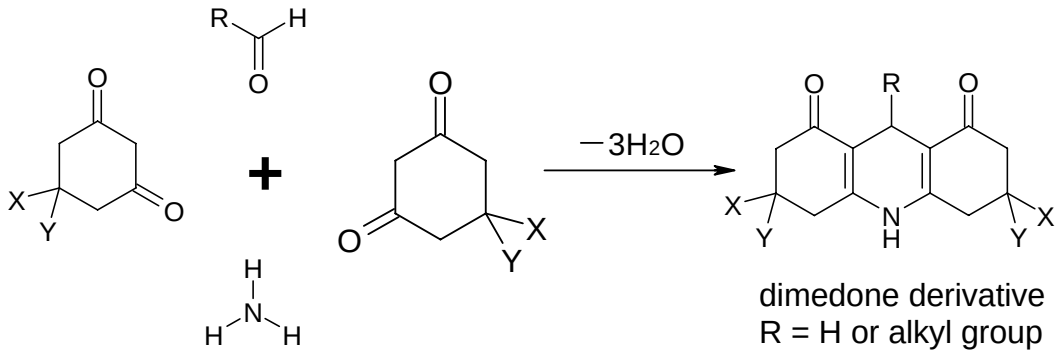

Figure 1.2.1. Aldehyde derivatization. The reaction proceeded by cyclization of 2 β-dicarbonyl compounds and an aldehyde in the presence of ammonia to form a heterocyclic system (110).

Derivatizing Agent

Aldehydes were derivatized by heating them with appropriate amounts of a stock dimethyl CHD derivatizing agent solution, as described below. This solution was prepared by combining 10 g ammonium acetate, 10 mL glacial acetic acid, 0.25 g dimethyl CHD and diluting to 100 mL with water. (62) CHD and methyl CHD derivatizing solutions were prepared in a similar fashion.

Standard Aldehyde Derivatives for Quantitative Analysis

For the aliphatic aldehydes (C_1-C_6), a standardized aldehyde solution mixture was prepared by adding precalculated, *weighed* amounts of stock aliphatic aldehydes (C_1-C_6) to a class A volumetric flask and diluting with methanol. A separate solution of heptanal internal standard was prepared in a similar manner. A set of standardized solutions with increasing concentration of aldehydes (~$1x10^{-9}$ g/mL to ~$3x10^{-7}$ g/mL) was prepared in volumetric glassware by adding suitable amounts of the aliphatic aldehyde mixture, an excess of derivatizing agent, a fixed amount of internal standard and diluting to the mark with methanol. The aldehyde solutions, upon derivatization, were calculated to provide 1 pg/µL to 300 pg/µL. The standardized solutions were incubated in a 60°C water bath for 1 h and subsequently desalted with C_{18} SPE cartridges. The derivatized aldehydes were then eluted with 2 mL methanol (Figure 1.2.2).

For the unsaturated aldehydes (acrolein and HNE), standardized solutions of acrolein and HNE were prepared in a similar manner as described above for the aliphatic species. The internal standard employed here was octanal (Figure 1.2.2).

Brain Tissue

For aldehyde analysis, 100 mg of tissue sample was homogenized using 5 mL HEPES buffer (pH 7.4) with 137 mM NaCl, 4.6 mM KCl, 1.1 mM KH_2PO_4, 0.6 mM $MgSO_4$, pepstatin (0.7 µg/mL), leupeptin (0.5 µg/mL), aprotinin (0.5 µg/mL) and phenylmethylsulfonyl fluoride (40 µg/mL). Next, 500 µL aliquots of homogenate were added to glass test tubes, followed by appropriate volumes of standardized internal standard solution (in methanol). Heptanal was chosen as the internal standard for the

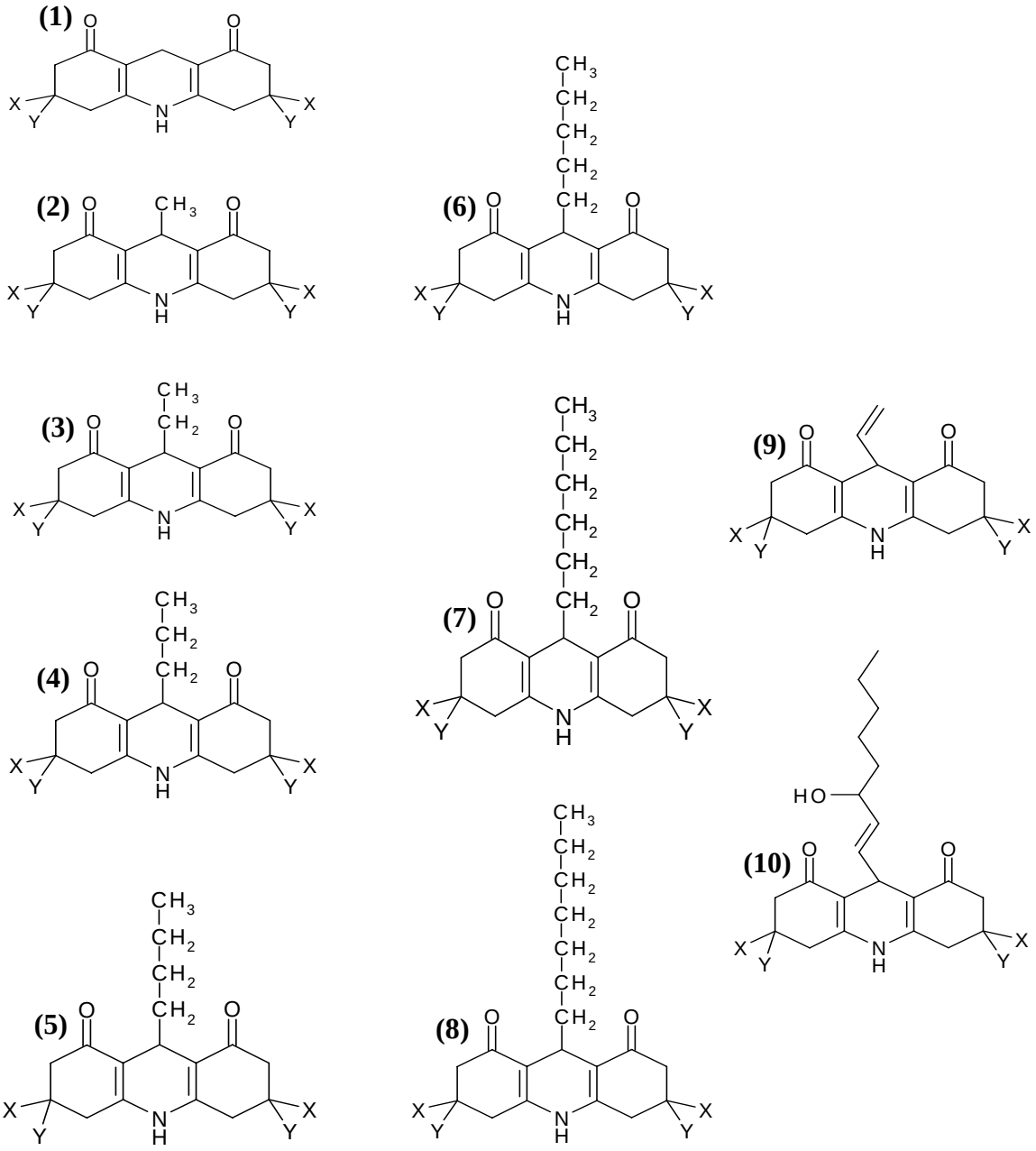

Figure 1.2.2. Biogenic aldehyde derivatives investigated. Aldehydes derivatized included (1) methanal, (2) ethanal, (3) propanal, (4) butanal, (5) pentanal, (6) hexanal, (7) heptanal (internal standard for aliphatic aldehydes), (8) octanal (internal standard for unsaturated aldehydes), (9) acrolein and (10) HNE.

aliphatic and octanal for the unsaturated aldehydes. Octanal internal standard was added at a 10-fold lower concentration compared to heptanal so that solvent concentration of the final derivatized brain sample by 10 enabled accurate quantification of low abundance unsaturated aldehydes. A review of the literature on aldehyde quantification in the brain indicates that this is adequate for acrolein and HNE analysis (49, 50, 62). Samples were vortexed for 30 sec for aldehyde extraction and centrifuged (850 x g for 10 min). A 500 µL aliquot of supernatant was then mixed with 1 mL of dimethyl CHD derivatizing reagent and heated in a 60^{o}C water bath for one hour. After cooling to room temperature, the reaction mixture was added to preconditioned C_{18} SPE columns, which were then washed with water to remove excess ammonium acetate. Derivatized aldehydes were eluted with methanol (62).

Construction of a C_{18} HPLC Column

Fused silica tubing (Polymicro Technologies) with an internal diameter of 320 µm and an outer diameter of 440 µm was used to create the HPLC column. All other column constructing supplies came from Upchurch Scientific. Column length (containing packing material) was 15 cm. The base of the column was prepared from an assembly of a zero dead volume (ZDV) union, 2 µm stainless steel frit, poly ether ether ketone (PEEK) sleeve, ferrule and nut. The column was packed with Macrosphere C_{18} material with a 300 Å pore size and 5 µm particle diameter (Alltech Associates, Inc.). A 10 mg/ml solution of this packing material was prepared in a solvent solution of 90% ACN and 10% water. Prior to column packing, the solution slurry was sonicated and thoroughly stirred to assure homogeneity. The column was packed in-house under helium gas pressure (1000 psi) using a specially designed stainless steel reservoir, also known as a column bomb (Figure 1.2.3).

Instrumentation

A Hewlett Packard LC system (1100 series) with a home-made C_{18} reversed phase capillary LC column was employed in the separation of aldehyde derivatives for quantitative analysis. A mobile phase mixture of water and ACN, each containing 0.1%

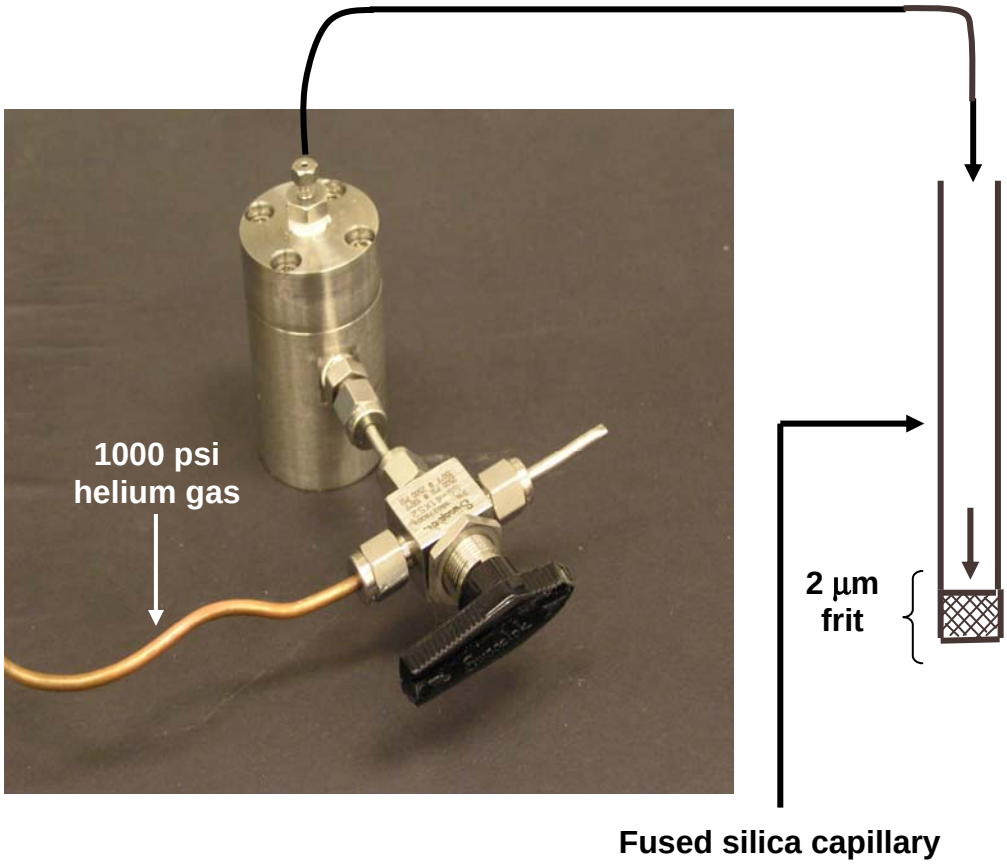

Figure 1.2.3. LC column packing scheme. A 15 cm length reversed-phase column was packed with 5 µm (300 Å) macrosphere C_{18} particles.

formic acid, was used in all experiments. The acid assisted in enhancing chromatographic peak shape and provided a source of protons in reversed-phase LC/MS. The binary pump of the HPLC offered gradient generation by high-pressure mixing. Programmed gradient elution was utilized in these experiments to enhance the separation of analytes. Each experiment, lasting one hour, was begun with a large excess of the weak eluting solvent water in the mobile phase, followed by steady additions of increasing proportions of the strong eluting solvent acetonitrile (ACN) during the course of the separation. For the first 2 minutes of a given run, the mobile phase composition was kept at 5% ACN. In the next 8 minutes, the proportion of ACN was linearly increased to 20%. Another linear increase in percent ACN occurred for 20 more minutes to reach a concentration of 70%. In the following 20 minutes, the percent ACN was linearly changed to 90%. During the last 5 minutes of the run, ACN content rose, once again linearly, to a maximum concentration of 95%. The column was restored to starting mobile phase conditions prior to beginning the next run (Figure 1.2.4).

LC solvent flow rate was maintained at 4 μL/min throughout the course of each chromatographic experiment using a laboratory constructed 50 to 1 splitter between the pump and injector. Manual injections were performed with a six-port Rheodyne injection valve (model # 7725i) equipped with a 5 μL sample loop.

A Finnigan LCQ Classic quadrupole ion trap mass spectrometer was interfaced to the LC system for reversed phase LC-MS/MS analyses (Figure 1.2.5). Samples with derivatized aldehydes were introduced into the LCQ following LC separation or by direct infusion in which case no chromatographic separation was achieved. The electrospray source was operated in positive ion mode. Desolvated ions migrated from the source into the ion trap, guided by several electrostatic focusing elements, including octopole lenses. Ions in the ion trap were subjected to mass analysis, sequentially ejected and detected by an electron multiplier.

Tuning LCQ Parameters

Dimethyl CHD heptanal was infused into the LCQ mass spectrometer and instrument parameters, such as lens offsets, capillary voltages, etc., were tuned for this

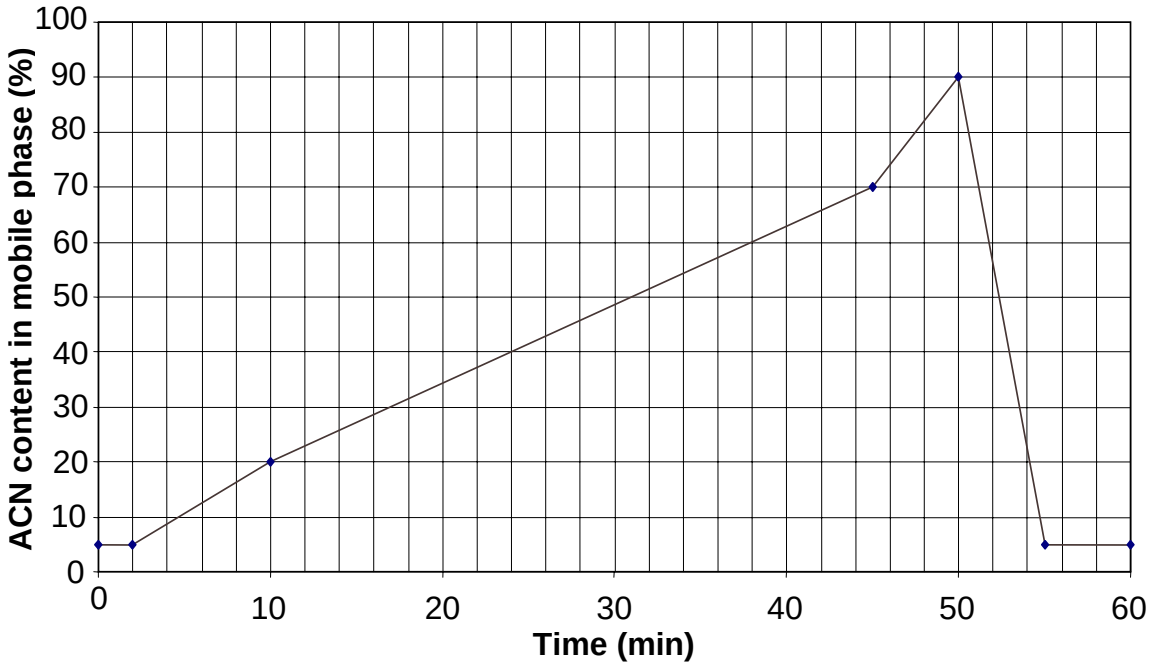

Figure 1.2.4. HPLC method.

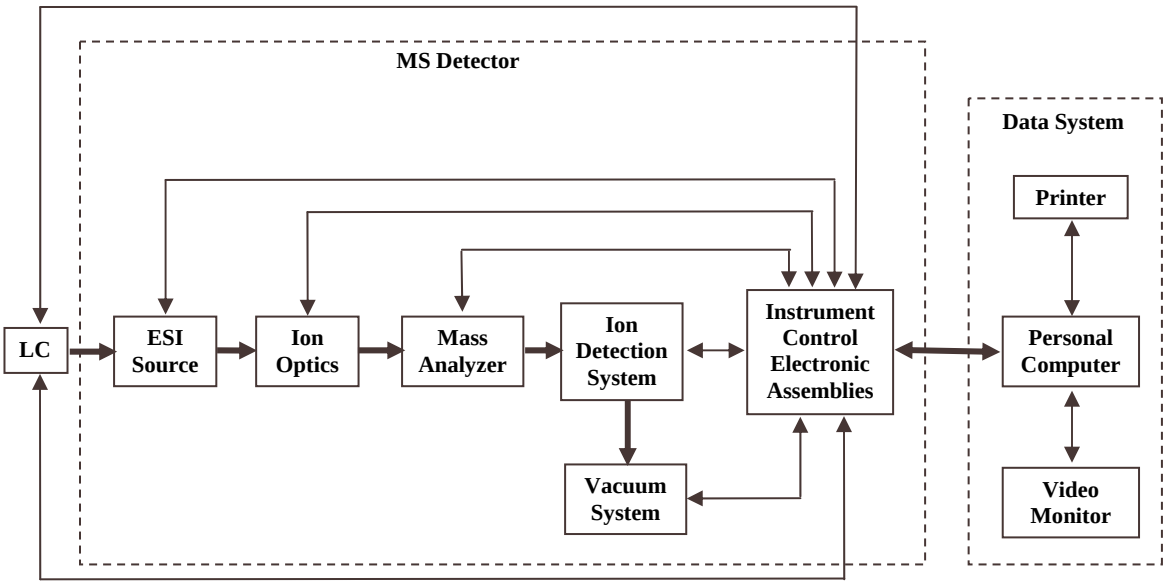

Figure 1.2.5. Functional block diagram of the Finnigan LCQ system. Broad, single headed arrows represent flow of sample molecules through the instrument. Narrow, double headed arrows represent electrical connections.

compound to improve the quality of LC-MS/MS data obtained for aldehyde derivatives. Electrospray source parameters were tuned to the following values: 4 kV applied voltage, 20 arbitrary units of sheath gas flow, 45 V inlet capillary voltage and 175^{o}C inlet capillary temperature. Other mass spectrometric parameters were as follows: 37 V tube lens offset, -5 V multipole 1 offset, -9 V multipole 2 offset, 430 V_{p-p} multipole *rf* amplitude, -15 V lens voltage and -10 V trap *dc* offset. Similar values were assumed for the other derivatives.

Results and Discussion

Initial experiments were performed to determine retention times for the aldehyde derivatives. In data-dependent scanning, the instrument acquires a full scan mass spectrum, evaluates the relative intensities of ions in a given mass range, then isolates the ion with the highest intensity for fragmentation and analysis (MS/MS mode). Masses utilized as precursors for MS/MS experiments are placed on an exclusion list and are not sampled again for a pre-selected time window. CHD, methyl CHD and dimethyl CHD derivatives of standard aldehyde solutions and several brain tissue samples with derivatized aldehydes (SMTG), were analyzed in this manner. Apart from its simplicity and compatibility with LC-MS/MS analyses, the Hantzsch reaction offers a high efficiency (above 90%), which was well suited for these studies (100).

After determining the retention times for each derivatized aldehyde peak, method files for segmented analysis were constructed to perform MS/MS analysis on the aldehyde derivatives. In segmented analysis, acquisition time is divided into segments for exclusive MS/MS analysis of particular analytes. This offers a dramatically improved signal-to-noise ratio and the isolation of the desired species in this manner for exclusive MS/MS analysis is a means of ion purification. When a species is isolated for segmented analysis, several parameters must be considered and enhanced for spectral data improvement. It is also desired to obtain as much of the product ions as possible without completely obliterating the parent species. Therefore, upon establishing the time-windows for segmented analysis of the aldehyde derivatives through data-dependent

studies, other parameters such as percent normalized collision energy (percent NCE or percent CID) and CID time were explored to improve the data from such experiments. This, in conjunction with tuning the ion trap as described in the Experimental section, enabled improved LC/MS analysis of aldehyde derivatives.

As was discussed in Chapter 1.1, the resonance excitation process is used to induce fragmentation in an ion trap. Upon increasing the amplitude of the applied supplemental *rf* voltage, the precursor ion dissociates to fragments over a narrow energy range. The collision energy needed to achieve optimum fragmentation has a mass dependency, which is compensated by the LCQ as normalized collision energy. In other words, CID is the amplitude of the resonance excitation *rf* voltage scaled to the precursor mass as follows: *rf* amplitude = (%CID/30%)(precursor ion mass × tick amp slope + tick amp intercept). The tick amp slope and tick amp intercept are instrument-specific values. CID time is the time during which the resonant *rf* signal is applied to the end-cap electrodes for ion excitation. The *rf* voltage causes increased ion motion between the end-caps, leading to fragmentation by increased collisions with helium gas. Infusion studies measuring ion intensity as a function of percent CID and CID time were performed to determine suitable conditions for segmented analysis of aldehyde derivatives.

Aldehyde derivative solutions (nanograms per microliter) were infused into the LCQ at a rate of 3 µl/min. Percent CID and CID time were separately ramped in increments of 5% from 0 to 100% while acquiring data on precursor and product ion intensities. Each data point represents an average of approximately thirty mass spectral scans. A plot of precursor and product ion intensities as a function of percent CID and CID time revealed the values of these parameters at which *most* of the precursor was converted into products. For the ion intensity versus percent CID plot of dimethyl CHD heptanal (Figure 1.2.6), conversion of precursor to products at higher collision energies was about 80%. A similar situation was observed when varying ion intensity with CID time for this species (Figure 1.2.7). At 38% CID and 30 ms CID time, most (>95%) of the precursor ion current was converted into products, with a little precursor species remaining intact. Indeed, all the aliphatic aldehydes provided similar responses.

In the case of ion intensity versus percent CID for dimethyl CHD acrolein, approximately 50% of precursor ion current was converted to products (Figure 1.2.8)

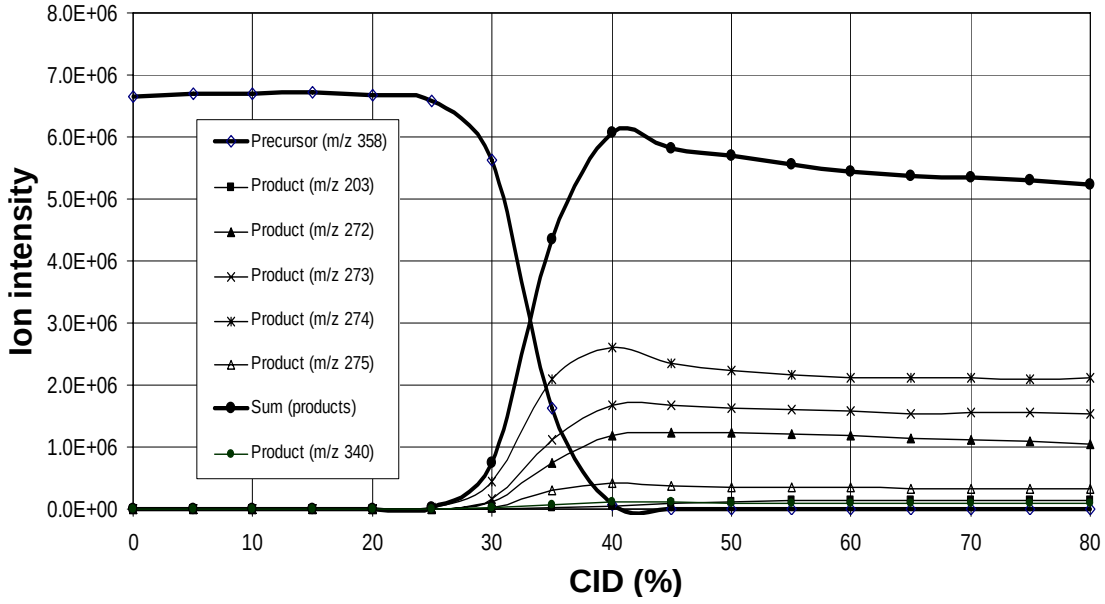

Figure 1.2.6. Ion intensity versus percent CID curve for dimethyl CHD heptanal. Data represents a single infusion experiment. Each data point is an average of thirty mass spectral scans.

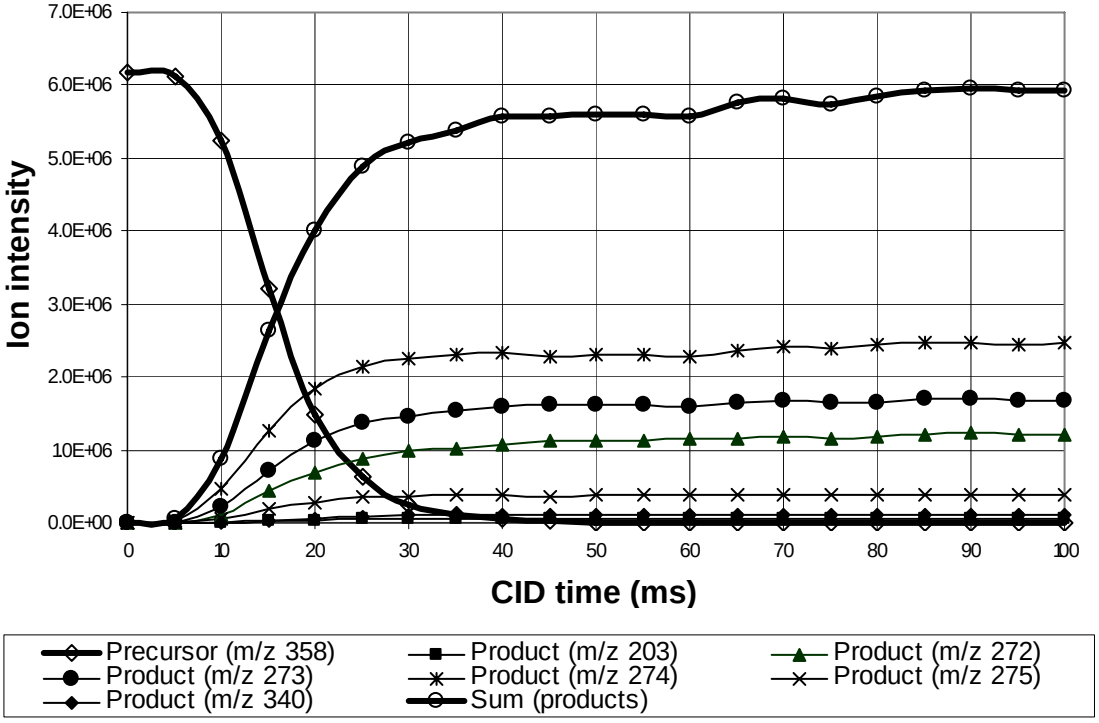

Figure 1.2.7. Ion intensity versus CID time (ms) for dimethyl CHD heptanal. Data represents a single infusion experiment. Each data point is an average of approximately thirty mass spectral scans.

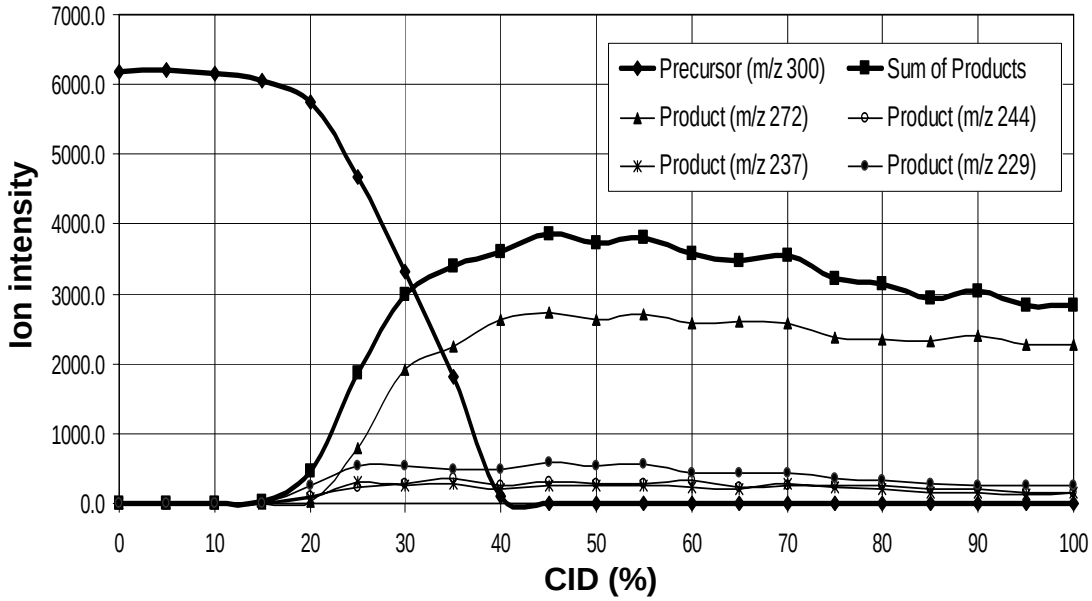

Figure 1.2.8. Ion intensity versus percent CID curve for dimethyl CHD acrolein. Data represents a single infusion experiment. Each data point is an average of approximately thirty mass spectral scans.

while in the case of the HNE derivative, only a third of the precursor ion current resulted in product formation (Figure 1.2.9). It is possible that some major products are below the low-mass cutoff of the ion trap and are therefore not detected.

All aldehyde derivatives required similar percent CID (~38%) and CID times (~30 msec) for LC/MS analysis. Using the optimized parameters for aldehyde derivatives in the mass spectrometric methods resulted in *>95%* reduction in precursor ion counts and subsequent conversion to products.

Data from Segmented Analysis

Segmented MS/MS analysis of aldehyde derivatives worked very well with LC gradient elution. The binary mobile phase system of water and acetonitrile generated well-resolved chromatograms for all the analytes. Gradient elution is particularly useful when the mixture of solutes to be analyzed has a wide range of capacity factors (ratio of analyte masses in the stationary phase and mobile phase). This was the case in the analytes described here, as the larger aldehyde derivatives were more hydrophobic and had greater retention times compared to their smaller counterparts. Starting mobile phase composition for every LC run was 5% ACN. It is important to start the gradient with some organic content in the mobile phase, especially for C_{18} columns, where the very long, very hydrophobic alkyl chains can mat down on the silica particle in an effort to get away from the high aqueous environment. When the alkyl chains mat down in this manner, they are unable to efficiently capture the target analyte, reducing the overall efficiency of the separation.

CHD, methyl CHD and dimethyl CHD aldehydes were studied using segmented analysis. The dimethyl CHD derivatized aldehydes offered the best data in terms of chromatographic peak quality. A possible explanation for this observation is that the greater hydrophobic nature of the dimethyl CHD derivatives promoted increased chromatographic focusing at the head of the column, thereby reducing peak width and improving the overall separation process. As such, this derivative was used exclusively for all further experiments.

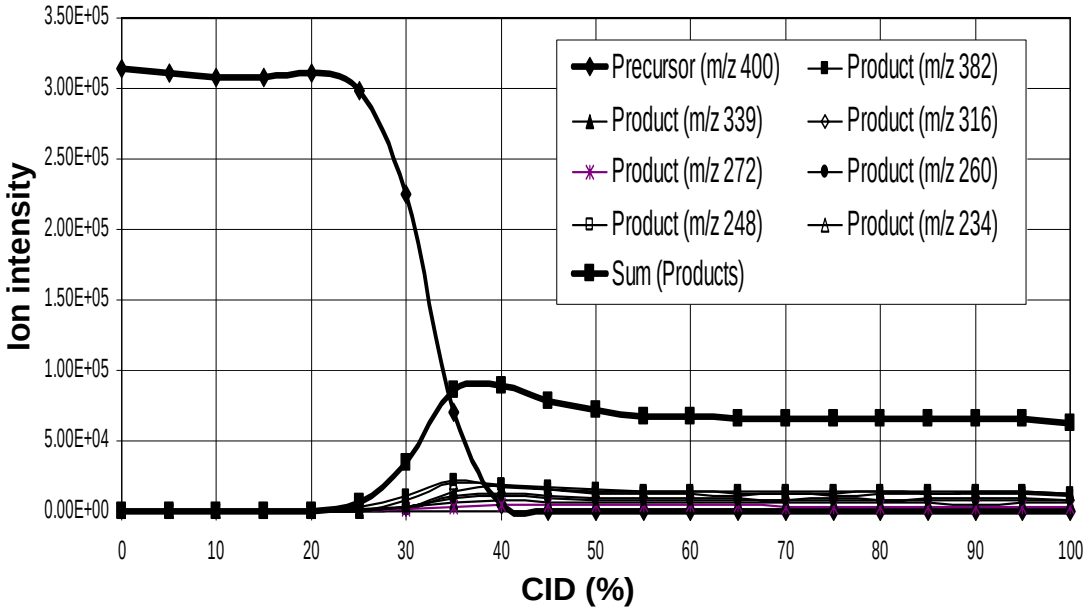

Figure 1.2.9. Ion intensity versus percent CID curve for dimethyl CHD HNE. Data represents a single infusion experiment. Each data point is an average of approximately thirty mass spectral scans.

Chromatographic Data

The aliphatic aldehyde derivatives displayed increasing retention times with increasing mass of aldehyde derivative (Figure 1.2.10) in good agreement with the rise in hydrophobicity associated with greater mass. Reconstructed ion chromatograms for dimethyl CHD methanal to dimethyl CHD heptanal formed a stair-step of peaks. For the unsaturated aldehydes, dimethyl CHD acrolein had a shorter retention time than dimethyl CHD HNE, as was expected due to the increased mass of the latter (Figure 1.2.11). Indeed, the acrolein and propanal derivatives showed similar retention times, in agreement with their similar masses. Keeping with this hydrophobicity trend, the internal standard for unsaturated aldehydes, dimethyl CHD octanal, had the longest retention time of all. The R group (Figure 1.2.2) of dimethyl CHD HNE has a hydrophilic –OH group at the γ position from the dimedone ring which reduces its hydrophobicity compared to aliphatic derivatives of similar size. So, this species has a shorter retention time than dimethyl CHD heptanal, which has a 6-carbon chain and no hydroxyl moiety.

Mass Spectrometric Data

The aliphatic aldehyde derivatives fragmented in a characteristic pattern to produce a base peak of either *m/z* 273 or 274, depending on the size of the R group derived from the precursor aldehyde. The MS/MS spectra of aliphatic aldehyde derivatives is shown in Figure 1.2.12. For smaller aldehyde derivatives (C_1-C_4), the appearance of *m/z* 273 was consistent with a simple C-C bond dissociation between the dimedone group and the R group, followed by neutral loss of a saturated R radical. For larger aldehyde derivatives (C_5-C_8), a hydrogen rearrangement followed by cleavage of the (R-H) group became more feasible. For these derivatives, the C-H bond dissociation energies of 2^o carbon atoms in the R group were sufficiently low enough for a base peak of m/z 274 to be generated as a result of the loss of an unsaturated (R-H) species (137). For all the derivatives, the major bond cleavage was between the R group derived from the original aldehyde and the heterocyclic ring from the derivatizing agent, with the latter retaining the charge at the nitrogen atom. Dimethyl CHD acrolein fragmented to produce a base peak at m/z 272, which appeared to be the loss of ethylene from the precursor

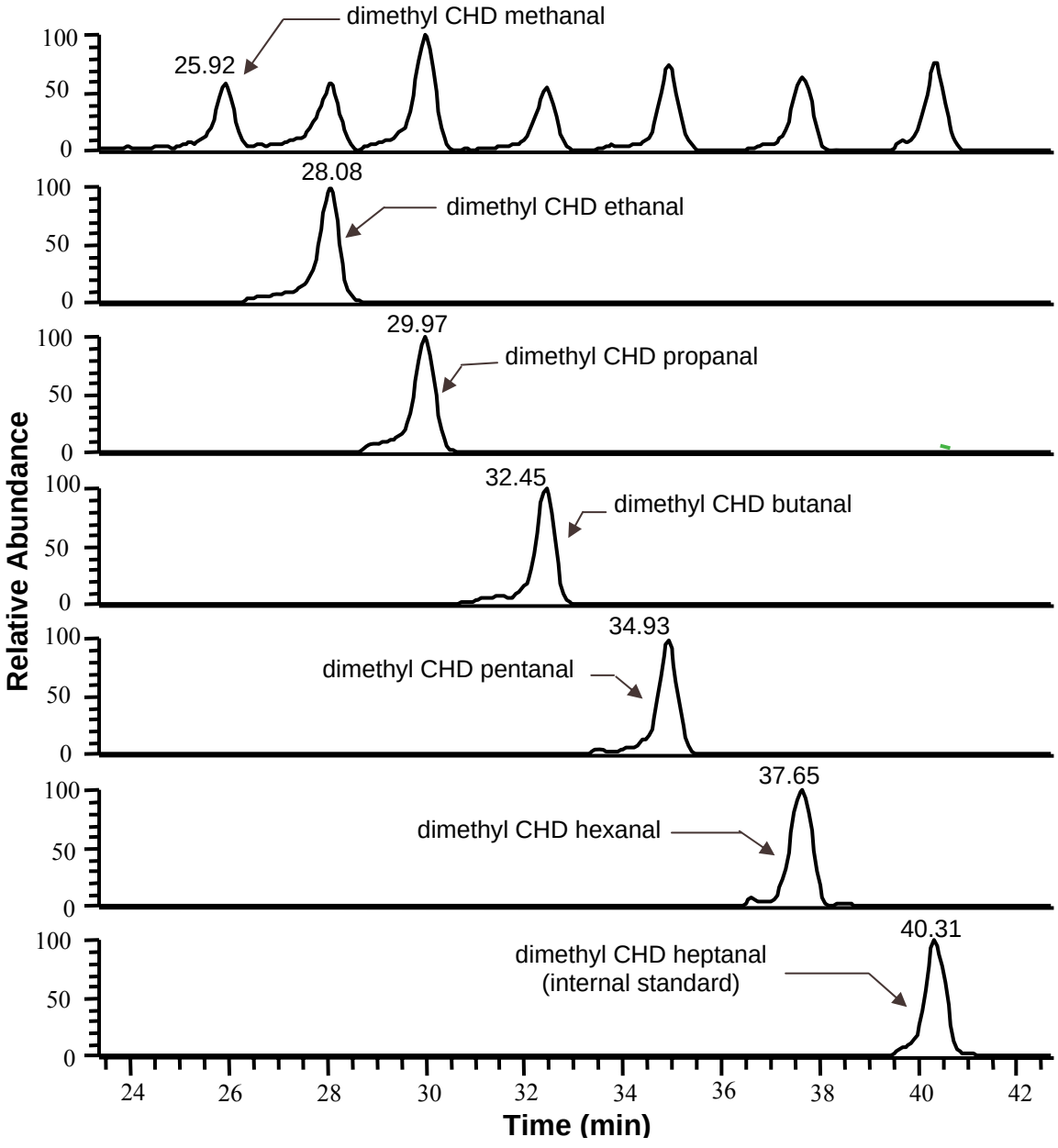

Figure 1.2.10. Segmented chromatograms of dimethyl CHD aliphatic aldehydes.

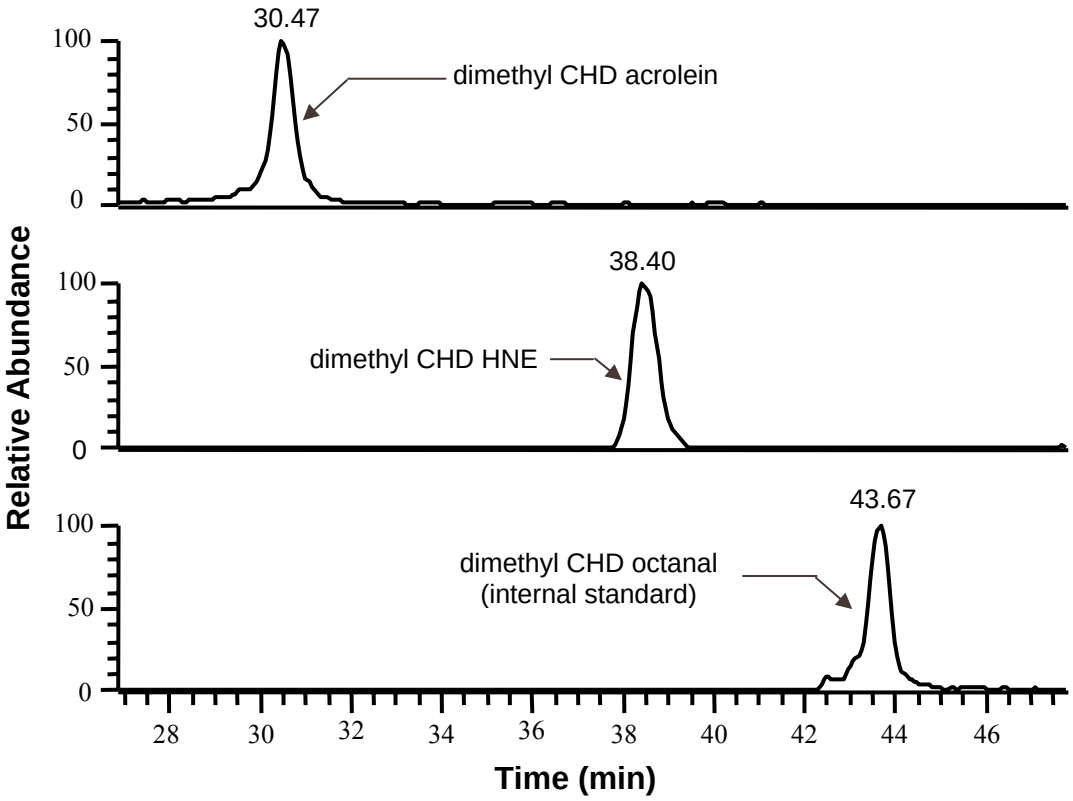

Figure 1.2.11. Segmented chromatograms of dimethyl CHD unsaturated aldehydes.

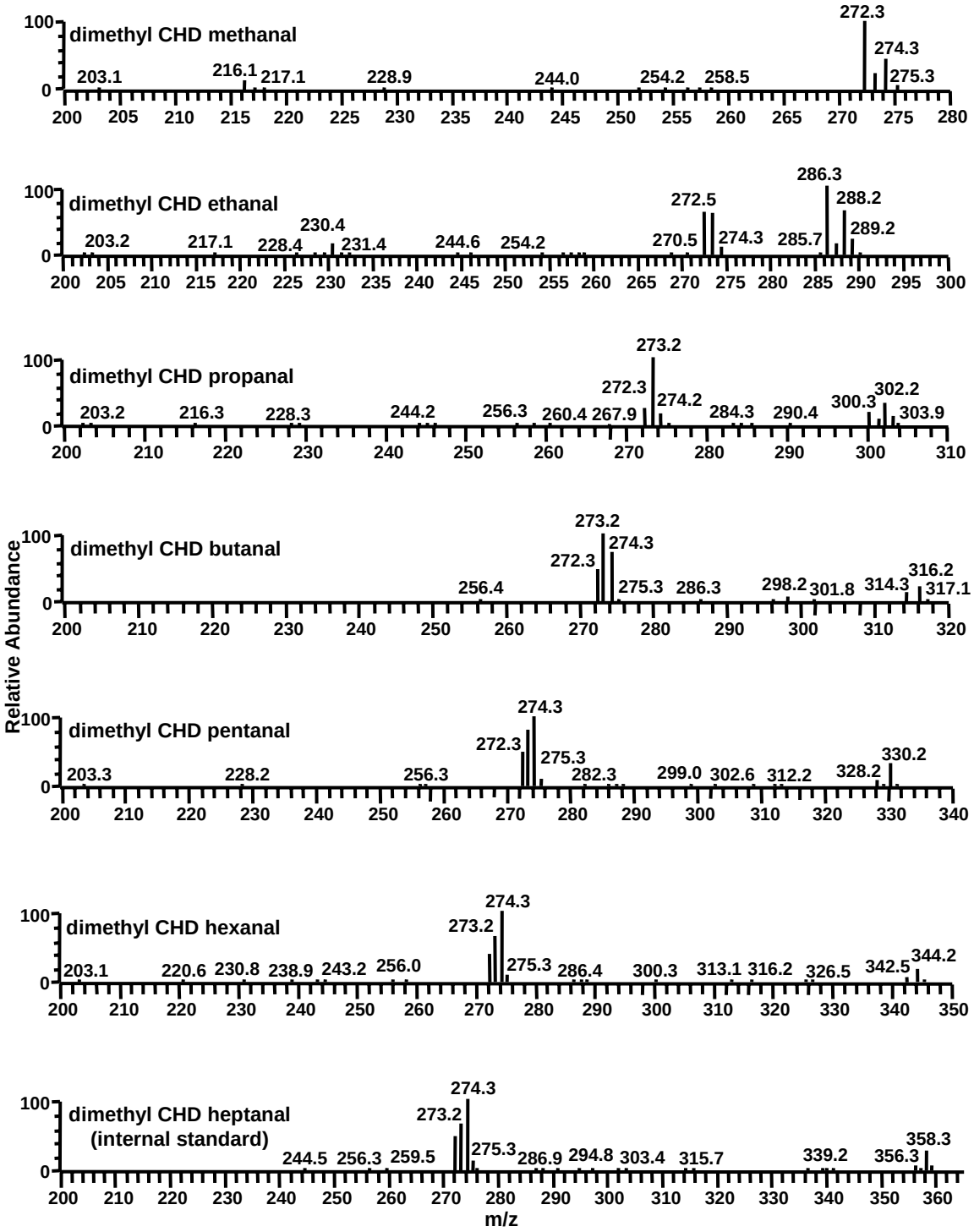

Figure 1.2.12. MS/MS spectra of dimethyl CHD aliphatic aldehydes.

species. In the case of dimethyl CHD HNE, the base peak was at m/z 339 but a significant peak was also observed at m/z 382 (Figure 1.2.13). It is probable that m/z 382 was produced from the loss of water with a subsequent loss of 43 amu (equivalent in mass to a propyl radical) resulting in the formation of the m/z 339 species. Mass spectrometric data for all aldehyde derivatives is summarized in Table 1.2.1. Mechanistic studies would be required to confirm fragmentation pathways.

Construction of Calibration Plots

Prior to proceeding with quantitative analysis, standard dimethyl CHD heptanal solutions of increasing concentrations were analyzed by segmented LC-MS/MS to determine the linearity of a plot of area counts versus concentration. Each solution was analyzed in triplicate to obtain standard deviation data. Figure 1.2.14 demonstrates that the plot was linear and so the heptanal derivative was a good choice for an internal standard in these experiments. Additionally, neither heptanal nor octanal are present in brain tissues to any significant concentrations, minimizing concerns regarding contributions of these aldehydes to internal standard peak areas (62). Due to similarity in structure, the octanal derivative produced a similar response.

For each of the standardized solutions of increasing concentration prepared for aliphatic and unsaturated aldehyde derivatives, segmented analysis was performed in triplicate. The area counts of aldehyde derivative 'X' was divided by the area counts of internal standard to obtain the relative response factor (RRF) of aldehyde derivative 'X' with respect to its internal standard. Calibration plots were constructed by plotting the RRF of each aldehyde derivative versus the number of picograms on column delivered in each LC-MS/MS experiment. A review of the literature indicated that the lowest concentration of biogenic aldehydes in human brain is on the order of 0.02 nmol/mg protein (49, 75). Such levels were well-represented in the calibration plots presented here. For acrolein, 0.02 nmol/mg protein delivered ~15 pg on column. The calibration plot for this aldehyde derivative had one data point below this value.

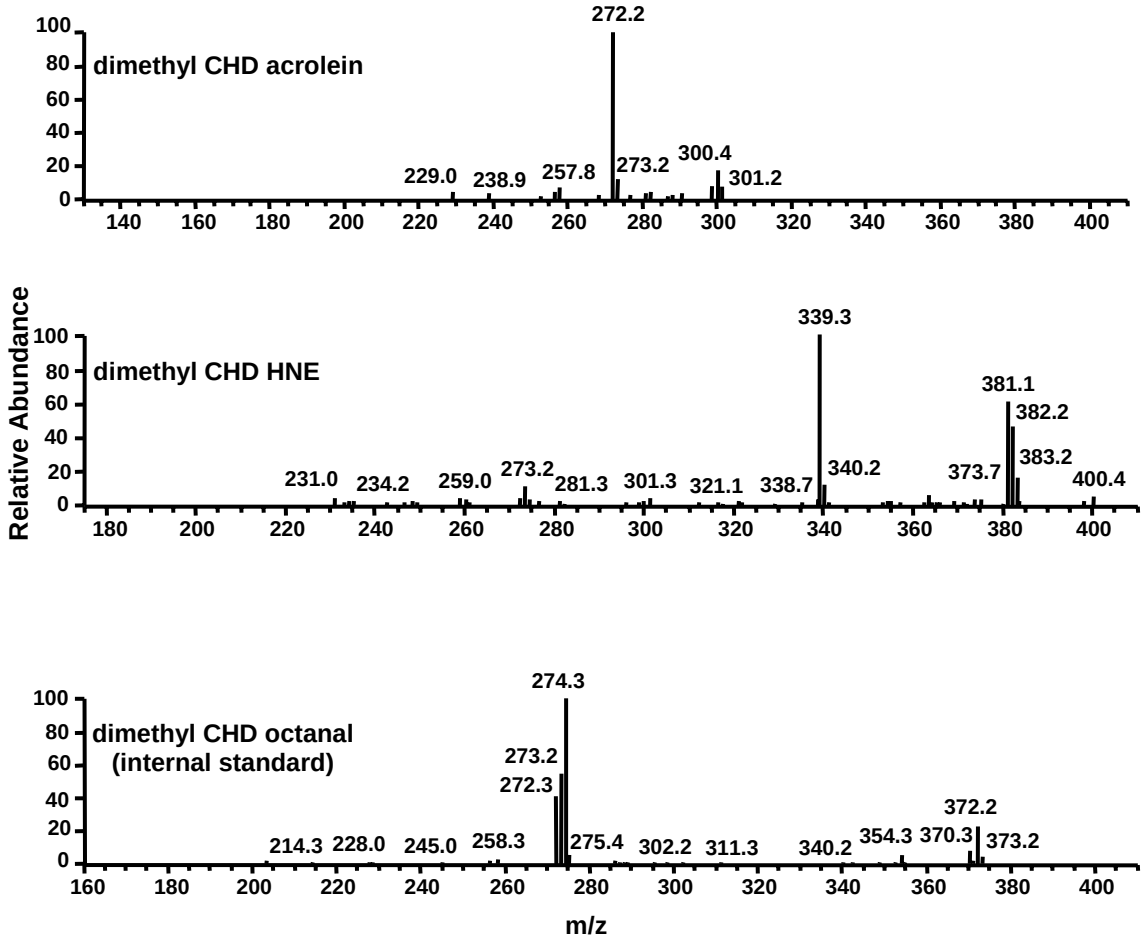

Figure 1.2.13. MS/MS spectra of dimethyl CHD unsaturated aldehydes.

Table 1.2.1. Mass spectrometric data of dimethyl CHD aldehyde derivatives.

Aldehyde	MW	Parent Molecular Ion of Derivative	Product Ion from Frag.	Neutral Loss from Fragmentation	
Methanal	30	$[M+H]^+ = 274$	m/z = 273	--	--
Ethanal	44	$[M+H]^+ = 288$	m/z = 273	CH_3	MW = 15
Propanal	58	$[M+H]^+ = 302$	m/z = 273	C_2H_5	MW = 29
Butanal	72	$[M+H]^+ = 316$	m/z = 273	C_3H_7	MW = 43
Pentanal	86	$[M+H]^+ = 330$	m/z = 274	C_4H_8	MW = 56
Hexanal	100	$[M+H]^+ = 344$	m/z = 274	C_5H_{10}	MW = 70
Heptanal	114	$[M+H]^+ = 358$	m/z = 274	C_6H_{12}	MW = 84
Octanal	128	$[M+H]^+ = 372$	m/z = 274	C_7H_{14}	MW = 98
Acrolein	56	$[M+H]^+ = 300$	m/z = 272	C_2H_4	MW = 28
HNE	156	$[M+H]^+ = 400$	m/z = 382, 339	H_2O, C_3H_7	MW = 18, 43

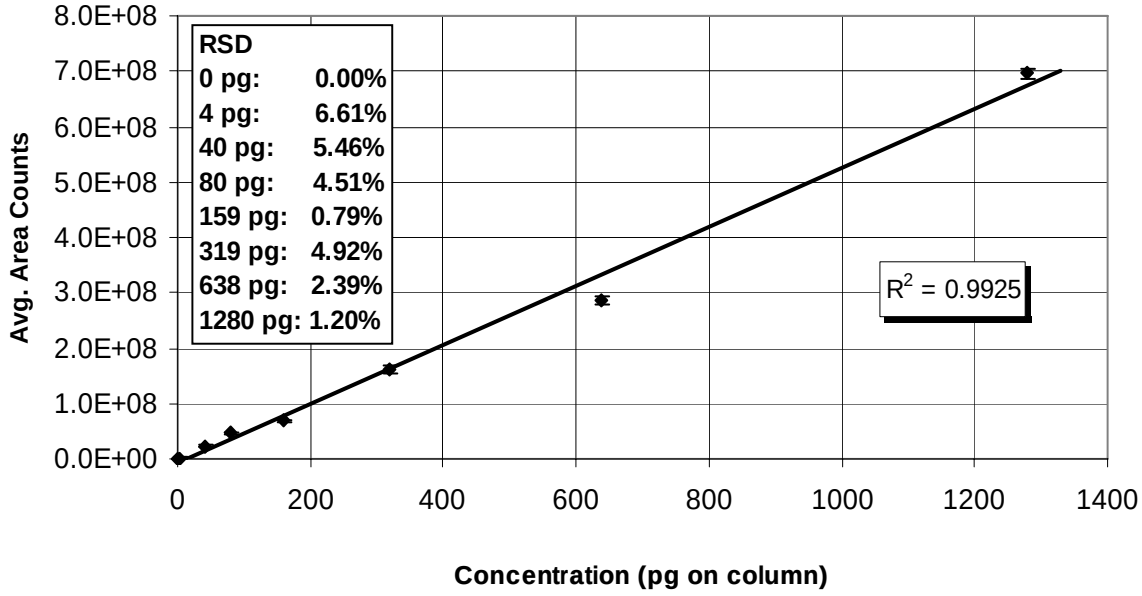

Figure 1.2.14. Average area counts versus concentration plot for dimethyl CHD heptanal.

The aliphatic aldehyde derivatives produced linear calibration plots with r^2 values ≥ 0.99 and relative standard deviations (RSD) of approximately ≤ 5% (Figures 1.2.15 to 1.2.20). The RRF values for these derivatives were comparable, with a slight trend towards lower RRFs with increasing aldehyde derivative mass, in agreement with their similarities in structure. The ethanal derivative showed a somewhat higher response factor compared to the others. The greatest RRFs would probably have been expected of the methanal derivative, which has the smallest mass. It should be noted, however, that methanal, which is a 37% stock solution, can exist in the form of other species, such as paraformaldehyde, which may not derivatize efficiently through the Hantzsch reaction or perhaps form different derivatives. This was evidenced by the observation of several 'extraneous' peaks at earlier retention times in the reconstructed ion chromatogram for dimethyl CHD methanal. As such, it may be that a somewhat lower proportion of the methanal (compared to the calculated value) is actually partaking in the derivatization process to form the *desired* heterocyclic derivative. In other words, if the stock methanal solution was indeed 37% 'pure methanal', then this derivative would probably have produced the highest RRF values compared to the other aliphatic aldehyde derivatives.

Calibration plots for unsaturated aldehyde derivatives were linear and with r^2 and RSD values comparable to their aliphatic counterparts (Figures 1.2.21 and 1.2.22). The HNE derivative had a much lower RRF than the acrolein derivative, in agreement with data from infusion studies (Figures 1.2.8 and 1.2.9). It should be noted that the area counts versus percent CID infusion experiment for dimethyl CHD HNE generated product ion curves at much lower intensity values (about a third of the initial ion intensity of the precursor species at low percent CID) compared to the acrolein derivative. Data from calibration plots for all the aldehyde derivatives are given in Table 1.2.2.

These calibration plots can be employed in the analysis of real tissue that has been subjected to oxidative stress for aldehyde content determination. As an example of how this methodology may be applied towards this purpose, brain samples (SMTG) from an AD subject and a suitable age-matched control (blind experiment) were analyzed in triplicate as described above. Data from these findings are summarized in Table 1.2.3.

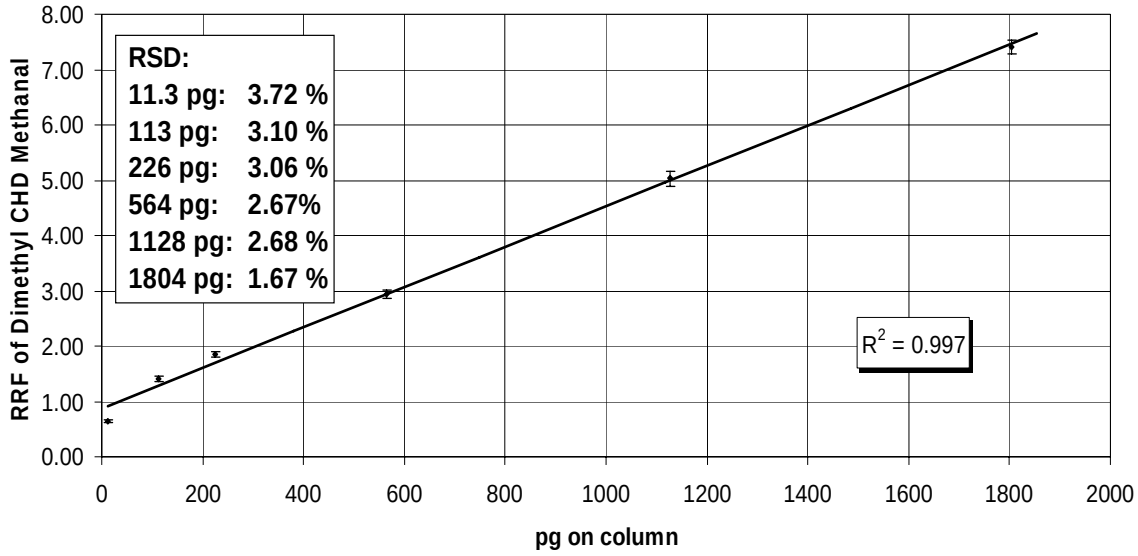

Figure 1.2.15. Calibration plot for dimethyl CHD methanal.

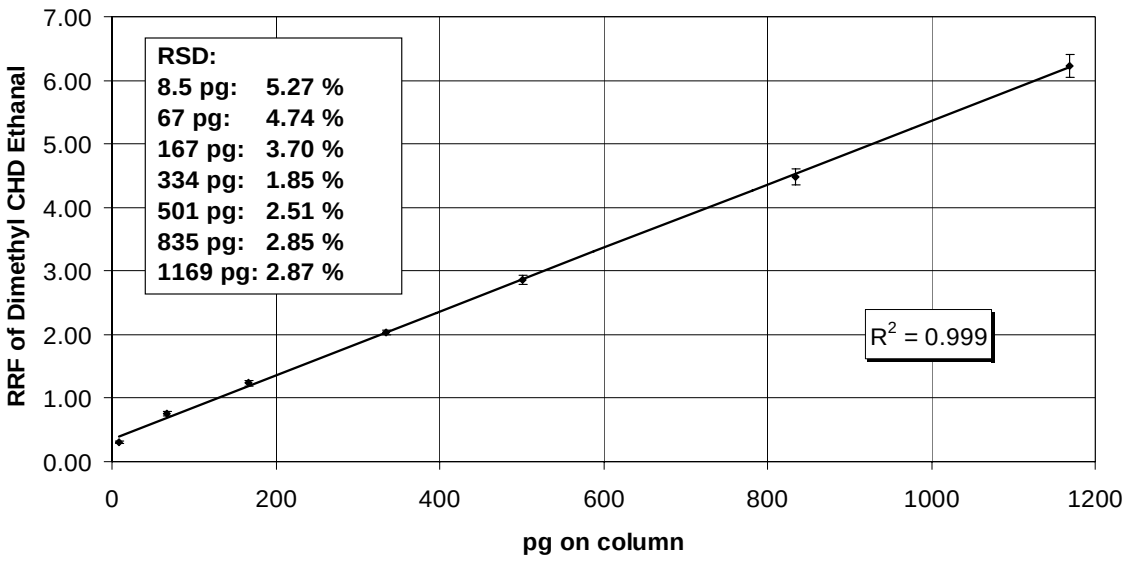

Figure 1.2.16. Calibration plot for dimethyl CHD ethanal.

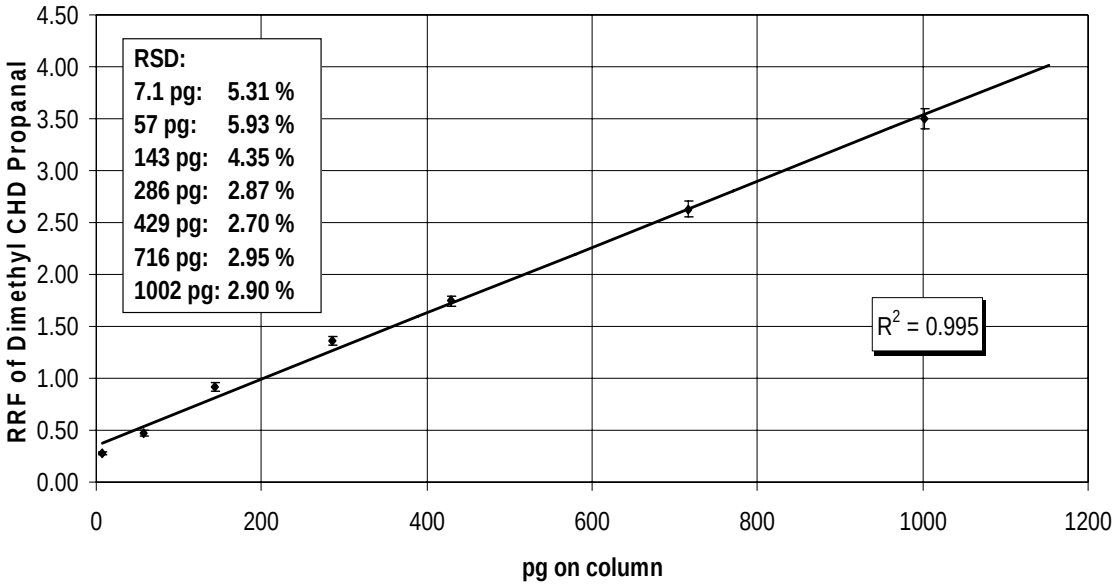

Figure 1.2.17. Calibration plot for dimethyl CHD propanal.

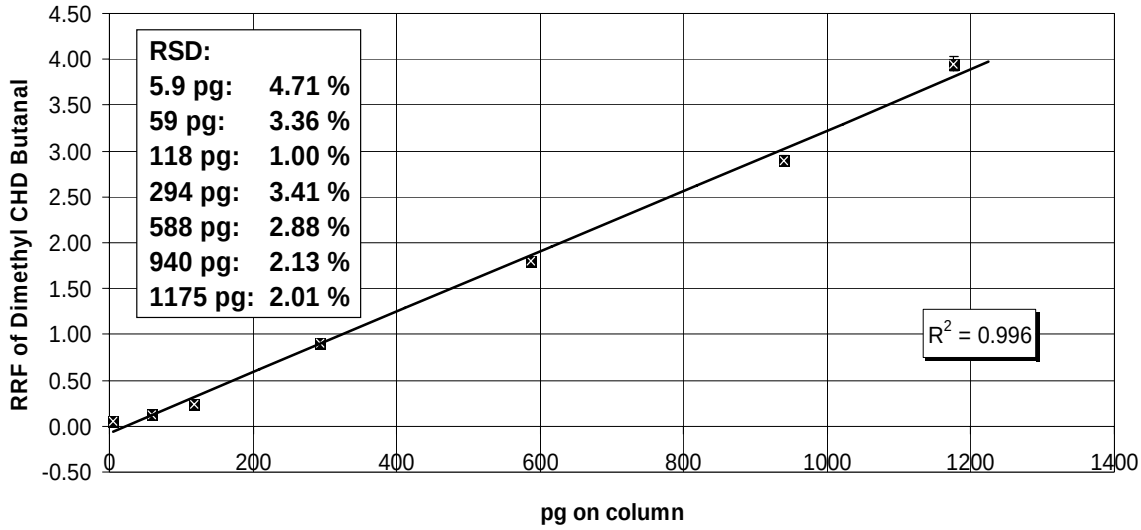

Figure 1.2.18. Calibration plot for dimethyl CHD butanal.

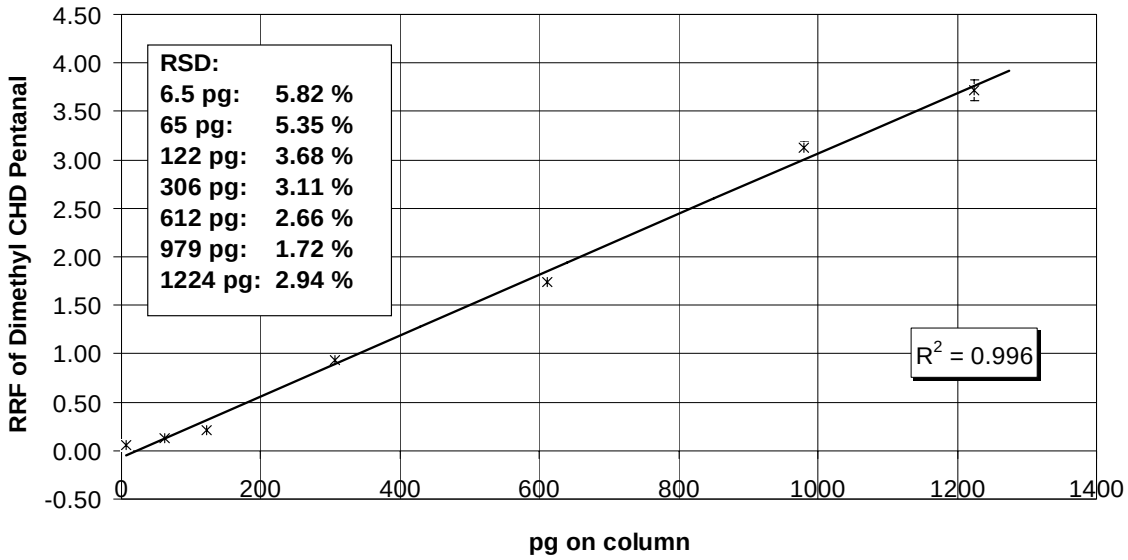

Figure 1.2.19. Calibration plot for dimethyl CHD pentanal.

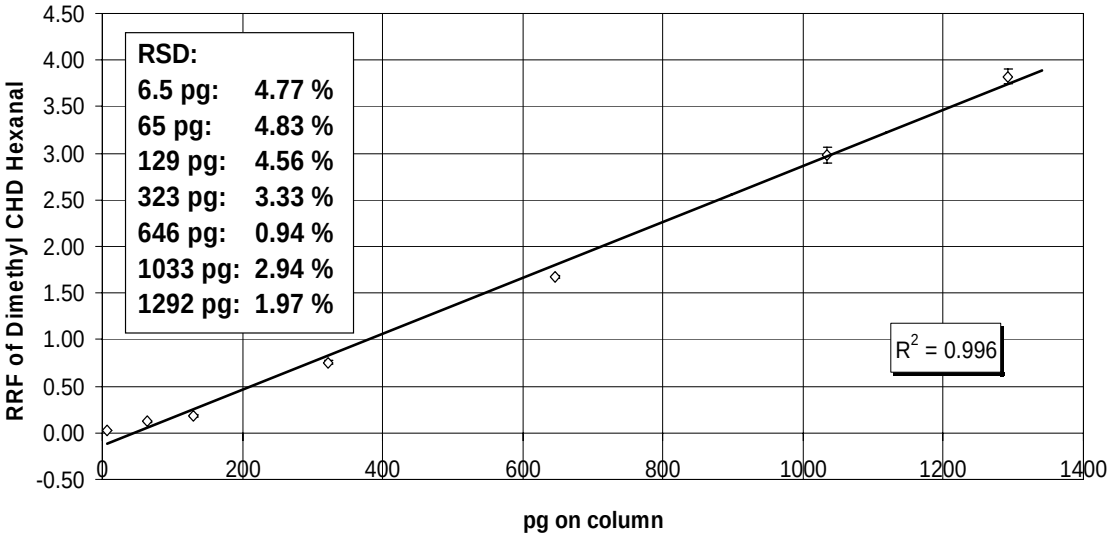

Figure 1.2.20. Calibration plot for dimethyl CHD hexanal.

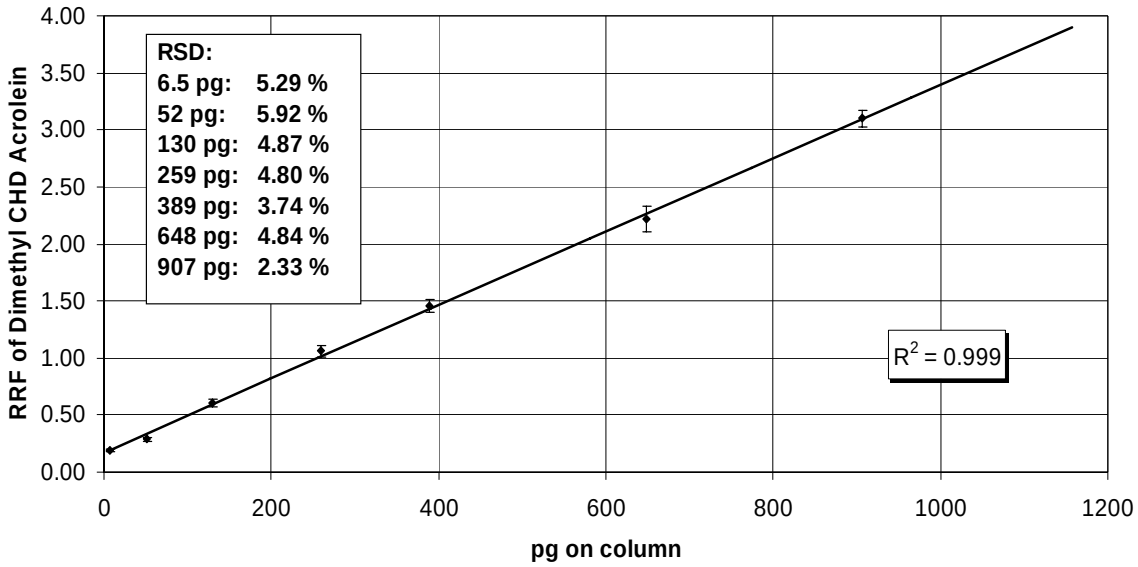

Figure 1.2.21. Calibration plot for dimethyl CHD acrolein.

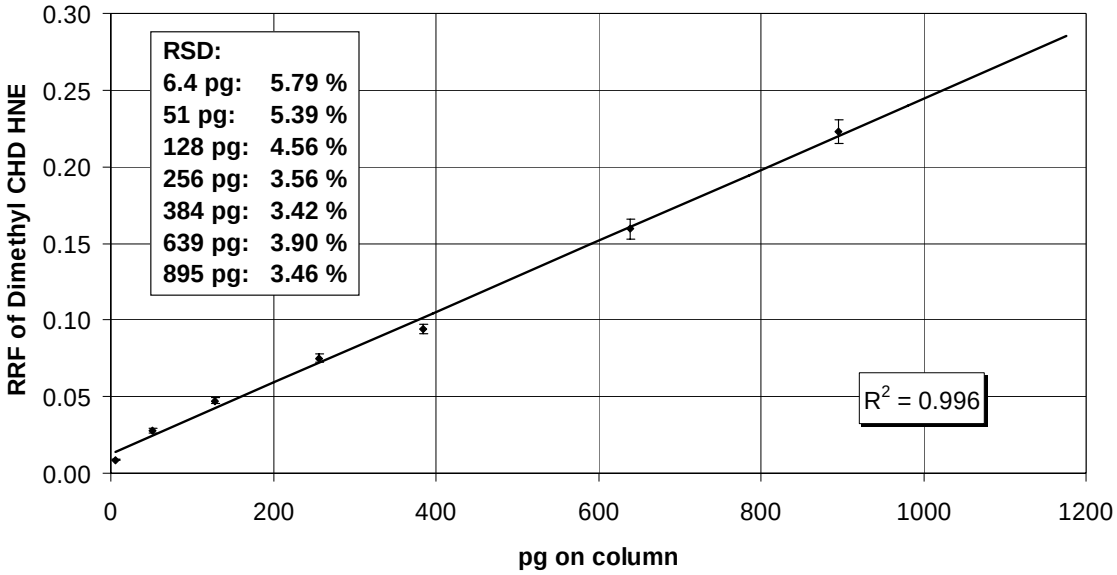

Figure 1.2.22. Calibration plot for dimethyl CHD HNE.

Table 1.2.2. Calibration plot data for dimethyl CHD aldehydes.

Aldehyde	r^2	pg on col. ald. deriv.	RRF*	RSD**	Aldehyde	r^2	pg on col. ald. deriv.	RRF*	RSD**
		11.3	0.65	3.72 %			6.5	0.19	5.29 %
		113	1.40	3.10 %			52	0.29	5.92 %
		226	1.85	3.06 %			130	0.61	4.87 %
methanal	0.997	564	2.94	2.67 %	acrolein	0.999	259	1.06	4.80 %
		1128	5.03	2.68 %			389	1.46	3.74 %
		1804	7.41	1.67 %			648	2.22	4.84 %
							907	3.10	2.33 %
		8.5	0.31	5.27 %			6.4	0.01	5.79 %
		67	0.76	4.74 %			51	0.03	5.39 %
		167	1.24	3.70 %			128	0.05	4.56 %
ethanal	0.999	334	2.03	1.85 %	HNE	0.996	256	0.08	3.56 %
		501	2.87	2.51 %			384	0.09	3.42 %
		835	4.48	2.85 %			639	0.16	3.90 %
		1169	6.23	2.87 %			895	0.22	3.46 %
		7.1	0.28	5.31 %					
		57	0.47	5.93 %					
		143	0.92	4.35 %					
propanal	0.995	286	1.36	2.87 %					
		429	1.74	2.70 %					
		716	2.63	2.95 %					
		1002	3.50	2.90 %					
		5.9	0.05	4.71 %					
		59	0.12	3.36 %					
		118	0.25	1.00 %					
butanal	0.996	294	0.91	3.41 %					
		588	1.80	2.88 %					
		940	2.89	2.13 %					
		1175	3.95	2.01 %					
		6.1	0.06	5.82 %					
		61	0.13	5.35 %					
		122	0.21	3.68 %					
pentanal	0.996	306	0.94	3.11 %					
		612	1.73	2.66 %					
		979	3.13	1.72 %					
		1224	3.72	2.94 %					
		6.5	0.02	4.77 %					
		65	0.12	4.83 %					
		129	0.18	4.56 %					
hexanal	0.996	323	0.76	3.33 %					
		646	1.67	0.94 %					
		1033	2.98	2.94 %					
		1292	3.82	1.97 %					

*Relative Response Factor **Relative Standard Deviation

Table 1.2.3. Comparison of aldehyde concentrations in the brains (superior and middle temporal gyrus or SMTG) of AD versus control subjects.

Aldehyde	**Subject with AD (nmol/mg protein) Mean ± SEM**	**Age-Matched Control (nmol/mg protein) Mean ± SEM**
methanal	133 ± 20	290 ± 39
ethanal	173 ± 21	175 ± 27
propanal	84.9 ± 14.5	91.0 ± 14.7
butanal	6.29 ± 1.09	8.42 ± 0.93
pentanal	9.99 ± 1.56	11.4 ± 2.0
hexanal	56.9 ± 5.7	13.8 ± 1.7
acrolein	1.45 ± 0.21	0.475 ± 0.077
HNE	0.550 ± 0.106	0.209 ± 0.039

Aldehyde content per milligram of protein from the brain tissue was reported as the mean value ± SEM (standard error of the mean). The AD sample showed similar levels of most aliphatic aldehydes and higher levels of unsaturated aldehydes, compared to the control. It is worth pointing out that AD development has been related to increased production of unsaturated aldehydes, in agreement with these findings (49, 50, 62, 68). The results indicated that the protocol outlined here can be effectively applied in aldehyde quantification in real tissues. Investigations on a larger set of tissues from various regions of the brain and from individuals presenting different levels of AD histopathology will provide an understanding on patterns of aldehyde generation in AD versus control subjects.

Conclusions

These studies aimed to develop sensitive, selective and reliable methods to analyze aldehydes in tissues using LC-MS/MS. It was shown that aldehydes typically found in brain tissues plagued by oxidative stress can be derivatized through the Hantzsch reaction to form cyclohexanedione (dimedone) derivatives, which can easily be quantified by MS. CHD, methyl CHD and dimethyl CHD derivatives were explored and it was determined that the dimethyl CHD derivatives provided the best LC/MS data. These compounds offered better peak quality due to their increased hydrophobicity, which resulted in greater chromatographic focusing of the sample at the head of the column. Analyte derivatization coupled with LC-MS/MS provided increased selectivity over established fluorescence methods (62, 98-101) for the analysis of low abundance biogenic aldehydes. Unsaturated aldehydes occur in the brain at much lower concentrations than their aliphatic counterparts and LC-MS/MS proved to be an ideal method for analyzing these two classes of compounds using two internal standards differing in concentration by an order of magnitude.

The developed method was applied to the analysis of samples of human brain (SMTG) from an AD patient and an age-matched control subject. In comparison to the control sample, the tissue obtained from the AD subject displayed similar concentrations of most aliphatic aldehydes, however, substantially elevated levels of acrolein and HNE

were detected. These results confirm that the protocol described here can be reliably applied in the quantification of aldehydes in brain tissue. Concentration variations of aliphatic and unsaturated aldehydes have been investigated using the methodology outlined here by exploring a larger data set of AD and control subjects, as well as by investigating several different regions of the brain, based on the level of AD pathology. The findings from this study are detailed in Chapter 1.3.

Chapter 1.3

Application of LC-MS Techniques to the Quantification of Biogenic Aldehydes *in vivo* in Alzheimer's Disease Brain

Introduction

Several different types of neurodegenerative conditions, such as AD, Parkinson's disease and Huntington's disease, are associated in etiology by the significant prevalence of lipid peroxidation (LPO) products in the brain (50). The importance of biogenic aldehydes in LPO and therefore neurodegenerative disease etiology has been well established by mounting evidence of neuronal damage that they initiate. These compounds could potentially serve as important biomarkers for AD and as such, a detailed study of their occurrence and quantification would be worthwhile. Of the different aldehyde derivatization techniques available for quantitative analysis, the Hantzsch reaction is well-suited by virtue of its simplicity and efficiency. Quantification is achieved with a suitable internal standard, using a variety of detection methods, as detailed in Chapters 1.1 and 1.2. Several reports have described the quantitative analysis of saturated and unsaturated biogenic aldehydes using this derivatization technique.

Lovell *et al.* (62) analyzed aldehydic markers of lipid peroxidation in biological specimens by high-pressure liquid chromatography. Biogenic straight-chain aldehydes and HNE were first derivatized through the Hantzsch reaction so as to make them amenable to fluorescence detection. The authors showed aldehydic products to be well-separated and minimum detection limits achieved for HNE were approximately 0.1 pmol. Shot to shot reproducibility of standard HNE solutions was about 3-5%, with a signal to noise ratio of the order of 50. The authors postulated that their results reflected levels of both free and protein-bound aldehydes. A potential problem associated with this type of analysis is the co-elution of other compounds with the aldehydes under investigation. However, the authors maintained that since the derivatization is dependent on the reaction between the aldehydic group and the β-dicarbonyl compounds, it was unlikely that other compounds without aldehydic groups would be derivatized.

Markesbery *et al*. (50) employed HPLC separation coupled to fluorescence detection to quantify HNE levels in multiple regions of the AD brain and suitable age-matched controls. Biogenic aldehydes in brain samples were chemically modified into stable, fluorescent, dimedone derivatives through the Hantzsch reaction for facile detection and quantification. The authors detected statistically significantly elevated levels of this aldehyde in the amygdala in AD (0.486 ± 0.096 nmol/mg) compared to controls (0.193 ± 0.062 nmol/mg) ($p = 0.008$) and in the hippocampus and parahippocampal gyrus in AD (0.543 ± 0.123 nmol/mg) compared to controls (0.265 ± 0.056 nmol/mg) ($p = 0.02$). Such areas of the brain typically show the most dramatic histopathological alterations in AD. The highest mean levels of the aldehyde (AD: 1.490 ± 0.376 nmol/mg; control: 1.404 ± 0.363 nmol/mg) were detected in the middle frontal gyrus. The authors also quantified several aliphatic aldehydes but found no statistical difference between AD and control subjects. The study demonstrated that HNE may be an important substance in the pathogenesis of neuron degeneration in AD.

In another report by Markesbery and co-workers (51), elevated HNE levels were detected and analyzed in the ventricular fluid of AD patients. Using HPLC separation coupled with fluorescence detection of dimedone derivatives of this aldehyde, free and protein-bound HNE levels were quantified in AD and control subjects. Free HNE levels were found to be significantly elevated in the ventricular fluid of individuals with AD (33.10 ± 8.9 nmol/mg protein), compared to control subjects 13.5 ± 3.8 nmol/mg protein) ($p = 0.0096$). The authors also employed dot-blot immunoassay to determine protein-bound HNE and reported that there were no significant differences between AD and age-matched controls. The levels of HNE in ventricular fluid observed in this study can potentially affect a host of molecular systems essential for neuron viability. The authors concluded that their results indicated increased lipid peroxidation in the AD brain and suggested a role for HNE in neurodegenerative mechanisms.

Mark *et al*. (75) explored the influence of HNE in oxidative stress, the disruption of ion homeostasis and neuronal death brought about by the amyloid β-peptide ($A\beta_{25-35}$). To determine whether Aβ induced production of HNE in hippocampal neurons, they exposed primary hippocampal cell cultures (18-day rat embryos) to 50 μM Aβ for 2 h and quantified the levels of free HNE in the cells by HPLC analysis with fluorescence

detection of dimedone derivatives. A 5- to10- fold increase in HNE concentration was observed as a result of the Aβ exposure, compared to control samples. The concentration of HNE in these cells was measured at ~4 μM. Western blot analysis of Aβ-exposed cultured neurons treated with physiologically dangerous HNE concentrations revealed increased HNE immunoreactivity in proteins, compared to controls. Since HNE had previously been established to be neurotoxic at physiologically relevant concentrations of 1-100 μM, the authors concluded that this aldehyde mediated Aβ-induced oxidative damage and eventual neuronal apoptosis.

Compared to HNE, there have been considerably fewer reports on the quantification and analysis of acrolein in association with neurodegenerative diseases. In a noteworthy study by Lovell *et al*. (49), this aldehyde was quantified in AD brain tissue and its effect on primary hippocampal cultures was investigated. As with other studies described earlier, aldehyde quantification was achieved by HPLC with fluorescence detection of dimedone derivatives. Increased mean concentrations of extracted acrolein were detected in all three brain regions studied, in comparison to age-matched controls. Statistical analysis of the data clearly demonstrated that acrolein was considerably elevated ($p < 0.05$) in the AD amygdala (2.5 ± 0.9 nmol/mg protein) compared to controls (0.3 ± 0.05 nmol/mg protein), and in the AD hippocampus and parahippocampal gyrus (5.0 ± 1.6 nmol/mg protein), compared to controls (0.7 ± 0.1 nmol/mg protein). Both these brain regions are characterized by marked pathological alterations in AD. Acrolein was also seen to be elevated in the AD inferior parietal lobule, although the disparity was not considered statistically significant. By exposing primary rat hippocampal neurons to increasing concentrations of acrolein, the authors demonstrated that this aldehyde is toxic to the cells in a time-and concentration-dependent manner. Indeed, neuronal death was shown to be brought about much more aggressively by acrolein exposure, compared to HNE exposure.

A thorough, quantitative study of biogenic aldehydes in different regions of the brain at different stages of AD would provide insight into patterns of aldehyde generation in the course of AD etiology. While there have been studies of HNE and acrolein in late-stage AD, there have been few studies of oxidative stress in the brain in subjects with mild cognitive impairment (MCI) or early AD (EAD). Mild cognitive impairment is

generally characterized by mild memory disturbances and is considered to be a transition between normal aging and AD (138-140). To determine if increased lipid peroxidation and generation of HNE and acrolein are associated with MCI and EAD, we measured levels of these neurotoxic aldehydic by-products in the hippocampus/parahippocampal gyrus (HPG), superior and middle temporal gyrus (SMTG) and cerebellum of MCI, EAD and age-matched control subjects. The methodology used in these investigations, described in Chapter 1.2, exploited the Hantzsch reaction to synthesize derivatized aldehyde mixtures for constructing appropriate calibration curves to quantify each aldehyde of interest (111). Since both aliphatic and unsaturated aldehydes are generated during lipid peroxidation, we described the analysis of both types of compounds with this approach. Interpretation of quantitative data from the different brain regions is provided and an explanation of their statistical significance is given. This is the first study to report an in-depth comparison of aldehyde levels between these three types of individuals. For the development of diagnostic tests and medication for AD, a thorough appreciation of the pathological and biochemical differences between MCI, EAD and normal subjects is becoming critical. In agreement with previous findings, we detected no statistical significance in the distribution of aliphatic aldehydes in the different brain regions and stages of AD under investigation. However, in agreement with earlier studies, the results presented here clearly show that HNE and acrolein are statistically significantly elevated in both MCI and EAD brain and suggest that oxidative damage occurs early in the pathogenesis of AD.

Experimental

Tissue Specimens

Specimens of HPG, SMTG and CER were obtained from short post mortem interval (PMI) autopsies of 7 subjects with MCI (3M, 4F), 6 subjects with EAD (3M, 3F), and 7 age-matched control subjects (5M, 2F). Specimens were immediately frozen in liquid nitrogen and stored at -80ºC until used for analysis. Control subjects were followed longitudinally in the control clinic of the University of Kentucky Alzheimer's Disease Center (UK-ADC) and had neuropsychologic testing annually and physical examinations

biannually. All control subjects had neuropsychologic scores in the normal range and showed no evidence of memory decline. Subjects with MCI and EAD were derived from the control cohort and were followed longitudinally in the memory disorders clinic of the UK-ADC.

The clinical criteria for diagnosis of amnestic MCI were those of Peterson *et al.* (139) and included: (a) memory complaints, (b) expected memory impairment for age and education, (c) normal general cognitive function, (d) intact activities of daily living (ADLs), and (e) the subject did not meet criteria for dementia. The clinical criteria for EAD were: (a) a decline in cognitive function from a previous higher level, (b) declines in one or more areas of cognition in addition to memory, (c) a clinical dementia rating score of 0.5 to 1 and (d) a clinical examination that excluded other causes of dementia. Objective memory test impairment was based on a score of ≤ 1.5 standard deviations from the mean of controls on the Consortium to Establish a Registry for Alzheimer's Disease (CERAD) Word List Learning Task (141). In several cases, the data were corroborated with the Free and Cued Selective Reminding Test (FCSRT). CERAD was established in 1986 by a grant from the National Institute of Aging (NIA) to standardize procedures for the evaluation and diagnosis of patients with AD. The CERAD test battery includes measures in the areas where impairments associated with AD first occur (verbal memory, naming) and is highly reliable for assessing memory dysfunction (142). The FCSRT is also a list-learning test which includes immediate category-cued recall and provides retrieval practice before the test phase.

Tissue Staining

Histopathologic examination of sections of neocortex, hippocampus, entorhinal cortex, amydgala, basal ganglia, nucleus basalis of Meynert, midbrain, pons, medulla and cerebellum were performed by staining with hematoxylin and eosin, the modified Bielschowsky stain, 10D-5 (for beta amyloid) and α-synuclein.

Hematoxylin and Eosin: This staining method employs two dyes – hematoxylin and eosin. A hematoxylin-metal complex, dark purple in color, acts as a basic dye and stains nucleic acids in the nucleus and the cytoplasm dark blue, brown or black. Eosin is

an acidic aniline dye which imparts a pink color to the more basic proteins within the cytoplasm and extracellular spaces. (143).

Bielschowsky Stain: This is a silver stain to determine the presence of NFTs, nerve fibers and SPs in the AD brain. A silver solution is employed to sensitize nerve fibers. The sections undergo treatment with ammoniacal silver and are then reduced to a visible metallic silver. Degenerating axons, NFTs and SPs develop a black stain and the background becomes yellow to brown (144).

10D-5: The 10D5 monoclonal antibody-DAB immunoperoxidase technique enables the detection of SPs in the AD brain. 10D-5 is an antibody to the Aβ peptide, which is the key component of SPs (145).

Alpha-Synuclein: This is a normal, unstructured and soluble protein commonly found in the brain. The function is unknown but it predominantly occurs as presynaptic neuronal protein and is sometimes detected in glial cells. Alpha-synuclein is a marker for Lewy bodies, pathologic feature in substantia nigra seen in Parkinson's disease and in neocortical regions of subjects with mixed Alzheimer's disease and Lewy body pathology. (146).

All of these staining experiments revealed only age-associated changes in the brain tissues in control subjects.

Staging of AD Pathology in Subjects

Braak Staging Scheme: The Braak method was employed for staging the severity of AD pathology in the brain tissues. This method, developed by Braak and Braak (147, 148), makes the assumption that the prevalence and nature of NFTs in the AD brain develops in a progressive and specific manner in the medial temporal lobe (MTL), subcortical nuclei and neocortical areas of the brain. A higher Braak score indicates greater spread of Alzheimer's pathology in the brain and vice versa. Six stages have been detailed, with a seventh stage or Stage 0, representing the absence of NFTs in the brain. The six stages can be collapsed into three stages. Stages I and II are the transentorhinal stages in which NFT pathology is in effect restricted to the transentorhinal and entorhinal cortex. Slight pathology may be observed in the CA1/CA2 regions of the hippocampus. In the limbic stages or Stages III and IV there is acute participation of the entorhinal

areas, modest pathology in the hippocampus and some expansion into the amygdala, thalamus, hypothalamus and basal forebrain. Symptoms of AD pathology usually appear in the neocortical stages or Stages V and VI. At this point, extensive NFT pathology is seen in the neocortex.

National Institute on Aging (NIA)-Reagan Institute Scheme: The NIA-Reagan Institute Consensus Conference proposed an AD progression scheme which can be used to corroborate the Braak scores. This scheme stresses topographic staging of both NFTs and SPs. It designates cases to categories of high, intermediate or low likelihood that the dementia is a result of AD (149).

Control subjects in this study showed Braak staging scores of I and II and met the NIA-Reagan low likelihood criteria for the histopathologic diagnosis of AD. The major difference between normal controls and MCI patients was a significant increase in neuritic plaques in neocortical regions and an increase in neurofibrillary tangles in the amygdala, hippocampus and entorhinal cortex (150). MCI subjects demonstrated Braak staging scores of III-V and met intermediate likelihood criteria for the histopathologic diagnosis of AD. EAD subjects showed Braak staging scores of V and met high likelihood criteria for the histopathologic diagnosis of AD.

Aldehyde Derivatization

Aldehydes were extracted and derivatized with a stock 5,5-dimethyl-1,3-cyclohexanedione derivatizing agent solution (0.25 g dimethyl CHD + 10 g ammonium acetate + 10 mL glacial acetic acid/100 ml water), as previously described (50, 98, 111). Briefly, 100 mg tissue was homogenized in 5 mL HEPES buffer (pH 7.4) containing 137 mM NaCl, 4.6 mM KCl, 1.1 mM KH_2PO_4, 0.6 mM $MgSO_4$, and the protease inhibitors pepstatin (0.7 μg/mL), leupeptin (0.5 μg/mL), aprotinin (0.5 μg/mL) and phenylmethylsulfonyl fluoride (40 μg/mL) using a chilled Dounce homogenizer. Heptanal was chosen as the internal standard for the aliphatic and octanal for the unsaturated aldehydes. Octanal internal standard was added at a 10-fold lower concentration compared to heptanal so that solvent concentration of the final derivatized brain sample by 10 enabled accurate quantification of low abundance unsaturated aldehydes. Aliquots of homogenate (500 μL) were added to glass test tubes and mixed

with 500 μL of methanol containing 2 μM heptanal and 0.2 μM octanal (Wako Pure Chemical Industries, Ltd., Osaka, Japan) as internal standards. Samples were vortexed for 30 sec for aldehyde extraction and centrifuged for 10 min at 850 x *g*. A 500 μL aliquot of supernatant was mixed with 1 mL of dimethyl CHD derivatizing reagent and heated in a 60^{o}C water bath for one hour. After cooling to room temperature, the reaction mixture was added to a C_{18} solid phase extraction (SPE) column (Fisher Scientific, Pittsburgh, PA) preconditioned with 10 mL methanol and 10 ml water. The column was washed with 2 mL water to remove excess ammonium acetate and derivatized aldehydes were eluted with 2 mL methanol.

In the interest of quality control, blank, spiked and duplicate analyses were performed for every brain region under investigation. Dimethyl CHD butanal was used as the aliphatic and dimethyl CHD acrolein as the unsaturated aldehyde for spiked analysis. As with the octanal internal standard for unsaturated aldehydes, acrolein was spiked at a 10-fold lower concentration compared to butanal.

Instrumentation

A Hewlett Packard 1100 series HPLC system was interfaced to a Finnigan LCQ Classic quadrupole ion trap mass spectrometer for reversed phase LC-ESI-MS/MS analyses. A mobile phase mixture of water and acetonitrile, each containing 0.1% formic acid, was used in all experiments. Details of HPLC gradient elution, LCQ instrument parameters and segmented LC-MS/MS analysis were as described previously (111).

Statistical Treatment of Data

Several statistical approaches were used to determine the significance of data obtained, including ANOVA with Dunnett's *post hoc* test (ABSTAT software), 2-tailed-*t*-test and the Mann-Whitney *U*-test.

ANOVA with Dunnett's *post hoc* Test

ANOVA (analysis of variance) is a procedure to compare and contrast the means of three or more populations, by comparing their variances, for the purposes of

establishing whether or not they came from identical populations. In situations where there are more than two populations under investigation, the Student's *t* test cannot be applied, making ANOVA very useful. There are three basic assumptions to ANOVA:

- The populations are normally distributed
- The populations have identical standard deviations (σ)
- The samples are selected independently

When these conditions are met, the *F* distribution is used as a test statistic. The null hypothesis (H_0) is that the population means are the same. H_0 would be rejected if the computed value of *F* is greater than the critical value. The strategy in ANOVA is to estimate the population variance by two separate methods and determine the ratio of these two estimates. If the ratio is close to 1, then the two estimates are the same and the population means are interpreted as being identical. If the ratio is different from 1, then it can be deduced that the population means are different. The *F* distribution determines when the ratio is too much different than 1 to have occurred by chance.

First, the sum of squares total (SS_{total}) is calculated. This is the sum of the squared differences between each observation and the overall mean:

$$SS_{total} = \sum X^2 - \frac{\left(\sum X\right)^2}{n} \tag{1.3.1}$$

where, $\Sigma X^2 = X$ values squared and then summed

$(\Sigma X)^2 = X$ values summed and then squared

n = total number of observations.

Next, the sum of squares due to treatments ($SS_{treatments}$), or the different populations under investigation, is determined:

$$SS_{treatments} = \sum\left(\frac{T_T^2}{n_T}\right) - \frac{\left(\sum X\right)^2}{n} \tag{1.3.2}$$

where, T_T = sum total for each treatment/population

n_T = number of observations for each treatment/population.

The sum of squares error (SS_{error}) is computed as follows:

$$SS_{error} = SS_{total} - SS_{treatments}\,. \tag{1.3.3}$$

Finally, the mean square for treatments ($MS_{treatments}$) and error (MS_{error}) is determined:

$$MS_{treatments} = \frac{SS_{treatments}}{df_1} \tag{1.3.4}$$

$$MS_{error} = \frac{SS_{error}}{df_2} \tag{1.3.5}$$

where, df_1 = number of treatments – 1

$df_2 = n$ – number of treatments.

The F statistic is the ratio of the mean square for treatments and error:

$$F = \frac{MS_{treatments}}{MS_{error}}. \tag{1.3.6}$$

The computed value of F is compared to the critical value to accept or reject the null hypothesis (151).

In situations when ANOVA shows a significant disparity between populations *and* one of the populations is a control, the Dunnett's Test is used as a *post hoc* test. The technique allows for comparisons to be made between the experimental populations and the control population. However, it does not permit experimental populations to be compared to one another other. In an experiment consisting of *a-1* treatments plus a control group, the Dunnett's test can test each treatment against the control mean:

H_0: $\mu_1 = \mu_c$

H_0: $\mu_2 = \mu_c$

H_0: $\mu_3 = \mu_c$

H_0: $\mu_{a-1} = \mu_c$

where, H_0 = null hypothesis

μ_i = mean of experimental population *i*

μ_c = mean of control population.

The *q'* statistics are calculated as follows:

$$q'_{obs} = \frac{\mu_c - \mu_i}{SE_{Dunnett}} \tag{1.3.7}$$

$$SE_{Dunnett} = \sqrt{(MS_{error})\left(\frac{1}{n_i} + \frac{1}{n_c}\right)} \tag{1.3.8}$$

where, n_i = total numbers in population *i*

n_c = total numbers in control population.

The critical value of the q' statistic (q_{crit}') is compared to the calculated value (q_{obs}'). At a given confidence level, if $q_{crit}' < q_{obs}'$, then the null hypothesis is accepted (152).

2-Tailed-*t*-Test

The Student's t test is a parametric test to determine the significance between means of two sample sets or between a mean and a theoretical value. The test presumes that all data points are distributed normally and the ratio of variances in the two samples is ≤ 3. In a 2-tailed-t-test, the area α under the distribution curve is split in half, placing half in each tail. The null hypothesis (H_0) in this case is a particular value and there are two alternative hypotheses (H_1), one positive and one negative:

H_0: $\mu = a$

H_1: $\mu \neq a$

The critical value of t (t_{crit}), is written with both a plus and minus sign (±). For instance, the critical value of t when there are 10 degrees of freedom ($df = 10$) and α is set to 0.05, is $t_{crit} = \pm 2.228$. The sampling distribution model used in a 2-tailed-t-test is given in Figure 1.3.1. When comparing the mean from a sample set to a theoretical or 'true' value, the critical value for rejecting the null hypothesis is as follows:

$$\mu - a = \pm \frac{ts}{\sqrt{N}} \tag{1.3.9}$$

where, N = total number of measurements
t = statistical parameter
s = standard deviation
μ = mean of measurements
a = true value.

The situation is slightly different when comparing the mean of one sample set to another, as in the case of N_x replicate analyses of X to yield a mean of μ_x and N_y analyses of Y to yield a mean of μ_y, the data being gathered in a similar manner. It can be considered that the standard deviations of the two measurement groups are identical. The 2-tailed-t-test can be used to determine if differences in measurements of X and Y are the result of random errors or because they happen to be two different samples. The null

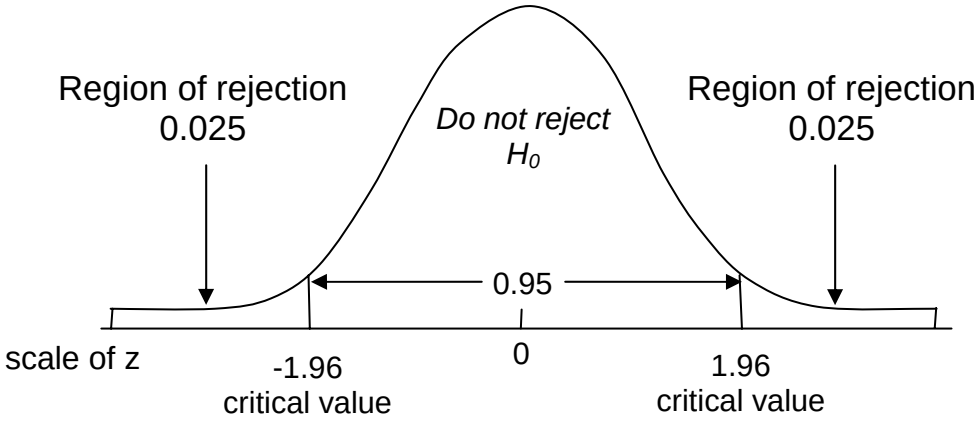

Figure 1.3.1. Regions of nonrejection and rejection for a 2-tailed-*t*-test. Significance level: 0.05.

hypothesis (H_0) is that X and Y are the same and any disparity (μ_x - μ_y) is due to random errors (153). The standard error of the means μ_x and μ_y are expressed as the ratio of the standard deviation to the square root of the number of data points:

$$s_{mx} = \frac{s_x}{\sqrt{N_x}} \tag{1.3.10}$$

$$s_{my} = \frac{s_y}{\sqrt{N_y}} \tag{1.3.11}$$

where, s_{mx} = standard error of μ_x

s_{my} = standard error of μ_y

s_x = standard deviation of x

s_y = standard deviation of y.

Therefore, the variance s_d^2 of the difference ($d = x - y$) between the two means is described as follows:

$$s_d^2 = s_{mx}^2 + s_{my}^2 . \tag{1.3.12}$$

Inserting values of s_d, s_{mx} and s_{my} into this equation:

$$\left(\frac{s_d}{\sqrt{N}}\right)^2 = \left(\frac{s_x}{\sqrt{N_x}}\right)^2 + \left(\frac{s_y}{\sqrt{N_y}}\right)^2 . \tag{1.3.13}$$

It can be supposed that the pooled standard deviation s_{pooled} is a reasonable approximation of both s_x and s_y:

$$\left(\frac{s_d}{\sqrt{N}}\right)^2 = \left(\frac{s_{pooled}}{\sqrt{N_x}}\right)^2 + \left(\frac{s_{pooled}}{\sqrt{N_y}}\right)^2 = s_{pooled}^2 \left(\frac{N_x + N_y}{N_x N_y}\right). \tag{1.3.14}$$

Substituting into Eqn (1.3.9) generates the following:

$$\mu_x - \mu_y = \pm t s_{pooled} \sqrt{\frac{N_x + N_y}{N_x N_y}} . \tag{1.3.15}$$

As such, the test value of t is given by:

$$t = \frac{\mu_x - \mu_y}{s_{pooled} \sqrt{\frac{N_x + N_y}{N_x N_y}}} \tag{1.3.16}$$

$$\text{for, } df = N_x + N_y - 2. \tag{1.3.17}$$

This test value of t is compared with t_{crit} obtained from appropriate statistical tables for the desired confidence level. If $|t| < t_{crit}$, the null hypothesis holds true. If, on the other hand, $|t| > t_{crit}$, it can be reasoned that there existas a significant difference between μ_x and μ_y (153).

Mann-Whitney *U* Test

Nonparametric tests are often used in place of their parametric counterparts when certain assumptions about the underlying population are questionable. For example, when comparing two independent samples, the Mann-Whitney *U* test does not assume that the difference between the samples is normally distributed whereas its parametric counterpart, the two sample-*t*-test, does. Nonparametric tests may be, and often are, more powerful in detecting population differences when certain assumptions are not satisfied. The Mann-Whitney *U* test is used to test the null hypothesis that two samples come from the same population (i.e. have the same median) or, alternatively, whether observations in one sample tend to be larger than observations in the other. The test assumes that the two distributions are similar in shape.

Consider a sample of n_x observations $\{x_1, x_2, \ldots, x_n\}$ in one group (from one population) and a sample of n_y observations $\{y_1, y_2, \ldots, y_n\}$ in another group (from another population). The Mann-Whitney *U* test is based on a comparison of every observation x_i, in the first sample set with every observation y_j in the other sample set. The total number of pairwise comparisons that can be made is $n_x n_y$. If the samples have the same median, then each x_i has an equal chance (i.e. probability ½) of being greater or smaller than each y_i. The null hypothesis is as follows:

H_0: P $(x_i > y_i) = ½$

while the alternate hypothesis is:

H_1: P $(x_i > y_i) \neq ½$.

The number of times (U_x) an x_i from sample X is greater than a y_i from sample Y is determined and vice versa. Under the null hypothesis, it would be expected that U_x and U_y are approximately equal.

First, all observations are arranged in order of magnitude. Each observation is denoted as being either from population *X* or *Y*. The number of *y*s that are smaller than every given *x* are counted (this indicates $x_i > y_j$) and vice versa (this indicates $y_j > x_i$). The total number of times (U_x) that $x_i > y_j$ is determined and vice versa (U_y). It should be noted that $U_x + U_y$ must equal $n_x n_y$. Finally, $U = \min(U_x, U_y)$ is determined. Statistical tables for the Mann-Whitney *U* test are used to find the probability of observing a value of *U* or lower. If the test is one-sided, this would be the *p*-value. If the test is two-sided, the probability is doubled to obtain the *p*-value.

If the number of observations is such that $n_x n_y$ is large enough (>20), a normal approximation can be used with

$$\mu_U = \frac{n_x n_y}{2} \tag{1.3.18}$$

$$\sigma_U = \sqrt{\frac{n_x n_y (N+1)}{12}} \tag{1.3.19}$$

where, $N = n_x + n_y$.

Sometimes, it may be that two or more observations are the same. If this is the case, *U* can still be calculated by allocating half of the tie to the *X* value and half of the tie to the *Y* value. However, in such a situation the normal approximation must then be used with an adjustment to the standard deviation. This becomes (154):

$$\sigma_U = \sqrt{\frac{n_x n_y}{N(N-1)} \times \left[\frac{N^3 - N}{12} - \sum_{j=1}^{g} \frac{t_j^3 - t_j}{12} \right]} \tag{1.3.20}$$

where, $N = n_x + n_y$

g = the number of groups of ties

t_j = the number of tied ranks in group j.

Results and Discussion

Aldehyde levels were compared statistically using ANOVA with Dunnett's *post hoc* test for individual differences and the commercially available ABSTAT software (AndersonBell, Arvada, CO). Age and PMI were compared using a 2-tailed *t*-test. Braak

staging scores were compared using non-parametric testing and the Mann-Whitney *U* test. Statistical significance was set at $P < 0.05$ (Table 1.3.1).

Levels of aliphatic aldehydes (C_1-C_6), HNE and acrolein were measured in the HPG, SMTG and CER of 7 subjects with MCI (3M, 4F), 6 subjects with EAD (3M, 3F) and 7 age-matched control subjects (5M, 2F) using an improved mass spectrometric method (LC/ESI/MS/MS) that provides unequivocal identification of the compounds of interest (111). Subject demographic data are shown in Table 1.3.1. There were no significant differences in PMI for any of the three subjects groups. There was a significant ($p < 0.05$) difference in age of EAD subjects (89.0 ± 1.8 y) compared to control subjects (81.4 ± 2.6 y). There was no significant difference in age between control and MCI subjects (88.4 ± 1.4 y). Median Braak staging scores were significantly higher in MCI (III) and EAD (V) subjects compared to controls (II). Delayed memory recall scores from the MMSE were significantly lower in MCI (4.1 ± 0.8) and EAD (4.2 ± 0.7) compared to control subjects (7.9 ± 0.7).

No *statistically significant* differences in the levels of aliphatic aldehydes were observed for the various brain regions and levels of AD pathology under investigation. Figure 1.3.2 shows that HNE levels were statistically significantly elevated in a disease progression-related manner in all three brain regions under investigation. *Post hoc* testing showed that HNE was significantly increased ($P < 0.05$) in EAD HPG (1.45 ± 0.5 nmol/mg protein) and MCI HPG (1.5 ± 0.3 nmol/mg protein) compared to control subjects (0.4 ± 0.1 nmol/mg protein). Levels of HNE were also significantly elevated in MCI SMTG (2.4 ± 0.3 nmol/mg protein) and EAD SMTG (2.9 ± 0.3 nmol/mg protein) compared to control SMTG (0.8 ± 0.1 nmol/mg protein). In contrast to a previous study of late-stage AD subjects (50), levels of HNE in CER were significantly elevated in MCI (1.5 ± 0.2 nmol/mg protein) compared to control CER (0.8 ± 0.1 nmol/mg protein). There were no significant differences in HNE between EAD and MCI for any of the brain regions analyzed. Comparison of regional differences showed a statistically significant elevation of HNE in SMTG compared to both HPG and CER in EAD and MCI.

Figure 1.3.3 shows that levels of acrolein increased in a disease progression related manner with statistically significant increases in EAD HPG (2.7 ± 0.2 nmol/mg protein) compared to control HPG (1.2 ± 0.3 nmol/mg protein). There were no significant

Table 1.3.1. Subject demographic data.

	Mean ± SEM Age (years)	**Sex**	**Mean ± SEM PMI (h)**	**Median Braak Score**
MCI	88.4 ± 1.4	3M, 4F	4.0 ± 1.0	III*
EAD	89.0 ± 1.8*	3M, 3F	5.4 ± 2.4	V*
Control	81.4 ± 1.4	5M, 2F	2.7 ± 0.3	II

* $p < 0.05$

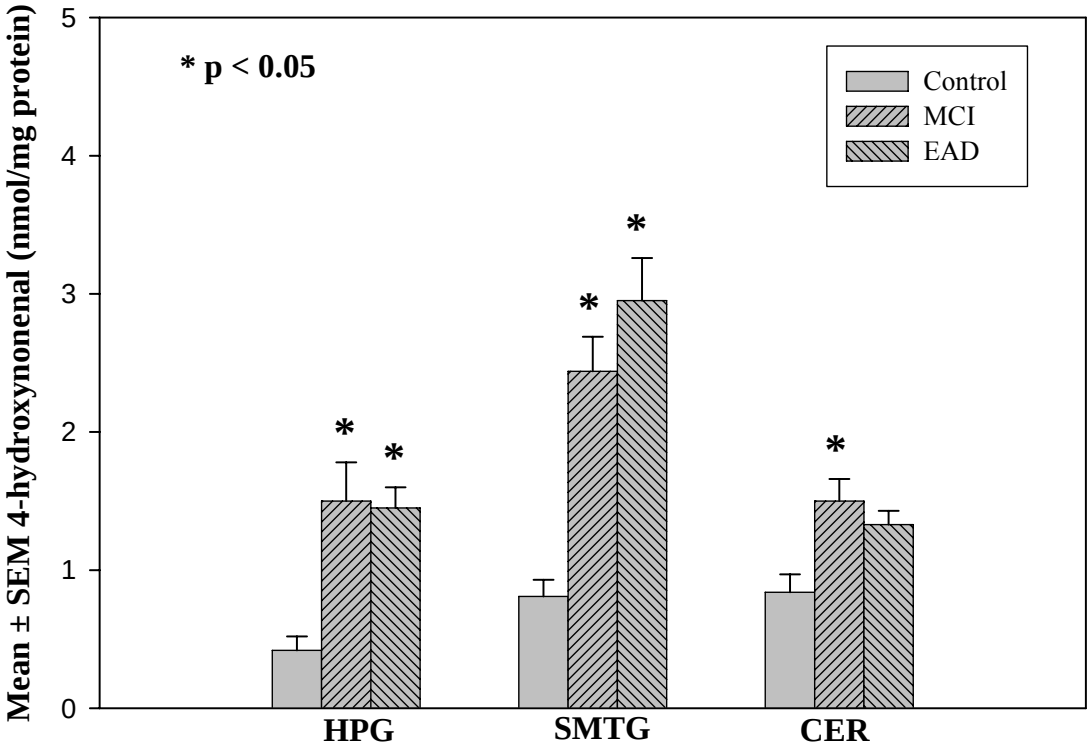

Figure 1.3.2. Mean ± SEM 4-hydroxynonenal (HNE) levels (nmol/mg protein) in MCI, EAD and control hippocampus/parahippocampal gyrus (HPG), superior and middle temporal gyrus (SMTG) and cerebellum (CER). There was a statistically significant ($p < 0.05$) elevation of HNE in MCI and EAD HPG and SMTG and in MCI CER.

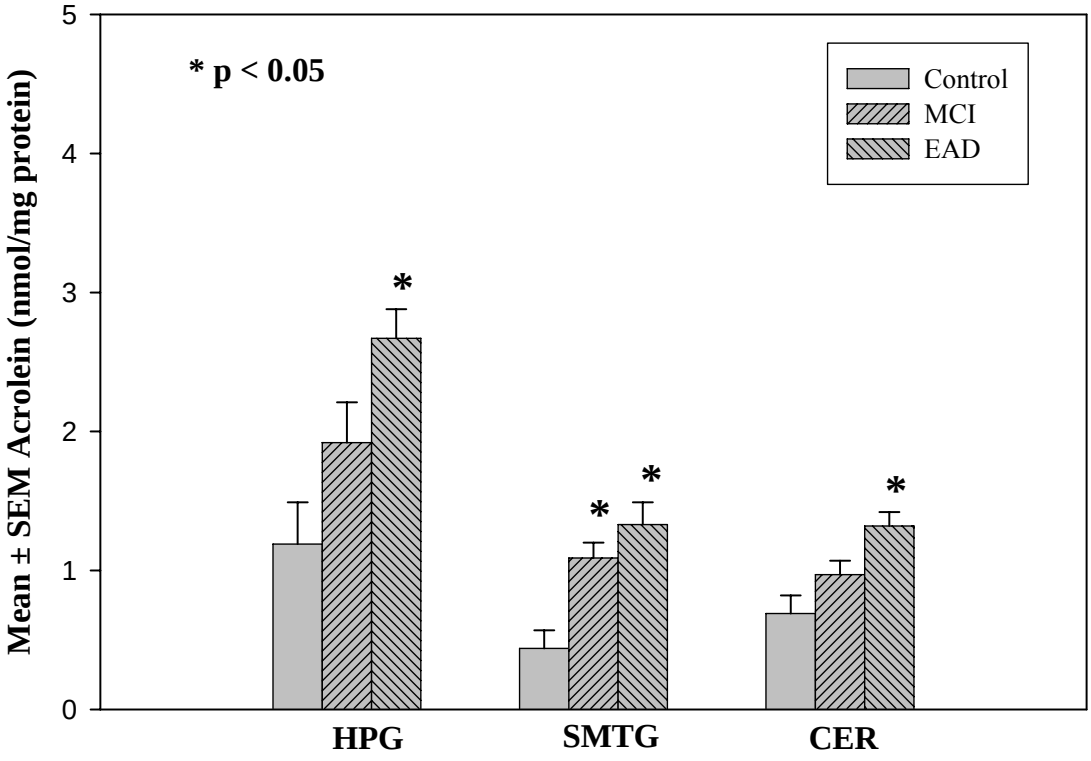

Figure 1.3.3. Mean ± SEM acrolein levels (nmol/mg protein) in MCI, EAD and control HPG, SMTG and CER. There was a statistically significant ($p < 0.05$) increase in acrolein in EAD HPG, SMTG and CER and in MCI SMTG.

differences in HPG acrolein between MCI and control subjects or between MCI and EAD subjects. In SMTG, there was a statistically significant increase in acrolein in MCI (1.1 ± 0.1 nmol/mg protein) and EAD (1.3 ± 0.2 nmol/mg protein) compared to control subjects (0.4 ± 0.1 nmol/mg protein). There were no significant differences in acrolein between MCI and EAD subjects. In contrast to a previous studies of late stage AD brain (49), EAD CER showed a significant increase in acrolein (1.3 ± 0.1 nmol/mg protein) compared to control subjects (0.7 ± 0.1 nmol/mg protein). Correlation analysis of Braak staging scores and HNE or acrolein levels showed no significant trends. Correlation analysis of HNE and acrolein levels with delayed memory recall scores showed negative trends although the results were not statistically significant.

This is the first study to quantify levels of specific, neurotoxic by-products of lipid peroxidation in brain specimens from subjects with MCI and EAD. The results clearly showed that HNE and acrolein increase in a disease progression-dependent manner with statistically significant elevations of HNE in MCI and EAD HPG and SMTG and in MCI CER. Acrolein levels were significantly elevated in EAD HPG and in MCI and EAD SMTG. In contrast to a previous study of late stage AD brain (50), the data presented here suggest that there is a generalized increase in oxidative damage in the brain in MCI, including the CER. In light of the potential role of lipid peroxidation and HNE generation in the pathogenesis of neuron degeneration, the observation of elevations of HNE in MCI CER where there is limited neuropathology may appear contradictory. However, a previous study of glutathione transferase (GST), the enzyme responsible for detoxification of reactive aldehydes including HNE and acrolein, showed that GST activity is significantly decreased in HPG and amygdala but remains unaltered in CER in late stage AD (155), suggesting that the AD brain retains the ability to detoxify HNE in areas unaffected by pathology, whereas brain regions showing increased neuropathology (HPG) do not.

Levels of HNE and acrolein measured in this current study using improved analytical methodology were comparable to those measured in previous studies of late-stage AD and control subjects (49, 50). Using HPLC with fluorescence detection, it has been shown HNE was significantly elevated in AD HPG (0.54 ± 0.12 nmol/mg protein) compared to age-matched control subjects (0.3 ± 0.1 nmol/mg protein). Similar to the

results of this study, previous analyses of late-stage AD brain showed the highest HNE levels in SMTG (1.5 ± 0.4 nmol/mg protein (AD); 1.4 ± 0.4 nmol/mg protein (control)). Levels of acrolein observed in EAD and MCI HPG in this study were also comparable to those observed in late stage AD (5.0 ± 1.6 nmol/mg protein) and age-matched controls (0.7 ± 0.1 nmol/mg protein). Slight differences in absolute levels of HNE and acrolein may be due to differences in analytical methods and slight subject to subject variability.

The increased levels of neurotoxic markers of lipid peroxidation in MCI and EAD reported here are consistent with previous studies of oxidative stress in extra cerebral fluids in MCI. Pratico *et al*. (156) showed substantially increased levels of isoprostane 8,12-iso-iP$F_{2\alpha}$-VI, a specific marker of lipid peroxidation, in plasma, urine and cerebrospinal fluid (CSF) of MCI subjects compared with age-matched controls. In a study of peripheral leukocytes in MCI and late-stage AD, Migliore *et al*. (157) showed substantially increased oxidative DNA damage in MCI and AD subjects compared to age-matched controls using comet assay analysis.

Keller *et al*. (85) showed substantially increased protein oxidation (protein carbonyls) in SMTG in MCI but not EAD, compared to age-matched control subjects. Additionally, significant elevations of thiobarbituric acid reactive substances (TBARs) and malondialdehyde, an aldehydic marker of lipid peroxidation with limited toxicity, were observed in MCI and EAD SMTG compared to control subjects. Although TBARs have been widely used as a marker for lipid peroxidation, the assay is subject to several interferences. This study, using LC-ESI-MS/MS, allows unequivocal identification of the target molecules based on their mass spectra and is free of possible confounding interferences. More recently, statistically significant elevations of 8-hydroxyguanine, a widely studied marker of DNA oxidation, were observed in nuclear DNA from frontal and temporal lobe specimens and in mitochondrial DNA from temporal lobe in MCI compared to age-matched control subjects (158). Statistically significant elevations of the markers of adenine oxidation (8-hydroxyadenine and 4,6-diamino-5-formamidopyrimidine) were also detected in nuclear and mitochondrial DNA in frontal, parietal and temporal lobes from MCI subjects compared to age-matched control subjects. No differences in DNA oxidation were observed in CER in MCI.

Conclusions

This study was conducted in the interest of obtaining a thorough understanding of the distribution of aldehydic products from LPO in different brain regions at different stages of AD. Here, we described the application of a previously developed, sensitive and selective LC-ESI-MS/MS methodology (111) in the quantification of aldehyde concentrations in the HPG, SMTG and CER of subjects with MCI and EAD compared to age-matched controls subjects (159). Individuals with amnestic MCI show memory impairment compared to normal controls, but lack the broader cognitive deficits of AD patients and likely represent the earliest stage of AD. Understanding the differences between MCI, EAD and normal subjects is becoming increasingly important in the interest of developing early diagnostic methods and viable treatments for this debilitating disease (159).

In agreement with previous studies, it was observed that aliphatic aldehydes do not display statistically significant differences when comparing HPG, SMTG and CER brain regions and different levels of AD pathology (50). The data given here coupled with other studies suggest that oxidative damage occurs early in the course of AD and reaches a plateau during EAD, consistent with the hypotheses of Nunomura *et al*. (160) and Perry *et al*. (161). These researchers suggested that oxidative damage is most pronounced early in AD development. However, a recent clinical study by Petersen *et al*. (162) showed that treatment of MCI subjects with Vitamin E did not alter the overall rate of progression from MCI to AD compared to subjects who received placebos, suggesting that limiting oxidative damage does not affect the progression of AD. Although the data presented here appear to contrast with the findings of the clinical study, it has been suggested that acrolein can inhibit the enzyme responsible for the reduction of Vitamin E radicals (13, 80) and thus may limit the therapeutic effects of Vitamin E. The observation of elevations of acrolein in MCI and EAD in this study may help to explain why Vitamin E showed no protective effects in MCI in the clinical trial. In addition, it has been shown that Vitamin E taken in conjunction with Vitamin C decreases markers of lipid peroxidation in CSF of AD patients (163). Vitamin C was not used in the clinical trial by Petersen *et al*. (162)

The observations from this study suggest that oxidative stress occurs as an early event in the progression of AD and that preventive measures for those at risk for AD should be initiated in the presymptomatic phase of the disease (at or prior to MCI) to be effective.

Chapter 1.4
Conclusions

Alzheimer's disease is a progressive, irrevocable ailment of the brain, the etiology and cure of which have eluded scientists and clinicians to this day. The disease attacks and gradually steals the minds of its victims. Symptoms of AD include judgment deterioration, mental confusion, loss of memory, changes in personality, disorientation, and impairment of language skills. Alzheimer's disease is the most common form of irreversible dementia amongst the elderly community. Due to the devastating nature of AD, considerable research is focused on developing early diagnostic methods, medication for symptom alleviation, as well as cures for the disease. The AD brain is marked by considerable oxidative stress and lipid peroxidation, particularly in areas responsible for cognition and memory. In recent years, various by-products of lipid peroxidation, including biogenic aldehydes, isoprostanes and neuroprostanes, have piqued the interest of the AD research community as potential biomarkers for lipid peroxidation and therefore, AD.

Since acrolein and HNE, amongst other biogenic aldehydes, are produced as a consequence of LPO, their prevalence above normal concentrations can be indicative of AD. As such, their quantification can serve as a measure of the progression of the disease. To this end, a sensitive, selective LC-ESI-MS/MS methodology for the detection and accurate quantification of acrolein, HNE and the aliphatic aldehydes C_1-C_6 was designed (111). This is the first report to describe the use of MS/MS analysis in brain aldehyde quantification. Researchers have explored spectrophotometric methods coupled to HPLC in biogenic aldehyde analysis but co-eluting species are difficult to analyze accurately using these techniques. Methods involving GC/MS come with high sensitivity, greater mass specificity and lower LODs, although different derivatization techniques are often required to analyze different classes of aldehydes. LC-ESI-MS/MS techniques are the some of the best analytical tools for biogenic aldehyde investigations as they offer greatly improved sensitivity, little sample cleanup and simultaneous analysis of multiple classes of aldehydes with a single derivatization method. Furthermore, in contrast to GC

experiments, analytes are not exposed to high temperatures in the analysis, which may not be suitable for some compounds.

The Hantzsch reaction proved to be a very beneficial means of easily derivatizing aldehydic species with high efficiencies for trace LC/MS analyses. This derivatization method offers high selectivity, as other carbonyl compounds do not react in a manner to generate dimedone derivatives. Furthermore, CHD derivatives of aldehydes have very good electrospray responses. The dimethyl CHD derivative demonstrated the best chromatographic response of all derivatives explored. The use of two internal standards for separate quantification of aliphatic and unsaturated aldehydes enabled accurate quantification of very low concentrations of acrolein and HNE typically observed in the brain. Standard aliphatic and unsaturated aldehydes gave linear responses over a wide concentration range.

The LC-ESI-MS/MS methodology was successfully applied in the detection and quantification of biogenic aldehydes *in vivo* (159). For the purposes of determining whether or not LPO-generation of aliphatic and unsaturated aldehydes occurred early in the pathogenesis of AD, levels of these aldehydes were studied in HPG, SMTG and CER of subjects with MCI, EAD and age-matched controls. This is the first study to report an in-depth comparison of aldehyde levels between MCI and EAD. At a 95% confidence level, no significant differences were observed in patterns of aliphatic aldehyde generation in different regions of the brain for MCI and EAD subjects, compared to the control group. This was in agreement with studies from other laboratories, as discussed in Chapter 1.3. However, also in agreement with previous findings, the results presented here clearly indicated statistically significant concentration differences for the unsaturated aldehydes HNE and acrolein. Noteworthy increases in HNE levels in HPG, SMTG and CER for MCI subjects were observed, compared to the control group. Individuals with MCI also demonstrated significantly elevated levels of acrolein in SMTG, compared to controls. In the case of subjects with EAD, a statistically significant increase in the production of HNE was detected in HPG and SMTG, compared to the control group. Furthermore, in contrast to the age-matched controls, significantly high concentrations of acrolein were observed in HPG, SMTG and CER in subjects with EAD.

A comparison of MCI and EAD subjects revealed no statistically significant differences in aldehyde levels.

The methodology developed here was very well-suited for detecting and quantifying biologically relevant aldehydes in AD progression. It was evident from the study of HNE and acrolein levels in different brain regions of individuals at different stages of AD that lipid peroxidation occurred early in the pathogenesis of AD, at the MCI stage of development, when little, if any, clinical symptoms are observed. Hence, our results indicated that effective diagnostic methods for AD must be designed to target the MCI stage. Furthermore, drug development for symptom alleviation and the ultimate cure of AD should also focus on subjects with MCI. As with any illness, the best mode of action is preventive medicine. While considerable research is devoted to determining the cause of AD, the answers still remain at large. In situations when preventive care is not possible or simply did not happen, early detection, diagnosis and treatment are the key ingredients to a better quality of life.

References

1. http://www.nlm.nih.gov/medlineplus/alzheimersdisease.html.
2. Markesbery, W. R. (**1997**) *Free Radic. Biol. Med.* ***23,*** 134-147.
3. Grootendorst, J., Bour, A., Vogel, E., Kelche, C., Sullivan, P. M., Dodart, J. C., Bales, K., and Mathis, C. (**2005**) *Behav. Brain Res.* ***159,*** 1-14.
4. Svennerholm, L., and Gottfries, C. G. (**1994**) *J. Neurochem.* ***62,*** 1039-1047.
5. Butterfield, D. A., Castegna, A., Lauderback, C. M., and Drake, J. (**2002**) *Neurobiol. Aging* ***23,*** 655-664.
6. Selkoe, D. J. (**1996**) *J. Biol. Chem.* ***271,*** 18295-18298.
7. Grundke-Iqbal, I., and Iqbal, K. (**1989**) *Prog. Clin. Biol. Res.* ***317,*** 745-753.
8. Grundke-Iqbal, I., Iqbal, K., Tung, Y. C., Quinlan, M., Wisniewski, H. M., and Binder, L. I. (**1986**) *Proc. Natl. Acad. Sci. USA* ***83,*** 4913-4917.
9. Lee, V. M., Balin, B. J., Otvos, L. J., and Trojanowski, J. Q. (**1991**) ***Science 251,*** 675-678.
10. Avilá, J. (**2000**) *FEBS Lett.* ***476,*** 89-92.
11. Hensley, K., Hall, N., Subramaniam, R., Cole, P., Harris, M., Aksenov, M., Aksenova, M., Gabbita, S. P., Wu, J. F., Carney, J. M., Lovell, M. A., Markesbery, W. R., and Butterfield, D. A. (**1995**) *J. Neurochem.* ***65,*** 2146-2156.
12. Varadarajan, S., Yatin, S., Aksenova, M., and Butterfield, D. A. (**2000**) *J. Struct. Biol.* ***130,*** 184-208.
13. Calingasan, N. Y., Uchida, K., and Gibson, G. E. (**1999**) *J. Neurochem.* ***72,*** 751-756.
14. Yatin, S., Varadarajan, S., and Butterfield, D. A. (**2000**) *J. Alzheimer's Dis.* ***2,*** 123-131.
15. Rottkamp, C. A., Raina, A. K., Zhu, X., Gaier, E., Bush, A. I., Atwood, C. S., Chevion, M., Perry, G., and Smith, M. A. (**2001**) *Free Rad. Biol. Med.* ***30,*** 447-450.
16. Atwood, C. S., Scarpa, R. C., Huang, X., Moir, R. D., Jones, W. D., Fairlie, D. P., Tanzi, R. E., and Bush, A. I. (**2000**) *J. Neurochem.* ***75,*** 1219-1233.
17. Arlt, S., Beisiegel, U., and Kontush, A. (**2002**) *Curr. Opin. Lipidol.* ***13,*** 289-294.

18. Perry, G., Castellani, R. J., Hirai, K., and Smith, M. A. (**1998**) *J. Alzheimer's Dis.* ***1,*** 45-55.
19. Smith, M. A., Drew, K. L., Nunomura, A., Takeda, A., Hirai, K., Zhu, X., Atwood, C. S., Raina, A. K., Rottkamp, C. A., Sayre, L. M., Friedland, R. P., and Perry, G. (**2002**) *Neurochem. Int.* ***40,*** 527-531.
20. Gómez-Ramos, A., Díaz-Nido, J., Smith, M. A., Perry, G., and Avilá, J. (**2003**) *J. Neurosci. Res.* ***71,*** 863-870.
21. Trojanowski, J. Q., and Lee, V. M. (**1995**) *FASEB J.* ***9,*** 1570-1576.
22. Lee, V. M., Goedert, M., and Trojanowski, J. Q. (**2001**) *Annu. Rev. Neurosci.* ***24,*** 1121-1159.
23. Iqbal, K., and Grundke-Iqbal, I. (**1997**) *Int. Psychogeriatr.* ***9,*** 289-296.
24. Mori, H., Kondo, J., and Ihara, Y. (**1987**) *Science* ***235,*** 1641-1644.
25. Perry, G., Friedman, R., Shaw, G., and Chau, V. (**1987**) *Proc. Natl. Acad. Sci. USA* ***84,*** 3033-3036.
26. Mattson, M. P. (**1995**) *Neurobiol. Aging* ***16,*** 447-457.
27. Takeda, A., Smith, M. A., Avilá, J., Nunomura, A., Siedlak, S. L., Zhu, X., Perry, G., and Sayre, L. M. (**2000**) *J. Neurochem.* ***75,*** 1234-1241.
28. Lovestone, S., and McLoughlin, D. M. (**2002**) *J. Neurol. Neurosurg. Psychiatry* ***72,*** 152-161.
29. Perez, M., Hernandez, F., Gomez-Ramos, A., Smith, M., Perry, G., and Avilá, J. (**2002**) *Eur. J. Biochem.* ***269,*** 1484-1489.
30. Liu, Q., Smith, M. A., Avilá, J., DeBernardis, J., Kansal, M., Takeda, A., Zhu, X., A., N., Honda, K., Moreira, P. I., Oliveria, C. R., Santos, M. S., Shimohama, S., Aliev, G., de la Torre, J., Ghanbari, H. A., Siedlak, S. L., Harris, P. L. R., Sayre, L. M., and Perry, G. (**2005**) *Free Radic. Biol. Med.* ***38,*** 746-754.
31. Zhu, X., Rottkamp, C. A., Boux, H., Takeda, A., Perry, G., and Smith, M. A. (**2000**) *J. Neuropathol. Exp. Neurol.* ***59,*** 880-888.
32. Zhu, X., Castellani, R. J., Takeda, A., Nunomura, A., Atwood, C. S., Perry, G., and Smith, M. A. (**2001**) *Mech. Ageing Dev.* ***123,*** 39-46.
33. Zhu, X., Lee, H., Raina, A. K., Perry, G., and Smith, M. A. (**2002**) *Neurosignals* ***11,*** 270-281.

34. Reynolds, C. H., Betts, J. C., Blackstock, W. P., Nebreda, A. R., and Anderton, B. H. (**2000**) *J. Neurochem.* ***74,*** 1587-1595.
35. Butterfield, D. A. (**2002**) *Free Radic. Biol. Med.* ***36,*** 1307-1313.
36. Praticó, D. (**2002**) *Drug Dev. Res.* ***56,*** 446-451.
37. O'Brien-Coker, I. C., and Mallet, G. P. A. I. (**2001**) *Rapid Commun. Mass Spectrom.* ***15,*** 920-928.
38. Porter, N. A., Lehman, L. S., Weber, B. A., and Smith, K. J. (**1981**) *J. Am. Chem. Soc.* ***103,*** 6447-6455.
39. Gabbita, S. P., Aksenov, M. Y., Lovell, M. A., and Markesbery, W. R. (**1999**) *J. Neurochem.* ***73,*** 1660-1666.
40. Esterbauer, H., Shchaur, R. J., and Zollner, H. (**1991**) *Free Rad. Biol. Med.* ***11,*** 81-128.
41. Mecocci, P., MacGarvey, U., and Beal, M. F. (**1994**) *Ann. Neurol.* ***36,*** 747-751.
42. Mecocci, P., Polidori, M. C., Ingegni, T., Cherubini, A., Chionne, F., Cecchetti, R., and Senin, U. (**1998**) *Neurology* ***51,*** 1014-1017.
43. Wang, J., Xiong, S., Markesbery, W. R., and Lovell, M. A. (**2005**) *J. Neurochem.* ***93,*** 953-962.
44. Prasad, M. R., Lovell, M. A., Yatin, M., Dhillon, H., and Markesbery, W. R. (**1998**) *Neurochem. Res.* ***23,*** 81-88.
45. Lovell, M. A., Ehmann, W. D., Butler, S. M., and Markesbery, W. R. (**1995**) *Neurology* ***45,*** 1594-1601.
46. Montine, T. J., Beal, M. F., Cudkowicz, M. E., O'Donnell, H., Margolin, R. A., McFarland, L., Bachrach, A. F., Zackert, W. E., Roberts, L. J., and Morrow, J. D. (**1999**) *Neurology* ***52,*** 562-565.
47. Montine, T. J., Markesbery, W. R., Morrow, J. D., and Roberts, L. J. n. (**1998**) *Ann. Neurol.* ***44,*** 410-413.
48. Nourooz-Zadeh, J., Liu, E. H., Yhlen, B., Anggard, E. E., and Halliwell, B. (**1999**) *J. Neurochem.* ***72,*** 734-740.
49. Lovell, M. A., Xie, C., and Markesbery, W. R. (**2001**) *Neurobiol. Aging* ***22,*** 187-194.
50. Markesbery, W. R., and Lovell, M. A. (**1998**) *Neurobiol. Aging* ***19,*** 33-36.

51. Lovell, M. A., Ehmann, W. D., Mattson, M. P., and Markesbery, W. R. (**1997**) *Neurobiol. Aging **18,*** 457-461.

52. Good, P. F., Werner, P., Hsu, A., Olanow, C. W., and Perl, D. P. (**1996**) *Am. J. Pathol. **149,*** 21-28.

53. Montine, K. S., Kim, P. J., Olson, S. J., Markesbery, W. R., and Montine, T. J. (**1997**) *J. Neuropathol. Exp. Neurol. **56,*** 866-871.

54. Smith, M. A., Perry, G., Richey, P. L., Sayre, L. M., Anderson, V. E., Beal, M. F., and Kowall, N. (**1996**) *Nature **382,*** 120-121.

55. Smith, M. A., Taneda, S., Richey, P. L., Miyata, S., Yan, S. D., Stern, D., Sayre, L. M., Monnier, V. M., and Perry, G. (**1994**) *Proc. Natl. Acad. Sci. U S A **91,*** 5710-5714.

56. Yan, S. D., Chen, X., Schmidt, A. M., Brett, J., Godman, G., Zou, Y. S., Scott, C. W., Caputo, C., Frappier, T., Smith, M. A., Perry, G., Yen, S. H., and Stern, D. (**1994**) *Proc. Natl. Acad. Sci. U S A **91,*** 7787-7791.

57. Montine, T. J., Neely, M. D., Quinn, J. F., Beal, M. F., Markesbery, W. R., Roberts II, L. J., and Morrow, J. D. (**2002**) *Free Rad. Biol. Med. **33,*** 620-626.

58. Morrow, J. D., and Roberts, L. J. (**2002**) *Am. J. Respir. Crit. Care Med. **166,*** S25-S30.

59. http://ccr.cancer.gov/faculties/documents/452/CRBWGmorrow.ppt.

60. Meagher, E. A., and FitzGerald, G. A. (**2000**) *Free Rad. Biol. Med. **28,*** 1745-1750.

61. Halliwell, B., and Grootveld, M. (**1987**) *FEBS Lett. **213,*** 9-14.

62. Lovell, M. A., and Markesbery, W. R. (**2003**) *Methods in Biological Oxidative Stress*, Humana Press, Totowa, NJ.

63. Sayre, L. M., Zelasko, D. A., Harris, P. L., Perry, G., Salomon, R. G., and Smith, M. A. (**1997**) *J. Neurochem. **68,*** 2092-2097.

64. Subramaniam, R., Roediger, F., Jordan, B., Mattson, M. P., Keller, J. N., Waeg, G., and Butterfield, D. A. (**1997**) *J. Neurochem. **69,*** 1161-1169.

65. Schneider, C., Tallman, K. A., Porter, N. A., and Brash, A. R. (**2001**) *J. Biol. Chem. **276,*** 20831-20838.

66. Mattson, M. P., Fu, W., Waeg, G., and Uchida, K. (**1997**) *Neuroreport **8,*** 2275-2281.

67. Drake, J., Petroze, R., Castegna, A., Ding, Q., Keller, J. N., Markesbery, W. R., Lovell, M. A., and Butterfield, D. A. (**2004**) *Neurosci. Lett. **356,*** 155-158.

68. McGrath, L. T., McGleenon, B. M., Brennan, S., McColl, D., McIlroy, S., and Passmore, A. P. (**2001**) *Q. J. Med. **94,*** 485-490.

69. Kruman, I., Bruce-Keller, A. J., Bredesen, D., Waeg, G., and Mattson, M. P. (**1997**) *J. Neurosci. **17,*** 5089-5100.

70. Rabacchi, S. A., Friedman, W. J., Shelanski, M. L., and Troy, C. M. (**2004**) *Neurobiol. Aging **25,*** 1057-1066.

71. Uchida, K. (**2000**) *Free Radic. Biol. Med. **28,*** 1685-1696.

72. Keller, J. N., Mark, R. J., Bruce, A. J., Blanc, E., Rothstein, J. D., Uchida, K., Waeg, G., and Mattson, M. P. (**1997**) *Neuroscience **80,*** 685-696.

73. Keller, J. N., Pang, Z., Geddes, J. W., Begley, J. G., Germeyer, A., Waeg, G., and Mattson, M. P. (**1997**) *J. Neurochem. **69,*** 273-284.

74. Lauderback, C. M., Hackett, J. M., Huang, F. F., Keller, J. N., Szweda, L. I., Markesbery, W. R., and Butterfield, D. A. (**2001**) *J. Neurochem. **78,*** 413-416.

75. Mark, R. J., Lovell, M. A., Markesbery, W. R., Uchida, K., and Mattson, M. P. (**1997**) *J. Neurochem. **68,*** 255-264.

76. Pedersen, W. A., Cashman, N. R., and Mattson, M. P. (**1999**) *Exp. Neurol. **155,*** 1-10.

77. Neely, M. D., Sidell, K. R., Graham, D. G., and Montine, T. J. (**1999**) *J. Neurochem. **72,*** 2323-2333.

78. Lovell, M. A., Xie, C., and Markesbery, W. R. (**2000**) *Free Radic. Biol. Med. **29,*** 714-720.

79. Uchida, K., Kanematsu, M., Sakai, K., Matsuda, T., Hattori, N., Mizuno, Y., Suzuki, D., Miyata, T., Noguchi, N., Niki, E., and Osawa, T. (**1998**) *Proc. Natl. Acad. Sci. U S A **95,*** 4882-4887.

80. Haenen, G. R., Vermeulen, N. P., Tai Tin Tsoi, J. N., Ragetli, H. M., Timmerman, H., and Blast, A. (**1988**) *Biochem. Pharmacol. **37,*** 1933-1938.

81. Uchida, K., Kanematsu, M., Morimitsu, Y., Osawa, T., Noguchi, N., and Niki, E. (**1998**) *J. Biol. Chem.* ***273,*** 16058-16066.

82. Uchida, K., Szweda, L. I., Chae, H. Z., and Stadtman, E. R. (**1993**) *Proc. Natl. Acad. Sci., U S A* ***90,*** 8742-8746.

83. Karas, G. B., Burton, E. J., Rombouts, S. A. R. B., van Schijndel, R. A., O'Brien, J. T., Scheltens, P., McKeith, I. G., Williams, D., Ballard, C., and Barkhof, F. (**2003**) *NeuroImage* ***18,*** 895-907.

84. Mouton, P. R., Martin, L. J., Calhoun, M. E., Forno, G. D., and Price, D. L. (**1998**) *Neurobiol. Aging* ***19,*** 371-377.

85. Keller, J. N., Schmitt, F. A., Scheff, S. W., Ding, Q., Chen, Q., Butterfield, D. A., and Markesbery, W. R. (**2005**) *Neurology* ***64,*** 1152-1156.

86. Smith, A. D. (**2001**) *Proc. Natl. Acad. Sci.* ***99,*** 4135-4137.

87. Detoledo-Morrell, L., Sullivan, M. P., Morrell, F., Wilson, R. S., A., B. D., and Spencer, S. (**1997**) *Neurobiol. Aging* ***18,*** 463-468.

88. Ohnishi, T., Matsuda, H., Tabira, T., Asada, T., and Uno, M. (**2001**) *AJNR Am. J. Neuroradiol.* ***22,*** 1680-1685.

89. http://en.wikipedia.org/wiki/Hippocampus (2005), Wikipedia.

90. http://www.psychology.nottingham.ac.uk/staff/cr1/concepts.pdf.

91. http://www.macalester.edu/~psych/whathap/UBNRP/StemCells/bird_three.html.

92. http://www.neuroskills.com/index.shtml?main=/tbi/btemporl.shtml.

93. http://www.health.qld.gov.au/abios/tbi/brain.asp (2003), Queensland Health.

94. Cordis, G. A., Bagchi, D., Maulik, N., and Das, D. K. (**1994**) *J. Chromatogr. A* ***661,*** 181-191.

95. Draper, H. H., Csallany, A. S., and Hadley, M. (**2000**) *Free Rad. Biol. Med.* ***29,*** 1071-1077.

96. Büldt, A., and Karst, U. (**1997**) *Anal. Chem.* ***69,*** 3617-3622.

97. Sim, A. S., Salonikas, C., Naidoo, D., and Wilcken, D. E. L. (**2003**) *J. Chromatogr. B* ***785,*** 337-344.

98. Yoshino, K., Matzuura, T., Sano, M., Saito, S., and Tomita, T. (**1986**) *Chem. Pharm. Bull.* ***34,*** 1694-1700.

99. Holley, A. E., Walker, M. K., Cheeseman, K. H., and Slater, T. E. (**1993**) *Free Rad. Biol. Med.* ***15,*** 281-289.

100. Bailey, A. L., Wortley, G., and Southon, S. (**1997**) *Free Rad. Biol. Med.* ***23,*** 1078-1085.

101. Matsuoka, M., Imado, N., and Maki, T. (**1996**) *Chromatographia* ***43,*** 501-506.

102. Spies-Martin, D., Sommerburg, O., Langhans, C.-D., and Leichsenring, M. (**2002**) *J. Chromatogr. B* ***774,*** 231-239.

103. Bruenner, B. A., Jones, A. D., and German, J. B. (**1996**) *Anal. Biochem.* ***241,*** 212-219.

104. Deng, C., and Zhang, X. (**2004**) *Rapid Commun. Mass Spectrom.* ***18,*** 1715-1720.

105. Luo, X. P., Yazdanpanah, M., Bhooi, N., and Lehotay, D. C. (**1995**) *Anal. Biochem.* ***228,*** 294-298.

106. Spiteller, G., Kern, W., and Spiteller, P. (**1999**) *J. Chromatogr. A.* ***843,*** 29-98.

107. Thomas, M. J., Robison, T. W., Samuel, M., and Forman, H. J. (**1995**) *Free Rad. Biol. Med.* ***18,*** 553-557.

108. Deighton, N., Magill, W. L., Bremner, D. H., and Benson, E. E. (**1997**) *Free Rad. Res.* ***27,*** 255-265.

109. Ravandi, A., Kuksis, A., Myher, J. J., and Marai, L. (**1995**) *J. Biochem. Biophys. Methods* ***30,*** 271-285.

110. Zurek, G., and Karst, U. (**1999**) *J. Chromatogr. A* ***864,*** 191-197.

111. Islam Williams, T., Lovell, M. A., and Lynn, B. C. (**2005**) *Anal. Chem.* ***77,*** 3383-3389.

112. Gioacchini, A. M., Calonghi, N., Boga, C., Cappadone, C., Masotti, L., Roda, A., and Traldi, P. (**1999**) *Rapid Commun. Mass Spectrom.* ***13,*** 1573-1579.

113. Robards, K., Haddad, P. R., and Jackson, P. E. (**2001**) Principles and Practice of Modern Chromatographic Methods, Bookcraft (Bath) Ltd., Somerset, UK.

114. Karger, B. L., Snyder, L. R., and Horvath, C. (**1973**) An Introduction to Separation Science, Wiley-Interscience, New York, NY.

115. http://www.shu.ac.uk/schools/sci/chem/tutorials/chrom/chrom1.htm.

116. Giddings, J. C. (**1991**) Unified Separation Science, Wiley, New York, NY.

117. Foley, J. P. (**1991**) *Analyst* ***116,*** 1275-1279.

118. http://www.ionsource.com/tutorial/chromatography/rphplc.htm (**2001**) (Guzzetta, A., Ed.).
119. Young, C. S., and Weigand, R. J. (**2002**) *LCGC North America **20,** 465-473*.
120. Covey, T. R., Lee, E. D., Bruins, A. P., and Henion, J. D. (**1986**) *Anal. Chem. **58,*** 1451A-1461A.
121. Volmer, D. A., and Vollmer, D. L. (**1996**) *LC-GC **14,*** 216-219.
122. Whitehouse, C. M., Dreyer, R. N., Yamashita, M., and Fenn, J. B. (1985) *Analytical Chemistry* **57,** 675-679.
123. Fenn, J. B., Mann, M., Meng, C. K., Wong, S. F., and Whitehouse, C. M. (1989) *Science* **246,** 64-71.
124. Yamashita, M., and Fenn, J. B. (1984) *Journal of Physical Chemistry* **88,** 4451-4459.
125. http://www.waters.com/WatersDivision/ContentD.asp?watersit=EGOO-66YNU9.
126. Glish, G. L., and Vachet, R. W. (**2003**) *Nature **2,*** 140-150.
127. Kebarle, P. (**2000**) *J. Mass Spectrom. **35,*** 804-817.
128. Jonscher, K. R., and Yates III, J. R. (**1997**) *Anal. Biochem. **244,*** 1-15.
129. March, R. E. (**1997**) *J. Mass Spectrom. **32,*** 351-369.
130. de Hoffmann, E., and Stroobant, V. (**1999**) Mass Spectrometry: Principles and Applications, John Wiley and Sons, Ltd., Chichester, England.
131. March, R. E., and Todd, J. F. J. (**1995**) Practical Aspects of Ion Trap Mass Spectrometry, CRC Press, Boca Raton, FL.
132. Paul, W. (**1990**) *Agnew. Chem. Int. Ed. **29,*** 739-746.
133. Wenner, B. R., and Lynn, B. C. (**2004**) *J. Am. Soc. Mass Spectrom. **15,*** 150-157.
134. Nash, T. (**1953**) *Biochemistry **55,*** 416-421.
135. Sawicki, E., and Carnes, R. A. (**1968**) *Mikrochim. Acta,* 148-159.
136. Compton, B. J., and Purdy, W. C. (**1980**) *Can. J. Chem. **58,*** 2207-2211.
137. McLafferty, F. W., and Tureček, F. (**1993**) *Interpretation of Mass Spectra*, University Science Books, Mill Valley, CA.
138. Petersen, R. C. (**2000**) *Neurologia **15,*** 93-101.
139. Petersen, R. C., Smith, G. E., Waring, S. C., Ivnik, R. J., Tangalos, E. G., and Kokmen, E. (**1999**) *Arch. Neurol. **56,*** 303-308.

140. Winblad, B., Palmer, K., Kivipelto, M., Jelic, V., Fratiglioni, L., Wahlund, L. O., Nordberg, A., Backman, L., Albert, M., Almkvist, O., Arai, H., Basun, H., Blennow, K., de Leon, M., DeCarli, C., Erkinjuntti, T., Giacobini, E., Graff, C., Hardy, J., Jack, C., Jorm, A., Ritchie, K., van Duijn, C., Visser, P., and Petersen, R. C. (**2004**) *J. Intern. Med.* ***256,*** 240-246.

141. Morris, J. C., Heyman, A., Mohs, R. C., Hughes, J. P., van Belle, G., Fillenbaum, G., Mellits, E. D., and Clark, C. (**1989**) *Neurology* **39,** 1159-1165.

142. Karrasch, M., Sinervä, E., Grönholm, P., Rinne, J., and Laine, M. (**2005**) *Acta Neurol. Scand.* ***111,*** 172-179.

143. http://www.sigmaaldrich.com/img/assets/7361/Primer-H&Emay04.pdf (Brown, H., Ed.), Sigma-Aldrich.

144. http://www.ihcworld.com/_protocols/special_stains/bielschowsky.htm, IHC World Online Information Center For Immunohistochemistry.

145. http://alzheimer.wustl.edu/adrc2/Research/Neuropathology/abeta_SP.html (**1995**), Daniel McKeel, M.D.

146. http://en.wikipedia.org/wiki/Alpha-synuclein (**2005**), Wikipedia: The Free Encyclopedia.

147. Braak, H., and Braak, E. (**1991**) *Acta Neuropathol.* ***82,*** 239-259.

148. Ohm, T. G., Muller, H., Braak, H., and Bohl, J. (1995) *Neuroscience* **64,** 209-217.

149. Newell, K. L., Hyman, B. T., Growdon, J. H., and Hedley-Whyte, E. T. (1999) *Journal of Neuropathology and Experimental Neurology* **58,** 1147-1155.

150. Markesbery, W. R., Schmitt, F. A., and Kryscio, R. J. (**2005**) *Arch. Neurol.* ***in press***.

151. McClave, J. T., Dietrich II, F. H., and T., S. (**1997**) Statistics, Prentice Hall, Inc., Upper Saddle River, NJ.

152. http://www.anselm.edu/homepage/jpitocch/anova/mcompex/multcompex.html (Pitocchelli, J., Ed.), Vol. **2001**, Saint Anselm College.

153. Skoog, D. A., West, D. M., Holler, F. J., and Crouch, S. R. (**2000**) Analytical Chemistry: An Introduction, Harcourt Inc., Orlando, FL.

154. http://learn.lboro.ac.uk/sci/ma/mlsc/documents/Mannwhitney.pdf (**2004**) (Shier, R., Ed.), Mathematics Learning Support Center.

155. Lovell, M. A., Xie, C., and Markesbery, W. R. (**1998**) *Neurology **51,*** 1562-1566.

156. Praticó, D., Clark, C. M., Liun, F., Lee, V. Y. M., and Trojanowski, J. Q. (**2002**) *Arch. Neurol. **59,*** 972-976.

157. Migliore, L., Fontana, I., Trippi, F., Colognato, R., Coppedé, F., Tognoni, G., Nucciarone, B., and Siciliano, G. (**2005**) *Neurobiol. Aging **26,*** 567-573.

158. Wang, J., Xiong, S., Xie, C., Markesbery, W. R., and Lovell, M. A. (**2005**) *Neurobiol. Aging **submitted for publication***.

159. Islam Williams, T., Lynn, B. C., Markesbery, W. R., and Lovell, M. A. (**2005**) *Neurobiol. Aging*.

160. Nunomura, A., Perry, G., Aliev, G., Hirai, K., Takeda, A., Balraj, E. K., Jones, P. K., Ghanbari, H., Wataya, T., Shimohama, S., Chiba, S., Atwood, C. S., Petersen, R. B., and Smith, M. A. (**2001**) *J. Neuropathol. Exp. Neurol. **60,*** 759-767.

161. Perry, G., Srinivas, R., Nunomura, A., and Smith, M. A. (**2003**) The role of oxidative mechanisms in neurodegenerative diseases, ISN Neuropath Press, Basel.

162. Petersen, R. C., Thomas, R. G., Grundman, M., Bennet, D., Doody, R., Ferris, S., Galasko, D., Jin, S., Kaye, J., Levey, A., Pfeiffer, E., Sano, M., van Dyck, C. H., and Thal, L. J. (**2005**) *N. Eng. J. Med. **352,*** 2379-2388.

163. Quinn, J. F., Montine, K. S., Moore, M., Morrow, J. D., Kaye, J. A., and Montine, T. J. (**2004**) *J. Alzheimer's Dis.* **6,** 93-97.

PART TWO

BACTERIAL CELL MEMBRANE PROTEOME INVESTIGATIONS

Chapter 2.1
Introduction

Ethanol Tolerance in Thermophilic Bacteria

Fossil fuels, including coal, oil and natural gas, are the major source of inexpensive energy that powers modern industrial civilization. These energy sources have been produced over millennia from the remains of prehistoric plants and animals. As humanity becomes increasingly advanced in technology, more energy is consumed to sustain the pace of changing requirements. Aside from heightened concerns about pollution, global warming and national security issues, existing reserves of this energy resource are depleting at a rapid rate. Use of fossil fuels has nearly doubled every 20 years since 1900. Petroleum geologists have known for the past 50 years that global oil production would hit the zenith and begin its inexorable decline soon after the year 2000. Furthermore, no renewable energy systems to date have the potential to generate more than a fraction of the power currently being delivered by fossil fuels. As a result, research in alternative sources of fuel has received considerable focus in recent years. Harnessing microbes to convert abundant fibrous biomass from the agricultural sector into ethanol for exploitation as fuel can offer an efficient and environmentally clean answer to the energy question. The thermophile *Clostridium thermocellum*, a gram-positive, chemotrophic, cellulolytic and obligately anaerobic bacterium, has generated considerable interest in the area of bio-ethanol production due to its ability to ferment complex carbohydrates, such as cellulose, in a single step reaction, thus eliminating the need for biomass pretreatment (1). When this organism grows on cellulose as the sole carbon source, ethanol, acetic acid, lactic acid and CO_2 are generated. The ability of *C. thermocellum* to ferment cellulose is a remarkable advantage over fungal species such as yeast, which can only ferment simple sugars via multi-step mechanisms.

Despite the benefits, *C. thermocellum* is strongly inhibited at low ethanol concentrations (< 2% v/v) and provides reduced ethanol yields compared to established industrial fermenters, including yeast (> 6% v/v). The restrained growth of the ethanol-challenged species displays a short time span of little or no inhibition followed by a

period of growth impediment, and finally a time of stunted but sustained exponential growth (2). This is in contrast to ethanol inhibition observed in yeast, where an immediate cessation of growth occurs. Studies have shown that inhibition of fermentation is due to a staling effect, which refers to accumulation of toxic metabolic byproducts from the organism (3). Recovery of alcohol at such low concentrations with conventional distillation techniques becomes unfavorably expensive. In order for *C. thermocellum* to be effectively exploited in ethanol production, it is necessary to increase the growth rate, improve cellulase activity and increase ethanol tolerance and production (4). Through sequential transfer techniques, several ethanol-tolerant strains have been developed, some able to tolerate as high as 8% ethanol (1, 4-7). The ability of these bacteria to sustain themselves on cellulose indicates the presence of a viable cellulase system that can generate ethanol. While none of the strains to date can match fungal ethanol tolerance, an understanding of the biochemistry behind this phenomenon can offer insight into the future development of more ethanol-tolerant derivatives of this organism.

The effects of ethanol on microbes have been investigated in some detail (2, 3, 8-12). The capacity of this alcohol to shut down metabolism is related to its partitioning between the aqueous and hydrophobic milieu in the cell. It has been shown that most of the effects of ethanol do not involve specific interactions or receptors but are the aftermath of a more generalized mechanism associated with hydrophobic associations (11). Nonionized species in the cellular matrix, including ethanol, influence membrane physiology through partitioning in lipid bi-layers and interfering with lipid-lipid and lipid-protein interactions (2). It is believed that the effect of ethanol may be due to physical disturbances of the bi-layer or perhaps more direct interactions with membrane proteins, such as permeases. Roberts and co-workers (2) have shown that when ethanol is added to *C. thermocellum* cultures, changes in membrane composition occur after the period of growth arrest. They reported an increase in the proportion of normal and *anteiso*-branched fatty acids (lower melting points) at the expense of *iso*-branched fatty acids (higher melting points), leading to increases in fluidity and permeability of the membrane. Studies have shown that key targets for microbe growth inhibition are hydrophobic in nature and that cessation of growth is directly proportional to the concentration of perturbing molecules that have partitioned into the hydrophobic

environment (2). Such evidence clearly highlights the vulnerability of the cell membrane to ethanol-induced changes.

Since a significant contributor to bacterial death at elevated ethanol concentrations is the disruption of the cellular permeability barrier (3), it is most likely that a majority of the changes brought about by ethanol adaptation center around the membrane proteome (Figure 2.1.1). Herrero *et al*. proposed that effects of ethanol on membrane fluidity and inhibition of certain enzymes associated with sugar metabolism lead to low tolerance of the bacterium to ethanol (2). In ethanol-challenged systems, the leakage of appreciable quantities of proteins also indicates membrane disruption (11). Hydrophobic associations are elemental in the preservation of membrane integrity and structure, protein folding and quaternary structure of proteins. The hydrogen bonding network of water is largely responsible for the strength of hydrophobic associations. While ethanol does form hydrogen bonds, its presence in aqueous solutions can limit the freedom of the hydrogen bonding lattice structure. This decline in the strength of the hydrophobic interactions can weaken the membrane by weakening van der Waal's interactions among acyl chains and hydrophobic protein surfaces, further increasing membrane permeability (3). It is also believed that ethanol can increase the polarity and dehydrate the cell membrane. By replacing water, ethanol induces altered protein folding and interactions within the bi-layer (11). While the exact mechanism of bacterial growth inhibition and adaptation to ethanol is unknown, analysis of differentially expressed membrane proteins in wild type and ethanol-adapted strains through proteomics studies can provide the insight necessary to tackle questions about the nature of ethanol tolerance.

Proteomic Analysis of Cell Membranes

Proteomics is the study of the structural and functional aspects of the protein complement of the genome. The term was created to draw parallels with genomics, although it is significantly more complicated. While the genome of an organism is rather static, the proteome can differ radically and is constantly changing through biochemical interactions with the genome and the environment. Protein expression can also vary with

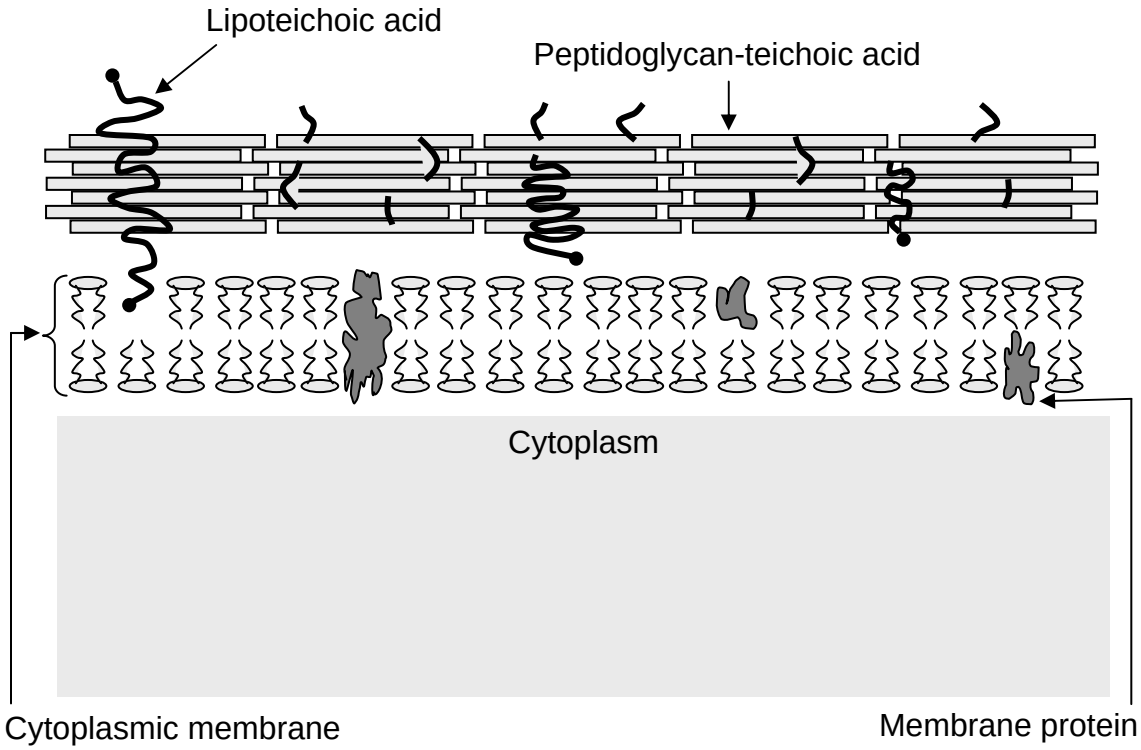

Figure 2.1.1. The Gram positive bacterial cell envelope.

changing stages of the cell cycle and environmental conditions. Needless to say, proteomics investigations have played a dominant role in the field of biological mass spectrometry in the aftermath of the human genome project. As such, a considerable amount of resources and manpower have been dedicated to the improvement of protein separation and analysis techniques. Despite its limitations, sodium dodecyl sulfate polyacrylamide gel electrophoresis (SDS-PAGE) is still the gold-standard of protein separation for subsequent analysis by mass spectrometry. Pre-fractionation techniques (i.e. to separate hydrophobic membrane proteins from cytosolic proteins) coupled to SDS-PAGE have been useful in studying the proteome at increasingly detailed levels. However, the cell membrane sub-proteome is frequently under-represented on 2D gel maps. This has largely been attributed to their low abundance, hydrophobicity and solubility issues encountered in the first dimension or isoelectric focusing step of standard 2D-PAGE (13). By virtue of the unique nature of the cell membrane as the site of first contact of the external environment with the cell, a detailed understanding of the membrane proteome is critical in many biological investigations.

In recent years, shotgun analyses have become popular 'gel-free' alternatives. MudPIT (Multidimensional Protein Identification Technology) is a technique for the separation and identification of complex protein and peptide mixtures that has developed considerable interest (14-16). In place of 2D gel electrophoresis, MudPIT separates peptides in 2D liquid chromatography, which allows the direct interfacing with a mass spectrometer. In the MudPIT experiment, biphasic columns are constructed of strong cation exchange (SCX) stationary phase in series with reversed phase (RP) material inside fused silica capillaries. The chromatography proceeds in cycles, each comprising an increase in salt concentration to free peptides from the SCX resin, after which they bind to the RP resin. A typical RP gradient to increasing hydrophobicity is then applied to progressively elute peptides from the RP into the ion source for analysis by mass spectrometry. A disadvantage to this methodology is that data interpretation and analysis is often not as straightforward compared to 2D-PAGE (17).

Despite the problems encountered with gel-based approaches, they are effective in providing a useful analytical tool for the generation of membrane protein profiles, along with quantitative comparisons of numerous proteins concurrently. Significant research

and methods development has been focused in the gel electrophoresis of membrane proteins to exploit the many advantages of this technique in membrane proteome analyses. Organic solvents and chemical modifiers in IEF solubilization buffers followed by analysis on one-dimensional gels or carefully modified two-dimensional gels (excluding isoelectric focusing) provide effective alternatives for improving membrane protein representation in these techniques. However, it should be noted that no approach offers a universal solution for all membrane proteins, and, experimental conditions ought to be optimized for the particular membrane-enriched sample at hand.

Polyacrylamide Gel Electrophoresis

The polyacrylamide gel electrophoresis technique (PAGE) was introduced by Raymond and Weintraub in 1959 (18). Since then, the methodology has been improved and adapted to various applications in a variety of scientific fields. SDS-PAGE is the most widely used method for qualitatively analyzing protein mixtures. Separation is based primarily on molecular weight (19). SDS (CH_3-$(CH_2)_{10}$-$CH_2OSO_3^-Na^+$) is an anionic detergent that can bind to hydrophobic portions of a protein (one SDS anion to two amino acids), disrupting its three dimensional structure and allowing it to exist stably in solution in an extended conformation. As a result, all the proteins contain primary structure only, have a large negative charge and the length of the SDS-protein complex is proportional to its molecular weight.

During an SDS-PAGE experiment, current is applied to opposite ends of an acrylamide gel support matrix (stationary phase) in the presence of an appropriate running buffer. Sample proteins are loaded on the cathode end of the assembly. The current from the cathode repels the negatively charged SDS-protein complexes while the anode, on the opposite end of the gel, simultaneously attracts them. The macromolecules are thus forced to move through the pores when electrical current is applied. Their rate of migration through the electric field depends on the strength of the field, size and shape of the molecules, relative hydrophobicity of the samples and the ionic strength and temperature of the buffer in which the molecules are moving. After staining, the separated macromolecules can be observed on the gel. The relative ease of execution and

wide application of SDS-PAGE have made it an important analytical technique in many areas, particularly macromolecular separations.

Electrophoresis Theory

Electrophoresis instruments are simple electrical circuits that operate in accordance with Ohm's law:

$$V = IR \tag{2.1.1}$$

where, V = electrical field in volts
I = current in milliamperes
R = resistance in ohms.

For a given an amount of voltage, a constant amount of current will flow through the circuit. With increasing resistance across any element, the total applied voltage increases. The resistance is inversely proportional to the ionic strength of the buffer, as well as the cross sectional area of a given element. As such, gel analysis can be fine-tuned by manipulating these parameters.

The electrophoresis technique is based on the property of charged molecules migrating in an electric field (20). A particular molecule with charge q in an electric field (E) experiences a force (F) as follows:

$$F = qE\ . \tag{2.1.2}$$

The molecule quickly reaches a velocity (v) in which the electric field is balanced by the frictional force:

$$qE = fv \tag{2.1.3}$$

where, f = frictional coefficient.

The electrophoretic mobility of the molecule (μ) is the velocity per unit field strength. It is expressed as a ratio of the net charge to the frictional coefficient.

$$\mu = \frac{v}{E} = \frac{q}{f} (cm^2/V\text{-}sec). \quad (2.1.4)$$

The frictional coefficient can be defined as:

$$f = 6\pi\eta r \quad (2.1.5)$$

where, η = viscosity of the medium

r = stokes radius of the molecule.

In 'free' electrophoresis, mobility is dependent on charge-to-mass-ratio. However, there are some complications to this simplistic view. The charges and frictional coefficients of a molecule are not only determined by size, shape and composition but by solvent conditions as well, including pH, counter-ions and temperature. Furthermore, counter-ions can shield the migrating analyte from the electric field, reducing the effective field strength it experiences.

Acrylamide Polymerization

First introduced by Chrambach and Rodbard (21), polyacrylamide is a synthetic polymer prepared by polymerizing the acrylamide monomer into long chains, cross-linked into three-dimensional structures. Cross-linked gels are prepared from the polymerization of acrylamide monomer in the presence of smaller amounts of N,N'-methylene-bis-acrylamide (*bis*), as shown in Figure 2.1.2. This type of polymerization is an example of free-radical catalysis, brought about by the addition of ammonium persulfate (APS) and the base N,N,N',N'-tetramethylenediamine (TEMED). TEMED catalyzes the decomposition of the persulfate ion to produce a free radical (22):

$$S_2O_8^{2-} + e^- \rightarrow SO_4^{2-} + SO4^{-\bullet} \quad (2.1.6)$$

The polymerization reaction can be represented as follows:

$$R^{\bullet} + M \rightarrow RM^{\bullet}$$

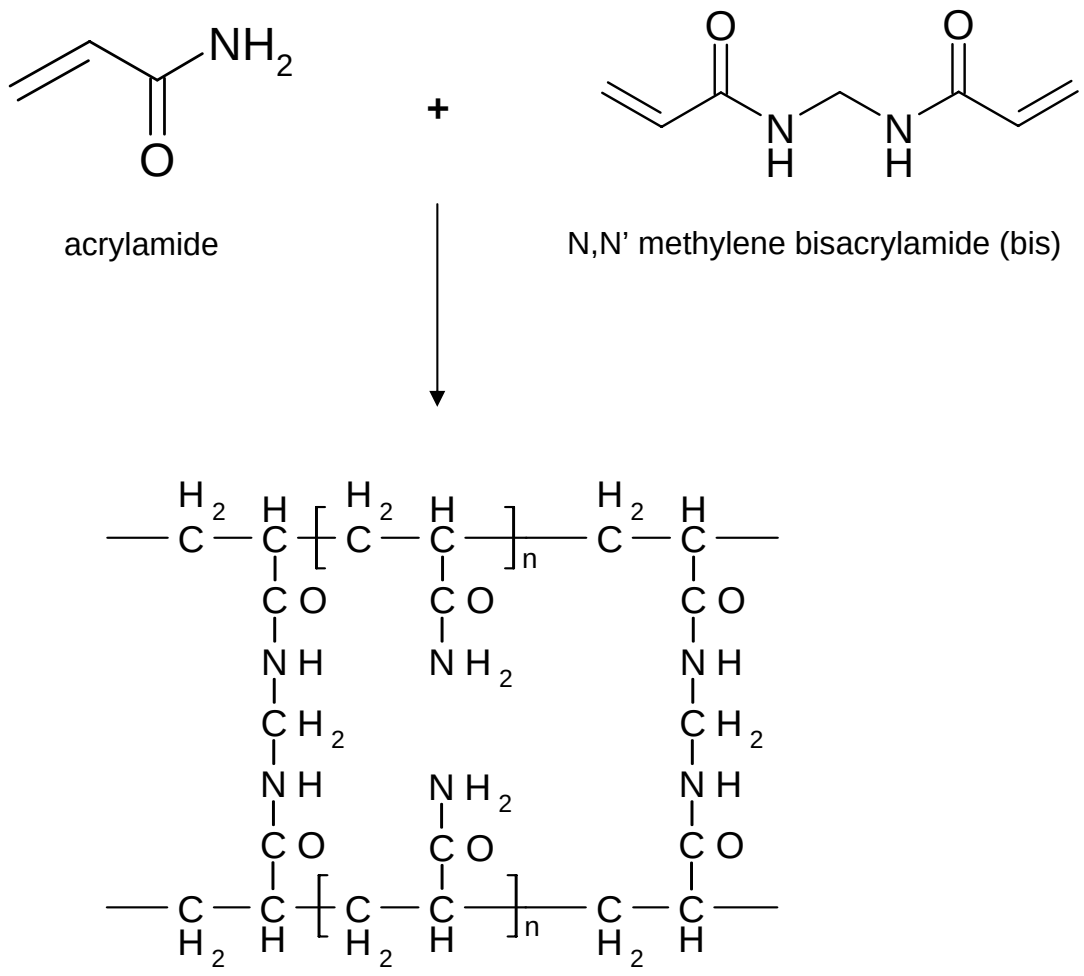

Figure 2.1.2. Polymerization of acrylamide.

$$RM^{\bullet} + M \rightarrow RMM^{\bullet}$$
$$RMM^{\bullet} + M \rightarrow RMMM^{\bullet} \text{ and so forth} \qquad (2.1.7)$$

where, $R^{\bullet}$ = sulfate radical

M = acrylamide monomer.

In this manner, long chains of acrylamide are synthesized, which are then cross-linked by the introduction of the occasional *bis*-acrylamide molecule. Oxygen has a tendency to quench free radical reactions and so the gel mixture is normally degassed prior to addition of catalyst. The polymerization efficiency can range from 95 – 98%. The polyacrylamide gel serves two purposes. It facilitates the diffusion of convective currents that would result in localized heating in the matrix, causing irregular migration patterns. The gel also provides a molecular sieve that enhances analyte separation based on molecular weight.

The SDS-PAGE Experiment

Gel solutions for SDS-PAGE are usually prepared with appropriate amounts of SDS (to maintain denaturing conditions) and Tris buffer (to maintain the desired pH and create a greater ionic strength within the gel). The stacking gel is usually prepared with a pH of 6.8 while the separating gel has a pH of 8.8. Catalysts are added immediately before pouring the gel sandwich between two glass plates. The main separating gel solution is poured first and allowed to polymerize. Next, a shorter stacking gel is poured on top of the separating gel, and it is in this gel that wells are formed and proteins loaded. Samples for SDS-PAGE analysis are boiled for 5 min in sample buffer (pH 6.8) to denature the proteins. The β-mercaptoethanol in this buffer is added to prevent oxidation of cysteine residues of protein disulfide bridges while SDS binds to the proteins. The end result is a collection of completely denatured, rod-shaped protein-SDS complexes with net negative charge. These charges overwhelm the inherent charge of the proteins and give every protein the same charge-to-mass ratio. Bromphenol blue or some other ionizable dye in the sample buffer allows the progress of the electrophoresis experiment to be tracked. The cathodic and anodic ends of the electrophoresis setup are filled with Tris-based running buffer. Sucrose or glycerol, present in the sample buffer, increases the

density of the sample solution thus enabling the sample to settle through the electrophoresis buffer to the bottom when injected into the loading well.

Electrophoresis is conducted under constant voltage or constant current conditions. Once all samples have passed through the stacking gel and entered the separating gel, the negatively charged protein-SDS complexes continue to move toward the anode. Since they have the same charge per unit length, these complexes migrate into the separating gel with the same mobility for a given electric field. During passage through the separating gel, the proteins separate as a result of the molecular sieving properties of the gel. Smaller proteins can travel more quickly compared to larger ones, which are successively retarded by frictional resistance. Being a small molecule, the bromphenol blue dye is almost totally unretarded and therefore indicates the electrophoresis front. As soon as the dye front reaches the bottom of the gel, the power is turned off and the gel is removed from between the glass plates for subsequent protein staining and analysis.

Polyacrylamide gels can be cast in a single percentage of acrylamide or with varying gradients. The gradient gels provide continuous decrease in pore size from the top to the bottom of the gel, either exponentially or linearly, and can offer improved resolution of proteins. During electrophoresis in gradient gels, proteins continue to migrate until the decreasing pore size impedes further advancement. Once the pore limit is reached, the protein banding pattern remains more or less the same with time, although migration does not cease completely. The main advantage of using gradient gels is that a much greater range of protein MW range can be interrogated, compared to a fixed-percentage gel. It is possible for larger proteins to enter the gel but they start to separate immediately because of the sieving effect of the gel (22).

The use of a short stacking gel on top of the separating gel also allows for better resolution. The stacking gel aids in the concentration of the protein sample into a sharp band prior to entering the main separating gel. By preparing a stacking gel with large pore size, the proteins can migrate freely and concentrate under the electric field, as a result of isotachophoresis. This band sharpening effect relies on the fact that the trailing ions (i.e. glycine in standard Laemmli-SDS-PAGE) in electrophoresis buffers have a

lower electrophoretic mobility than the protein-SDS complexes, which in turn have lower mobility than the leading ions (i.e. Cl^-) in regions of high field strength (22).

Protein Visualization

A suitable staining protocol can be used to visualize separated proteins on a polyacrylamide gel. The Colloidal Coomassie (Coomassie Brilliant Blue G 250) staining protocol offers a sensitive, consistent, simple method and provides nanogram-level detection of proteins (23). The technique is based on the colloidal properties of Coomassie Blue dyes generated in methanol-water binary solvents containing inorganic acids and high salt concentrations (Figure 2.1.3). The anionic form of the dye is produced in acidic staining media and combines with the protonated amino groups of proteins through electrostatic interactions. The free dye in solution is greatly reduced due to the hydrophobic effect, resulting in low background staining and high affinity binding of the dye to the proteins fixed in the gel.

In the Colloidal Coomassie Blue staining protocol, gels are fixed for one hour with a solution containing 80% water, 20% methanol and 1% *o*-phosphoric acid. This ensures that the separated proteins do not diffuse and migrate. Overnight staining is performed in an aqueous solution of 0.001 g/mL Coomassie G-250 dye, 0.08 g/mL ammonium sulfate, 20% methanol and 1.6% *o*-phosphoric acid. The gel is then transferred into neutralization buffer (0.1M Tris, pH 6.5) for 1-3 min. This is followed by washing with 25% methanol for less than a minute. Then, the gel is immersed in an aqueous stabilizing solution of 0.2 g/mL ammonium sulfate. The gels can be safely stored in 1% aqueous glycerol solutions until further analysis.

In-Gel Digestion

As staining methods with increasing sensitivity were developed, protein identification became limited by the sensitivity of Edman sequencing, since this was the most well-established method for protein analysis. With the development of ESI-MS and MALDI-TOF-MS, mass spectrometry became recognized as a much more sensitive and worthwhile tool for such purposes. Following separation on a polyacrylamide gel,

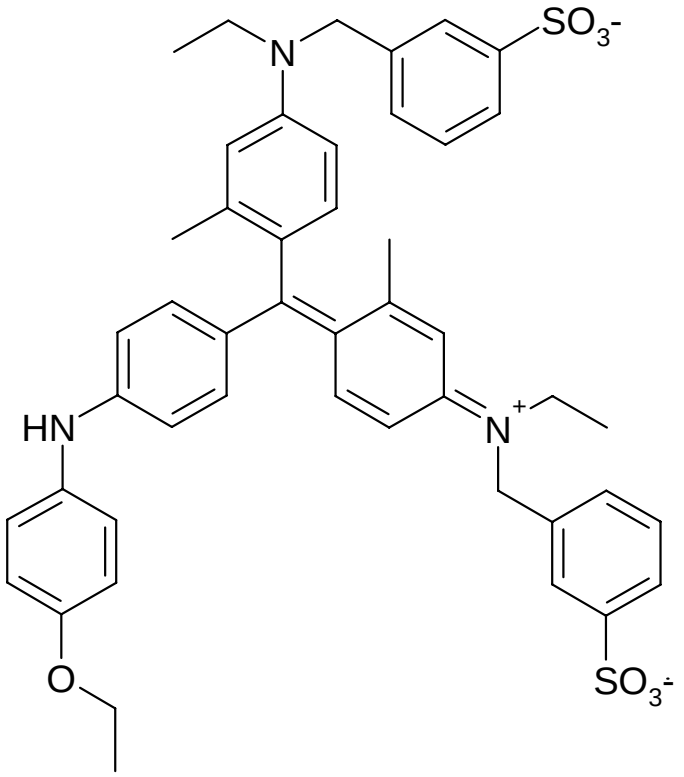

Figure 2.1.3. Coomassie Brilliant Blue G 250.

proteins are excised, digested and the resulting peptides subjected to peptide mass fingerprinting (PMF) methods. For protein identification, PMF uses the peptide masses to search the protein databases for *in silico* or theoretical digest patterns that match the experimental data. Mass spectrometric analyses can now be performed on picomole and sub-picomole levels of PAGE-separated proteins following in-gel digestion procedures to fragment the proteins into peptides.

In-gel digestion techniques can vary from laboratory to laboratory but they all share some basic components. It is essential that contamination from human keratins be reduced as far as possible, so that peptide signals are not suppressed during mass spectrometric experiments. Protein spots/bands are excised from the gel. SDS, unpolymerized acrylamide and other buffer constituents that could potentially generate a high background in MS analyses are removed from the excised gel plugs in several NH_4HCO_3/ACN washing steps. One particular method employs a 25 mM NH_4HCO_3 as the first wash (10 min), followed by a 1:1 mixture of 25 mM NH_4HCO_3 and ACN (10 min), terminating with a pure ACN wash (10 min). The washing steps dry the gel pieces, which are subsequently rehydrated with a 25 mM NH_4HCO_3 buffer containing a proteolytic enzyme, such as trypsin. In most work, trypsin is the protease of choice of peptide mass fingerprinting because it is very reliable and substrate-specific. Tryptic digests produce peptides with C-terminal basic residues (Arg and Lys), rendering them easily ionizable, thus facilitating mass spectrometric analyses. Approximately 10% of all bonds in a protein are suitable cleavage sites for this enzyme. Trypsin is usually dissolved in ice cold buffer, just prior to use, so as to limit auto-proteolysis. The gel pieces are incubated in trypsin at 4^{o}C for 40 min, following which the enzyme solution is removed and fresh 25 mM NH_4HCO_3 buffer (~10 µL) is added. After incubation of the gel pieces at 50^{o}C for 4 hours, 1 µL of formic acid is added to encourage protonation of tryptic peptides. The resulting peptides are then subjected to mass spectrometric analysis.

MALDI-TOF-MS

Matrix-assisted laser desorption/ionization or MALDI was first introduced by Karas and Hillenkamp in 1988 (24). They discovered that the incorporating the analyte

into the crystalline structure of small UV-absorbing organic molecules (matrix) provided a vehicle for ions to be created from polar or charged biomolecules. This assured that the once restrictive mass limitations of laser desorption/ionization could be circumvented. Since then, MALDI has evolved into a powerful ionization method for biological molecules and synthetic polymers. MALDI coupled to time-of-flight MS (TOF-MS), a mass analyzer designed in 1955 by Wiley and McLaren (25), has evolved into the workhorse and benchmark macromolecule analyses. Since MALDI ions are produced by a pulsed laser, these ion sources can be conveniently coupled to TOF mass spectrometers, which require a well-defined start time. With the establishment of proteomics as a key area of research in mass spectrometry, interest in the analysis of biomolecules has risen dramatically and with it, interest in MALDI-TOF-MS.

The MALDI Process

In the MALDI technique, the sample is mixed with an excess of an appropriate matrix and irradiated with a laser beam of short (10 – 20 ns) pulses. The laser power is normalized with respect to the irradiated area (~ 50 μm), with power densities in the range of ~10^6 W/cm^2 irradiance power (26). Multiple laser pulses are usually averaged to enhance signal-to-noise ratio (SNR). The primary function of the matrix is to absorb radiation at the wavelength of the laser and subsequently transfer it to the analyte. Absorption of energy from the laser beam causes desorption of the matrix, along with analyte molecules. Ionization of the analyte follows through gas-phase proton-transfer reactions. MALDI is amenable to both positive and negative ion analyses. The MALDI mass spectra of proteins and peptides typically display singly protonated analyte molecules, along with their oligomeric ions (i.e. $[M+H]^+$, $[2M+H]^+$, etc.). In some instances, doubly and triply charged protonated ions of low abundance can also be generated. The higher the mass of the analytes, the greater their propensity to form multiply charged ions.

Sample Preparation

In a MALDI experiment, analyte and matrix is spotted onto a MALDI target (Figure 2.1.4) and subjected to laser irradiation. There are several methods available for

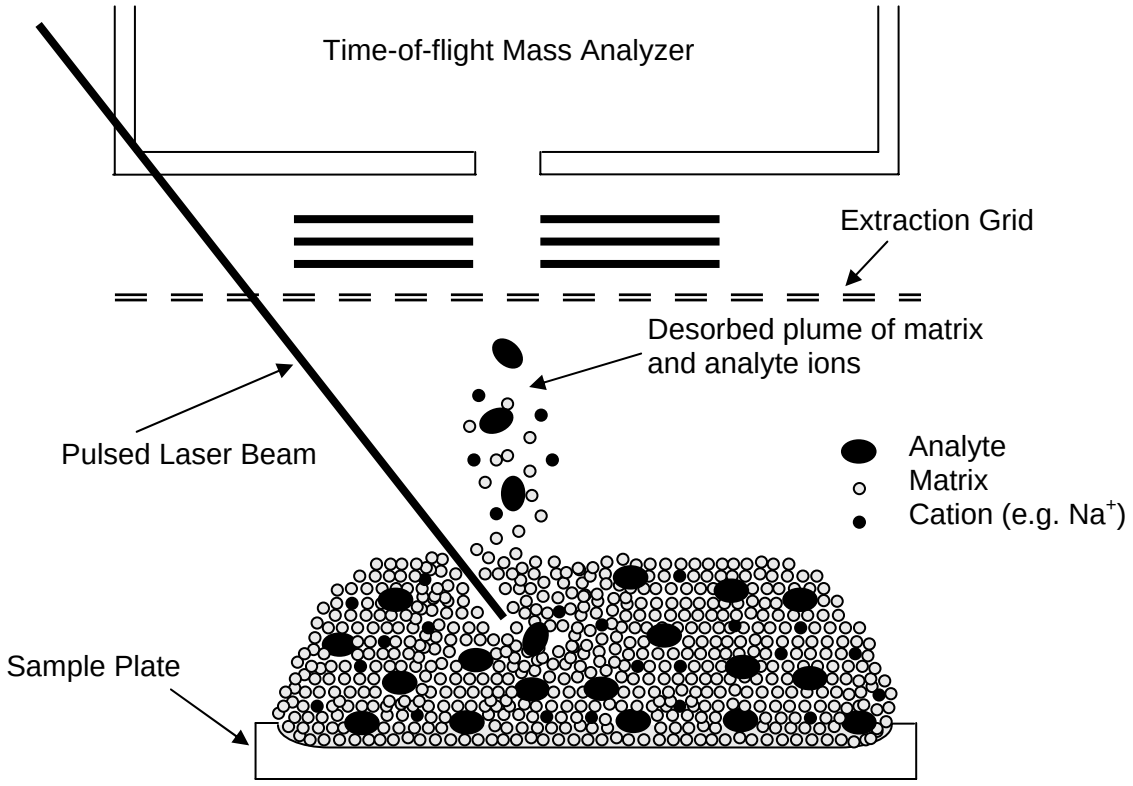

Figure 2.1.4. The MALDI process.

sample preparation and a good choice is made based on the needs of the sample at hand. For the analysis of tryptic peptides, the *fast matrix evaporation method* can be used (27). Matrix solution (in a volatile solvent, such as acetone) is applied to the surface of the MALDI target (Figure 2.1.5) to create a thin film of crystals. HCCA or α-cyano-4-hydroxycinnamic acid (Figure 2.1.6) is a well-suited matrix for peptide samples. This matrix can be prepared as a 10 mg/mL solution in acetone : 0.1% aqueous TFA = 9:1. Once the matrix layer is dry, about 0.8 μL of a protein digest is added on top of the polycrystalline film. Upon drying, the sample spots are washed with 0.1% aqueous TFA to remove unwanted salts. The matrix/analyte spots are dried again and subjected to MS.

Analysis by MALDI-TOF-MS is very sensitive to sample preparation and so care must be taken at each step to avoid contamination and eliminate any potential interference that could mask peptide peaks. By virtue of the homogeneous crystal structure generated, the fast matrix evaporation approach provides higher resolution, sensitivity and signal reproducibility compared to other sample preparation methods.

Mechanism of Desorption and Ion Formation

The mechanism by which molecules are desorbed and photoionized is not very well understood (Figure 2.1.4). However, three different models are now recognized as viable candidates for explaining this phenomenon. The first one involves quasithermal evaporation as a result of increased molecular motion. The second model describes the expulsion of upper lattice layers in the MALDI process. Finally, the third possibility explains desorption/ionization from a standpoint of increases in the hydrodynamic pressure due to rapidly expanding molecules in the crystal lattice (26). Regardless, all three hypotheses agree that the MALDI matrix plays a pivotal role in sample ionization. A good MALDI matrix should have high molar absorptivity at the selected laser wavelength (337 nm for a nitrogen laser), be able to form microcrystals with the analyte, have low sublimation temperature and possess the ability to engage in photochemical reactions (27). Laser radiation strikes the matrix, causing absorption of energy and heating of matrix crystals when they emit the absorbed energy. Matrix molecules sublime due to the heat generation, sending both matrix and analyte molecules into a dense gaseous plume.

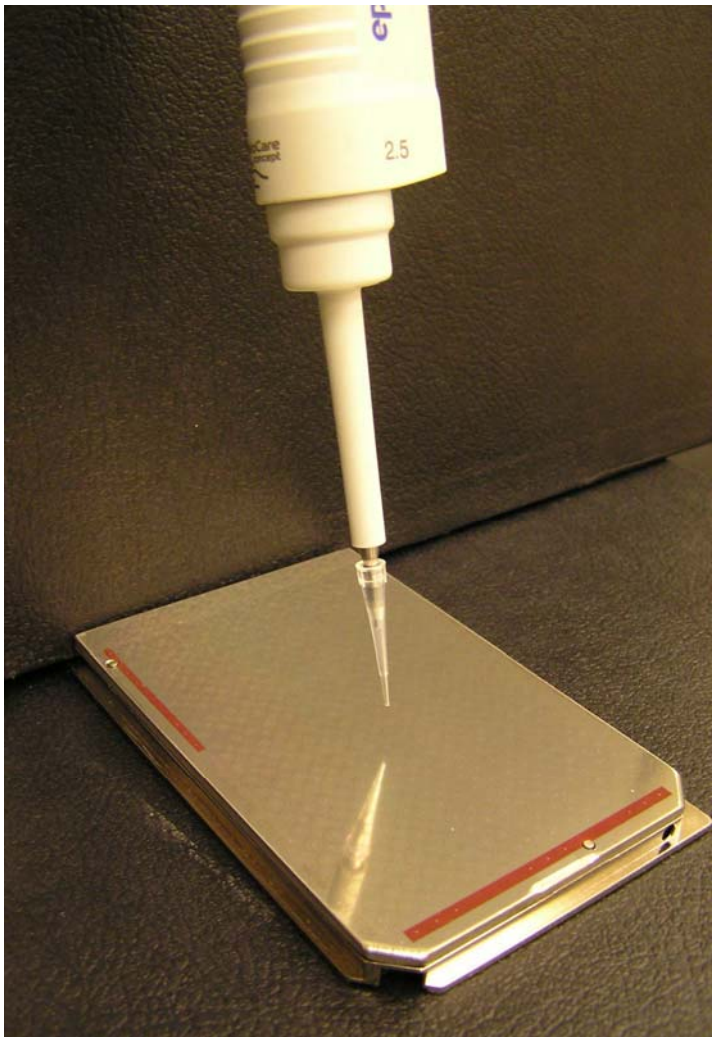

Figure 2.1.5. The MALDI target.

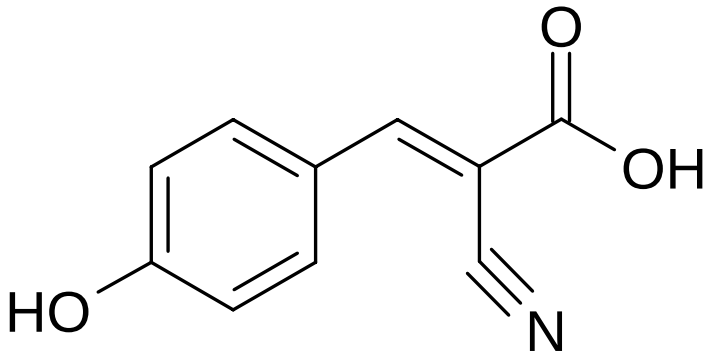

Figure 2.1.6. MALDI matrix: α-cyano-4-hydroxycinnamic acid (HCCA).

Since the analyte is embedded within the matrix during sample preparation, this process can also remove buffer and salt contaminants (26).

One popular hypothesis (26) states that following desorption as neutral species, the analyte molecules become ionized through acid-base reactions with the protonated matrix. This is said to occur within the plume of particles ablated by the laser pulse and just above the matrix layer. The protonated matrix molecules are produced by photochemical reactions. Another possibility is that the singly excited matrix molecules (and not the photoionized matrix molecules) are responsible for analyte ionization. According to this model, two excited matrix molecules are needed to produce ionized gaseous analyte ions. Karas *et al.* (28) suggested the formation of initial matrix clusters, protonated/deprotonated analyte molecules and counter-ions, as well as the desolvation of desorbed clusters to generate free ionic species through acid/base reactions and evaporation of neutrals. Electrons generated during matrix photoionization are captured by charged clusters to form singly charged ions. Electron capture is also believed to be responsible for fragmentation (26).

TOF-MS

A time-of-flight mass spectrometer is one of the simplest mass analyzing devices (Figure 2.1.7) available. It is commonly used for MALDI-MS because ion pulses produced in MALDI provide the sampling mode required by TOF analyzers. A TOF mass spectrometer is a velocity spectrometer, in which ion separation occurs as a result of velocity differences. Following laser desorption, a short pulse of ions leaves the MALDI source and is dispersed in time by allowing it to drift in a field-free region (FFR) of a long flight tube. It is in this FFR where separation based on *m/z* occurs. TOF mass analyzers offer a variety of advantages, including high analysis speed, simplicity of design, high transmission, (theoretically) unlimited mass range, concurrent detection of all ions (multiplex advantage), as well as compatibility with pulsed ionization sources, such as MALDI (26).

Ions produced by a laser pulse through MALDI are extracted into the TOF analyzer by an electrical field *V*. The principle behind the mass analysis is that after acceleration to a constant kinetic energy, the ions travel at velocities, *v*, that are inversely

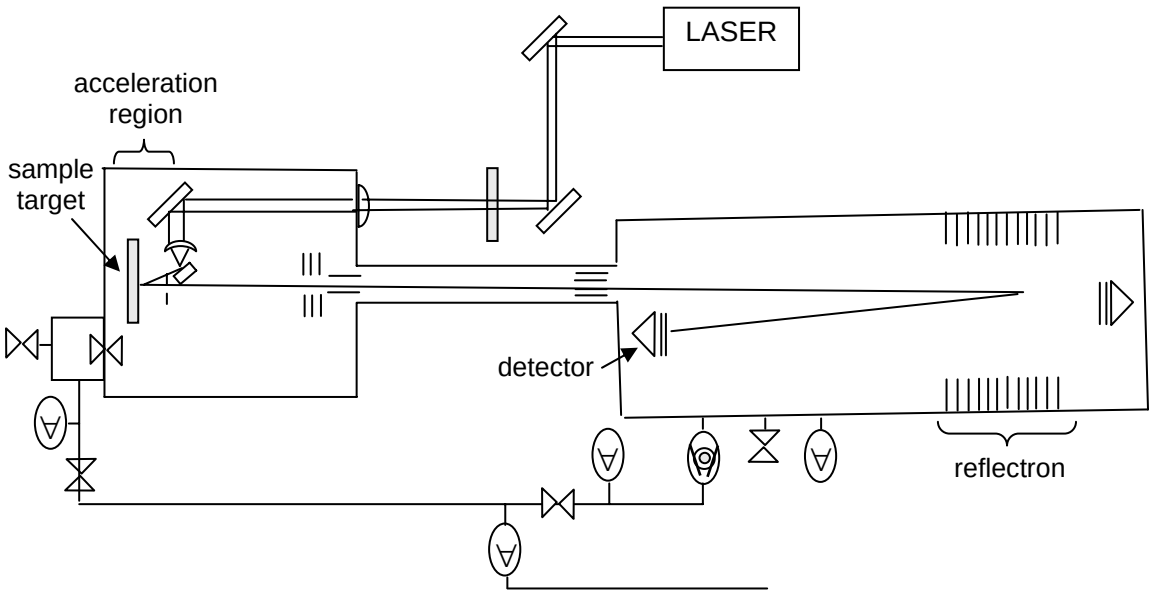

Figure 2.1.7. Time-of-flight (TOF) mass spectrometry.

proportional to the square root of their *m/z* values. The kinetic energy can be expressed as follows (27):

$$KE = zeV \tag{2.1.8}$$

where, z = charge of molecular ion

e = charge of an electron (Coulombs)

V = electric field strength (Volts).

In ideal situations, all ions, small and large, enter the FFR with the same kinetic energy. According to Newton's law:

$$KE = \left(\frac{1}{2}\right)mv^2 = \left(\frac{1}{2}\right)m\left(\frac{dx}{dt}\right)^2 . \tag{2.1.9}$$

Therefore,

$$zeV = \left(\frac{1}{2}\right)m\left(\frac{dx}{dt}\right)^2 . \tag{2.1.10}$$

Compared to the flight path and time of flight, the source region is very short and ions spend comparatively little time there. Thus, the velocity can be considered to be constant in these equations. As such, the instantaneous velocity can be expressed as a ratio of the total field free flight path (Δx) and flight time (Δt). The *m/z* for a given ion can be calculated as follows (27):

$$m/z = 2eV\frac{\Delta t^2}{\Delta x^2} \tag{2.1.11}$$

where, m = mass (kg)

Δx = flight path length (m)

Δt = flight time (s).

The short ion pulse is eventually dispersed into packets of iso-mass ions, as it travels through the flight tube. Ion arrival time can be used to perform mass analysis:

$$\Delta t = \frac{\Delta x}{v} = \Delta x\left(\frac{m}{2zeV}\right)^{1/2} . \tag{2.1.12}$$

If all ions obtain the same kinetic energy, the ions of lesser *m/z* will have greater velocity than ions of greater *m/z*. Therefore, as ions traverse the analyzer, they separate in space. A detector is positioned at the end of the analyzer to measure the arrival time of ions. The ions of lesser *m/z* arrive first, followed by ions of greater *m/z* (26).

Since MALDI typically generates singly charged ions, a mass analyzer with high mass range is required. In theory, TOF has an unlimited mass range, which places strict requirements on the detector because they are velocity-sensitive detectors. Due to the fact that velocity decreases inversely with the square root of the mass, the sensitivity of TOF-MS is lower for larger ions.

Pulsed Ion Extraction

When ions are formed in MALDI, they have a kinetic energy, directional, spatial and temporal spread due to the ionization process, which can cause peak broadening. By generating ions in a weak electric field and applying a high voltage extracting field following a time delay, the effect of this spread can be minimized. Ions are first allowed to expand into a field-free region in the source and after a certain delay (hundreds of nanoseconds to several microseconds) a voltage pulse is applied to extract the ions outside the source (26).

The Reflectron

Further improvements in resolution can be achieved by incorporating a reflectron (29) in the TOF instrument. Due to the large kinetic energy spread of the ions (which increases with mass) produced at the surface of the sample/matrix spot, linear TOF (Figure 2.1.8) analyzers are unable to offer high mass resolution in the absence of any compensation. The reflectron TOF (Figure 2.1.9) features two linear field-free regions and an ion mirror, which corrects for kinetic energy and spatial dispersions of ions of the same *m/z*. The ion mirror consists of an array of electrical lenses, each having progressively higher repelling potential. The initial spatial spread is translated to a velocity spread, which can be easily corrected by the mirror.

Ions entering the reflectron, after traversing the first FFR, are slowed down and then their direction of motion is reversed. This is followed by acceleration into a second FFR. Ions of a given *m/z* with faster velocities spend less time in the drift regions, but penetrate to a greater depth into the reflecting field. As a result, they spend more time in the reflectron, which compensates for the shorter flight times of faster ions in the drift regions. The end result is that all ions of the same *m/z* arrive simultaneously at the

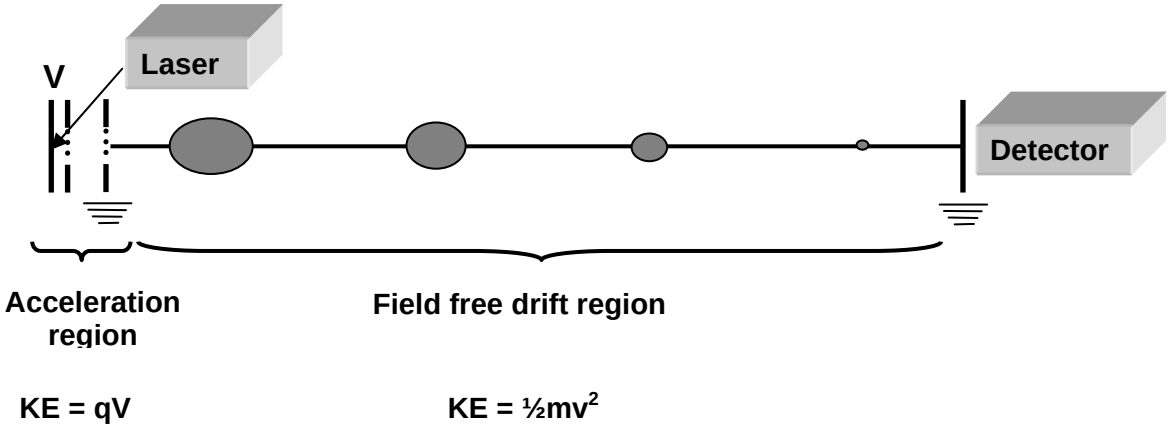

Figure 2.1.8. Linear mode TOF-MS operation.

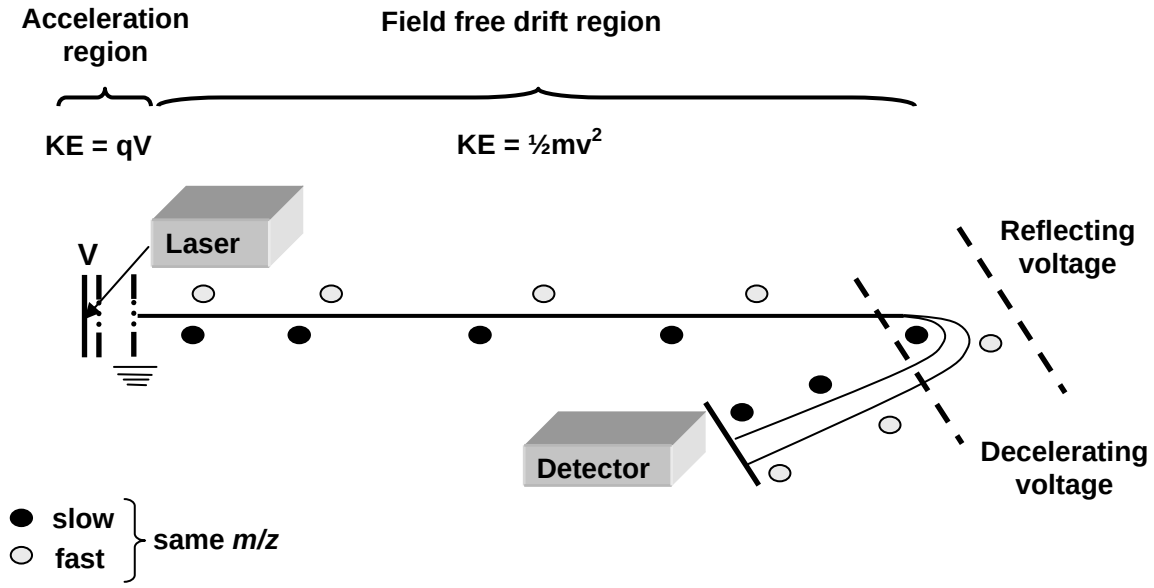

Figure 2.1.9. Reflectron mode TOF-MS operation.

detector, situated at the end of the flight path. Considerable improvements in mass resolution can be achieved in this manner. An additional contributing factor in improving the mass resolution is the longer path length provided by reflectron. Dramatic improvements are realized over linear TOF-MS instruments for <10 kDa molecular mass compounds. The total flight time of an ion in the reflectron is given by:

$$t = \left(\frac{m}{2zeV}\right)^{1/2} \left(L_1 + L_2 + 4d\right) \qquad (2.1.13)$$

where, L_1 = first field-free region

L_2 = second field-free region

d = depth of ion penetration into the reflecting field.

Reflectrons can be either single-stage or dual-stage. A single-stage reflectron is a simple ion mirror that provides a singe retarding-reflecting field. The device consists of an entrance grid electrode and a series of ring electrodes. With a single-stage reflectron, first order correction for the kinetic energy spread is achieved. Dual-stage reflectrons feature two linear retarding voltage regions separated by an additional grid and can provide improved resolution at the expense of sensitivity (26).

Protein Identification by MALDI-TOF-MS

MALDI-TOF-MS is a powerful technique for proteomics analyses. Mass spectrometric analysis generates a mass fingerprint or profile which is unique to a particular protein. Comparison of this peptide mass fingerprint (PMF) with databases of known protein digest fingerprints provides the means of protein identification. PMF works well with analytical proteomics because it combines a conceptually simple approach with robust, high-throughput instrumentation. The quality of protein identifications made depend on the quality of the MS data, the accuracy of the databases and power of the search algorithms and software used.

Database Searching

An algorithm is a set of rules that specify how to solve a well-formulated problem in a finite number of steps. The problem is described in terms of inputs and outputs and

the algorithm facilitates the conversion of inputs to outputs. As the field of proteomics acquires momentum in the wake of the genomics era, several algorithms and computer programs have been described for protein identification. Many programs involve the interrogation of a sequence database with mass spectrometric data from the unknown protein. An *in silico* digestion of the entire sequence database according to suitable fragmentation rules (depending upon the proteolytic enzyme being used) produces a list of theoretical peptide mass values which can be compared to the experimental data. Equivalent peptide masses are tallied or scored such that the peptide or protein providing the closest match with experimental data can be identified (30).

In situations where the target protein is not present in the database, entries with homology similar to the protein in question are identified. These entries are usually proteins of similar structure and/or function from related organisms. Of the protein identification algorithms available, the MASCOT algorithm offers the substantial advantage of probability-based scoring. In this approach to peptide mass scoring, a straightforward mathematical rule can be employed to evaluate the significance of the result, thereby avoiding false positives. Furthermore, it is possible to draw comparisons between these scores and those derived from other types of searches, including determination of sequence homology. Finally, the search parameters can be optimized through iteration (30).

With MASCOT, the database can be searched using a peptide mass fingerprint (PMF), sequence query and MS/MS information from target proteins. MASCOT was originally designed as an extension of the MOWSE (Molecular Weight Search) scoring algorithm (31). In a typical MOWSE search, the theoretical peptide masses for all the entries in the sequence database are compared with the experimental data. A match is said to occur when a calculated value falls within a pre-defined mass tolerance of an experimental mass. A molecular weight range for the intact protein from gel electrophoresis data can be applied as a pre-filter. MOWSE assigns a statistical weight to each peptide match by considering several empirically determined factors.

In the MOWSE approach, a matrix **F** of all the weighting factors of *in silico* peptides is calculated during the database build stage. Each row in this matrix represents a 100 Da interval in peptide fragment mass while each column is an interval of 10 kDa in

intact protein mass. With the analysis of each sequence entry, the appropriate matrix elements f_{ij} are incremented to generate statistical information on the size distribution of peptide masses as a function of protein mass. Matrix normalization is achieved by dividing the elements of each 10 kDa column in **F** by the largest number in the column. This produces the MOWSE factor matrix **M**:

$$m_{ij} = \frac{f_{ij}}{\left| f_{ij} \right|_{j\max}} . \tag{2.1.14}$$

Experimental mass values are searched against the theoretical peptide mass database and the score for each entry is determined:

$$Score = \frac{50000}{M_{prot} \times \prod_{n} m_{ij}} \tag{2.1.15}$$

where, M_{prot} = molecular weight of the entry.

The product term in the denominator is determined from the MOWSE factor elements for each match between the experimental data set and peptide masses calculated from the entry (32).

The MASCOT algorithm uses a probability-based approach of the MOWSE algorithm. As such, it incorporates the significant benefits of MOWSE, including the ability of this program to accurately model the behavior of a proteolytic enzyme. There are noteworthy differences between MOWSE and MASCOT aside from probability-based scoring, such as the removal of pre-built indexes (30). A FASTA format of the sequence database is directly compatible with MASCOT. To maximize search speed, the FASTA format can be compressed and incorporated into the computer memory.

The basic *modus operandi* in MASCOT is the determination of the likelihood that the observed match between the experimental data set and each sequence database entry occurs at random. The match securing the lowest probability is reported as the best match. This match may or may not be a significant one, depending upon the size of the database. A generally accepted significance threshold is that the probability of the observed result being a chance event is less than 5% ($p < 0.05$). MASCOT reports the scores as $-10\text{Log}_{10}P$, where P is the probability. MASCOT accepts MS data as lists of centroided mass values (peak lists), and if preferred, with associated intensity values as

well. When using MS/MS data, it is also necessary to detect the peaks in the chromatogram. Several spectra from a single peptide may be added together while at the same time eliminating spectra from the chromatogram baseline that would otherwise contribute to noise (32).

One of the challenges in using PMF data with MASCOT is the elimination of false positive results. Some basic assumptions are associated with a MASCOT search. Experimental data are considered to be independent measurements taken from the larger population of all possible measurements. In situations when data are not independent, the absolute score becomes an unreliable indication of significance. Another problem is the frequent observation of identical masses. For pairs of duplicate masses, if one matches, then so will the other. The score determined on the presumption that these are autonomous matches, is higher than it should be. In PMF data, this can occur because the mass error window specified by the user is too large. Another possibility is that the peaks are split by noise or poor calibration. For MS/MS data, scans for a single chromatographic peak may not have been averaged. In some situations, particularly when non-quantitative modifications are applied, data lacking duplicate values can produce statistically significant scores in searches against the random database. It is possible that the data contain pairs of masses differing by the mass difference of the modification. For these pairs, if one of the values happens to match a theoretical sequence containing the modifiable residue, the likelihood of the other value matching the same sequence becomes significant. The experimental data are then not independent and the score is higher than it ought to be (30). While the use of probability-based scoring in MASCOT is a significant improvement over other approaches, there is certainly much room for further improvements in protein identification technology.

Goals

The importance of research in alternative sources of fuel, particularly biofuels research, has been highlighted in this chapter. The applicability of bacterial fermenters in industrial bio-ethanol production was considered and an overview of the current knowledge in bacterial ethanol tolerance and adaptation has been provided. In light of

evidence suggesting that a majority of changes associated with ethanol adaptation occur in the bacterial membrane proteome, a closer look at membrane protein expression patterns is warranted. The advantages and pitfalls associated with membrane protein analysis using gel-based approaches were discussed, along with other gel-free alternatives. A review of the literature clearly indicates that gel electrophoresis methods are still the gold standard of protein separation. A description of gel-based proteomic analyses is provided, including a discussion of polyacrylamide gel electrophoresis, in-gel digestion of proteins, methods for protein visualization, MALDI-TOF mass spectrometry of protein digests, as well as protein identification using database searching.

Through careful study of the gel electrophoresis experiment, a new and more improved SDS-PAGE methodology was developed which could be effectively applied to the analysis of membrane proteins, particularly those of the bio-ethanol producer *Clostridium thermocellum*. Information from these investigations should provide a better understanding of ethanol adaptation by this organism. Chapter 2.2 describes the design of doubled SDS-PAGE (dSDS-PAGE) methodologies for membrane protein analysis. The wild type *C. thermocellum* membrane proteome was chosen as the model system for these experiments. Standard glycine-based running buffers (Laemmli protocol) (19), along with tricine-based (33) and the newly developed bicine-based buffer systems (34) were examined in their suitability for separation of such proteins. The parameter space of gel preparation in Tricine- and Bicine-dSDS-PAGE was explored and a description of the optimization of these parameters is given. The compatibility of these dSDS-PAGE methods with mass spectrometric analysis of digested proteins extracted from the gel was investigated. The improved suitability of bicine-based running buffers in membrane proteome analyses was explained through capillary electrophoresis experiments.

Chapter 2.3 focuses on the application of the Bicine-dSDS-PAGE methodology in the analysis of membrane proteins derived from wild type and ethanol-adapted *C. thermocellum* strains. Definitive changes in membrane protein expression patterns were observed between these bacteria and a discussion of differentially expressed proteins in the backdrop of ethanol tolerance is provided.

Chapter 2.4 offers some concluding remarks and highlights the significance and future direction of this work.

Chapter 2.2

Methods Development in Two-Dimensional Polyacrylamide Gel Electrophoresis for Membrane Proteins

Introduction

Since Laemmli's introduction of the discontinuous SDS-PAGE system (19), several modifications and improvements have led to significant strides in gel-based protein separations. Inclusion of urea has shown benefits in terms of resolution and enabling the use of higher levels of cross-linker (%C - N',N'-methylenebisacrylamide or Bis) for the separation of low molecular weight proteins (35-38). However, despite these benefits, urea can carbamylate proteins, thus complicating proteomic analysis, particularly for larger proteins. Other reports have explored high Tris concentrations in the buffer and gel (39), glycerol in the gel (40) and running buffer modifiers (35, 36, 41) in lieu of or in addition to urea. These investigations have led to benefits in dynamic range, resolution and protein representation. The advent of 2D-SDS-PAGE enabled orthogonal protein separation by both charge and size, further improving the technique and vastly increasing protein representation (42). However, with all these advances also came the realization that the cellular proteome is comprised of many sub-proteomes which often require different sample preparation conditions for optimum separation.

One particular sub-proteome that has been notoriously resistant to detailed analysis by 2D-SDS-PAGE includes the proteins associated with cell membranes. Many of these proteins are hydrophobic in nature, which makes them very difficult to solubilize in the first dimensional or isoelectric focusing (IEF) step (13). Typically used IEF sample buffers are detergent free and are not adequate to dissolve these proteins and furthermore, dissolved membrane proteins have a tendency to precipitate at their isoelectric points (15). As a consequence, they are quite consistently under-represented in traditional 2D-SDS-PAGE. Improvements that have been suggested include the use of various ionic, zwitterionic and nonionic detergents, as well as different combinations of these, to promote solubilization (43-54). Other reports described the substitution of dithiothreitol (DTT) with the uncharged reducing agent tributyl phosphine (TBP; (44, 55-57)), which

assists in maintaining reducing conditions during IEF and lowers the likelihood of precipitation that could occur through aggregation initiated by disulfide bonding. Subproteomics and prefractionation techniques have recently been explored to improve representation of membrane proteins expressed in low copy numbers (58, 59). Selective enrichment of certain classes of proteins, such as periplasmic proteins, to enhance their abundance in 2D gels has also been described (60). While all these approaches have improved membrane protein analysis to some extent, solubility issues associated with IEF have not been fully eliminated.

Since the main problems with membrane protein separation arise during IEF separation, alternatives to the standard 2D-PAGE approach that circumvent this step have been considered. Schägger and co-workers (17) described a doubled SDS-PAGE (dSDS-PAGE) experiment in which SDS-PAGE separation of membrane proteins in the first dimension was followed by an additional SDS-PAGE separation in a second dimension to generate a diagonal arrangement of protein spots. The effectiveness of this dSDS-PAGE approach is influenced by the type of buffer system (e.g. glycine- or tricine-based), presence of urea and acrylamide content in the gels. Indeed, highly hydrophobic membrane proteins from bovine heart mitochondria were successfully separated with this approach (17). In a similar set of experiments, Sánchez *et al*. (61) separated outer membrane protein complexes and heat-modifiable proteins in *Neisseria* strains. The authors explored different combinations of non-denaturing and denaturing conditions in 1D and 2D for the purposes of optimizing separation. Eliminating β-mercaptoethanol from the 1D sample buffer enhanced spot resolution. They also postulated that incubating the 1D sample strip under denaturing conditions prior to running the second dimension offered better separation and spot resolution compared to incubation under non-denaturing conditions. Despite these benefits of dSDS-PAGE, the technique is still not widely used and in fact, there are few other reports of its application (62, 63).

Tricine-based running buffer systems (17) have been successfully applied in the separation of various types of proteins (17) and cell surface structures (e.g., bacterial lipopolysaccharides) (33, 64-73). Advantages of tricine over glycine-based buffers include improved protein migration, especially in the presence of potentially interfering substrates (72); and improved stacking and destacking of middle (64) and low (67)

molecular weight proteins, resulting in better resolution. This improved resolution was theoretically (74-76) and experimentally (77) explained by increases in ionic strength, as would be associated with a Tricine-SDS-PAGE buffer system.

As with any separation method, modification of the mobile phase or running buffer can change the separation process. Since Tricine-dSDS-PAGE is a powerful tool in membrane protein separation, we explored other buffer systems in conjunction with the dSDS-PAGE approach and describe an orthogonal Bicine-dSDS-PAGE method for the analysis of membrane proteins from the anaerobic bacterium, *Clostridium thermocellum*. This organism produces ethanol from fibrous biomass but has low tolerance to ethanol build-up in the medium. Recently, strains able to tolerate up to 8% ethanol have been developed and studies have shown that changes in the membrane proteome are elicited by ethanol (78). Comparisons of Bicine-dSDS-PAGE to Tricine-dSDS-PAGE and the standard Glycine-dSDS-PAGE (Laemmli method) revealed a considerably better separation method for membrane-associated proteins, as well as highly basic proteins, in addition to the advantage of circumventing solubility issues in the first dimension of standard 2D-SDS-PAGE experiments. These differences between bicine, tricine and glycine were explained through capillary electrophoresis investigations of electrophoretic migrations. Both Bicine- and Tricine-dSDS-PAGE were amenable to protein spot analysis and identification by mass spectrometry.

Experimental

Materials

All materials and chemicals for the growth of bacterial cultures were from Sigma (St. Louis, MO) except yeast extract, which was obtained from Difco Laboratories (Detroit, MI). Laemmli sample buffer, Coomassie stains, Tris base, SDS, acrylamide, N,N-methylene-bis-acrylamide (bis), ammonium persulfate (APS), N,N,N,N-tetramethyl-ethylenediamine (TEMED), glycine and tricine were obtained from Bio-Rad (Hercules, CA). Bicine, ammonium bicarbonate and the MALDI matrix α-cyano-4-hydroxycinnamic acid (HCCA) came from Sigma. Methanol, glycerol, *o*-phosphoric acid, hydrochloric acid, formic acid, trifluoroacetic acid (TFA), boric acid, acetonitrile

and trypsin were purchased from Fisher Scientific (Pittsburg, PA). Ammonium sulfate was obtained from EMD Chemicals (Gibbstown, NJ).

Bacterial Strains and Growth Conditions

Clostridium thermocellum ATCC 27405 was obtained from the American Type Culture Collection and cultured in a medium that contained 10.8 mM Na_2HPO_4, 11.05 mM KH_2PO_4, 9.35 mM NH_4Cl, 3.79 mM $(NH_4)_2SO_4$, 0.44 mM $MgCl_2.6H_2O$, 0.27 mM $CaCl_2$, 2.0 g/L yeast extract, 0.5 g of cysteine, 10 mL of a vitamin standard mixture (79), 5 mL of a modified micromineral mixture (79) and 1 mg/L of the oxygen indicator resazurin. The stock micromineral mixture was modified to provide 10 mg of $Na_2WO_4.2H_2O$ and 1 mg of Na_2SeO_3 per liter of medium. The basal medium was adjusted to pH 6.7 with 10% NaOH and autoclaved for 10 min to remove dissolved gases. Carbon dioxide was then immediately bubbled through the solution until it was cooled to room temperature and an anaerobic solution containing 4 g of Na_2CO_3 was then added. The medium was anaerobically dispensed into culture tubes and bottles and sterilized by autoclaving for 20 min. This basal medium was supplemented with an anaerobic solution of cellobiose to provide a final concentration of 4 g/L.

Cell cultures were grown at 55ºC and harvested once the optical density at 600 nm had reached approximately 1.0. The cultures were then centrifuged at 15,000 x *g* for 10 min at 4^{o}C. The supernatant was discarded and the pellets re-suspended with 40 mL of 50 mM Tris, pH 7.5. This was followed by another 10 min centrifugation and an additional wash step. Cell pellets were finally re-suspended in the Tris buffer to a final optical density of approximately 50. The concentrated cells were stored at -80^{o}C.

Preparation of Membrane Protein Fractions

Concentrated *C. thermocellum* cells were thawed and phenylmethylsulfonylfluoride (PMSF) and DTT were added to achieve final concentrations of 5 mM for each. The cells were then lysed by passage through a French Press (SLM Aminco, Urbana, IL) three times at 137 MPa. The broken cells were centrifuged for 10 min at 5,700 x *g* and 4^{o}C. The pellets were discarded and the supernatant centrifuged at 200,000 x *g* and 4^{o}C for 45 min. The resulting membrane

pellet was re-suspended in 10 mL of 10 mM Tris, pH 7.5. Next, the pellet was centrifuged twice (200,000 x *g*, 4°C, 45 min), and finally re-suspended in 10 mM Tris, pH 7.5, to obtain a protein concentration of approximately 6.4 mg/mL. Protein content was determined using the Lowry assay (80). Aliquots of re-suspended proteins were stored at -80°C until further use.

The dSDS-PAGE Experiment

Small (7 cm x 8 cm) and large (20 cm x 20 cm) format gel experiments were performed at 4°C with Mini PROTEAN II and PROTEAN II xi electrophoresis cells (Bio-Rad), respectively. Linear acrylamide gradients in the second dimension of dSDS-PAGE were generated using a Model 485 Gradient Former and all gels were run at 4°C. The first dimension of a dSDS-PAGE experiment consisted of a 4% acrylamide stacking gel and a 10% separating gel. Gel thickness was 0.75 mm and 1.0 mm for small and large formats, respectively. The Laemmli protocol (19) was used to separate the proteins in the first dimension for Glycine-, Tricine- and Bicine-dSDS-PAGE. Small format gels were run at a constant 200 V, with run times of approximately 50 min. The large format gels were run at 16 mA/gel for protein migration through the stacking gel, and this was then increased to 24 mA/gel when the dye front entered the separating gel. Run times for large format 1D gels were approximately 7 h.

Membrane proteins were then further resolved in the second dimension by a 9-12% linear acrylamide gradient gel. After staining with Coomassie R-250 overnight, gel strips (approximately 5 mm wide) were excised from the first dimension, swelled for 30 min in buffer (100 mM Tris, 150 mM HCl, approximately pH 2) (17), and then placed in between the glass plates and on top of the separating gel of the second dimension (Figure 2.2.1). Gaps between the excised gel lane and spacers of the second dimension were filled with gel mixtures that contained 10% acrylamide, the same composition as in the 1D strip. Gel and running buffer preparation for the second dimension of Glycine-dSDS-PAGE followed the Laemmli protocol (19). In the case of Tricine-dSDS-PAGE, the second dimension running buffer was prepared as described by Hunte *et al*. (81) and a similar system was designed for Bicine-dSDS-PAGE (Table 2.2.1). In the interest of methods development and optimization, a series of experiments were performed for the

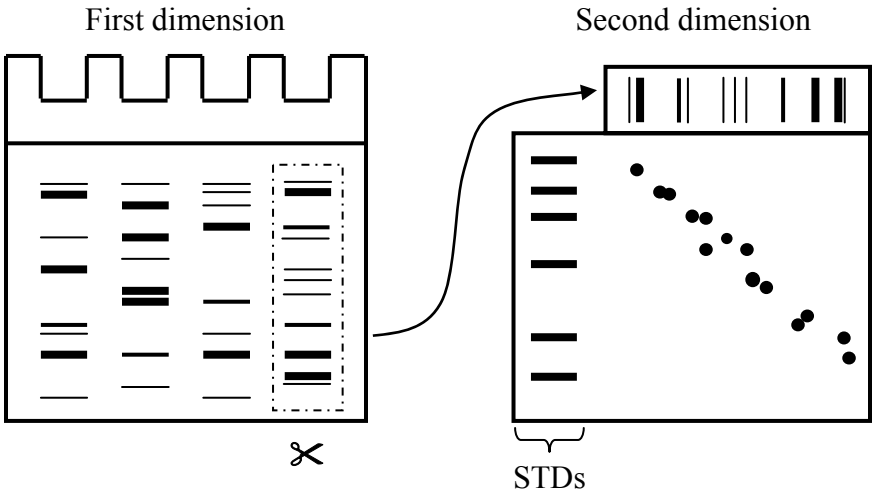

Figure 2.2.1. Doubled SDS-PAGE (dSDS-PAGE) experiment with molecular weight-based separations in two dimensions. A first dimensional separation was performed (Laemmli protocol) using a 4% stacking gel and 10% resolving gel. The 1D sample strip was then further separated in the second dimension by a 9-12% linear acrylamide gradient gel using glycine-, tricine- or bicine-based buffer systems.

Table 2.2.1. Running buffer composition of second dimension dSDS-PAGE gels.

	Glycine-dSDS-PAGE[a]	Bicine-dSDS-PAGE	Tricine-dSDS-PAGE[b]
Anode Buffer	25 mM Tris 192 mM glycine 0.1% SDS pH 8.3	200 mM Tris pH 8.9	200 mM Tris pH 8.9
Cathode Buffer	25 mM Tris 192 mM glycine 0.1% SDS pH 8.3	100 mM Tris 100 mM bicine 0.1% SDS pH 8.3	100 mM Tris 100 mM tricine 0.1% SDS pH 8.3

[a]As previously described (19)

[b]As previously described (33)

second dimension of Tricine- and Bicine-dSDS-PAGE. In all second dimension experiments, the gel thickness for the small and large formats was 1 mm and 1.5 mm, respectively. For the second dimension of Bicine- and Tricine-dSDS-PAGE small format gels, electrophoresis was performed by applying a constant 100 V for 30 min to allow protein migration through the width of the 1D strip and overlay gel. When the dye front entered the separating gel, the voltage was increased to and maintained at 150 V. Run times were typically 2.5 h. For large format gels in the second dimension of Bicine- and Tricine-dSDS-PAGE, running conditions were 90 V for the first 30 min and 120 V thereafter, with run times of approximately 24 h. All second dimension gels were stained with G-250 Colloidal Coomassie (23).

Image Analyses

Gel images were captured using a Bio-rad Versadoc Imaging System and analysis of 1D and 2D images was performed by Bio-Rad Quantity One and PDQuest software, respectively. Images shown in figures are Gaussian representations generated by the software.

Protein Identification

Tryptic digests of membrane proteins were examined in positive ion mode using a Bruker Autoflex MALDI-TOF or a Finnigan LCQ Classic quadrupole ion trap mass spectrometer. HCCA was used as the matrix of choice for protein samples. MALDI spectra were internally calibrated using peptides generated from trypsin autolysis. Peptide mass fingerprinting data (PMF) with monoisotopic peak mass lists were analyzed using the MASCOT algorithm and the *C. thermocellum* database (82). Protein spots that could not be identified by MALDI were subjected to LC-ESI-MS/MS and *C. thermocellum* database searching with MASCOT.

A Hewlett Packard LC system (1100 series) with a custom-made C_{18} capillary LC column was interfaced to the ion trap mass spectrometer for reversed phase LC-MS/MS analyses. A mobile phase mixture of water and acetonitrile (ACN), each containing 0.1% formic acid, was used in all experiments. Gradient elution was employed in these studies,

similar to the profile described in Chapter 1.2 of Part 1. LCQ data was also analyzed by the MASCOT algorithm and the *C. thermocellum* database.

Capillary Electrophoresis

Capillary electrophoresis (CE) experiments were performed on a Groton Biosystem CE equipped with a UV detector (Boxborough, MA). The detection wavelength was set at 290 nm. An uncoated fused silica capillary (Polymicro Technologies, Phoenix, AZ) with dimensions of 95 cm (70 cm effective length) x 75 μm I.D was used for separation. A background electrolyte (BGE) containing 100 mM borate buffer at the desired pH and 10 mM 2-methyl-1,3-cyclohexanedione was used in all experiments. Prior to use, the capillary was rinsed with 1.0 M NaOH for 10 min, followed by 0.1 M NaOH for 10 min, water for 5 min and finally with BGE for 10 min. After each run, the capillary was rinsed with 0.1 M NaOH for 1 min, methanol for 1 min and with BGE for 5 min. Samples were injected hydrodynamically at a pressure of 50 mbar for 6 seconds. BGE was replaced after every alternate run. Analytes were identified by indirect UV detection and 2-methy-1,3-cyclohexanedione was included in the BGE as a UV-absorbing probe.

Results and Discussion

Optimization of the dSDS-PAGE Experiment

As with any separation experiment, manipulation of the mobile and stationary phases can often yield improved sensitivity and resolution. Therefore, the parameter space of gel preparation (stationary phase) and the running buffer system (mobile phase) were manipulated to arrive at the optimal separation conditions for *C. thermocellum* membrane proteins. Tricine-dSDS-PAGE and the newly developed Bicine-dSDS-PAGE were explored in this regard. Bicine or N,N-bis(2-hydroxyethyl)glycine is a tertiary amine and has buffering capacity for the pH range of 7.6 – 9.0 (pk_{a1} = 1.84 and pk_{a2} = 8.35). Tricine or N-tris-(hydroxymethyl)-methylglycine is a secondary amine buffer for the pH range of 7.4 – 8.8 (pk_{a1} = 2.3 and pk_{a2} = 8.15). SDS-PAGE gels and running buffers are normally operated in the 6.6 – 8.8 pH range, which makes bicine- and tricine-

based buffer systems somewhat more suitable as the range is within a reasonable proximity of their pk_{a2} values. To ensure maximum buffering action of bicine and tricine, the pH of running buffers based on these ions were adjusted to be close to their pK_{a2} values. Operating at higher pH to accommodate the pH range of 8.8 – 10.6 buffering region of the primary amine glycine (pk_{a1} = 2.35 and pk_{a2} = 9.78) used in the Laemmli approach of dSDS-PAGE is not advised due to the susceptibility of acrylamide to hydrolysis (83).

Optimization of gel preparation parameters was performed using small format gels. We previously determined that a 10% acrylamide gel in the first dimension, followed by a 9-12% linear gradient gel in the second dimension of dSDS-PAGE provided reasonable protein spot resolution across the entire molecular weight range of the *C. thermocellum* membrane proteome (84). An overlay gel containing the same acrylamide percentage as the 1D sample strip and 150 mM Tris-HCl, pH 7.4, provided electrical conductivity similar to that of the 1D strip and maintained a neutral pH for efficient polymerization of acrylamide (17). Running buffer compositions for all experiments are given in Table 2.2.1. The method of Schägger *et al*. (81) was used to prepare running buffer for Tricine-dSDS-PAGE and a suitable protocol was designed for Bicine-dSDS-PAGE. Preliminary investigations involved applying the standard Laemmli gel preparation protocol with these two buffer systems. Bicine- and Tricine-dSDS-PAGE resulted in similar spot number, which was much poorer compared to Glycine-dSDS-PAGE. Considerable vertical streaking was observed and overall, it was evident that the Laemmli method for gel preparation was not well-suited for use with these buffer systems, as shown in Figures 2.2.2(A) and (B).

There have been reports of enhanced electrophoretic performance by incorporating glycerol in the gel, due to improved sieving (36) and mechanical stability (40). Enhanced resolution, particularly for peptides, is a result of either exclusion or ordering of water in the resolving gel (39). Furthermore, due to its viscous nature, glycerol is believed to aid in the separation and staining processes by reducing diffusion (40). In our experiments, addition of glycerol to the gel solution while keeping all other ingredients similar to the Laemmli protocol did not result in any significant increases in spot numbers for Tricine-dSDS-PAGE, although there were marginal increases in the

(A)

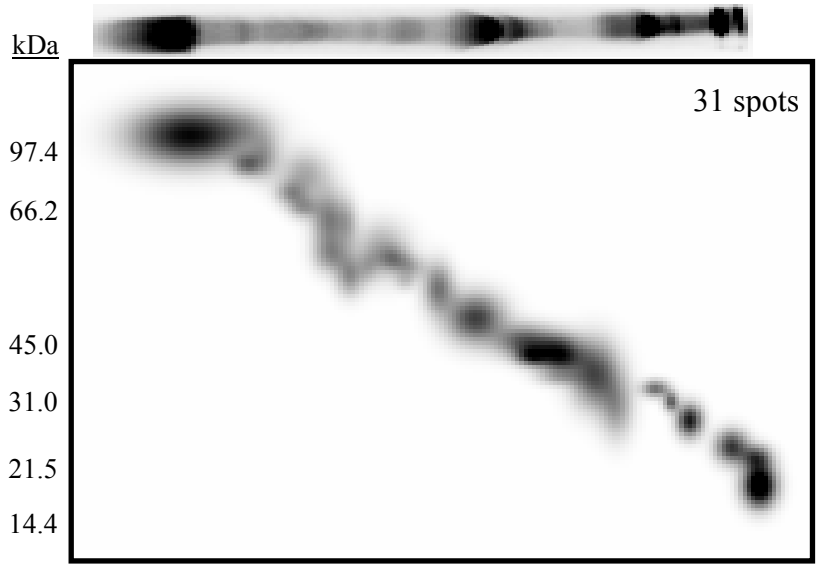

(B)

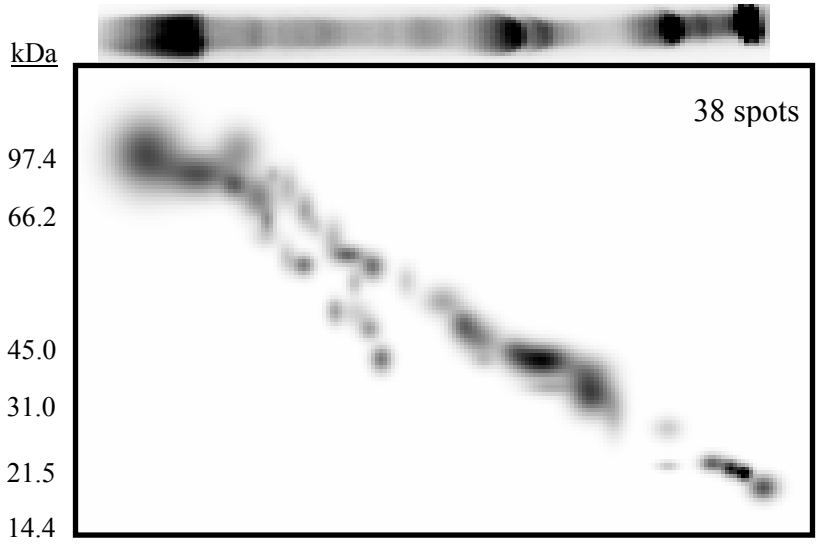

Figure 2.2.2. Standard Laemmli protocol in gel preparation for (A) Bicine-dSDS-PAGE and (B) Tricine-dSDS-PAGE.

case of Bicine-dSDS-PAGE. Vertical streaking remained a significant problem. However, there appeared to be improvements in spot resolution, particularly in Tricine-dSDS-PAGE, as shown in Figures 2.2.3(A) and (B).

The effect of increasing the Tris concentration in the gel solution was also investigated, as theoretical (74-76) and experimental (39, 77) evidence suggested that increased ionic strength can play a pivotal role in the successful stacking, migration and resolution of proteins. Just as with glycerol, high amounts of Tris in the resolving gel is also believed to improve resolution by excluding or ordering water in the gel (39). Keeping all other gel preparation parameters the same as the Laemmli protocol, higher concentrations of Tris were explored in the gel recipie for Bicine- and Tricine-dSDS-PAGE. Compared to the gels with glycerol, no detectable increases in protein spot numbers were observed in either case. Problems with vertical streaking were improved, especially for Tricine-dSDS-PAGE. In addition, spot resolution was better (spots less diffuse) for both Bicine- and Tricine-dSDS-PAGE, as shown in Figures 2.2.4(A) and (B).

Dramatic improvements were observed when both glycerol and increased Tris concentrations were incorporated into the gel solutions for Bicine- and Tricine-dSDS-PAGE. Gels that had glycerol and a high Tris concentration displayed remarkable improvements in spot number for Bicine-dSDS-PAGE. Spot resolution was better in both systems and furthermore, vertical streaking was negligible. The improved gel sieving offered by glycerol in conjunction with a high ionic strength produced a stationary phase with better resolving power, as shown in Figures 2.2.5(A) and (B). A tighter separating gel mesh with narrower sieve was also investigated for the purposes of improving the separation. Previous studies have indicated that such a gel offers better resolution and reduced leakage of low molecular weight proteins from the gel during the protein staining process (38). Gels made with a higher percentage cross-linker (6%) showed improvement in spot number for Bicine- and Tricine-dSDS-PAGE, as shown in Figures 2.2.6(A) and (B). Spot resolution improved and virtually no vertical streaking was observed. Other parameters, such as presence of different types of spacer gels, were explored (data not shown) and determined to have little effect in enhancing the separation process. Based on these results, the optimized parameters for gel preparation in Bicine- and Tricine-dSDS-

(A)

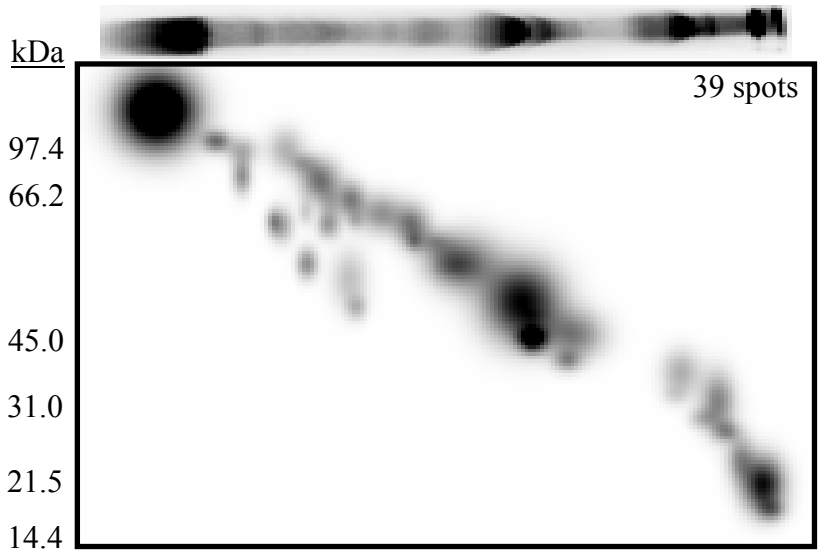

(B)

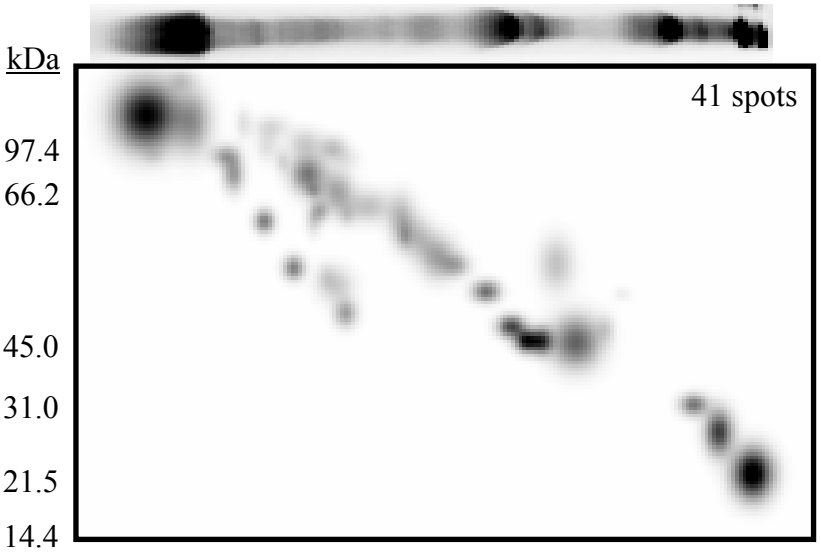

Figure 2.2.3. Effect of glycerol in gel preparation for (A) Bicine-dSDS-PAGE and (B) Tricine-dSDS-PAGE.

(A)

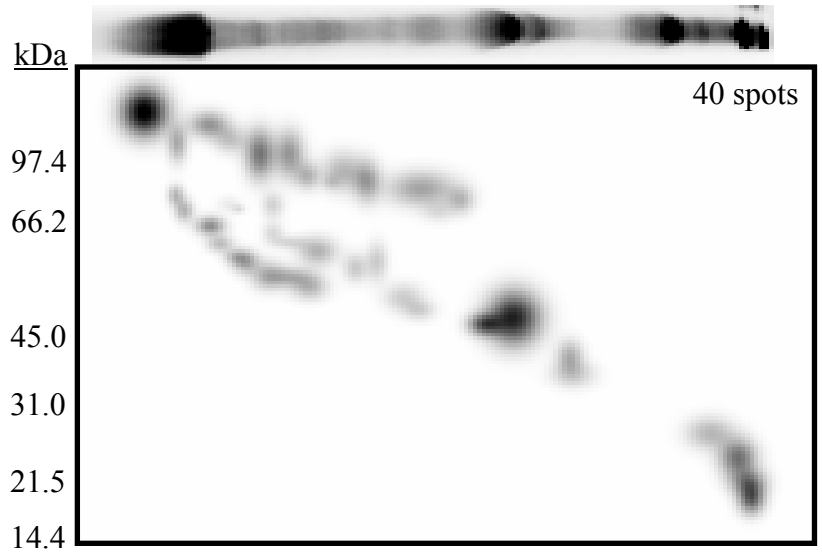

(B)

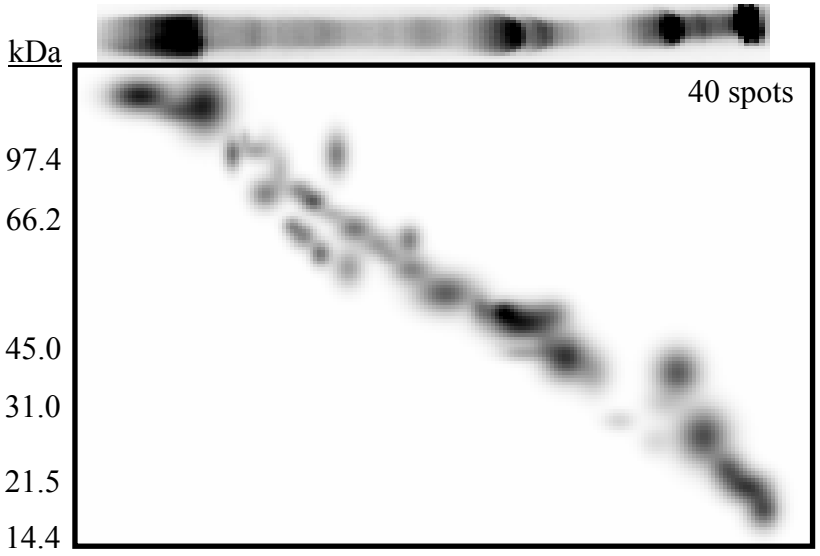

Figure 2.2.4. Effect of increased Tris buffer in gel preparation for (A) Bicine-dSDS-PAGE and (B) Tricine-dSDS-PAGE.

(A)

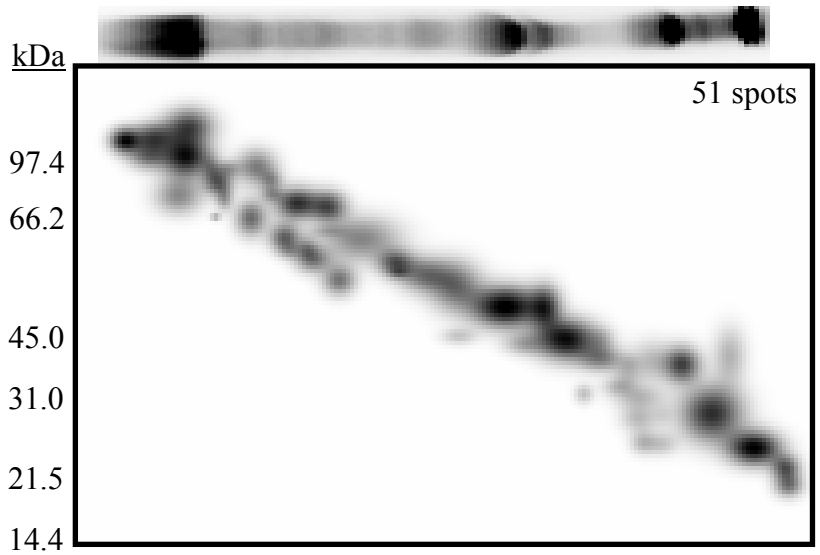

(B)

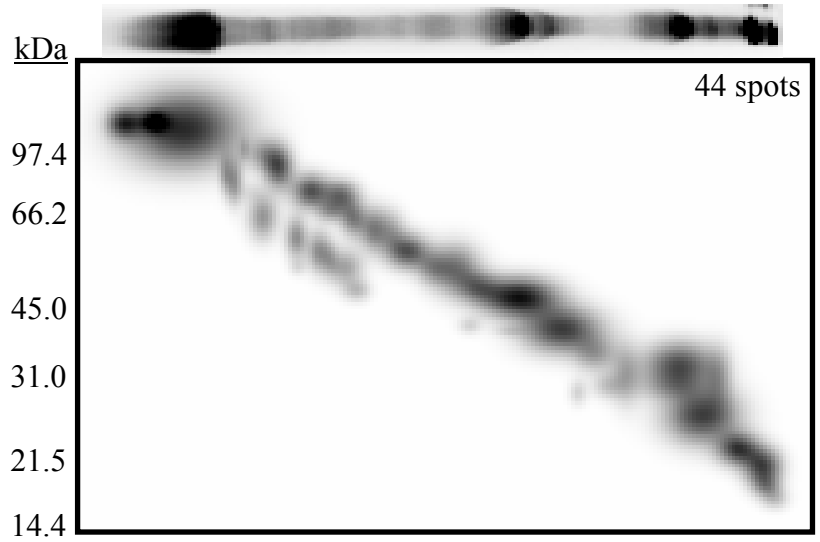

Figure 2.2.5. Effect of glycerol and increased Tris buffer in gel preparation for (A) Bicine-dSDS-PAGE and (B) Tricine-dSDS-PAGE.

(A)

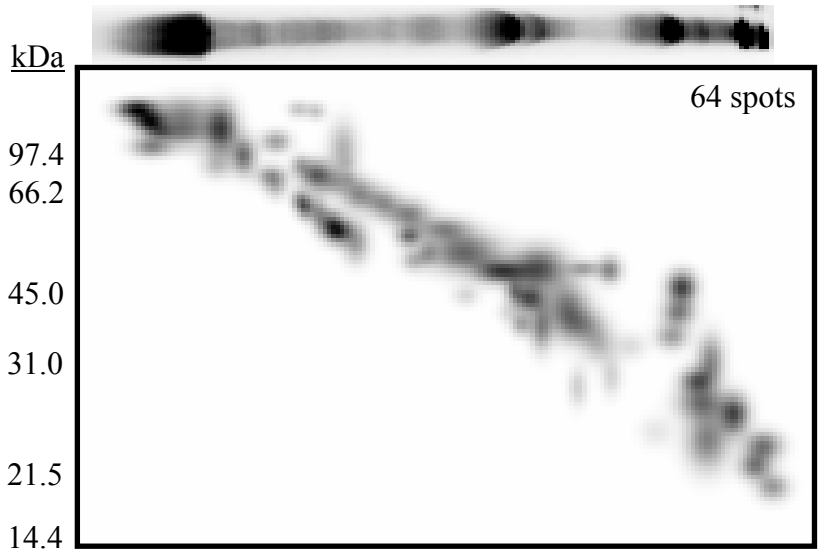

(B)

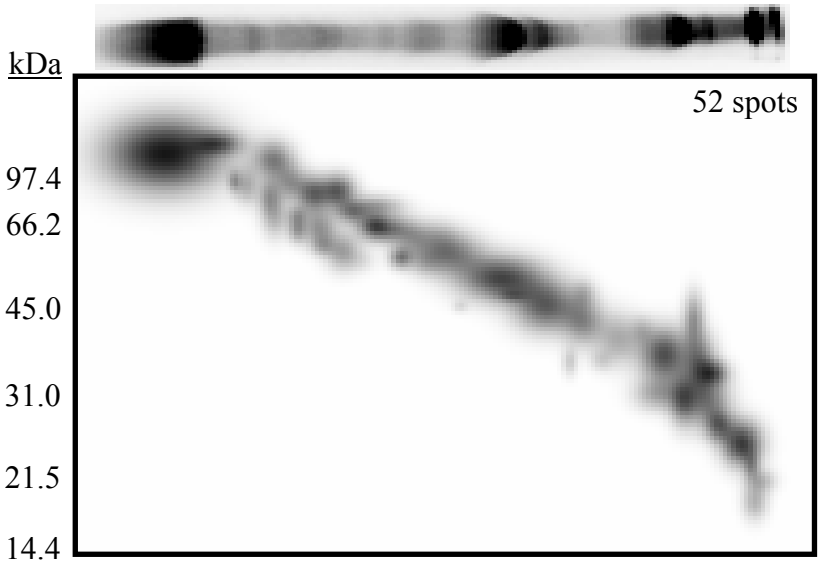

Figure 2.2.6. Effect of glycerol, increased Tris buffer and high percentage cross-linker in gel preparation for (A) Bicine-dSDS-PAGE and (B) Tricine-dSDS-PAGE.

PAGE were 10.7% glycerol, 1 M Tris, 0.1% SDS and 6% bis-acrylamide cross-linker, along with 0.05% APS and 0.05% TEMED for polymerization.

Large Format Gel Experiments with Optimized Parameters

To further improve protein representation and increase protein loading capacity of the gel, large format experiments for Laemmli-, Bicine- and Tricine-dSDS-PAGE were performed using optimized gel preparation protocols, as shown in Figures 2.2.7 to 2.2.9. Comparing these optimized large format gels for the three buffer systems, it was clear that Bicine dSDS-PAGE offered significant improvements in spot number over Tricine- and Glycine-dSDS-PAGE. Tricine-dSDS-PAGE showed a 112% increase in protein spot number and Bicine-dSDS-PAGE showed a 151% increase over Glycine-dSDS-PAGE. Spot resolution in Bicine-dSDS-PAGE was also dramatically better, particularly in the high molecular weight range. Although Tricine- and Glycine-dSDS-PAGE showed similar spot count, resolution of spots was superior in the former. Protein spot excision, in-gel digestion and MALDI-TOF analysis demonstrated that both Bicine- and Tricine-dSDS-PAGE were compatible with mass spectrometry (Figures 2.2.7 to 2.2.9). The dSDS-PAGE experiment was well-suited for the analysis of hydrophobic proteins and highly basic proteins, unlike traditional 2D-PAGE approaches. Combining this power with the added advantages of improved spot resolution and protein representation observed in a bicine-based system produced a separation method that is amenable to detailed probing of the membrane proteome.

Since all dSDS-PAGE techniques investigated involved identical first dimensions using the Laemmli protocol, the resolving power of each method can be effectively demonstrated when considering the conversion of total number of protein bands in the first dimension to total number of protein spots in the second dimension in large format gels. For Glycine-dSDS-PAGE, 42 bands in the first dimension were translated into 109 second dimensional protein spots. In the case of Tricine-dSDS-PAGE, 42 1D bands were converted into 122 second dimension spots. Finally for Bicine-dSDS-PAGE, 42 protein bands were resolved into 165 protein spots in the second dimension. The identical first dimensional experiments in each protocol served as a normalizing factor in clearly demonstrating the relative resolving capabilities of each dSDS-PAGE technique.

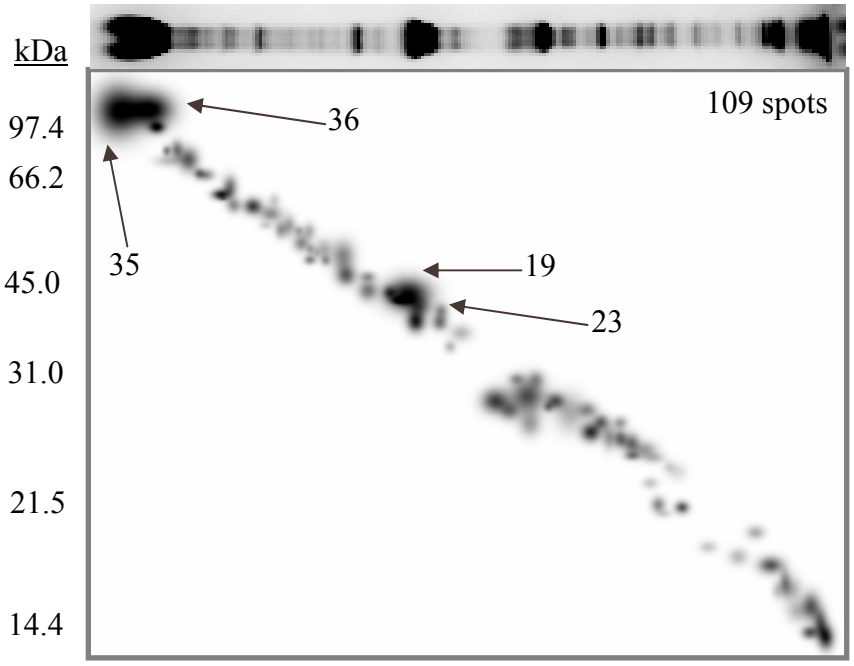

Figure 2.2.7. Standard Laemmli-dSDS-PAGE separation of *C. thermocellum* membrane proteins. A 10% acrylamide 1D experiment was followed by a 9-12% 2D acrylamide gradient gel separation. Proteins identified by mass spectrometry included S-layer proteins (#35 and 36), extracellular solute-binding protein (19) and small GTP-binding protein domain (23).

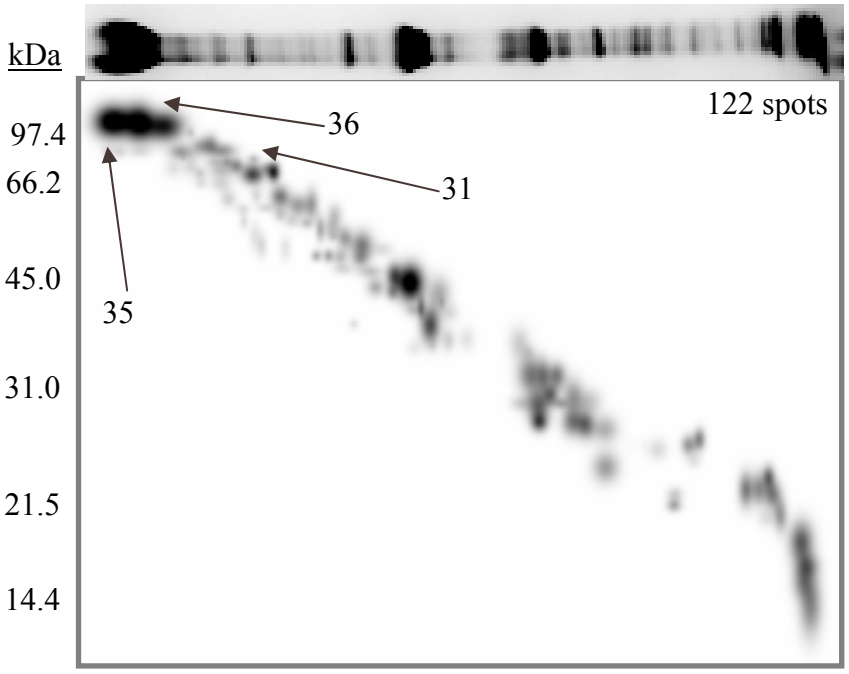

Figure 2.2.8. Tricine-dSDS-PAGE of *C. thermocellum* membrane proteins. A 10% acrylamide 1D experiment was followed by a 9-12% 2D acrylamide gradient gel separation. Proteins identified by mass spectrometry included S-layer proteins (#35 and 36) and molecular chaperone (31).

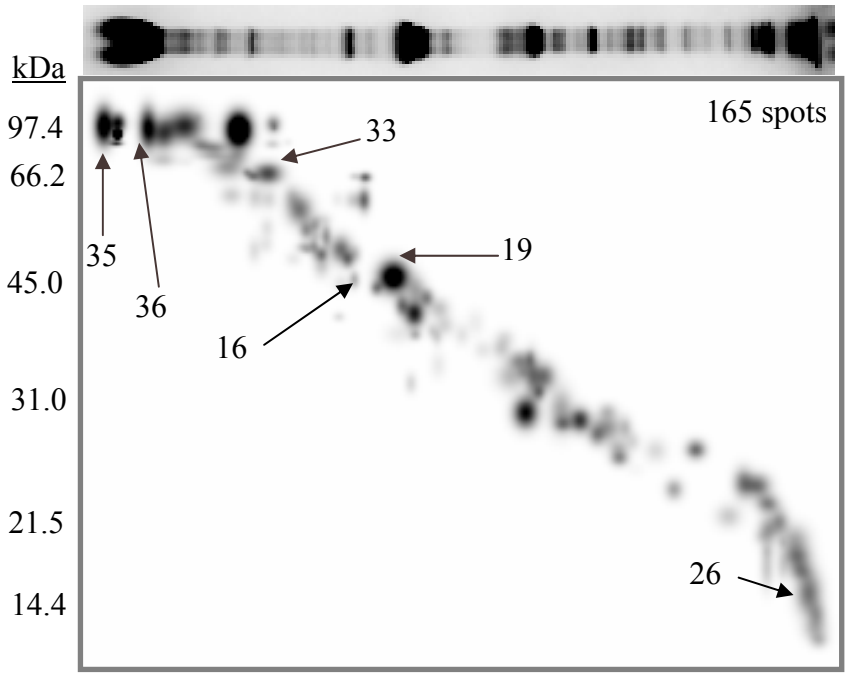

Figure 2.2.9. Bicine-dSDS-PAGE of *C. thermocellum* membrane proteins. A 10% acrylamide 1D experiment was followed by a 9-12% 2D acrylamide gradient gel separation. Proteins identified by mass spectrometry included S-layer proteins (#35 and 36), glycoside hydrolase family 10 enzyme (33), ribosomal protein L16 (26), extracellular solute-binding protein (19) and ABC transporter (16).

A closer look at the electrophoresis process offers insight into the observed differences in resolving powers for the three dSDS-PAGE methods. Tricine-based buffer systems have been typically used for the separation of low-molecular weight proteins and peptides. The stacking of low molecular weight polypeptides (5 kDa) by Glycine-SDS-PAGE is complicated by the fact that their complex with SDS has about the same size as that of the SDS micelle (18-32 kDa) (33). The small proteins stack together with the SDS from the sample buffer and they co-migrate in the resolving gel together with SDS, producing inferior resolution. Substituting the trailing ion glycine in the electrode buffer with the faster moving tricine prevents stacking of the SDS ions with the low molecular weight protein bands, thus improving their resolution. Ion mobility depends on charge density of a molecule and the voltage gradient. Under gel electrophoresis pH conditions, more tricine is in the migrating anionic form, compared to glycine. As a result, tricine migrates faster than glycine under such conditions, despite the fact that tricine has the higher molecular weight (Table 2.2.2). Evidence from previous studies suggests that highly hydrophobic peptides are unable to bind with SDS at high SDS:protein ratios, suggesting a greater role of the trailing ion in electrophoretic separations (85). A similar argument can be considered for hydrophobic membrane proteins, indicating that a faster ion than glycine would be more suitable to obtain better resolution. Unlike peptides, however, membrane proteins are considerably larger in size and less mobile. As such, a very fast ion, such as tricine, would not be able to provide sufficient time and opportunity for optimum separation and resolution.

Capillary Electrophoresis Experiments

The driving force for ion motion in gel electrophoresis is electrophoretic mobility, as electroosmotic flow is non-existent. An examination of the electrophoretic mobilities of trailing ions in the three buffer systems can provide insight into the selectivity and separation efficiency offered by Glycine-, Bicine- and Tricine-dSDS-PAGE. To this end, capillary electrophoresis with indirect UV detection was performed on glycine, bicine, and tricine. In CE, ion mobility is a vector addition of electroosmotic flow (μ_{eo}) and electrophoretic mobility (μ_e). Electroosmotic flow is the movement of a liquid in contact with the solid capillary surface when a tangential electric field is applied. The migration

Table 2.2.2. Charge states of various gel electrophoresis buffers.

pH	6	7	8	9	10	11	12	13	14
Glycine $pk_{a1} = 2.35$ $pk_{a2} = 9.78$	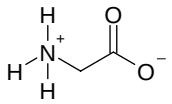				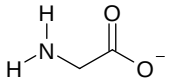				
Bicine $pk_{a1} = 1.84$ $pk_{a2} = 8.35$	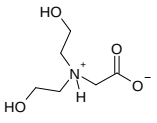				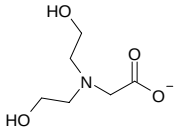				
Tricine $pk_{a1} = 2.30$ $pk_{a2} = 8.15$	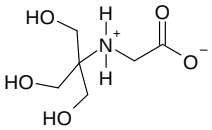				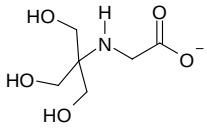				
Tris $pk_a = 8.30$	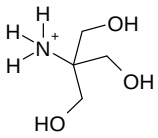				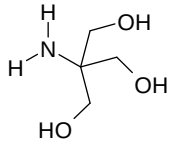				

of a charged species under the influence of this electric field is known as electrophoretic mobility. Analyte mobility is dependent not only on the charge density of the solute but on the dielectric constant and viscosity of the electrolyte as well. The apparent mobility of a species (μ) in CE is expressed as (86):

$$\mu = \mu_{eo} \pm \mu_e . \tag{2.2.1}$$

A positive sign indicates that μ_e for the ion has same direction as μ_{eo} and vice-versa.

For a given CE experiment, μ_{eo} is a constant and dominant factor in the apparent mobility of analytes. Therefore, separation of analytes will be exclusively dictated by differences in their μ_e, as given by the following (86):

$$\mu_e = \frac{lL}{V(t_{eo} - t)} . \tag{2.2.2}$$

where L is the capillary length, l is the capillary length to the detector, V is the applied voltage, t_{eo} is the μ_{eo} front migration time and t is the analyte migration time.

In the standard CE operation mode, the sample is injected at the anodic end of the capillary and detection occurs at the cathodic end. The electroosmotic flow front under such conditions will travel from anode to cathode. On applying a suitable voltage, analytes migrate toward the electrode of opposite charge according to their μ_e. If μ_e were the dominant or sole driving force in ion mobility, anions, such as bicine and tricine at basic pH, would hardly migrate from the anode and never reach the detector. Since the magnitude of μ_{eo} is much greater than that of μ_e, the apparent mobilities of all species dictate a unidirectional flow from anode to cathode. The direction of μ_e for cations is the same as that of the electroosmotic flow front, enabling cations to migrate faster than μ_{eo} and reach the detector first. Neutral species travel along with μ_{eo}, reaching the detector after cations. The anions reach the detector last, as their μ_e vector is in the opposite direction of μ_{eo}.

The electrophoretic mobilities of glycine, bicine and tricine at pH 8.3 and 8.9 were evaluated by performing standard CE experiments on mixtures of these analytes. These pH values were chosen because they are identical to the pH of gel electrophoresis running buffers in dSDS-PAGE. For identification purposes and to determine migration times, individual analytes were also run separately at each pH. The electropherograms

generated from experiments conducted at BGE pH 8.3 and 8.9 are given in Figures 2.2.10(A) and (B). At both pH values, glycine displayed the shortest migration time, followed by bicine, and tricine had the longest migration time. Since apparent mobility (μ) is inversely proportional to migration time (86), these experiments demonstrated that of the three analytes, glycine showed the highest μ, followed by bicine, with tricine having the lowest μ.

Eqn (2.2.1) dictates that μ for anions will be less than the μ_{eo}. Thus, a higher value of μ implies a smaller μ_e since μ_{eo} is constant for a given system. So glycine displayed the smallest μ_e (0.12×10^{-4} $cm^2V^{-1}s^{-1}$), followed by bicine (1.50×10^{-4} $cm^2V^{-1}s^{-1}$), and tricine displayed the highest μ_e (2.27×10^{-4} $cm^2V^{-1}s^{-1}$). These results are in direct agreement with the pH-dependent charge states of the various analytes (Table 2.2.2). The predominant equilibrium for all analytes at the experimental pH values occurs between the zwitterionic and anionic forms. At pH 8.3, approximately 50% of bicine is anionic, slightly greater than 50% of tricine exists as anions, and a large majority of glycine is zwitterionic. Since a larger fraction of tricine is anionic compared to the other analytes, tricine migrated the slowest. The constant re-equilibration between the zwitterionic and anionic glycine during the course of migration was enough to retard this species and give it a slightly greater migration time than μ_{eo}. A similar migration order with longer migration times was observed for pH 8.9, at which greater amounts of each analyte exists as anions. As in CE, bicine would also show intermediate μ_e in gel electrophoresis experiments. It is likely that the intermediate μ_e of bicine provides the key to better resolution in dSDS-PAGE of hydrophobic membrane proteins compared to tricine and glycine.

Conclusions

With the typically low abundance of membrane proteins in biological systems, it is imperative that analytical protocols for studying such proteins afford the highest resolution and protein representation possible. Increased resolution and representation of membrane proteins was achieved by exploring electrophoretic buffer systems other than the traditional Laemmli approach. Tricine-dSDS-PAGE provided better spot count and

(A)

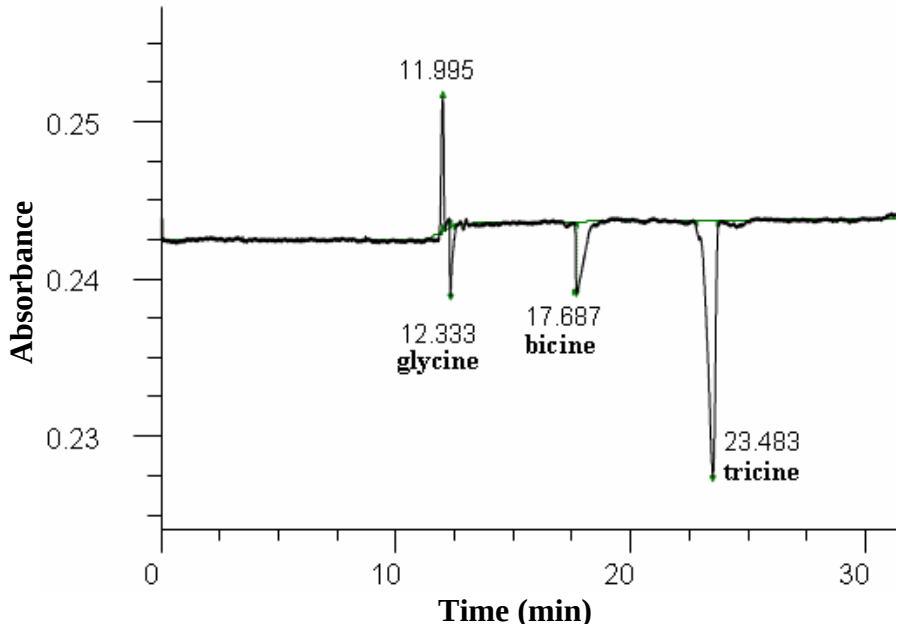

(B)

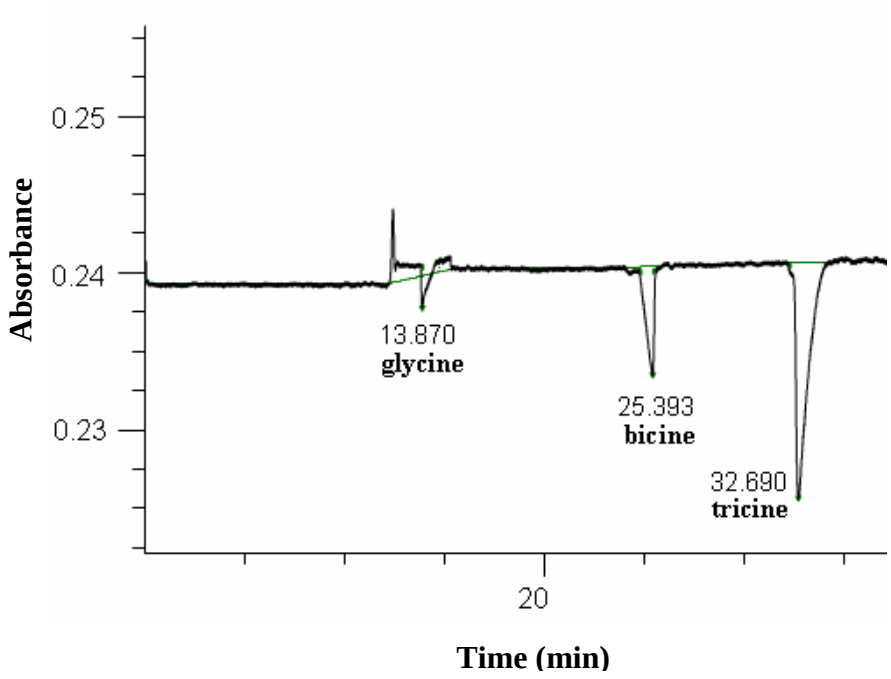

Figure 2.2.10. Electropherograms of a mixture of glycine, bicine and tricine dissolved in background electrolyte (BGE). The BGE used was 100 mM borate + 10 mM 2-methyl-1,3-cyclohexanedione at (A) pH 8.3 and (B) pH 8.9; capillary dimensions 75 µm x 100 cm; distance to detector 75 cm.

resolution compared to Glycine-dSDS-PAGE (112% increase in spot count over Glycine-dSDS-PAGE) and Bicine-dSDS-PAGE (151% increase in spot count over Glycine-dSDS-PAGE) provided the best separation conditions of all. Gels with low water content, high ionic strength and improved sieving capabilities were better suited for Tricine- and Bicine-dSDS-PAGE, compared with the standard Laemmli protocol for gel preparation.

Due to the hydrophobic nature of membrane proteins, they typically have low SDS:protein binding ratios and as such, their migration in an electric field is more strongly dictated by the trailing ion in the running buffer. Tricine-dSDS-PAGE, with a faster trailing ion than the glycine-based system, provided better electrophoretic separation of membrane proteins, as demonstrated by increased spot number in the optimized gels. Tricine-based systems have been previously demonstrated to be well-suited for analysis of peptides, due to their low molecular weight and high mobilities, in an electric field. However, with slower moving membrane proteins, a slightly slower trailing ion such as bicine can provide adequate time for improved stacking and separation. Capillary electrophoresis experiments with indirect UV detection suggested that CE data can provide a suitable guide for selection of the trailing ion in gel electrophoresis running buffers. In this way, the dSDS-PAGE experiment can be appropriately tailored to the particular sample under investigation so as to produce optimum separation conditions. The Bicine-dSDS-PAGE approach has been successfully applied towards the analysis of differentially expressed proteins in wild type and ethanol-adapted *C. thermocellum* membranes to obtain a better understanding of the nature of ethanol tolerance (Chapter 2.3).

Chapter 2.3

Analysis of Proteomic Profile Changes in Membranes of Ethanol-Adapted *Clostridium thermocellum*

Introduction

The effects of ethanol on microbes have been investigated extensively (2, 3, 8-12), but the mechanisms contributing to growth inhibition are many and complex. A major cause of the negative effects of elevated ethanol levels is disturbance and disruption of membrane permeability (3), and so it is likely that changes induced by ethanol adaptation involve membrane physiology and the membrane proteome. A thorough analysis of membrane protein expression in wild type and ethanol-adapted cells would shed light on the biochemistry of ethanol tolerance. Due to the disadvantages of membrane protein analysis using 2D-PAGE, Schägger and co-workers (17) described a doubled SDS-PAGE (dSDS-PAGE) experiment in which SDS-PAGE separation of membrane proteins in the first dimension is followed by SDS-PAGE separation in the second dimension. They applied tricine-based and standard glycine-based running buffers in the analyses. While these buffer systems were suitable for membrane protein analysis, the newly designed Bicine-dSDS-PAGE method (34), described in Chapter 2.2, offered the best resolution and protein spot representation of the three approaches. A two-part Bicine-dSDS-PAGE analysis was performed on wild type and ethanol-adapted *C. thermocellum* membrane proteins to bring different regions of the membrane proteome into focus and obtain a clear picture of differential protein expression patterns.

Although wild type strains of *C. thermocellum* are typically inhibited by ethanol concentrations less than 2%, strains able to tolerate as high as 8% have been generated (1, 2, 8-10) through sequential transfer techniques. Previous investigations (78) indicated that cell surface proteins could be accumulating at the site of manufacture (cytosol) in ethanol-adapted cells. Based on the hypothesis that membrane protein expression in wild type and ethanol-tolerant strains is different, the proteomes of these cultures were evaluated and compared. Understanding membrane protein expression changes instigated by ethanol adaptation is essential in the interest of developing more robust microbes with

increased abilities to tolerate and produce biogenic ethanol. To our knowledge, this is the first investigation on differential membrane protein expression in *C. thermocellum*.

Experimental

Materials

All chemicals and materials for the growth of bacterial cultures were purchased from Sigma (St. Louis, MO) except yeast extract, which was obtained from Difco Laboratories (Detroit, MI). Laemmli sample buffer, Coomassie G-250, Coomassie R-250, Tris base, SDS, acrylamide, N,N-methylene-bis-acrylamide (bis), ammonium persulfate (APS) and N,N,N,N-tetramethyl-ethylenediamine (TEMED) were obtained from Bio-Rad (Hercules, CA). Bicine, ammonium bicarbonate and the MALDI matrix α-cyano-4-hydroxycinnamic acid (HCCA) came from Sigma. Methanol, glycerol, *o*-phosphoric acid, hydrochloric acid, formic acid, trifluoroacetic acid (TFA), acetonitrile and trypsin were purchased from Fisher Scientific (Pittsburg, PA). Ammonium sulfate was obtained from EMD Chemicals (Gibbstown, NJ).

Bacterial Strains and Growth Conditions

C. thermocellum ATCC 27405 was obtained from the American Type Culture Collection. Adaptation of wild type cells to 5% ethanol was brought about using a sequential transfer procedure as previously described (78). Briefly, the wild-type strains were initially grown in a basal medium containing 0.5% (w/v) ethanol. The rate and extent of growth were monitored and upon cessation of growth, cultures were immediately transferred to fresh medium containing ethanol at 0.5% (w/v). Several (typically 3 or 4) repeated transfers of this sort were performed to ensure that ethanol tolerance was not lost. The ethanol concentration was then raised to 1%. Additional rounds of repeated transfers were performed and involved incrementally increasing the ethanol concentration by 0.5% to arrive at bacteria that could tolerate 5% ethanol.

The organisms were cultured in a medium that contained 10.8 mM Na_2HPO_4, 11.05 mM KH_2PO_4, 9.35 mM NH_4Cl, 3.79 mM $(NH_4)_2SO_4$, 0.44 mM $MgCl_2.6H_2O$, 0.27 mM $CaCl_2$, 2.0 g/L yeast extract, 0.5 g of cysteine, 10 mL of a vitamin standard mixture

(79) and 5 mL of a modified micromineral mixture stock (79). This micromineral mixture also contained 10 mg of $Na_2WO_4.2H_2O$ and 1 mg of Na_2SeO_3 per liter of stock, as well as 1 mg/L of the oxygen indicator resazurin. The basal medium was adjusted to pH 6.7 with 10% NaOH and autoclaved for 10 min to remove dissolved gases. Carbon dioxide was then immediately bubbled through the solution until it was cooled to room temperature, following which an anaerobic solution of Na_2CO_3 was added to provide 4 g per liter (final concentration). The medium was then anaerobically dispensed into culture tubes and bottles and sterilized by autoclaving for 20 min. This basal medium was supplemented with an anaerobic solution of cellobiose (final concentration of 4 g/L). Ethanol-adapted cell cultures were grown in a similar medium that also contained 5% (w/v) ethanol.

Preparation of Crude Membrane Protein Fractions

Cell cultures were grown at 55ºC and harvested once the optical density at 600 nm had reached approximately 1.0. The cultures were then centrifuged (15,000 x *g*, 10 min, 4^{o}C) and the supernatant was discarded and the pellets re-suspended with 40 mL buffer (50 mM Tris, pH 7.5). This was followed by another 10 min centrifugation and finally by an additional wash step. Cell pellets were then re-suspended in buffer to a final optical density of approximately 50. The concentrated cells were stored at -80^{o}C until further use.

Concentrated cells were thawed and phenylmethylsulfonylfluoride (PMSF) and dithiothreitol (DTT) were added to achieve final concentrations of 5 mM for each. The cells were then lysed by passage through a French Press (SLM Aminco, Urbana, IL) three times at 137 MPa. The broken cells were centrifuged (5,700 x *g*, 10 min, 4^{o}C). The pellets were then discarded and the supernatant centrifuged (200,000 x *g*, 45 min, 4^{o}C). The resulting membrane pellet was re-suspended in 10 mL of 10 mM Tris, pH 7.5 and this was centrifuged twice (200,000 x *g*, 45 min, 4^{o}C). The washed pellets were finally re-suspended in 10 mM Tris, pH 7.5, to obtain a protein concentration of approximately 6.4 mg/mL using the Lowry assay (80). Aliquots of re-suspended proteins were stored at -80^{o}C until further use.

Sucrose Isopycnic Density Gradient Centrifugation

In order to obtain a more defined membrane fraction for subsequent mass spectrometric analyses, the crude membranes from wild type and ethanol-adapted *C. thermocellum* were subjected to sucrose isopycnic density gradient centrifugation (SIDGC). The gradient was prepared by layering solutions of increasing sucrose percentages in 11 mL centrifuge tubes (bottom to top) as follows: one part 55%, two parts 45%, two parts 40%, two parts 35%, three parts 30% and finally one part sample. The tubes were then centrifuged in a swinging bucket rotor (270,000 x *g*, 47 h, 4^{o}C). Aliquots (0.5 mL) were removed and protein concentration was estimated by absorbance at 280 nm. Fractions were pooled based on their absorbance and these pools were diluted approximately 3-fold with 10 mM Tris (pH 7.5). Membrane proteins were then collected by centrifugation (48,300 x *g*, 2 h, 4^{o}C). The resultant pellets were washed twice with 10 mM Tris (pH 7.5) and the final resuspension yielded a protein concentration between 11 and 20 µg/µl.

Bicine-dSDS-PAGE

A previously developed Bicine-dSDS-PAGE approach (34) was used to separate membrane proteins. Large (20 cm x 20 cm) format gel experiments were performed with the PROTEAN II xi electrophoresis cell (Bio-Rad). Linear acrylamide gradients in the second dimension of dSDS-PAGE were generated using a Model 485 Gradient Former and all gels were run at 4^{o}C. The first dimension of a dSDS-PAGE experiment consisted of a 4% acrylamide stacking gel and an 8 or 11% separating gel (1 mm thick). The two separating gel percentages provided enhanced resolution of different regions of the bacterial membrane proteome. The Laemmli protocol (19) was used to separate the proteins in the first dimension of Bicine-dSDS-PAGE and gels were run at 16 mA/gel for protein migration through the stacking gel. This was then increased to 24 mA/gel when the dye front entered the separating gel. Run times for large format 1D gels were typically 7 h.

Membrane proteins were then further resolved in the second dimension by a 7-12% linear acrylamide gradient gel of 1.5 mm thickness. After staining with Coomassie R-250 overnight, gel strips (approximately 5 mm wide) were excised from the first

dimension, swelled for 30 min in buffer (100 mM Tris, 150 mM HCl, approximately pH 2), and then placed in between the glass plates and on top of the separating gel of the second dimension (17). Gaps between the excised gel lane and the spacers of the second dimension were filled with gel mixtures that contained 10% acrylamide, the same composition as in the 1D strip. Gel and running buffer preparation for the second dimension of Bicine-dSDS-PAGE were described previously (34). Running conditions for second dimensional gels were 90 V for 30 min and 120 V thereafter, with run times of approximately 24 h. All second dimension gels were stained with G-250 Colloidal Coomassie (23).

Image Analyses

Gel images were captured using a Bio-rad Versadoc Imaging System and analysis of 1D and 2D images was performed by Bio-Rad Quantity One and PDQuest software, respectively. Images shown in figures are Gaussian representations generated by the software.

Protein Identification

Tryptic digests of membrane proteins were examined in positive ion mode using a Bruker Autoflex MALDI-TOF or a Finnigan LCQ Classic quadrupole ion trap mass spectrometer. HCCA was used as the matrix for MALDI-TOF protein analyses. MALDI spectra were internally calibrated using peptides from trypsin autolysis (*m/z* 842.51 and 2211.10). Peptide mass fingerprinting data (PMF) with monoisotopic peak mass lists were analyzed using the MASCOT algorithm and the *C. thermocellum* database (82). Protein spots that could not be identified by MALDI were subjected to LC-ESI-MS/MS.

A Hewlett Packard LC system (1100 series) with a custom-made C_{18} capillary LC column was interfaced to the ion trap mass spectrometer for reversed phase LC-MS/MS analyses. A mobile phase mixture of water and acetonitrile (ACN), each containing 0.1% formic acid, was used in all experiments. Gradient elution was employed in these studies, as described in Chapter 1.2 of Part 1. LCQ data was also analyzed by the MASCOT algorithm and the *C. thermocellum* database.

Results

The Bicine-dSDS-PAGE analysis provided a diagonal arrangement of *C. thermocellum* membrane protein spots and a total of 145 proteins were identified from crude and SIDGC membrane preparations using MALDI-TOF MS and MASCOT database searching. The MALDI-TOF mass spectrum of a histidine kinase identified from *C. thermocellum* membrane preparations is given in Figure 2.3.1. Analysis of crude membrane fractions revealed that 45% of all proteins identified from this fraction were cytosolic (based on the absence of protein transmembrane domains or TMDs). In contrast, the highly purified samples from SIDGC contained dramatically lower amounts (14%) of such proteins. Since the SIDGC fractions were more highly enriched with non-cytosolic proteins, these samples were used in subsequent experiments.

The Bicine-dSDS-PAGE analysis of highly purified membrane fractions revealed similar spot diversity for wild type and ethanol-adapted *C. thermocellum* in both the high and low molecular weight ranges. Gel experiments aimed at better resolution and representation of high molecular weight proteins (8% first dimension separating gel) resolved 76 spots in the wild type organism (Figure 2.3.2(A)) and 72 spots in the ethanol-adapted strain (Figure 2.3.3(A)). For dSDS-PAGE experiments geared towards low molecular weight protein analysis (11% first dimension separating gel), wild type *C. thermocellum* membranes yielded 123 spots (Figure 2.3.2(B)) whereas the ethanol-adapted organism provided 117 spots (Figure 2.3.3(B)). Despite the similarities in protein spot numbers between the two cultures, it was evident that many proteins were present at higher levels in wild type membranes compared to ethanol-adapted bacteria. Analysis of the relative expression values indicated a fairly even distribution of differentially expressed proteins throughout the molecular weight range under investigation (Table 2.3.1).

Further examination of the proteins from the SIDGC fractions by measures of relative hydrophobicity can provide information on their propensity of being membrane-associated. TMD analyses revealed that a majority of these proteins have two or more TMDs and nearly half had positive Grand Average of Hydropathicity (GRAVY) scores (Table 2.3.2). As a general trend, higher numbers of TMDs corresponded with more

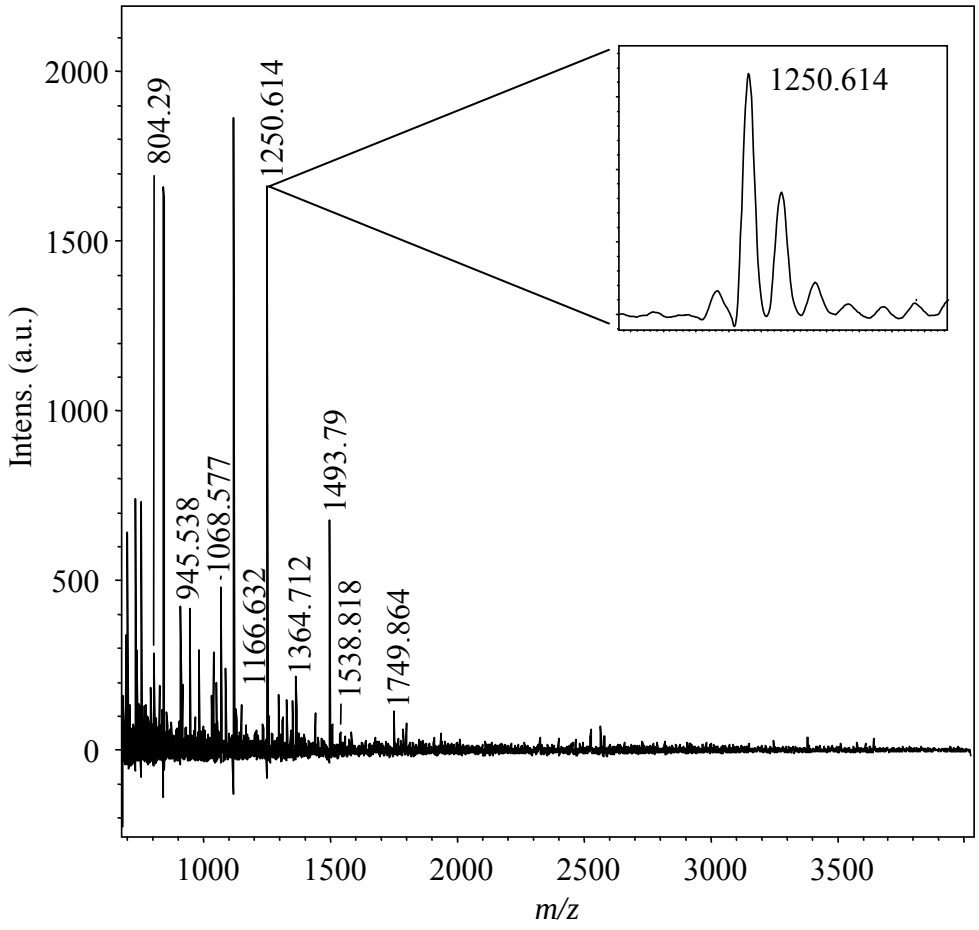

Figure 2.3.1. MALDI-TOF mass spectrum of histidine kinase, HAMP region: bacterial chemotaxis sensory transducer (#32: gi 67874049).

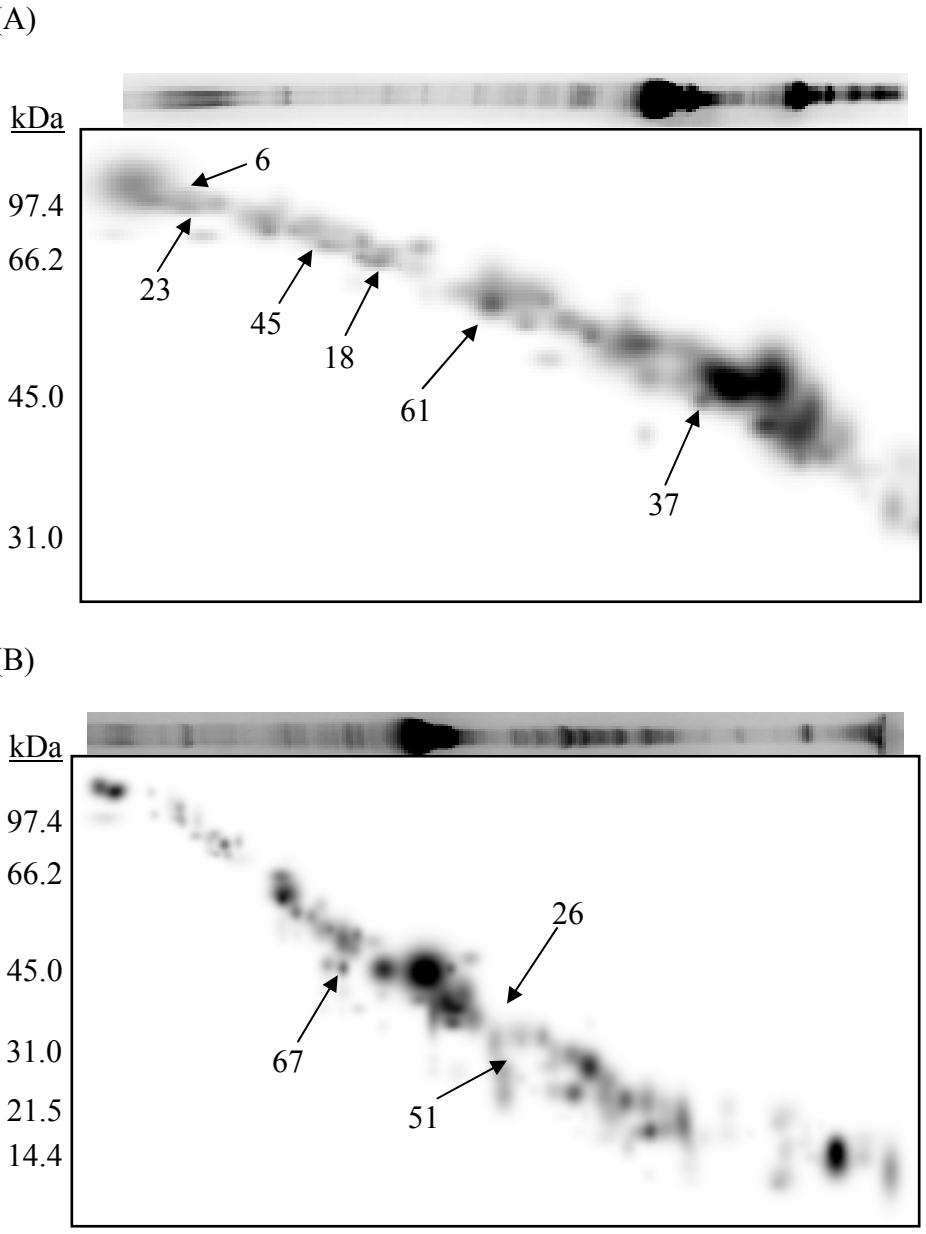

Figure 2.3.2. Bicine-dSDS-PAGE of the wild type *C. thermocellum* membrane proteins: (A) 8% acrylamide and (B) 11% acrylamide 1D experiments were followed by a 9-12% 2D acrylamide gradient gel separation. Highlighted proteins identified by mass spectrometry include glycoside hydrolase (#45: gi 67874975), SecA (#6: gi 67916795), chemotaxis sensory transducer (#37: gi 67873910), flagellar biosynthetic protein FlhB (#67: gi 67875429), Mg^{2+}-transporter protein, CorA-like (#26: gi 67875293), divalent cation transporter (#61: gi 67916199), amino acid-binding ACT: MgtC/SapB transporter (#51: gi 67916179) and S-layer proteins (#18: gi 67917201 and #23: gi 67916324).

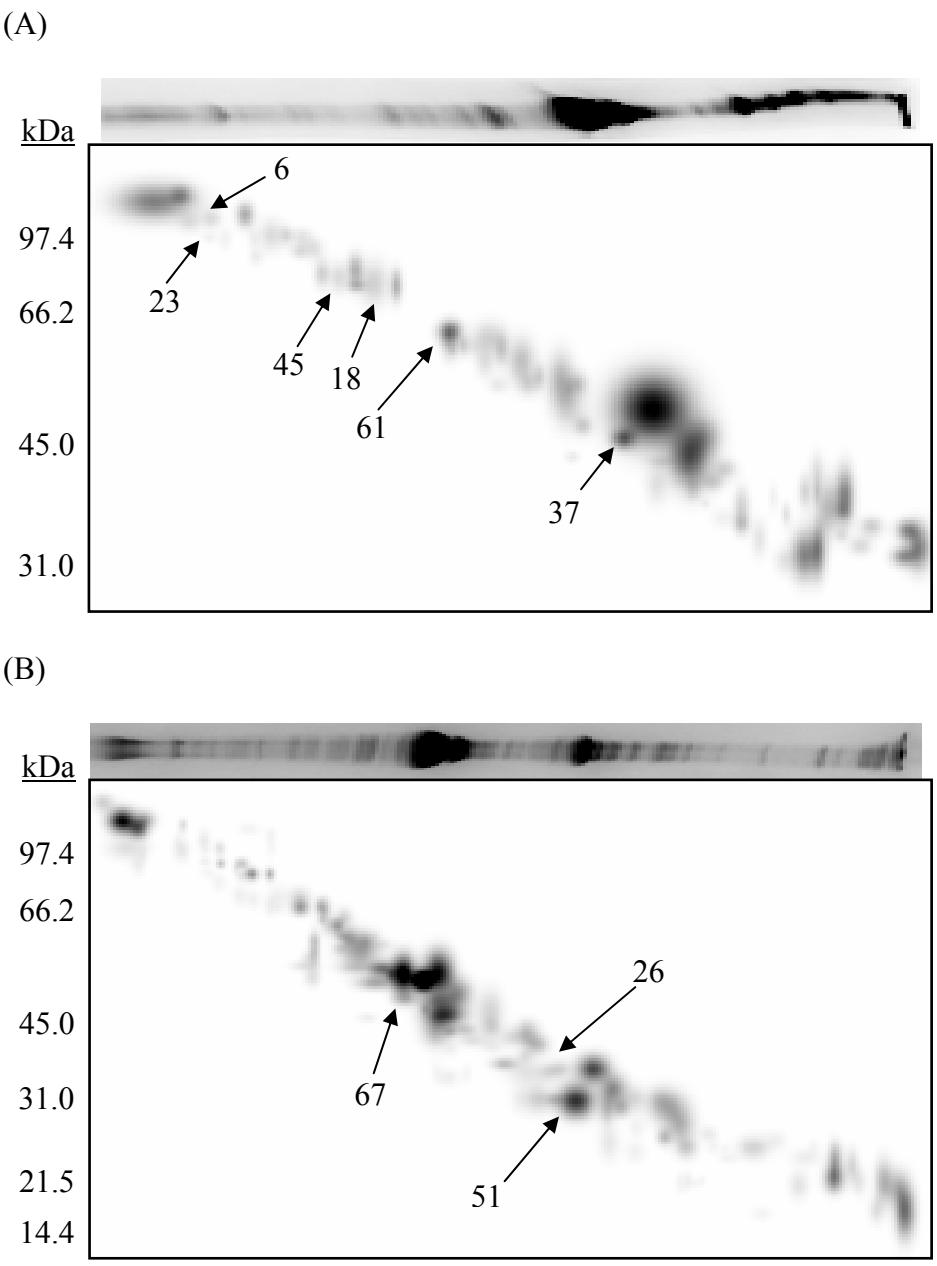

Figure. 2.3.3. Bicine-dSDS-PAGE of the ethanol-adapted *C. thermocellum* membrane proteins: (A) 8% acrylamide and (B) 11% acrylamide 1D experiments were followed by a 9-12% 2D acrylamide gradient gel separation. Highlighted proteins identified by mass spectrometry include glycoside hydrolase (#45: gi 67874975), SecA (#6: gi 67916795), chemotaxis sensory transducer (#37: gi 67873910), flagellar biosynthetic protein FlhB (#67: gi 67875429), Mg^{2+}-transporter protein, CorA-like (#26: gi 67875293), divalent cation transporter (#61: gi 67916199), amino acid-binding ACT: MgtC/SapB transporter (#51: gi 67916179) and S-layer proteins (#18: gi 67917201 and #23: gi 67916324).

Table 2.3.1. Proteins identified from purified membrane fractions: gel analysis data.

#	gi	Protein Name	MW	pI	MOWSE Score	Seq. cov. (%)	Ratio* WT/EA
1	67876078	Chaperonin Cpn60/TCP-1	57474	4.96	425	43	0.88
2	67876077	Chaperonin Cpn10	10156	5.22	38	30	1.35
3	67874556	AMP-dependent synthetase and ligase	64507	8.72	177	37	1.05
4	67874931	Cysteine synthase K/M: Cysteine synthase K	33398	6.62	652	43	1.19
5	67916452	Anthranilate synthase component I	56020	6.30	33	12	2.73
6	67916795	SecA protein	104612	6.38	132	24	2.57
7	67916027	H^+-transporting two-sector ATPase	65363	5.30	159	30	1.18
8	67875538	NADH dehydrogenase (ubiquinone)	68124	6.55	102	22	1.23
9	67916533	Ferredoxin: 4Fe-4S ferredoxin, iron-sulfur binding domain: Iron hydrogenase, small subunit: Hydrogenase large subunit, C-terminal	64013	6.25	34	11	1.78
10	67916676	Acetate kinase	43966	7.12	34	14	1.39
11	67916856	Clostridium cellulosome enzyme, dockerin type I: Carbohydrate binding module, family 6	105247	6.03	38	7	2.12
12	67916907	Glycoside hydrolase, family 5: Clostridium cellulosome enzyme, dockerin type I: Carbohydrate binding domain, family 11	102415	5.61	33	6	1.18
13	67874442	Polysaccharide deacetylase	36292	5.39	100	17	2.42
14	67875254	Glycoside hydrolase, family 9: Clostridium cellulosome enzyme, dockerin type I	68642	5.57	32	6	3.21
15	67875618	Conserved hypothetical protein	40466	5.64	32	5	2.54
16	67917396	Periplasmic binding protein	34968	4.98	43	25	2.08
17	67916519	Peptide chain release factor 3: Small GTP-binding protein domain	60641	5.95	32	9	1.18
18	67917201	S-layer protein (SLH domain): Bacterial Ig-related	64851	4.50	354	12	3.78
19	67875524	Glycoside hydrolase, family 9: Clostridium cellulosome enzyme, dockerin type 1: Carbohydrate-binding, CenC-like: Glycoside hydrolase family 9, N-terminal, Ig-like	100621	5.29	32	5	2.20
20	67874774	Glycoside hydrolase, family 9: Bacterial type 3a cellulose-binding domain: Clostridium	82122	5.49	32	5	4.17

		cellulosome enzyme, dockerin type 1					
21	67876088	Clostridium cellulosome enzyme, dockerin type I	55169	8.55	97	17	2.01
22	67916212	Putative esterase: Glycoside hydrolase, family 10: Clostridium cellulosome enzyme, dockerin type 1: Carbohydrate-binding, CenC-like	119664	5.45	33	3	2.76
23	67916324	Similar to S-layer domain	89952	5.12	32	7	2.08
24	67875819	Hypothetical protein CtheDRAFT_2053	17520	9.61	48	25	2.96
25	67917091	ATP-binding region, ATPase-like: Histidine kinase A, N-terminal	39499	7.33	86	19	1.62
26	67875293	Mg^{2+} transporter protein, CorA-like	36590	4.91	73	25	0.44
27	67916045	CheW-like protein:ATP-binding region, ATPase-like: Signal transducing histidine kinase, homodimeric domain: Hpt	78305	4.94	95	5	0.40
28	67916751	Glycosyl transferase, group 1: Phospholipid/glycerol acyltransferase	71359	9.80	36	6	2.35
29	67916159	Clostridium cellulosome enzyme, dockerin type I: Glycosyl hydrolase, BNR repeat	92364	5.19	73	7	2.44
30	67916443	Protein of unknown function DUF 1432	35303	8.73	253	56	2.95
31	67916720	Glycosyl transferase, family 2	36155	8.69	48	13	2.76
32	67874049	Histidine kinase, HAMP region: Bacterial chemotaxis sensory transducer	68286	5.02	46	21	0.50
33	67916032	AAA ATPase, central region: Peptidase M41, FtsH	43874	8.82	132	24	1.32
34	67875125	Glycoside hydrolase, family 9: Bacterial type 3a cellulose-binding domain: Clostridium cellulosome enzyme, dockerin type 1	79810	5.23	51	10	2.22
35	67873911	ABC1	64815	6.29	113	20	2.26
36	67874822	MotA/TolQ/ExbB proton channel	30847	5.62	98	10	1.60
37	67873910	Chemotaxis sensory transducer	45710	4.92	103	32	0.38
38	67875410	Flagellar FliF M-ring protein	57822	4.90	41	8	0.43
39	67876339	UDP-N-acetylglucosamine 1-carboxyvinyltransferase	44383	7.80	112	10	0.99
40	67916760	ATP-binding region, ATPase-like: Histidine kinase A, N-terminal	40280	5.46	83	15	1.65
41	67874555	Serine-type D-Ala-D-Ala carboxypeptidase	47984	6.95	44	5	2.54

42	67916336	Chemotaxis sensory transducer	46229	4.99	33	6	0.25
43	67876447	Serine-type D-Ala-D-Ala carboxypeptidase	46650	5.68	53	17	2.14
44	67874093	Hypothetical protein CtheDRAFT_3149	30329	9.31	49	7	1.84
45	67874975	Glycoside hydrolase, family 15	73680	5.52	32	7	2.29
46	67916154	Conserved hypothetical protein	25138	9.09	74	26	1.86
47	67876065	Peptidase C39, bacteriocin processing	33754	8.55	102	22	2.10
48	67917031	Putative sugar transport system permease ABC transporter protein	18113	9.30	76	12	2.92
49	67917112	ABC transporter, transmembrane region	29046	8.97	35	7	1.80
50	67873242	Similar to Flp pilus assembly protein TadB	30626	5.42	55	9	0.49
51	67916179	Amino acid-binding ACT: MgtC/SapB transporter	25495	9.04	50	10	0.35
52	67916824	Histidine kinase, HAMP region: Cache domain: Bacterial chemotaxis sensory transducer	91309	5.06	32	13	0.91
53	67875449	Holin, toxin secretion/phage lysis	14926	8.31	32	6	1.13
54	67916023	H^+-transporting two-sector ATPase, C subunit	15977	6.62	48	13	1.45
55	67915993	MscS Mechanosensitive ion channel	31354	8.80	42	9	0.47
56	67916702	ABC transporter, transmembrane region: ABC transporter	71856	8.51	58	18	2.44
57	67875027	Hedgehog/Intein hint domain, N-terminal	60427	6.41	98	19	0.73
58	67916960	Lipopolysaccharide biosynthesis	47526	5.18	75	22	1.11
59	67916966	Glycosyl transferase, family 2	44800	8.88	103	33	1.10
60	67876364	CDP-diacylglycerol-glycerol-3-phosphate 3-phosphatidyltransferase	22566	9.59	27	2	2.30
61	67916199	Divalent cation transporter	50239	5.03	48	8	0.24
62	67916249	Amino acid ABC transporter, permease protein, 3-TM region, His/Glu/Gln/Arg/opine	24788	9.54	53	13	2.22
63	67873370	GGDEF: Uncharacterized HDIG domain	60702	8.34	36	4	2.11
64	67875548	Small basic protein	13797	9.27	77	12	2.08
65	67874594	Permease	13024	9.60	42	11	3.02
66	67916392	Cobalt transport protein	30127	9.36	44	15	0.59
67	67875429	Flagellar biosynthetic protein FlhB	44294	9.52	49	13	0.50
68	67875120	Hypothetical protein CtheDRAFT_2575	37170	9.00	55	10	1.85
69	67875688	ABC transporter, transmembrane region: ABC transporter	70505	7.19	73	3	1.70

70	67873849	H^+-transporting two-sector ATPase, A subunit	28464	5.59	39	8	0.99
71	67917176	Phosphatidate cytidylyltransferase	22273	9.14	61	9	2.06
72	67873913	Cation transporting ATPase, N-terminal: Haloacid dehalogenase-like hydrolase: Cation transport ATPase, C-terminal: E1-E2 ATPase-associated region	93885	6.40	75	10	2.28

* Spot density ratio

Table 2.3.2. Proteins identified from purified membrane fractions: Grand Average of Hydropathicity (GRAVY) and transmembrane domain (TMD) analysis.

#	gi	Protein Name	F. Class*	GRAVY†	# TMDs‡
1	67876078	Chaperonin Cpn60/TCP-1	O	-0.081	0
2	67876077	Chaperonin Cpn10	O	-0.068	0
3	67874556	AMP-dependent synthetase and ligase	I	0.193	0
4	67874931	Cysteine synthase K/M: Cysteine synthase K	E	-0.129	0
5	67916452	Anthranilate synthase component I	EH	-0.276	0
6	67916795	SecA protein	U	-0.546	0
7	67916027	H^+-transporting two-sector ATPase	C	-0.228	0
8	67875538	NADH dehydrogenase (ubiquinone)	C	-0.209	0
9	67916533	Ferredoxin: 4Fe-4S ferredoxin, iron-sulfur binding domain: Iron hydrogenase, small subunit: Hydrogenase large subunit, C-terminal	C	-0.202	0
10	67916676	Acetate kinase	C	-0.089	0
11	67916856	Clostridium cellulosome enzyme, dockerin type I: Carbohydrate binding module, family 6	G	-0.238	1
12	67916907	Glycoside hydrolase, family 5: Clostridium cellulosome enzyme, dockerin type I: Carbohydrate binding domain, family 11	G	-0.456	1
13	67874442	Polysaccharide deacetylase	G	-0.264	1
14	67875254	Glycoside hydrolase, family 9: Clostridium cellulosome enzyme, dockerin type I	G	-0.445	1
15	67875618	Conserved hypothetical protein	S	-0.639	1
16	67917396	Periplasmic binding protein	P	-0.346	1
17	67916519	Peptide chain release factor 3: Small GTP-binding protein domain	O	-0.319	1
18	67917201	S-layer protein (SLH domain): Bacterial Ig-related	V	-0.208	1
19	67875524	Glycoside hydrolase, family 9: Clostridium cellulosome enzyme, dockerin type 1: Carbohydrate-binding, CenC-like: Glycoside hydrolase family 9, N-terminal, Ig-like	G	-0.532	1
20	67874774	Glycoside hydrolase, family 9: Bacterial type 3a cellulose-binding domain: Clostridium cellulosome enzyme, dockerin type 1	G	-0.327	1
21	67876088	Clostridium cellulosome enzyme, dockerin type I	G	-0.212	1
22	67916212	Putative esterase: Glycoside hydrolase, family 10: Clostridium cellulosome enzyme, dockerin type 1: Carbohydrate-binding, CenC-like	G	-0.358	1
23	67916324	Similar to S-layer domain	V	-0.190	2
24	67875819	Hypothetical protein CtheDRAFT_2053	S	0.193	2
25	67917091	ATP-binding region, ATPase-like: Histidine kinase A, N-terminal	T	-0.034	2
26	67875293	Mg^{2+} transporter protein, CorA-like	P	0.036	2
27	67916045	CheW-like protein: ATP-binding region, ATPase-like: Signal transducing histidine kinase, homodimeric domain: Hpt	T	-0.148	2
28	67916751	Glycosyl transferase, group 1: Phospholipid/glycerol acyltransferase	G	-0.029	2

29	67916159	Clostridium cellulosome enzyme, dockerin type I: Glycosyl hydrolase, BNR repeat	G	-0.298	2
30	67916443	Protein of unknown function DUF 1432	S	0.177	2
31	67916720	Glycosyl transferase, family 2	G	0.130	2
32	67874049	Histidine kinase, HAMP region: Bacterial chemotaxis sensory transducer	T	-0.284	2
33	67916032	AAA ATPase, central region: Peptidase M41, FtsH	O	-0.151	2
34	67875125	Glycoside hydrolase, family 9: Bacterial type 3a cellulose-binding domain: Clostridium cellulosome enzyme, dockerin type 1	G	-0.360	2
35	67873911	ABC1	O	-0.034	2
36	67874822	MotA/TolQ/ExbB proton channel	U	0.084	2
37	67873910	Chemotaxis sensory transducer	T	-0.057	2
38	67875410	Flagellar FliF M-ring protein	N	-0.403	2
39	67876339	UDP-N-acetylglucosamine 1-carboxyvinyltransferase	M	0.130	2
40	67916760	ATP-binding region, ATPase-like: Histidine kinase A, N-terminal	T	-0.159	2
41	67874555	Serine-type D-Ala-D-Ala carboxypeptidase	O	-0.054	2
42	67916336	Chemotaxis sensory transducer	T	-0.179	2
43	67876447	Serine-type D-Ala-D-Ala carboxypeptidase	O	0.069	2
44	67874093	Hypothetical protein CtheDRAFT_3149	S	-0.140	2
45	67874975	Glycoside hydrolase, family 15	G	-0.335	3
46	67916154	Conserved hypothetical protein	S	0.657	3
47	67876065	Peptidase C39, bacteriocin processing	O	0.120	3
48	67917031	Putative sugar transport system permease ABC transporter protein	G	0.957	3
49	67917112	ABC transporter, transmembrane region	R	0.528	3
50	67873242	Similar to Flp pilus assembly protein TadB	N	0.217	3
51	67916179	Amino acid-binding ACT: MgtC/SapB transporter	E	0.356	3
52	67916824	Histidine kinase, HAMP region: Cache domain: Bacterial chemotaxis sensory transducer	T	-0.244	3
53	67875449	Holin, toxin secretion/phage lysis	V	0.635	3
54	67916023	H+-transporting two-sector ATPase, C subunit	C	1.126	3
55	67915993	MscS Mechanosensitive ion channel	V	0.223	3
56	67916702	ABC transporter, transmembrane region: ABC transporter	R	0.036	3
57	67875027	Hedgehog/Intein hint domain, N-terminal	T	0.044	3
58	67916960	Lipopolysaccharide biosynthesis	GI	-0.239	3
59	67916966	Glycosyl transferase, family 2	G	-0.093	4
60	67876364	CDP-diacylglycerol-glycerol-3-phosphate 3-phosphatidyltransferase	I	0.776	4
61	67916199	Divalent cation transporter	P	0.265	4
62	67916249	Amino acid ABC transporter, permease protein, 3-TM region, His/Glu/Gln/Arg/opine	E	0.793	4
63	67873370	GGDEF: Uncharacterized HDIG domain	FT	0.064	4
64	67875548	Small basic protein	S	0.791	4
65	67874594	Permease	R	1.046	4
66	67916392	Cobalt transport protein	P	0.619	4
67	67875429	Flagellar biosynthetic protein FlhB	N	-0.011	4

68	67875120	Hypothetical protein CtheDRAFT_2575	S	0.416	4
69	67875688	ABC transporter, transmembrane region: ABC transporter	R	0.132	5
70	67873849	H+-transporting two-sector ATPase, A subunit	C	0.793	5
71	67917176	Phosphatidate cytidylyltransferase	F	1.005	5
72	67873913	Cation transporting ATPase, N-terminal: Haloacid dehalogenase-like hydrolase: Cation transport ATPase, C-terminal: E1-E2 ATPase-associated region	P	0.159	9

* Function class of protein (see Appendix for function class names)
† Grand Average of Hydropathicity (GRAVY) score
‡ Number of transmembrane domains (TMDs)

positive GRAVY values, indicating greater hydrophobicity of the protein. Overall, these results showed that the SIDGC fractions indeed were enriched with relatively hydrophobic proteins that are probably associated with the cell membrane.

Approximately 60% of the identified proteins in the purified fraction were differentially expressed in the wild type and ethanol-adapted strains. Of these differentially expressed proteins, 74% were up-regulated by a factor of two or more in the wild type strain with the remaining 26% up-regulated in the ethanol-adapted bacterium. Approximately half of the up-regulated proteins in the wild type organism were involved with carbohydrate transport and metabolism. Some of the up-regulated proteins in the ethanol-adapted species were associated with chemotaxis and signal transduction.

Discussion

The *C. thermocellum* Membrane Proteome

The 3214 putative proteins in the *C. thermocellum* proteome were interrogated for membrane proteins using the Sosui algorithm (87). This program predicts the number of TMDs in the amino acid sequences of proteins. Based on the analysis, 935 proteins (29.1% of the total proteome) were found to contain at least one TMD. Furthermore, 492 proteins in the database contained at least two TMDs. Proteins containing such hydrophobic domains were considered as integral membrane proteins. A virtual 2D gel map of the *C. thermocellum* membrane proteome was generated using web-based JVirGel software (88), as shown in Figure 2.3.4.

Membrane Proteome Analysis with Bicine-dSDS-PAGE

The highly purified membrane protein fraction obtained through SIDGC enabled relative quantification of differentially expressed proteins in wild type and ethanol-adapted *C. thermocellum* (Table 2.3.1). Many of these proteins were not observed in the crude fraction, perhaps because of their low abundance compared to other proteins in the sample, particularly cytosolic proteins. These experiments clearly demonstrated the benefits of employing sample purification procedures to enrich membrane proteins, as well as gel-based separation methods that are attentive to their physicochemical nature.

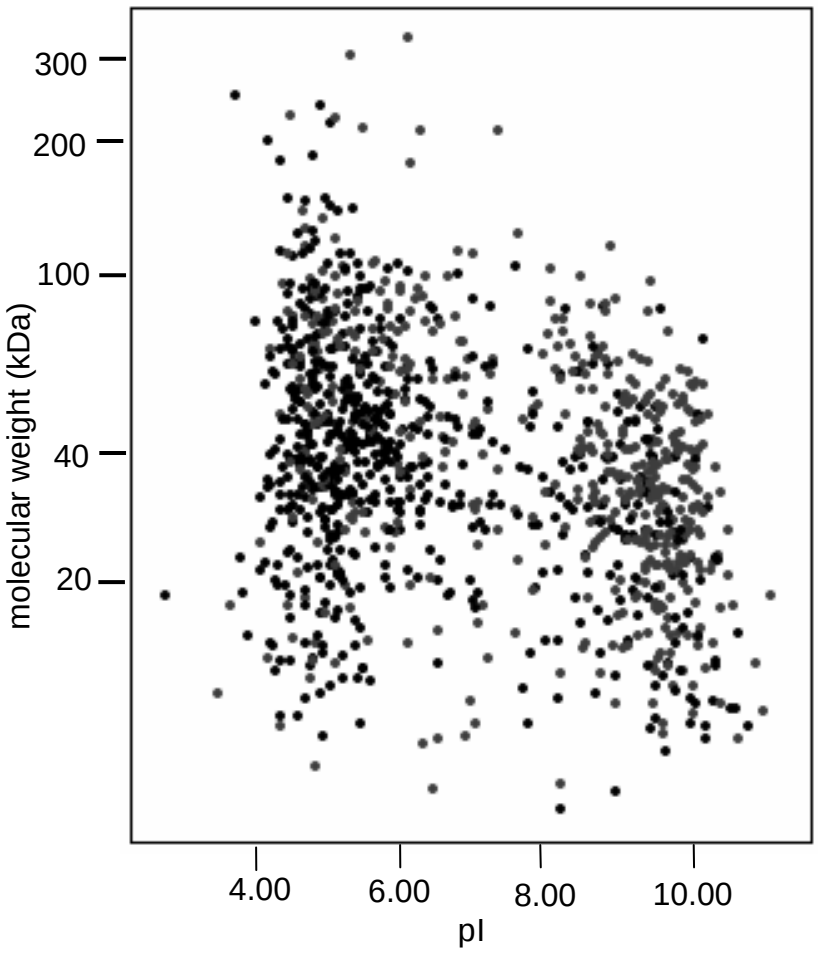

Figure 2.3.4. Theoretical 2D gel of the *C. thermocellum* membrane proteome.

The two-stage Bicine-dSDS-PAGE analyses of wild type (Figures 2.3.2(A) and (B)) and ethanol-adapted (Figures 2.3.3(A) and (B)) cells displayed similar protein spot representation in the high and low molecular weight range. The tendency of membrane proteins to have basic pI values is a significant contributor to their under-representation in traditional 2D-PAGE (13). However, as demonstrated by the data presented here, pI was not a limiting factor in the Bicine-dSDS-PAGE analyses (Table 2.3.1). In addition, the generally hydrophobic nature of membrane proteins further contributes to their low abundance in 2D gel maps. Here again, Bicine-dSDS-PAGE analyses proved to be a suitable approach due to the fact that solubility issues of membrane proteins in the first dimension or isoelectric focusing step of 2D-PAGE are completely circumvented by applying molecular weight-based separations in both dimensions.

TMD and GRAVY Analysis of Membrane Proteins

The presence of hydrophobic domains in a majority of the proteins identified from the SIDG fractions supported the contention that these proteins are intimately associated with the cell membrane (Table 2.3.2). The membrane protein distribution as a function of the number of transmembrane domains (TMDs) in both the *C. thermocellum* database and the experimentally determined membrane proteins from SIDGC fractions revealed a marked decline in the number of proteins with high numbers of TMDs, particularly in the theoretical membrane population (Figures 2.3.5(A) and (B)). While the theoretical membrane population showed a substantially high proportion of proteins with only one TMD (47% of all predicted membrane proteins), this was not the case for the experimentally determined set (17% of proteins). It should be noted that a sizable fraction of proteins with only one TMD may not be true membrane proteins and the fact that this set was under-represented in the experimental population is a measure of the effectiveness of our sample preparation procedures in eliminating non-membrane protein components. The experimental set also differed from the theoretical membrane protein population in the representation of proteins with large numbers of TMDs. A possibility for the under-representation of these highly hydrophobic proteins is likely related to sample solubilization issues. Use of solubilizing detergents in the sample buffer in

(A)

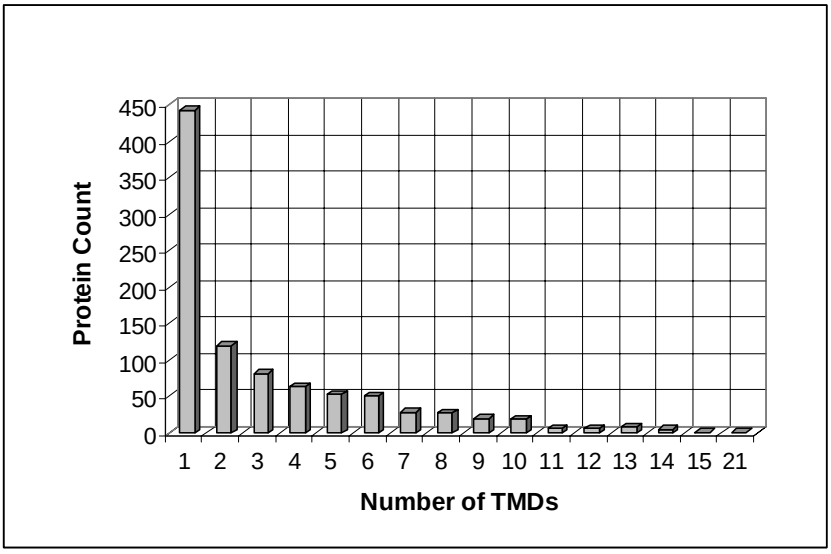

(B)

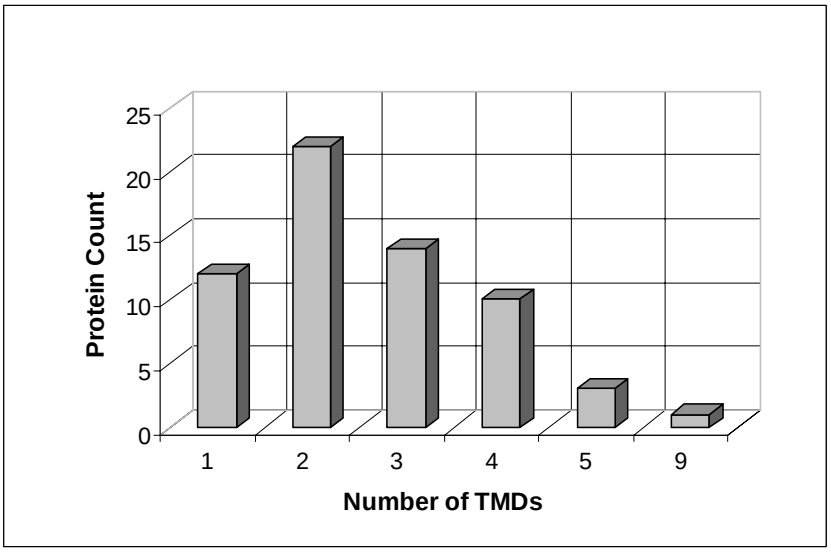

Figure 2.3.5. Membrane protein distribution as a function of the number of transmembrane domains (TMDs) in (A) the *C. thermocellum* database and (B) the experimentally determined membrane proteins from SIDGC fractions.

conjunction with the first dimension of dSDS-PAGE could perhaps enhance the presence of such proteins in the gels.

In a majority of the cases, proteins with a high number of TMDs corresponded with more positive GRAVY values. The GRAVY analysis of identified proteins should be considered with caution, however, as these scores represent the overall hydrophobicity of the entire protein and not just the regions of TMDs. Integral membrane proteins often have sizable hydrophilic sequences that are not embedded within the lipid bi-layer which can contribute to the overall reduction (more negative) of the GRAVY score. An example of such a protein is a glycosyl transferase (#59: gi 67916966). This protein had four TMDs but its GRAVY score was slightly negative (-0.093). On the opposite end, AMP-dependent synthetase and ligase (#3: gi 67874556) was determined to have no TMDs but GRAVY analysis resulted in a very positive score (0.193). It is possible that such a protein is associated with the cell membrane through protein – protein interactions but is not necessarily an integral membrane protein.

Differential Protein Expression in *C. thermocellum* Strains

Herrero *et al*. (2) proposed that ethanol effects on membrane fluidity and the inhibition of certain membrane-bound enzymes associated with carbohydrate metabolism contributed to the ethanol sensitivity of the bacterium. Our results clearly demonstrated that a significant proportion of membrane-associated proteins involved with carbohydrate transport and metabolism, such as glycoside hydrolase (#45: gi 67874975), were present at over 2-fold lower concentrations in the ethanol-adapted strain, compared to the wild type organism. It is possible that these proteins are not being properly incorporated into the ethanol-challenged cell membrane.

Studies have shown that in ethanol-challenged systems, membrane damage is manifested by the leakage of small, albeit significant, quantities of proteins (11). A survey of the proteins present in higher concentrations in the wild type strain showed that one of the members of this category is the protein SecA (#6: gi 67916795). This is a soluble protein, as demonstrated by the absence of TMDs and negative GRAVY score. However, it binds peripherally to membranes with high affinity and supports translocation of proteins across the cell membrane (89). Passive leakage of proteins

through the membrane lipid bi-layer can potentially account for the down-regulation of this protein observed in ethanol-adapted cells.

Previous investigations have reported that ethanol-challenged cells are characterized by the acceleration of a diverse range of processes, including survival, chemotaxis, growth and spore germination, particularly at very low ethanol concentrations (89). While only a few of the analyzed proteins were found to be up-regulated in the ethanol-adapted organisms, several of these proteins were observed to have signal transduction and/or chemotaxis function, such as the chemotaxis sensory transducer (#37: gi 67873910). Some proteins involved with cell motility, such as the flagellar biosynthetic protein FlhB (#67: gi 67875429), were also present at higher levels in the ethanol-adapted cell membrane.

Some membrane-bound magnesium ion transporters were up-regulated in the ethanol-tolerant organism. These included the Mg^{2+}-transporter protein, CorA-like (#26: gi 67875293) and the divalent cation transporter (#61: gi 67916199). Earlier investigations (11) have demonstrated that fermentation rates are closely related to cellular magnesium concentrations. Leaky membranes, as are characteristic of ethanol-challenged organisms, can effect the loss of appreciable quantities of small, inorganic ions, such as magnesium. It is possible that when adapting to ethanol, the organism attempts to incorporate more magnesium ion transporters into the cell membrane, so as to counterbalance the passive loss of this ion through the lipid bi-layer. Another protein associated with magnesium transport that was up-regulated in ethanol-adapted strains was the amino acid-binding ACT: MgtC/SapB transporter (#51: gi 67916179). This protein is believed to act as an accessory protein for MgtB, thus mediating magnesium influx into the cytosol (89).

Ethanol Exposure and the Membrane Proteome

A closer look at the physiological effects of ethanol on cell membranes may offer explanations for the differential expression of membrane proteins observed in *C. thermocellum* strains under investigation. The hydrophobic interior of the membrane lipid bi-layer provides a barrier to the passive transport of polar molecules in and out of the cell. The primary physiological effect of an ethanolic environment is a general tightening

of the bi-layer as it becomes interspersed with ethanol molecules (11). The polarity of the hydrophobic core is increased and the cell responds through mechanisms that attempt to offset this increase in membrane rigidity. Ethanol-induced stress causes a reduction in the hydrophobic interactions among acyl side chains and hydrophobic domains of proteins. Increases in coulombic interactions stimulate a decrease in ionization and an elevation in the strength of charge repulsions between the polar heads of membrane phospholipids. The overall effect is an increase in surface area occupied per phospholipids molecule, reduction in membrane thickness and increases in membrane fluidity (3). Ethanol exposure clearly compromises lipid-lipid and lipid-protein interactions within the cell membrane.

Roberts and co-workers (2) have shown that when ethanol is added to *C. thermocellum* cultures, changes in membrane composition occur after the period of growth arrest. They detected an increase in the proportion of normal and *anteiso*-branched fatty acids (lower melting points) at the expense of *iso*-branched fatty acids (higher melting points), which causes fluidizing of the membrane. Studies have shown that key cellular targets for growth inhibition are hydrophobic in nature and that cessation of growth is directly proportional to the concentration of perturbing molecules that have partitioned into the hydrophobic milieu (2). It is evident that the cell membrane is an organelle most vulnerable to ethanol-induced changes.

Hydrophobic interactions are the major driving force for the biological self-assembly of membranes and both electrostatic and hydrophobic interactions are involved in preserving the spatial organization of membrane components, such as membrane-associated and integral membrane proteins (11). The positioning of proteins within the lipid bi-layer is brought about through a complex balance of charge interactions and hydrophobic associations. While the physical principles of ethanol action would be similar for all proteins, both cytosolic and membrane-bound, the specific consequences for a given protein would clearly depend on the physicochemical properties, structure and immediate environment of that particular protein. Ethanol-induced changes in the mechanics and chemical environment of the cell membrane can significantly affect the tertiary and quaternary structure of membrane proteins, resulting in their inefficient assimilation and folding within the lipid bi-layer. Previous investigations from our

laboratory (78) have suggested that cell surface proteins, such as different S-layer components, could be accumulating at their site of manufacture (the cytosol), perhaps due to the failure of chaperones and protein folding agents to successfully incorporate membrane proteins into the cell membrane. It is worthwhile to mention that S-layer proteins (#18: gi 67917201 and #23: gi 67916324) were observed to be up-regulated in the wild-type organism in the investigations reported here.

Conclusions

Proteomics is a very powerful analytical tool for understanding how organisms respond to environmental stress, such as ethanol exposure and adaptation. Nevertheless, the use of proteomic techniques with *C. thermocellum* is limited. In fact, to our knowledge, this is the first study of the *C. thermocellum* membrane proteome using carefully designed proteomics approaches. In recent years, the realization that cellular proteomes are comprised of diverse sub-proteomes which often require different methodologies for effective characterization and analysis has brought about a marked increase in resources dedicated to methods development for membrane proteome analysis. The recently developed Bicine-dSDS-PAGE method was very well-suited for studying differential protein expression in wild type and ethanol-adapted *C. thermocellum* strains (34). Dramatic strides in membrane protein representation and reduction of cytosolic protein contaminants were achieved through sucrose isopycnic density gradient centrifugation techniques. This was corroborated by transmembrane domain (TMD) and hydropathy (GRAVY) analyses of identified proteins.

It is evident from these investigations that the membrane proteomes of wild type and ethanol-adapted species are dissimilar, with a majority of differentially expressed proteins being under-represented in the ethanol-adapted bacterium (90). A close investigation of differential protein expression can offer insights into the true nature of ethanol tolerance. It is probable that the under-represented proteins are being produced in lower quantities in the ethanol-adapted cells. Another possibility is that the organism simply fails to incorporate the proteins into the cell membrane. The latter option would perhaps result in a build-up of integral membrane and membrane-associated proteins in

the cytosol, hinting at an inadequate environment in the lipid bi-layer for proper protein assimilation and folding to occur. Investigations to determine which possibility is the more likely answer are definitely worthwhile in the interest of better understanding ethanol adaptation.

Chapter 2.4
Conclusions

Proteomics has emerged, in the wake of the genomics era, as a powerful analytical tool for the large-scale study of proteins in cells, the minute specks of universe termed living. While the genome is a rather constant, unchanging entity, the proteome differs from cell to cell and is frequently altered through biochemical interactions with the genome and the environment. An organism will have radically different protein expression patterns in different parts of the body, during different stages of the life cycle and in different types of environmental conditions. A host of environmental stressors, such as disease, climactic changes, fluctuations in nutrient levels and the presence of toxins can cause specific alterations in the cellular proteome that can be effectively studied using proteomics approaches. A survey of the diversity of living organisms and the ecological niches they occupy, ranging from hot sulfur springs to the polar ice caps, is a clear indication of the adaptability and versatility of life. It has long been known that fermenting organisms, such as yeast and certain thermophilic bacteria including *Clostridium thermocellum*, can be adapted to an environment of accumulating fermentation byproducts, such as ethanol. These organisms and their ability to generate ethanol have recently generated interest in bio-fuels research and development. This area of research has become increasingly important in the current geo-political climate, as the trend towards developing cleaner and more efficient fuels becomes critical. A study of differential protein expression can offer clues into how these organisms respond to an ethanolic environment in an effort to adjust and adapt to existing living conditions.

Industrial-scale production of bio-ethanol has traditionally been the realm of yeast. However, this fungus has the significant drawback of only being able to ferment expensive simple sugars, such as maize starch, through multi-step mechanisms. The cost of generating large quantities of ethanol through yeast is a definite limitation in exploiting this organism for competing with, and ultimately replacing, fossil fuels as the chief energy source for human consumption. This is in contrast to anaerobic, cellulolytic, thermophilic bacteria, such as *C. thermocellum*, that can ferment cheap cellulose byproducts from the agricultural and forestry sectors via a single step process. Despite the

benefits, *C. thermocellum* is inhibited by low ethanol concentrations (< 2%) in its immediate environment, unlike yeast, which can tolerate high levels of ethanol (> 10%) in the media. Through sequential transfer procedures, *C. thermocellum* strains able to tolerate as high as 8% ethanol have been developed and preliminary proteomics investigations have clearly demonstrated that critical changes in the membrane proteome are brought about by ethanol adaptation. A closer look at the bacterial membrane protein expression could therefore provide insight into how ethanol tolerance is developed.

With increasing research and development dedicated to understanding global protein expression and changes came the understanding that the cellular proteome is composed of many sub-proteomes that often require different experimental conditions for optimum analysis. One such sub-proteome that stands apart from other cellular protein components is the class of proteins in the cell membrane. These proteins are difficult to analyze using traditional gel-based approaches that are the cornerstone of proteomics investigations. This is largely due to their high hydrophobicity and solubility issues in the first dimension or isoelectric focusing step of 2D-PAGE. A solid understanding of differential protein expression in the *C. thermocellum* membrane proteome demands the design of suitable proteomic methodologies geared towards the analysis of membrane proteins. The newly developed Bicine-dSDS-PAGE method, described in Chapter 2.2, provided a more effective means of separating membrane proteins compared to other dSDS-PAGE and traditional 2D-PAGE approaches. This methodology featured molecular weight-based separations in both dimensions of SDS-PAGE and completely circumvented problems associated with pI-based separations (34).

Orthogonality of separation in Bicine-dSDS-PAGE was achieved through manipulation of the parameter space for gel and electrophoresis buffer preparation. Hydrophobicity and the relatively high pI values commonly observed in *C. thermocellum* membrane proteins did not pose as a significant drawback in Bicine-dSDS-PAGE analyses, in contrast to traditional 2D-PAGE. A comparison of this technique with the established Glycine (Laemmli)- and Tricine-dSDS-PAGE protocols revealed significant improvements in membrane protein representation and abundance. These differences were explained to be the effect of differential electrophoretic migration of the trailing ions in the three dSDS-PAGE approaches: bicine for Bicine-dSDS-PAGE, tricine for

Tricine-dSDS-PAGE and glycine for Laemmli-dSDS-PAGE. While faster-moving tricine is well-suited for separation of small proteins and the slower glycine is appropriate for cytosolic proteins, intermediate mobility of bicine was adequate for effective separation and resolution of membrane proteins.

The Bicine-dSDS-PAGE method was successfully applied towards the study of differential protein expression in wild type and ethanol-adapted *C. thermocellum* strains, as described in Chapter 2.3. To our knowledge, this is the first study of differential protein expression in wild type and ethanol-adapted *C. thermocellum* cells (90). Highly purified membrane fractions, obtained through sucrose isopycnic density gradient centrifugation procedures (SIDGC), were employed. Hydropathy (GRAVY) and transmembrane domain (TMD) analyses revealed substantial representation of membrane proteins and dramatically reduced cytosolic proteins, compared to crude membrane preparations. It was evident from these investigations that while protein spot representation was fairly similar between the two strains, there were dramatic differences in the abundance of several proteins. A majority of the proteins that were differentially expressed in these studies were observed to be up-regulated in the wild type strain, particularly those intimately involved with carbohydrate transport and metabolism. Of the few proteins that were present in higher abundance in the ethanol-challenged strain, several were associated with chemotaxis and sensory transduction. It is possible that the lower levels of different proteins in the ethanol-adapted organism is likely due to the failure of chaperones and protein folding agents to properly incorporate membrane proteins into the very fluid lipid bi-layer that is so characteristic of these cells.

These investigations have clearly highlighted the importance of careful sample preparation and methods development in proteomics investigations. A solid understanding of the chemistry and biochemistry of the target analytes, such as membrane proteins, in the development of appropriate methodologies can substantially improve the quality of data obtained. The study of the *C. thermocellum* membrane proteome with specially designed gel-based technology provided a basic understanding of ethanol-induced changes. A closer look at these proteins, investigations into their metabolic pathways and whether or not they are under-produced or inefficiently incorporated into the cell membrane will no doubt significantly add to existing

knowledge about ethanol adaptation. These are the key initial steps towards the eventual design of more ethanol-resistant *C. thermocellum* strains and their exploitation as bio-energy producers.

Appendix

COG function classes of proteins and their abbreviations.

C	Energy production and conversion
D	Cell cycle control, cell division, chromosome partitioning
E	Amino acid transport and metabolism
F	Nucleotide transport and metabolism
G	Carbohydrate transport and metabolism
H	Coenzyme transport and metabolism
I	Lipid transport and metabolism
J	Translation, ribosomal structure and biogenesis
K	Transcription
L	Replication, recombination and repair
M	Cell wall/membrane/envelope biogenesis
N	Cell motility
O	Posttranslational modification, protein turnover, chaperones
P	Inorganic ion transport and metabolism
Q	Secondary metabolites biosynthesis, transport and catabolism
R	General function prediction only
S	Function unknown
T	Signal transduction mechanisms
U	Intracellular trafficking, secretion, and vesicular transport
V	Defense mechanisms

References

1. Sudha Rani, K., Swamy, M. V., and Seenayya, G. (**1998**) *Process Biochem.* ***33,*** 435-440.
2. Herrero, A. A., Gomez, R. F., and Roberts, M. F. (**1982**) *Biochim. Biophys. Acta* ***693,*** 195-204.
3. Ingram, L. O., and Buttke, T. M. (**1984**) *Adv. Microb. Physiol.* **25,** 253-300.
4. Bender, J., Vatcharapijarn, Y., and Jeffries, T. W. (**1985**) *Appl. Environ. Microbiol.,* 475-477.
5. Sudha Rani, K., and Seenayya, G. (**1999**) *World J. Micro. Biotech.* ***15,*** 173-178.
6. Tailliez, P., Girard, H., Longin, R., Beguin, P., and Millet, J. (**1989**) *Appl. Environ. Microbiol.,* 203-206.
7. Tailliez, P., Girard, H., Millet, J., and Beguin, P. (**1989**) *Appl. Environ. Microbiol.,* 207-211.
8. Herrero, A. A., and Gomez, R. F. (**1980**) *Appl. Environ. Microbiol.,* 571-577.
9. Lamed, R., and Zeikus, J. G. (**1980**) *J. Bacteriol.* ***144,*** 569-578.
10. Jones, R. P. (**1989**) *Enzyme Microb. Technol.* **11,** 130-153.
11. Ingram, L. O. (**1990**) *Crit. Rev. Biotechnol.* ***9,*** 305-319.
12. Kundu, S., Ghose, T. K., and Mukhopadhyay, S. N. (**1983**) *Biotechnol. Bioeng.* **25,** 1109-1126.
13. Santoni, V., Molloy, M., and Rabilloud, T. (**2000**) *Electrophoresis* ***21,*** 1054-1070.
14. Washburn, M. P., Wolters, D., and Yates, J. R., 3rd (**2001**) *Nat. Biotechnol.* ***19,*** 242-247.
15. Wu, C. C., and Yates, J. R., 3rd (**2003**) *Nat. Biotechnol.* ***21,*** 262-267.
16. Wu, C. C., MacCoss, M. J., Howell, K. E., and Yates, J. R., 3rd (2003) *Nat. Biotechnol.* ***21,*** 532-538.
17. Rais, I., Karas, M., and Schägger, H. (**2004**) *Proteomics* ***4,*** 2567-2571.
18. Raymond, S., and Weintraub, L. (**1959**) *Science* ***130,*** 711.
19. Laemmli, U. K. (**1970**) *Nature* ***227,*** 680-685.
20. Viney, C., and Fenton, R. A. (**1998**) *Eur. J. Phys.* ***19,*** 575-580.
21. Chrambach, A., and Rodbard, D. (**1971**) *Science* ***172,*** 440-451.

22. Walker, J. M. (**2002**) *The Protein Protocols Handbook*, Humana Press, Totowa, NJ.
23. Neuhoff, V., Arold, N., Taube, D., and Ehrhardt, W. (**1988**) *Electrophoresis **9,*** 255-262.
24. Karas, M., and Hillenkamp, F. (**1988**) *Anal. Chem. **60,*** 2299-2301.
25. Wiley, W. C., and Mclaren, I. H. (**1955**) *Review of Scientific Instruments **26,*** 1150-1157.
26. Dass, C. (**2001**) Principles and Practice of Biological Mass Spectrometry, Wiley-Interscience, New York, NY.
27. Muddiman, D. C., Bakhtiar, R., Hofstadler, S. A., and Smith, R. D. (**1997**) *J. Chem. Educ. **74,*** 1288-1292.
28. Karas, M., Gluckmann, M., and Schafer, J. (**2000**) *J. Mass Spectrom. **35,*** 1-12.
29. Mamyrin, B. A., Karateev, V. I., Shmikk, D. V., and Zagulin, V. A. (**1973**) *Sov. Phys. JETP* **37,** 45-48.
30. Perkins, D. N., Pappin, D. J., Creasy, D. M., and Cottrell, J. S. (**1999**) *Electrophoresis **20,*** 3551-3567.
31. Pappin, D. J., Hojrup, P., and Bleasby, A. J. (**1993**) *Curr. Biol. **3,*** 327-332.
32. http://www.matrixscience.com/ (**2003**), Vol. 2005, Matrix Science.
33. Schägger, H., and von Jagow, G. (**1987**) *Anal. Biochem. **166,*** 368-379.
34. Islam Williams, T., Combs, J. C., Thakur, A. P., Strobel, H. J., and Lynn, B. C. (2005) *Electrophoresis, in press.*
35. Kyte, J., and Rodriguez, H. (**1983**) *Anal. Biochem. **133,*** 515-522.
36. Anderson, B. L., Berry, R. W., and Telser, A. (**1983**) *Anal. Biochem. **132,*** 365-375.
37. Swank, R. T., and Munkres, K. D. (**1971**) *Anal. Biochem. **39,*** 462-477.
38. Hashimoto, F., Horigome, T., Kanbayashi, M., Yoshida, K., and Sugano, H. (**1983**) *Anal. Biochem. **129,*** 192-199.
39. Fling, S. P., and Gregerson, D. S. (**1986**) *Anal. Biochem. **155,*** 83-88.
40. DeWald, D. B., Adams, L. D., and Pearson, J. D. (**1986**) *Anal. Biochem. **154,*** 502-508.
41. Bothe, D., Simonis, M., and von Dohren, H. (**1985**) *Anal. Biochem. **151,*** 49-54.

42. O'Farrell, P. H. (**1975**) *J. Biol. Chem.* ***250,*** 4007-4021.
43. Molloy, M. P., Phadke, N. D., Maddock, J. R., and Andrews, P. C. (**2001**) *Electrophoresis* ***22,*** 1686-1696.
44. Molloy, M. P., Herbert, B. R., Walsh, B. J., Tyler, M. I., Traini, M., Sanchez, J. C., Hochstrasser, D. F., Williams, K. L., and Gooley, A. A. (**1998**) *Electrophoresis* ***19,*** 837-844.
45. Pessione, E., Giuffrida, M. G., Prunotto, L., Barello, C., Mazzoli, R., Fortunato, D., Conti, A., and Giunta, C. (**2003**) *Proteomics* ***3,*** 1070-1076.
46. Phadke, N. D., Molloy, M. P., Steinhoff, S. A., Ulintz, P. J., Andrews, P. C., and Maddock, J. R. (**2001**) *Proteomics* ***1,*** 705-720.
47. Schaffer, S., Weil, B., Nguyen, V. D., Dongmann, G., Gunther, K., Nickolaus, M., Hermann, T., and Bott, M. (**2001**) *Electrophoresis* ***22,*** 4404-4422.
48. Hermann, T., Finkemeier, M., Pfefferle, W., Wersch, G., Kramer, R., and Burkovski, A. (**2000**) *Electrophoresis* ***21,*** 654-659.
49. Agudo, D., Mendoza, M. T., Castanares, C., Nombela, C., and Rotger, R. (**2004**) *Proteomics* ***4,*** 355-363.
50. Chitlaru, T., Ariel, N., Zvi, A., Lion, M., Velan, B., Shafferman, A., and Elhanany, E. (**2004**) *Proteomics* ***4,*** 677-691.
51. Huang, F., Parmryd, I., Nilsson, F., Persson, A. L., Pakrasi, H. B., Andersson, B., and Norling, B. (**2002**) *Mol. Cell. Proteomics* ***1,*** 956-966.
52. Molloy, M. P., Herbert, B. R., Slade, M. B., Rabilloud, T., Nouwens, A. S., Williams, K. L., and Gooley, A. A. (**2000**) *Eur. J. Biochem.* ***267,*** 2871-2881.
53. Nouwens, A. S., Cordwell, S. J., Larsen, M. R., Molloy, M. P., Gillings, M., Willcox, M. D., and Walsh, B. J. (**2000**) *Electrophoresis* ***21,*** 3797-3809.
54. Antelmann, H., Yamamoto, H., Sekiguchi, J., and Hecker, M. (**2002**) *Proteomics* ***2,*** 591-602.
55. Herbert, B. R., Molloy, M. P., Gooley, A. A., Walsh, B. J., Bryson, W. G., and Williams, K. L. (**1998**) *Electrophoresis* ***19,*** 845-851.
56. Molloy, M. P. (**2000**) *Anal. Biochem.* **280,** 1-10.
57. Herbert, B. (**1999**) *Electrophoresis* ***20,*** 660-663.

58. Cordwell, S. J., Nouwens, A. S., Verrills, N. M., McPherson, J. C., Hains, P. G., Van Dyk, D. D., and Walsh, B. J. (**1999**) *Electrophoresis **20,*** 3580-3588.
59. Cordwell, S. J., Nouwens, A. S., Verrills, N. M., Basseal, D. J., and Walsh, B. J. (**2000**) *Electrophoresis **21,*** 1094-1103.
60. Ames, G. F., Prody, C., and Kustu, S. (**1984**) *J. Bacteriol. **160,*** 1181-1183.
61. Sánchez, S., Arenas, J., Abel, A., Criado, M. T., and Ferreirós, C. M. (**2005**) *J. Proteome Res. **4,*** 91-95.
62. Brookes, P. S., Pinner, A., Ramachandran, A., Coward, L., Barnes, S., Kim, H., and Darley-Usmar, V. M. (**2002**) *Proteomics **2,*** 969-977.
63. Camacho-Carvajal, M. M., Wollscheid, B., Aebersold, R., Steimle, V., and Schamel, W. W. (**2004**) *Mol. Cell. Proteomics **3,*** 176-182.
64. Patton, W. F., Chung-Welch, N., Lopez, M. F., Cambria, R. P., Utterback, B. L., and Skea, W. M. (**1991**) *Anal. Biochem. **197,*** 25-33.
65. Pardo, M. F., and Natalucci, C. L. (**2002**) *Acta Farm. Bonarense **21,*** 57-60.
66. Khalkhali-Ellis, Z. (**1995**) *Prep. Biochem. **25,*** 1-9.
67. Maskell, J. P. (**1991**) *J. Med. Microbiol. **34,*** 253-257.
68. Lesse, A. J., Campagnari, A. A., Bittner, W. E., and Apicella, M. A. (**1990**) *J. Immunol. Methods. **126,*** 109-117.
69. Maskell, J. P. (**1994**) *Antonie Van Leeuwenhoek **65,*** 155-161.
70. Firoozkoohi, J., Zandi, H., and Olsen, I. (**1997**) *Endod. Dent. Traumatol. **13,*** 13-18.
71. Marshall, T., and Williams, K. M. (**1994**) *Appl. Theor. Electrophor. **4,*** 25-31.
72. Martinez, M., Newbold, C. J., Wallace, R. J., and Moyano, F. J. (**2002**) *Electrophoresis **23,*** 1-7.
73. Fountoulakis, M., Juranville, J. F., Roder, D., Evers, S., Berndt, P., and Langen, H. (**1998**) *Electrophoresis **19,*** 1819-1827.
74. Jovin, T. M. (**1973**) *Biochemistry **12,*** 871-879.
75. Jovin, T. M. (**1973**) *Biochemistry **12,*** 879-890.
76. Jovin, T. M. (**1973**) *Biochemistry **12,*** 890-898.
77. Baumann, G., and Chrambach, A. (**1976**) *Proc. Natl. Acad. Sci., U S A **73,*** 732-736.

78. Strobel, H. J., and Lynn, B. C. (**2004**) *in* American Society for Microbiology, New Orleans, LA.
79. Cotto, M. A., and Russell, J. B. (**1982**) *J. Dairy Sci.* ***65,*** 226-234.
80. Lowry, O. H., Rosebrough, N. J., Farr, A. L., and Randall, R. J. (**1951**) *J. Biol. Chem.* ***193,*** 265-275.
81. Hunte, C., von Jagow, G., and Schägger, H. (**2003**) Membrane Protein Purification and Crystallization: A Practical Guide, Academic Press, San Diego, CA.
82. http://www.ncbi.nlm.nih.gov/genomes/framik.cgi?db=genome&gi=5118, NCBI.
83. Yim, S. K., Ahn, T., Kim, J. S., and Yun, C. H. (**2002**) *Anal. Biochem.* ***305,*** 277-279.
84. Islam Williams, T., Combs, J. C., Strobel, H. J., and Lynn, B. C. (**2005**) *in* American Society for Mass Spectrometry, San Antonio, TX.
85. O'Brien, V., Grindlay, G. J., and Campo, M. S. (**2001**) *J. Biol. Chem.* ***276,*** 33861-33868.
86. Wehr, T., Rodriguez-Diaz, R., and Zhu, M. (1999) Capillary electrophoresis of proteins, Marcel Dekker, Inc., New York, NY.
87. http://sosui.proteome.bio.tuat.ac.jp/cgi-bin/sosui.cgi?/sosui_submit.html.
88. http://www.jvirgel.de/ (2003) (Hiller, K., Ed.).
89. http://www.ebi.ac.uk/interpro/, European Bioinformatics Institute.
90. Islam Williams, T., Combs, J. C., Lynn, B. C., and Strobel, H. J. (*Manuscript in Preparation*).

CONCLUSIONS

In the year 1803, when John Dalton proposed that matter was composed of small, indivisible particles called atoms, it was popularly believed that mankind was fast approaching the frontiers of what can be known about the fabric of the cosmos. Smashing the atom quickly dissipated such ideas as matter was probed at increasingly detailed levels to reveal a whole new universe of understanding in quantum mechanics. A major contributor to the power of mass spectrometry, particularly in the bioanalytical world, lies in its ability to deliver sensitive and selective quantitative and qualitative data at vanishingly lower detection levels, resulting in very accurate and detailed analysis. Full exploitation of such characteristics of this analytical tool is realized through careful methods development geared towards specific analytes. By repeatedly challenging the frontiers of mass spectrometry through instrument development and experimental design, it can be possible to broaden the scope of scientific analysis to even lower limits of detection and quantification. The ability to measure minute quantities of analytes, such as detection of subtle changes between diseased and control data sets, can vastly improve knowledge of the biological system under investigation, both in the realms of small and large molecule research. How low is low enough? The pioneers of string theory and M theory would probably say “as low as technologically possible and then lower”.

Discovery of biomarkers, which have traditionally been small organic molecules, in disease progression research would be of little use for the development of disease diagnostics and cures if those biomarkers could not be accurately detected and quantified. There are numerous diseases with poor diagnostic methods and treatments that claim untold lives every year. Of all the cancers that afflict women, ovarian cancer is one of the deadliest and by the time it is diagnosed, the odds of a cure have generally dropped to little more than 1 in 10. While there are many terminal diseases, such as AIDS, Alzheimer’s disease and several types of cancer, in many cases, early diagnosis renders the diseases treatable, if not curable, in a manner that can improve the quality of life during the lifetime of the afflicted individual. The ultimate goal of disease research should be the development of complete cures. However, in the interest of those who will succumb before such cures come to pass, an equally strong emphasis ought to be placed

on early detection and symptom alleviation. Human lives and the quality of life itself depend on the design of reliable, sensitive and accurate clinical diagnostics.

Retirement of the baby boom generation will place a significant fraction of the elderly populace, unmatched in history, in the hands of the geriatric physician. The aging population, particularly in the western world, will clearly demand greater medical and social attention for diseases of the elderly, such as Alzheimer's disease. The first part of this dissertation described the development of MS-based sensitive, selective and accurate methodologies for the quantification of biogenic aldehydes, potential biomarkers for this debilitating illness. This was achieved through a solid understanding of the chemistry of these analytes, along with careful experimental design in HPLC separation and mass spectrometry. The reliability of biogenic aldehydes as AD biomarkers renders them well-suited for exploitation as a clinical diagnostic, through analysis of human cerebrospinal fluid (CSF) samples, for instance. It can be possible to improve the quantitative power of this methodology through the use of radioactively labeled internal standards in isotope dilution mass spectrometry. Greater similarity between the physicochemical properties of internal standard and target analyte will produce a more effective and reliable analytical methodology.

Application of the developed LC-MS method to measuring biogenic aldehydes in different regions of the human brain for individuals who displayed varying levels of AD pathology clearly demonstrated the power of MS-based methods development in disease progression research. The data confirmed that AD pathology appeared early in the disease, at the mild cognitive impairment (MCI) stage. To design reliable diagnostics and effect a cure for AD, it is imperative that research focus on the MCI stage. A sizable proportion of acrolein and HNE are known to be bound to proteins in the AD brain. Tapping into these reservoirs of biogenic aldehydes using similarly designed LC/MS methods can offer a clearer understanding of their prevalence in the brain. No doubt, one can also envision developing LC/MS techniques for the analysis of other possible AD biomarkers, such as isoprostanes. Metabolic and mutation studies coupled to LC/MS for detection of these compounds can further provide information on the circumstances of lipid peroxidation and AD occurrence. The possibilities of applying LC/MS-based methods for biomarker studies in other diseases are also very promising, especially in

view of the large parameter space of LC/MS experiments – ranging from LC column makeup to ion fragmentation techniques in MS – which can be manipulated to tailor experimental design towards the analyte of interest.

The knowledge base for Alzheimer's disease has grown significantly in the past decade and many believe that a viable clinical diagnostic lies within the foreseeable future. Understanding the etiology of the disease will pave the way to the discovery of effective biomarkers. The MCI stage is considered to be the earliest time when AD pathology appears. It is very likely that with improvements in the detection of AD pathology, a time even earlier than the MCI stage can be targeted in the development of clinical tests. Early detection is the key. A deeper understanding of AD biomarker generation, biochemistry, as well as careful evaluation of their relative abundance in the body (as demonstrated in Part 1 of this dissertation) can only strengthen the power of diagnostics based on these compounds. With the detection and quantification potential available in mass spectrometry, it is not difficult to see why an MS-based clinical diagnostic is a very practical and worthwhile avenue to pursue.

The power of mass spectrometry is such that it can be interfaced to a host of separation techniques, in no way limited to chromatography, for the analysis of a variety of compounds. While LC-based separations coupled to MS have had success in the area of large molecule research such as proteomics studies, the Laemmli protocol of 2D-SDS-PAGE remains the gold standard for protein separations. But proteins are a diverse group of macromolecules which simply cannot be grouped together and effectively analyzed through a single gel-based separation approach. Such an assumption produced consistently low representation of cell membrane proteins in standard 2D gel maps. Closer scrutiny of these proteins revealed that their hydrophobicity, generally basic pI values and poor solubility in isoelectric focusing (first dimension of 2D-SDS-PAGE) buffers rendered them unsuitable for analysis using traditional 2D-SDS-PAGE. Since the membrane is the site of first contact of the cell with the exterior, membrane proteins play a critical role in cellular processes, especially during changes in the organism's immediate environment. This was evident in ethanol tolerance studies of the thermophilic, anaerobic, cellulolytic bacterium *Clostridium thermocellum*. This organism has received attention in the area of bio-fuels research for its ability to ferment

inexpensive cellulose-based biomass to ethanol. With changing climactic conditions from burning of fossil fuels, national security issues, as well as predictions of an impending energy crisis, the development of alternative sources of energy for human consumption has become critical.

The second part of this dissertation focused on *Clostridium thermocellum* membrane proteome research in an effort to obtain a clear understanding of membrane protein expression patterns in wild type and ethanol-adapted strains. As with the AD investigations in Part 1, careful methods development in gel-based separations of membrane proteins proved to be highly beneficial in achieving desired goals. Bicine-based electrophoresis buffers in conjunction with dSDS-PAGE approaches that circumvented solubility concerns encountered in the first dimension of 2D-SDS-PAGE were well-suited for low abundance membrane protein analysis. Greater protein spot representation was observed with Bicine-dSDS-PAGE, compared with conventional dSDS-PAGE techniques. The rationale for the applicability of bicine as a trailing ion in these investigations was explained through electrophoretic mobility studies using capillary electrophoresis experiments (CE). One can envision the careful selection of trailing ions through CE for specific analytes at hand to dramatically improve selectivity and separation efficiency of electrophoresis methods. Tailoring analysis to the target analyte, rather than employing generalized protocols for dissimilar classes of compounds, will ensure reliable data. Chromatography has enjoyed decades of analytical research culminating in a variety of mobile and stationary phases, as well as separation techniques. There is no reason why similar success in broadening the versatility and applications of gel electrophoretic methodologies should not be realized in the near future.

The Bicine-dSDS-PAGE method was successfully applied towards the analysis of differential protein expression in the wild type and ethanol-adapted *C. thermocellum* membrane proteomes. Definitive changes were observed, with a majority of differentially expressed proteins being present at higher concentrations in the wild-type organism. It was postulated that these proteins were either being under-produced by the ethanol-adapted strain or the organism was unable to properly incorporate them into the membrane proteome. The latter possibility would imply that membrane protein build-up could be occurring at the site of manufacture (cytosol). While investigations presented

here offered a basic foundation for understanding ethanol tolerance at the membrane level, a closer examination of the biochemistry of differentially expressed proteins will surely provide a deeper appreciation of the underlying mechanisms for this phenomenon. Many proteins in the *C. thermocellum* cell membrane have been studied but a sizable fraction of the entire membrane proteome remains unexplored. One can envision using multi-dimensional chromatographic separation methods (MudPIT) coupled with isotope labeling to probe this class of proteins on a deeper level and obtain accurate relative quantification data.

The ethanol adapted *C. thermocellum* strain is considerably less robust than its wild type counterpart. Once a thorough understanding of differential protein expression of the entire *C. thermocellum* membrane proteome is obtained, mutation studies and metabolic experiments can shed light on which pathways are critical for ethanol adaptation to develop and which mechanisms contribute to the poor growth and overall health of the ethanol-adapted organism. Results from these investigations can definitely enable the production of specially designed, genetically engineered ethanol-adapted bacteria. These 'super bugs' would have certain genes with increased capabilities of up-regulating ethanol production routes. Manipulation of other genes that effectively control metabolic pathways, rendering the bacteria more robust than their ethanol-challenged cousins, would also be beneficial. *C. thermocellum* strains with even as much ethanol tolerance as yeast, the current industrial bio-ethanol producer, would be a remarkable success. Unlike yeast which can only ferment expensive simple sugars, such bacterial strains would be able to effectively produce ethanol from inexpensive cellulose-based by-products out of the agricultural and forestry sectors. With high demands on cleaner, more efficient fuel sources, along with increasing emphasis on recycling materials for human consumption, a bacterium able to mass-produce bio-ethanol from cellulose waste would be a highly promising outcome indeed.

The possibilities with methods development in MS investigations interfaced with separation technology in the biological arena are truly limitless. No matter what the analytes under investigation, be they small or large molecules, hydrophilic or hydrophobic, acidic or basic, reliable quantification is only achieved through careful consideration of analyte properties, as opposed to using generalized methodologies that

have little regard for the specific needs of target compounds. The versatility of various chromatographic and gel-based methods, coupled to the variety of ionization sources and mass analyzers available, culminate in a marriage of incredible analytical potential. In terms of biological systems that scientists desire to study and the permutations of separation-based MS methods available with which to study them, we are truly at the tip of a bioanalytical iceberg and the iceberg is growing every day.

BIBLIOGRAPHY

Agudo, D., M. T. Mendoza, et al. (**2004**). "A proteomic approach to study Salmonella typhi periplasmic proteins altered by a lack of the DsbA thiol: disulfide isomerase." *Proteomics* ***4***(2): 355-363.

Ames, G. F., C. Prody, et al. (**1984**). "Simple, rapid, and quantitative release of periplasmic proteins by chloroform." *J. Bacteriol.* ***160***(3): 1181-1183.

Anderson, B. L., R. W. Berry, et al. (**1983**). "A sodium dodecyl sulfate--polyacrylamide gel electrophoresis system that separates peptides and proteins in the molecular weight range of 2500 to 90,000." *Anal. Biochem.* ***132***(2): 365-375.

Antelmann, H., H. Yamamoto, et al. (**2002**). "Stabilization of cell wall proteins in *Bacillus subtilis*: a proteomic approach." *Proteomics* ***2***(5): 591-602.

Arlt, S., U. Beisiegel, et al. (**2002**). "Lipid peroxidation in neurodegeneration: new insights into Alzheimer's disease." *Curr. Opin. Lipidol.* ***13***: 289-294.

Atwood, C. S., R. C. Scarpa, et al. (**2000**). "Characterization of Copper Interactions with Alzheimer Amyloid β Peptides: Identification of an Attomolar-Affinity Copper Binding Site on Amyloid β1-42." *J. Neurochem.* ***75***: 1219-1233.

Avilá, J. (**2000**). "Tau aggregation into fibrillar polymers: tauopathies." *FEBS Lett.* ***476***: 89-92.

Bailey, A. L., G. Wortley, et al. (**1997**). "Measurement of Aldehydes in Low Density Lipoprotein by High Performance Liquid Chromatography." *Free Rad. Biol. Med.* ***23***(7): 1078-1085.

Baumann, G. and A. Chrambach (**1976**). "Gram-preparative protein fractionation by isotachophoresis: isolation of human growth hormone isohormones." *Proc. Natl. Acad. Sci., U S A* ***73***(3): 732-736.

Bender, J., Y. Vatcharapijarn, et al. (**1985**). "Characteristics and adaptability of some new Isolates of *Clostridium thermocellum*." *Appl. Environ. Microbiol.*: 475-477.

Bothe, D., M. Simonis, et al. (**1985**). "A sodium dodecyl sulfate-gradient gel electrophoresis system that separates polypeptides in the molecular weight range of 1500 to 100,000." *Anal. Biochem.* ***151***(1): 49-54.

Braak, H. and E. Braak (**1991**). "Neuropathological Staging of Alzheimer-Related Changes." *Acta Neuropathol.* ***82***(4): 239-259.

Brookes, P. S., A. Pinner, et al. (**2002**). "High throughput two-dimensional blue-native electrophoresis: a tool for functional proteomics of mitochondria and signaling complexes." *Proteomics* ***2***(8): 969-977.

Bruenner, B. A., A. D. Jones, et al. (**1996**). "Simultaneous Determination of Multiple Aldehydes in Biological Tissues and Fluids Using Gas Chromatography/Stable Isotope Dilution Mass Spectrometry." *Anal. Biochem.* ***241***: 212-219.

Büldt, A. and U. Karst (**1997**). "1-Methyl-1-(2,4-dinitrophenyl)hydrazine as a New Reagent for the HPLC Determination of Aldehydes." *Anal. Chem.* ***69***: 3617-3622.

Butterfield, D. A. (**2002**). "Amyloid beta-peptide (1-42)-indued Oxidative Stress and Neurotoxicity: Implications for Neurodegeneration in Alzheimer's Disease Brain. A Review." *Free Radic. Biol. Med.* ***36***(12): 1307-1313.

Butterfield, D. A., A. Castegna, et al. (**2002**). "Evidence that amyloid beta-peptide-induced lipid peroxidation and its sequelae in Alzheimer's disease brain contribute to neuronal death." *Neurobiol. Aging* ***23***: 655-664.

Calingasan, N. Y., K. Uchida, et al. (**1999**). "Protein-Bound Acrolein: A Novel Marker of Oxidative Stress in Alzheimer's Disease." *J. Neurochem.* ***72***: 751-756.

Camacho-Carvajal, M. M., B. Wollscheid, et al. (**2004**). "Two-dimensional Blue native/SDS gel electrophoresis of multi-protein complexes from whole cellular lysates: a proteomics approach." *Mol. Cell. Proteomics* ***3***(2): 176-182.

Chitlaru, T., N. Ariel, et al. (**2004**). "Identification of chromosomally encoded membranal polypeptides of *Bacillus anthracis* by a proteomic analysis: prevalence of proteins containing S-layer homology domains." *Proteomics* ***4***(3): 677-691.

Chrambach, A. and D. Rodbard (**1971**). "Polyacrylamide gel electrophoresis." *Science* ***172***(982): 440-451.

Compton, B. J. and W. C. Purdy (**1980**). "The mechanism of the reaction of the Nash and Sawicki aldehyde reagent." *Can. J. Chem.* ***58***: 2207-2211.

Cordis, G. A., D. Bagchi, et al. (**1994**). "High Performance Liquid Chromatographic Method for the Simultaneous Detection of Malondialdehyde, Acetaldehyde,

Formaldehyde, Acetone and Propionaldehyde to Monitor Oxidative Stress in the Heart." *J. Chromatogr. A* ***661***: 181-191.

Cordwell, S. J., A. S. Nouwens, et al. (**2000**). "Subproteomics based upon protein cellular location and relative solubilities in conjunction with composite two-dimensional electrophoresis gels." *Electrophoresis* ***21***(6): 1094-1103.

Cordwell, S. J., A. S. Nouwens, et al. (**1999**). "The microbial proteome database--an automated laboratory catalogue for monitoring protein expression in bacteria." *Electrophoresis* ***20***(18): 3580-3588.

Cotto, M. A. and J. B. Russell (**1982**). "Effect of peptides and amino acids on efficiency of ruminal bacterial protein synthesys in continuous culture." *J. Dairy Sci.* ***65***: 226-234.

Covey, T. R., E. D. Lee, et al. (**1986**). "Liquid Chromatography/Mass Spectrometry." *Anal. Chem.* ***58***(14): 1451A-1461A.

Dass, C. (**2001**). Principles and Practice of Biological Mass Spectrometry. New York, NY, Wiley-Interscience.

de Hoffmann, E. and V. Stroobant (**1999**). Mass Spectrometry: Principles and Applications. Chichester, England, John Wiley and Sons, Ltd.

Deighton, N., W. L. Magill, et al. (**1997**). "Malondialdehyde and 4-hydroxy-2-nonenal in plant tissue cultures: LC-MS determination of 2,4-dinitrophenylhydrazone derivatives." *Free Rad. Res.* ***27***(3): 255-265.

Deng, C. and X. Zhang (**2004**). "A simple, rapid and sensitive method for determination of aldehydes in human blood by gas chromatography/mass spectrometry and solid-phase microextraction with on-fiber derivatization." *Rapid Commun. Mass Spectrom.* ***18***: 1715-1720.

Detoledo-Morrell, L., M. P. Sullivan, et al. (**1997**). "Alzheimer's Disease: In Vivo Detection of Differential Vulnerability of Brain Lesions." *Neurobiol. Aging* ***18***(5): 463-468.

DeWald, D. B., L. D. Adams, et al. (**1986**). "A nonurea electrophoretic gel system for resolution of polypeptides of Mr 2000 to Mr 200,000." Anal. Biochem. ***154***(2): 502-508.

Drake, J., R. Petroze, et al. (**2004**). "4-Hydroxynonenal oxidatively modifies histones: implications for Alzheimer's disease." *Neurosci. Lett.* ***356***: 155-158.

Draper, H. H., A. S. Csallany, et al. (**2000**). "Urinary aldehydes as indicators of lipid peroxidation in vivo." *Free Rad. Biol. Med.* ***29***(11): 1071-1077.

Esterbauer, H., R. J. Shchaur, et al. (**1991**). "Chemistry and biochemistry of 4-hydroxynonenal, malondialdehyde and related aldehydes." *Free Rad. Biol. Med.* ***11***: 81-128.

Fenn, J. B., M. Mann, et al. (1989). "Electrospray Ionization for Mass-Spectrometry of Large Biomolecules." Science **246**(4926): 64-71.

Firoozkoohi, J., H. Zandi, et al. (**1997**). "Comparison of lipopolysaccharides from Bacteroides, Porphyromonas, Prevotella, Campylobacter and Wolinella spp. by tricine-SDS-PAGE." *Endod. Dent. Traumatol.* ***13***(1): 13-18.

Fling, S. P. and D. S. Gregerson (**1986**). "Peptide and protein molecular weight determination by electrophoresis using a high-molarity tris buffer system without urea." *Anal. Biochem.* ***155***(1): 83-88.

Foley, J. P. (**1991**). "Resolution Equations for Column Chromatography." *Analyst* ***116***: 1275-1279.

Fountoulakis, M., J. F. Juranville, et al. (**1998**). "Reference map of the low molecular mass proteins of *Haemophilus influenzae*." *Electrophoresis* ***19***(10): 1819-1827.

Gabbita, S. P., M. Y. Aksenov, et al. (**1999**). "Decrease in peptide methionine sulfoxide reductase in Alzheimer's disease brain." *J. Neurochem.* ***73***: 1660-1666.

Giddings, J. C. (**1991**). Unified Separation Science. New York, NY, Wiley.

Gioacchini, A. M., N. Calonghi, et al. (**1999**). "Determination of 4-Hydroxy-2-nonenal at Cellular Levels by Means of Electrospray Mass Spectrometry." *Rapid Commun. Mass Spectrom.* ***13***: 1573-1579.

Glish, G. L. and R. W. Vachet (**2003**). "The Basics of Mass Spectrometry in the Twenty-First Century." *Nature* ***2***: 140-150.

Gómez-Ramos, A., J. Díaz-Nido, et al. (**2003**). "Effect of the Lipid Peroxidation Product Acrolein on Tau Phosphorylation in Neural Cells." *J. Neurosci. Res.* ***71***: 863-870.

Good, P. F., P. Werner, et al. (**1996**). "Evidence of neuronal oxidative damage in Alzheimer's disease." *Am. J. Pathol.* ***149***: 21-28.

Grootendorst, J., A. Bour, et al. (**2005**). "Human apoE targeted replacement mouse lines: h-apoE4 and h-apoE3 mice differ on spatial memory performance and avoidance behavior." Behav. Brain Res. ***159***(1): 1-14.

Grundke-Iqbal, I. and K. Iqbal (**1989**). "Neuronal cytoskeleton in the biology of Alzheimer's disease." *Prog. Clin. Biol. Res.* ***317***: 745-753.

Grundke-Iqbal, I., K. Iqbal, et al. (**1986**). "Abnormal phosphorylation of the microtubule-associated protein tau (tau) in Alzheimer cytoskeletal pathology." *Proc. Natl. Acad. Sci. USA* ***83***(13): 4913-4917.

Haenen, G. R., N. P. Vermeulen, et al. (**1988**). "Activation of the microsomal glutathione-S-transferase and reduction of the glutathione dependent protection against lipid peroxidation by acrolein." *Biochem. Pharmacol.* ***37***: 1933-1938.

Halliwell, B. and M. Grootveld (**1987**). "The Measurement of Free Radical Reactions in Humans." *FEBS Lett.* ***213***(1): 9-14.

Hashimoto, F., T. Horigome, et al. (**1983**). "An improved method for separation of low-molecular-weight polypeptides by electrophoresis in sodium dodecyl sulfate-polyacrylamide gel." *Anal. Biochem.* ***129***(1): 192-199.

Hensley, K., N. Hall, et al. (**1995**). "Brain Regional Correspondence Between Alzheimer's Disease Histopathology and Biomarkers of Protein Oxidation." *J. Neurochem.* ***65***: 2146-2156.

Herbert, B. (**1999**). "Advances in protein solubilisation for two-dimensional electrophoresis." *Electrophoresis* ***20***(4-5): 660-663.

Herbert, B. R., M. P. Molloy, et al. (**1998**). "Improved protein solubility in two-dimensional electrophoresis using tributyl phosphine as reducing agent." *Electrophoresis* ***19***(5): 845-851.

Hermann, T., M. Finkemeier, et al. (**2000**). "Two-dimensional electrophoretic analysis of *Corynebacterium glutamicum* membrane fraction and surface proteins." *Electrophoresis* ***21***(3): 654-659.

Herrero, A. A. and R. F. Gomez (**1980**). "Development of ethanol tolerance in *Clostridium thermocellum*: effect of growth temperature." *Appl. Environ. Microbiol.*: 571-577.

Herrero, A. A., R. F. Gomez, et al. (**1982**). "Ethanol-induced changes in the membrane lipid composition of *Clostridium thermocellum*." Biochim. Biophys. Acta ***693***(1): 195-204.

Holley, A. E., M. K. Walker, et al. (**1993**). "Measurement of n-alkanals and hydroxyalkanals in biological samples." *Free Rad. Biol. Med.* ***15***: 281-289.

http://alzheimer.wustl.edu/adrc2/Research/Neuropathology/abeta_SP.html. (**1995**). "Amyloid-Beta Alzheimer Plaques."

http://ccr.cancer.gov/faculties/documents/452/CRBWGmorrow.ppt. "The Quantification of Isoprostanes as an Index of Oxidant Stress In Vitro and In Vivo: Uses and Controversies."

http://en.wikipedia.org/wiki/Alpha-synuclein. (**2005**). "Alpha-synuclein."

http://en.wikipedia.org/wiki/Hippocampus. (2005). "Hippocampus."

http://learn.lboro.ac.uk/sci/ma/mlsc/documents/Mannwhitney.pdf. (**2004**). "Statistics: 2.3 The Mann-Whitney U Test."

http://sosui.proteome.bio.tuat.ac.jp/cgi-bin/sosui.cgi?/sosui_submit.html. "Transmembrane domain predictor."

http://www.anselm.edu/homepage/jpitocch/anova/mcompex/multcompex.html. "Anova and Multiple Comparisons." **2001**.

http://www.ebi.ac.uk/interpro/. "InterPro."

http://www.health.qld.gov.au/abios/tbi/brain.asp. (2003). "Brain Functions and Map."

http://www.ihcworld.com/_protocols/special_stains/bielschowsky.htm. "Bielschowsky's Silver Staining for Nerve Fibers, Axons, Neurofibrillary Tangles and Senile Plaques on Paraffin Sections."

http://www.ionsource.com/tutorial/chromatography/rphplc.htm. (**2001**). "Reverse Phase HPLC Basics for LC/MS." Retrieved July 22.

http://www.jvirgel.de/. (2003). "JVirGel."

http://www.macalester.edu/~psych/whathap/UBNRP/StemCells/bird_three.html.

http://www.matrixscience.com/. (**2003**). "MASCOT." 2005.

http://www.ncbi.nlm.nih.gov/genomes/framik.cgi?db=genome&gi=5118. "*Clostridium thermocellum* ATCC 27405 Genome."

http://www.neuroskills.com/index.shtml?main=/tbi/btemporl.shtml. "Traumatic Brain Injury Resource Guide: Temporal Lobes."

http://www.nlm.nih.gov/medlineplus/alzheimersdisease.html. "MedlinePlus: Alzheimer's Disease."

http://www.psychology.nottingham.ac.uk/staff/cr1/concepts.pdf.

http://www.shu.ac.uk/schools/sci/chem/tutorials/chrom/chrom1.htm. "Chromatography - Introductory Theory."

http://www.sigmaaldrich.com/img/assets/7361/Primer-H&Emay04.pdf. "Hematoxylin & Eosin (The Routine Stain)."

http://www.waters.com/WatersDivision/ContentD.asp?watersit=EGOO-66YNU9. "LC/MS - Interfacing HPLC and MS."

Huang, F., I. Parmryd, et al. (**2002**). "Proteomics of *Synechocystis* sp. strain PCC 6803: identification of plasma membrane proteins." *Mol. Cell. Proteomics* ***1***(12): 956-966.

Hunte, C., G. von Jagow, et al. (**2003**). Membrane Protein Purification and Crystallization: A Practical Guide. San Diego, CA, Academic Press.

Ingram, L. O. (**1990**). "Ethanol tolerance in bacteria." *Crit. Rev. Biotechnol.* ***9***(4): 305-319.

Ingram, L. O. and T. M. Buttke (**1984**). "Effects of alcohols on micro-organisms." *Adv. Microb. Physiol.* **25**: 253-300.

Iqbal, K. and I. Grundke-Iqbal (**1997**). "Elevated levels of tau and ubiquitin in brain and cerebrospinal fluid in Alzheimer's disease." *Int. Psychogeriatr.* ***9***: 289-296.

Islam Williams, T., J. C. Combs, et al. (*Manuscript in Preparation*). "Proteomic profile changes in membranes of ethanol-tolerant *Clostridium thermocellum*."

Islam Williams, T., J. C. Combs, et al. (**2005**). The Membrane Proteome of *Clostridium thermocellum* by MALDI-TOF-MS. American Society for Mass Spectrometry, San Antonio, TX.

Islam Williams, T., J. C. Combs, et al. (2005). "A novel bicine running buffer system for doubled sodium dodecyl sulfate-polyacrylamide gel electrophoresis of membrane proteins." *Electrophoresis, in press.*

Islam Williams, T., M. A. Lovell, et al. (**2005**). "Analysis of Derivatized Biogenic Aldehydes by LC Tandem Mass Spectrometry." *Anal. Chem.* ***77***: 3383-3389.

Islam Williams, T., B. C. Lynn, et al. (**2005**). "Increased levels of 4-hydroxynonenal and acrolein, neurotoxic markers of lipid peroxidation, in the brain in Mild Cognitive Impairment and early Alzheimer's disease." *Neurobiol. Aging*.

Jones, R. P. (**1989**). "Biological principles for the effects of ethanol." *Enzyme Microb. Technol.* **11**: 130-153.

Jonscher, K. R. and J. R. Yates III (**1997**). "The Quadrupole Ion Trap Mass Spectrometer - A Small Solution to a Big Challenge." *Anal. Biochem.* ***244***: 1-15.

Jovin, T. M. (**1973**). "Multiphasic zone electrophoresis. I. Steady-state moving-boundary systems formed by different electrolyte combinations." *Biochemistry* ***12***(5): 871-879.

Jovin, T. M. (**1973**). "Multiphasic zone electrophoresis. II. Design of integrated discontinuous buffer systems for analytical and preparative fractionation." *Biochemistry* ***12***(5): 879-890.

Jovin, T. M. (**1973**). "Multiphasic zone electrophoresis. III. Further analysis and new forms of discontinuous buffer systems." *Biochemistry* ***12***(5): 890-898.

Karas, G. B., E. J. Burton, et al. (**2003**). "A Comprehensive Study of Gray Matter Loss in Patients with Alzheimer's Disease Using Optimized Voxel-Based Morphometry." *NeuroImage* ***18***: 895-907.

Karas, M., M. Gluckmann, et al. (**2000**). "Ionization in matrix-assisted laser desorption/ionization: singly charged molecular ions are the lucky survivors." *J. Mass Spectrom.* ***35***(1): 1-12.

Karas, M. and F. Hillenkamp (**1988**). "Laser desorption ionization of proteins with molecular masses exceeding 10,000 daltons." *Anal. Chem.* ***60***(20): 2299-2301.

Karger, B. L., L. R. Snyder, et al. (**1973**). An Introduction to Separation Science. New York, NY, Wiley-Interscience.

Karrasch, M., E. Sinervä, et al. (**2005**). "CERAD test performances in amnestic mild cognitive impairment and Alzheimer's disease." *Acta Neurol. Scand.* ***111***: 172-179.

Kebarle, P. (**2000**). "A brief overview of the present status of the mechanisms involved in electrospray mass spectrometry." *J. Mass Spectrom.* ***35***(7): 804-817.

Keller, J. N., R. J. Mark, et al. (**1997**). "4-Hydroxynonenal, an aldehydic product of membrane lipid peroxidation, impairs glutamate transport and mitochondrial function in synaptosomes." *Neuroscience* ***80***(3): 685-696.

Keller, J. N., Z. Pang, et al. (**1997**). "Impairment of glucose and glutamate transport and induction of mitochondrial oxidative stress and dysfunction in synaptosomes by amyloid beta-peptide: role of the lipid peroxidation product 4-hydroxynonenal." *J. Neurochem.* ***69***: 273-284.

Keller, J. N., F. A. Schmitt, et al. (**2005**). "Evidence of increased oxidative damage in subjects with mild cognitive impairment." *Neurology* ***64***(7): 1152-1156.

Khalkhali-Ellis, Z. (**1995**). "An improved SDS-polyacrylamide gel electrophoresis for resolution of peptides in the range of 3.5-200kDa." *Prep. Biochem.* ***25***(1-2): 1-9.

Kruman, I., A. J. Bruce-Keller, et al. (**1997**). "Evidence that 4-hydroxynonenal mediates oxidative stress-induced neuronal apoptosis." *J. Neurosci.* ***17***(13): 5089-5100.

Kundu, S., T. K. Ghose, et al. (**1983**). "Bioconversion of cellulose into ethanol by *Clostridium thermocellum* - product inhibition." *Biotechnol. Bioeng.* **25**: 1109-1126.

Kyte, J. and H. Rodriguez (**1983**). "A discontinuous electrophoretic system for separating peptides on polyacrylamide gels." *Anal. Biochem.* ***133***(2): 515-522.

Laemmli, U. K. (**1970**). "Cleavage of structural proteins during the assembly of the head of bacteriophage T4." *Nature* ***227***(5259): 680-685.

Lamed, R. and J. G. Zeikus (**1980**). "Ethanol production by thermophilic bacteria: relationship between fermentation product yields of and catabolic enzyme activities in *Clostridium thermocellum* and *Thermoanaerobium brockii*." *J. Bacteriol.* ***144***(2): 569-578.

Lauderback, C. M., J. M. Hackett, et al. (**2001**). "The glial glutamate transporter, GLT-1, is oxidatively modified by 4-hydroxy-2-nonenal in the Alzheimer's disease brain: the role of Abeta1-42." *J. Neurochem.* ***78***: 413-416.

Lee, V. M., B. J. Balin, et al. (**1991**). "A68: a major subunit of paired helical filaments and derivatized forms of normal Tau." ***Science*** ***251***: 675-678.

Lee, V. M., M. Goedert, et al. (**2001**). "Neurodegenerative tauopathies." *Annu. Rev. Neurosci.* ***24***: 1121-1159.

Lesse, A. J., A. A. Campagnari, et al. (**1990**). "Increased resolution of lipopolysaccharides and lipooligosaccharides utilizing tricine-sodium dodecyl sulfate-polyacrylamide gel electrophoresis." *J. Immunol. Methods.* ***126***(1): 109-117.

Liu, Q., M. A. Smith, et al. (**2005**). "Alzheimer-specific epitopes of tau represent lipid peroxidation-induced conformations." *Free Radic. Biol. Med.* ***38***: 746-754.

Lovell, M. A., W. D. Ehmann, et al. (**1995**). "Elevated thiobarbituric acid-reactive substances and antioxidant enzyme activity in the brain in Alzheimer's disease." *Neurology* ***45***(8): 1594-1601.

Lovell, M. A., W. D. Ehmann, et al. (**1997**). "Elevated 4-hydroxynonenal in ventricular fluid in Alzheimer's disease." *Neurobiol. Aging* ***18***(5): 457-461.

Lovell, M. A. and W. R. Markesbery (**2003**). *Methods in Biological Oxidative Stress*. Totowa, NJ, Humana Press.

Lovell, M. A., C. Xie, et al. (**1998**). "Decreased glutathione transferase activity in brain and ventricular fluid in Alzheimer's disease." *Neurology* ***51***(6): 1562-1566.

Lovell, M. A., C. Xie, et al. (**2000**). "Acrolein, a product of lipid peroxidation, inhibits glucose and glutamate uptake in primary neuronal cultures." *Free Radic. Biol. Med.* ***29***(8): 714-720.

Lovell, M. A., C. Xie, et al. (**2001**). "Acrolein is increased in Alzheimer's disease brain and is toxic to primary hippocampal cultures." *Neurobiol. Aging* ***22***: 187-194.

Lovestone, S. and D. M. McLoughlin (**2002**). "Protein aggregates and dementia: is there a common toxicity?" *J. Neurol. Neurosurg. Psychiatry* ***72***: 152-161.

Lowry, O. H., N. J. Rosebrough, et al. (**1951**). "Protein measurement with the Folin phenol reagent." *J. Biol. Chem.* ***193***(1): 265-275.

Luo, X. P., M. Yazdanpanah, et al. (**1995**). "Determination of Aldehydes and Other Lipid Peroxidation Products in Biological Samples by Gas Chromatography-Mass Spectrometry." *Anal. Biochem.* ***228***: 294-298.

Mamyrin, B. A., V. I. Karateev, et al. (**1973**). *Sov. Phys. JETP* **37**: 45-48.

March, R. E. (**1997**). "An introduction to quadrupole ion trap mass spectrometry." *J. Mass Spectrom.* ***32***(4): 351-369.

March, R. E. and J. F. J. Todd (**1995**). Practical Aspects of Ion Trap Mass Spectrometry. Boca Raton, FL, CRC Press.

Mark, R. J., M. A. Lovell, et al. (**1997**). "A role for 4-hydroxynonenal, an aldehydic product of lipid peroxidation, in disruption of ion homeostasis and neuronal death induced by amyloid beta-peptide." *J. Neurochem.* ***68***: 255-264.

Markesbery, W. R. (**1997**). "Oxidative Stress Hypothesis in Alzheimer's Disease." *Free Radic. Biol. Med.* ***23***(1): 134-147.

Markesbery, W. R. and M. A. Lovell (**1998**). "Four-Hydroxynonenal, a Product of Lipid Peroxidation, is Increased in the Brain in Alzheimer's Disease." *Neurobiol. Aging* ***19***(1): 33-36.

Markesbery, W. R., F. A. Schmitt, et al. (**2005**). "The neuropathologic substrate of mild cognitive impairment." *Arch. Neurol.* ***in press***.

Marshall, T. and K. M. Williams (**1994**). "Analysis of snake venoms by sodium dodecyl sulfate-polyacrylamide gel electrophoresis and two-dimensional electrophoresis." *Appl. Theor. Electrophor.* ***4***(1): 25-31.

Martinez, M., C. J. Newbold, et al. (**2002**). "Effects of high-molecular-mass substrates on protein migration during sodium dodecyl sulfatepolyacrylamide gel electrophoresis." *Electrophoresis* ***23***(1): 1-7.

Maskell, J. P. (**1991**). "The resolution of bacteroides lipopolysaccharides by polyacrylamide gel electrophoresis." *J. Med. Microbiol.* ***34***(5): 253-257.

Maskell, J. P. (**1994**). "Electrophoretic analysis of the lipopolysaccharides of Bacteroides spp." *Antonie Van Leeuwenhoek* ***65***(2): 155-161.

Matsuoka, M., N. Imado, et al. (**1996**). "Determination of free aliphatic aldehydes by high-performance liquid chromatography of the 1,3-cyclohexanedione derivatives." *Chromatographia* ***43***(9/10): 501-506.

Mattson, M. P. (**1995**). "Degenerative and Protective Signaling Mechanisms in the Neurofibrillary Pathology of AD." *Neurobiol. Aging* ***16***(3): 447-457.

Mattson, M. P., W. Fu, et al. (**1997**). "4-Hydroxynonenal, a product of lipid peroxidation, inhibits dephosphorylation of the microtubule-associated protein tau." *Neuroreport* ***8***: 2275-2281.

McClave, J. T., F. H. Dietrich II, et al. (**1997**). Statistics. Upper Saddle River, NJ, Prentice Hall, Inc.

McGrath, L. T., B. M. McGleenon, et al. (**2001**). "Increased oxidative stress in Alzheimer's disease as assessed with 4-hydroxynonenal but not malondialdehyde." *Q. J. Med.* ***94***: 485-490.

McLafferty, F. W. and F. Tureček (**1993**). *Interpretation of Mass Spectra*. Mill Valley, CA, University Science Books.

Meagher, E. A. and G. A. FitzGerald (**2000**). "Indices of lipid peroxidation in vivo: strengths and limitations." *Free Rad. Biol. Med.* ***28***(12): 1745-1750.

Mecocci, P., U. MacGarvey, et al. (**1994**). "Oxidative damage to mitochondrial DNA is increased in Alzheimer's disease." *Ann. Neurol.* ***36***(5): 747-751.

Mecocci, P., M. C. Polidori, et al. (**1998**). "Oxidative damage to DNA in lymphocytes from AD patients." *Neurology* ***51***(4): 1014-1017.

Migliore, L., I. Fontana, et al. (**2005**). "Oxidative DNA damage in peripheral leukocytes of mild cognitive impairment and AD patients." *Neurobiol. Aging* ***26***: 567-573.

Molloy, M. P. (**2000**). "Two-dimensional electrophoresis of membrane proteins using immobilized pH gradients." *Anal. Biochem.* **280**(1): 1-10.

Molloy, M. P., B. R. Herbert, et al. (**2000**). "Proteomic analysis of the *Escherichia coli* outer membrane." *Eur. J. Biochem.* ***267***(10): 2871-2881.

Molloy, M. P., B. R. Herbert, et al. (**1998**). "Extraction of membrane proteins by differential solubilization for separation using two-dimensional gel electrophoresis." *Electrophoresis* ***19***(5): 837-844.

Molloy, M. P., N. D. Phadke, et al. (**2001**). "Two-dimensional electrophoresis and peptide mass fingerprinting of bacterial outer membrane proteins." *Electrophoresis* ***22***(9): 1686-1696.

Montine, K. S., P. J. Kim, et al. (**1997**). "4-hydroxy-2-nonenal pyrrole adducts in human neurodegenerative disease." *J. Neuropathol. Exp. Neurol.* ***56***(8): 866-871.

Montine, T. J., M. F. Beal, et al. (**1999**). "Increased CSF F2-isoprostane concentration in probable AD." *Neurology* ***52***(3): 562-565.

Montine, T. J., W. R. Markesbery, et al. (**1998**). "Cerebrospinal fluid F2-isoprostane levels are increased in Alzheimer's disease." *Ann. Neurol.* ***44***(3): 410-413.

Montine, T. J., M. D. Neely, et al. (**2002**). "Serial Review: Causes and Consequences of Oxidative Stress in Alzheimer's Disease." *Free Rad. Biol. Med.* ***33***(5): 620-626.

Mori, H., J. Kondo, et al. (**1987**). "Ubiquitin is a component of paired helical filaments in Alzheimer's disease." *Science* ***235***: 1641-1644.

Morris, J. C., A. Heyman, et al. (**1989**). "The Consortium to Establish a Registry for Alzheimer's Disease (CERAD). Part 1. Clinical and neuropsychological assessment of Alzheimer's disease." *Neurology* **39**(9): 1159-1165.

Morrow, J. D. and L. J. Roberts (**2002**). "The Isoprostanes: Their Role as an Index of Oxidant Stress Status in Human Pulmunary Disease." *Am. J. Respir. Crit. Care Med.* ***166***: S25-S30.

Mouton, P. R., L. J. Martin, et al. (**1998**). "Cognitive Decline Strongly Correlates with Cortical Atrophy in Alzheimer's Disease." *Neurobiol. Aging* ***19***(5): 371-377.

Muddiman, D. C., R. Bakhtiar, et al. (**1997**). "Matrix-Assisted Laser Desorption/Ionization Mass Spectrometry." *J. Chem. Educ.* ***74***(11): 1288-1292.

Nash, T. (**1953**). "The colorimetric estimation of formaldehyde by means of the Hantzsch reaction." *Biochemistry* ***55***: 416-421.

Neely, M. D., K. R. Sidell, et al. (**1999**). "The lipid peroxidation product 4-hydroxynonenal inhibits neurite outgrowth, disrupts neuronal microtubules, and modifies cellular tubulin." *J. Neurochem.* ***72***: 2323-2333.

Neuhoff, V., N. Arold, et al. (**1988**). "Improved staining of proteins in polyacrylamide gels including isoelectric focusing gels with clear background at nanogram sensitivity using Coomassie Brilliant Blue G-250 and R-250." *Electrophoresis* ***9***(6): 255-262.

Newell, K. L., B. T. Hyman, et al. (1999). "Application of the National Institute on Aging (NIA)-Reagan Institute criteria for the neuropathological diagnosis of Alzheimer disease." Journal of Neuropathology and Experimental Neurology **58**(11): 1147-1155.

Nourooz-Zadeh, J., E. H. Liu, et al. (**1999**). "F4-isoprostanes as specific marker of docosahexaenoic acid peroxidation in Alzheimer's disease." *J. Neurochem.* ***72***: 734-740.

Nouwens, A. S., S. J. Cordwell, et al. (**2000**). "Complementing genomics with proteomics: the membrane subproteome of *Pseudomonas aeruginosa* PAO1." *Electrophoresis* ***21***(17): 3797-3809.

Nunomura, A., G. Perry, et al. (**2001**). "Oxidative damage is the earliest event in Alzheimer's disease." *J. Neuropathol. Exp. Neurol.* ***60***(8): 759-767.

O'Brien, V., G. J. Grindlay, et al. (**2001**). "Cell transformation by the E5/E8 protein of bovine papillomavirus type 4. p27(Kip1), Elevated through increased protein synthesis is sequestered by cyclin D1-CDK4 complexes." *J. Biol. Chem.* ***276***(36): 33861-33868.

O'Farrell, P. H. (**1975**). "High resolution two-dimensional electrophoresis of proteins." *J. Biol. Chem.* ***250***(10): 4007-4021.

O'Brien-Coker, I. C. and G. P. A. I. Mallet (**2001**). "Aldehyde analysis by high performance liquid chromatography/tandem mass spectrometry." *Rapid Commun. Mass Spectrom.* ***15***: 920-928.

Ohm, T. G., H. Muller, et al. (1995). "Close-Meshed Prevalence Rates of Different Stages as a Tool to Uncover the Rate of Alzheimers Disease-Related Neurofibrillary Changes." Neuroscience **64**(1): 209-217.

Ohnishi, T., H. Matsuda, et al. (**2001**). "Changes in Brain Morphology in Alzheimer's Disease and Normal Aging: Is Alzheimer's Disease an Exaggerated Aging Process?" *AJNR Am. J. Neuroradiol.* ***22***: 1680-1685.

Pappin, D. J., P. Hojrup, et al. (**1993**). "Rapid identification of proteins by peptide-mass fingerprinting." *Curr. Biol.* ***3***(6): 327-332.

Pardo, M. F. and C. L. Natalucci (**2002**). "Electrophoretic analysis (Tricine-SDS-PAGE) of bovine caesins." *Acta Farm. Bonarense* ***21***(1): 57-60.

Patton, W. F., N. Chung-Welch, et al. (**1991**). "Tris-tricine and Tris-borate buffer systems provide better estimates of human mesothelial cell intermediate filament protein molecular weights than the standard Tris-glycine system." *Anal. Biochem.* ***197***(1): 25-33.

Paul, W. (**1990**). "Electromagnetic Traps for Charged and Neutral Particles." *Agnew. Chem. Int. Ed.* ***29***: 739-746.

Pedersen, W. A., N. R. Cashman, et al. (**1999**). "The lipid peroxidation product 4-hydroxynonenal impairs glutamate and glucose transport and choline acetyltransferase activity in NSC-19 motor neuron cells." *Exp. Neurol.* ***155***: 1-10.

Perez, M., F. Hernandez, et al. (**2002**). "Formation of aberrant phosphotau fibrillar polymers in neural cultured cells." *Eur. J. Biochem.* ***269***: 1484-1489.

Perkins, D. N., D. J. Pappin, et al. (**1999**). "Probability-based protein identification by searching sequence databases using mass spectrometry data." *Electrophoresis* ***20***(18): 3551-3567.

Perry, G., R. J. Castellani, et al. (**1998**). "Reactive Oxygen Species Mediate Cellular Damage in Alzheimer's Disease." *J. Alzheimer's Dis.* ***1***: 45-55.

Perry, G., R. Friedman, et al. (**1987**). "Ubiquitin is detected in neurofibrillary tangles and senile plaque neurites of Alzheimer's disease brains." *Proc. Natl. Acad. Sci. USA* ***84***(9): 3033-3036.

Perry, G., R. Srinivas, et al. (**2003**). The role of oxidative mechanisms in neurodegenerative diseases. Basel, ISN Neuropath Press.

Pessione, E., M. G. Giuffrida, et al. (**2003**). "Membrane proteome of *Acinetobacter radioresistens* S13 during aromatic exposure." *Proteomics* ***3***(6): 1070-1076.

Petersen, R. C. (**2000**). "Mild cognitive impairment: transition between aging and Alzheimer's disease." *Neurologia* ***15***(3): 93-101.

Petersen, R. C., G. E. Smith, et al. (**1999**). "Mild cognitive impairment: clinical characterization and outcome." *Arch. Neurol.* ***56***(3): 303-308.

Petersen, R. C., R. G. Thomas, et al. (**2005**). "Vitamin E and Donepezil for the Treatment of Mild Cognitive Impairment." *N. Eng. J. Med.* ***352***(23): 2379-2388.

Phadke, N. D., M. P. Molloy, et al. (**2001**). "Analysis of the outer membrane proteome of Caulobacter crescentus by two-dimensional electrophoresis and mass spectrometry." *Proteomics* ***1***(5): 705-720.

Porter, N. A., L. S. Lehman, et al. (**1981**). "Unified Mechanisms for Polyunsaturated Fatty Acid Autooxidation. Competition of Peroxy Radical Hydrogen Atom Abstraction, beta-Scission and Cyclization." *J. Am. Chem. Soc.* ***103***: 6447-6455.

Prasad, M. R., M. A. Lovell, et al. (**1998**). "Regional membrane phospholipid alterations in Alzheimer's disease." *Neurochem. Res.* ***23***(1): 81-88.

Praticó, D. (**2002**). "Oxidative imbalance and lipid peroxidation in Alzheimer's disease." *Drug Dev. Res.* ***56***: 446-451.

Praticó, D., C. M. Clark, et al. (**2002**). "Increase of Brain Oxidative Stress in Mild Cognitive Impairment." *Arch. Neurol.* ***59***(6): 972-976.

Quinn, J. F., K. S. Montine, et al. (**2004**). "Suppression of longitudinal increase in CSF F_2-isoprostanes in Alzheimer's Disease." *J. Alzheimer's Dis.* **6**: 93-97.

Rabacchi, S. A., W. J. Friedman, et al. (**2004**). "Divergence of the apoptotic pathways induced by 4-hydroxynonenal and amyloid beta-protein." *Neurobiol. Aging* ***25***: 1057-1066.

Rais, I., M. Karas, et al. (**2004**). "Two-dimensional electrophoresis for the isolation of integral membrane proteins and mass spectrometric identification." *Proteomics* ***4***(9): 2567-2571.

Ravandi, A., A. Kuksis, et al. (**1995**). "Determination of lipid ester ozonides and core aldehydes by high-performance liquid chromatography with on-line mass spectrometry." *J. Biochem. Biophys. Methods* ***30***: 271-285.

Raymond, S. and L. Weintraub (**1959**). "Acrylamide gel as a supporting medium for zone electrophoresis." *Science* ***130***: 711.

Reynolds, C. H., J. C. Betts, et al. (**2000**). "Phosphorylation Sites on Tau Identified by Nanoelectrospray Mass Spectrometry: Differences In Vitro Between the Mitogen-Activated Protein Kinases ERK2, c-Jun N-Terminal Kinase and P38, Glycogen Synthase Kinase-3β." *J. Neurochem.* ***74***: 1587-1595.

Robards, K., P. R. Haddad, et al. (**2001**). Principles and Practice of Modern Chromatographic Methods. Somerset, UK, Bookcraft (Bath) Ltd.

Rottkamp, C. A., A. K. Raina, et al. (**2001**). "Redox-Active Iron Mediates Amyloid-β Toxicity." *Free Rad. Biol. Med.* ***30***(4): 447-450.

Sánchez, S., J. Arenas, et al. (**2005**). "Analysis of outer membrane protein complexes and heat-modifiable proteins in Neisseria strains using two-dimensional diagonal electrophoresis." *J. Proteome Res.* ***4***(1): 91-95.

Santoni, V., M. Molloy, et al. (**2000**). "Membrane proteins and proteomics: un amour impossible?" *Electrophoresis* ***21***(6): 1054-1070.

Sawicki, E. and R. A. Carnes (**1968**). "Spectrophotofluorimetric determination of aldehydes with dimedone and other reagents." *Mikrochim. Acta*: 148-159.

Sayre, L. M., D. A. Zelasko, et al. (**1997**). "4-Hydroxynonenal-derived advanced lipid peroxidation end products are increased in Alzheimer's disease." *J. Neurochem.* ***68***: 2092-2097.

Schaffer, S., B. Weil, et al. (**2001**). "A high-resolution reference map for cytoplasmic and membrane-associated proteins of Corynebacterium glutamicum." *Electrophoresis* ***22***(20): 4404-4422.

Schägger, H. and G. von Jagow (**1987**). "Tricine-sodium dodecyl sulfate-polyacrylamide gel electrophoresis for the separation of proteins in the range from 1 to 100 kDa." *Anal. Biochem.* ***166***(2): 368-379.

Schneider, C., K. A. Tallman, et al. (**2001**). "Two distinct pathways of Formation of 4-Hydroxynonenal." *J. Biol. Chem.* ***276***(24): 20831-20838.

Selkoe, D. J. (**1996**). "Amyloid beta-Protein and the Genetics of Alzheimer's Disease." *J. Biol. Chem.* ***271***(31): 18295-18298.

Sim, A. S., C. Salonikas, et al. (**2003**). "Improved method for plasma malondialdehyde measurement by high-performance liquid chromatography using methyl malondialdehyde as an internal standard." *J. Chromatogr. B* ***785***: 337-344.

Skoog, D. A., D. M. West, et al. (**2000**). Analytical Chemistry: An Introduction. Orlando, FL, Harcourt Inc.

Smith, A. D. (**2001**). "Imaging the progressionof Alzheimer pathology through the brain." *Proc. Natl. Acad. Sci.* ***99***(7): 4135-4137.

Smith, M. A., K. L. Drew, et al. (**2002**). "Amyloid-b, tau alterations and mitochondrial dysfunction in Alzheimer's disease: the chicken or the eggs?" *Neurochem. Int.* ***40***: 527-531.

Smith, M. A., G. Perry, et al. (**1996**). "Oxidative damage in Alzheimer's." *Nature* ***382***: 120-121.

Smith, M. A., S. Taneda, et al. (**1994**). "Advanced Maillard reaction end products are associated with Alzheimer disease pathology." *Proc. Natl. Acad. Sci. U S A* ***91***: 5710-5714.

Spies-Martin, D., O. Sommerburg, et al. (**2002**). "Measurement of 4-hydroxynonenal in small volume blood plasma samples: modification of a gas chromatographic-mass spectrometric method for clinical settings." *J. Chromatogr. B* ***774***: 231-239.

Spiteller, G., W. Kern, et al. (**1999**). "Investigation of aldehydic lipid peroxidation products by gas chromatography-mass spectrometry." *J. Chromatogr. A.* ***843***: 29-98.

Strobel, H. J. and B. C. Lynn (**2004**). Proteomic analysis of ethanol sensitivity in *Clostridium thermocellum*. American Society for Microbiology, New Orleans, LA.

Subramaniam, R., F. Roediger, et al. (**1997**). "The lipid peroxidation product, 4-hydroxy-2-trans-nonenal, alters the conformation of cortical synaptosomal membrane proteins." *J. Neurochem.* ***69***: 1161-1169.

Sudha Rani, K. and G. Seenayya (**1999**). "High ethanol tolerance of new isolates of *Clostridium thermocellum* strains SS21 and SS22." *World J. Micro. Biotech.* ***15***: 173-178.

Sudha Rani, K., M. V. Swamy, et al. (**1998**). "Production of ethanol from various pure and natural cellulosic biomass by *Clostridium thermocellum* strains SS21 and SS22." *Process Biochem.* ***33***(4): 435-440.

Svennerholm, L. and C. G. Gottfries (**1994**). "Membrane Lipids, Selectively Diminished in Alzheimer Brains, Suggest Synapse Loss as a Primary Event in Early-Onset Form (Type 1) and Demyelination in Late-Onset Form (Type II)." *J. Neurochem.* ***62***: 1039-1047.

Swank, R. T. and K. D. Munkres (**1971**). "Molecular weight analysis of oligopeptides by electrophoresis in polyacrylamide gel with sodium dodecyl sulfate." *Anal. Biochem.* ***39***(2): 462-477.

Tailliez, P., H. Girard, et al. (**1989**). "Cellulose fermentation by an *Asporogenous* mutant and an ethanol-tolerant mutant of *Clostridium thermocellum*." *Appl. Environ. Microbiol.*: 203-206.

Tailliez, P., H. Girard, et al. (**1989**). "Enhanced cellulose fermentation by an *Asporogenous* and ethanol-tolerant mutant of *Clostridium thermocellum*." *Appl. Environ. Microbiol.*: 207-211.

Takeda, A., M. A. Smith, et al. (**2000**). "In Alzheimer's Disease, Heme Oxygenase is Coincident with Alz50, an Epitope of tau Induced by 4-Hydroxy-2-nonenal Modification." *J. Neurochem.* ***75***(3): 1234-1241.

Thomas, M. J., T. W. Robison, et al. (**1995**). "Detecting and identifying volatile aldehydes as dinitrophenylhydrazones using gas chromatography mass spectrometry." *Free Rad. Biol. Med.* ***18***(3): 553-557.

Trojanowski, J. Q. and V. M. Lee (**1995**). "Phosphorylation of paired helical filament tau in Alzheimer's disease neurofibrillary lesions: focusing on phosphatases." *FASEB J.* ***9***(15): 1570-1576.

Uchida, K. (**2000**). "Role of reactive aldehyde in cardiovascular diseases." *Free Radic. Biol. Med.* ***28***(12): 1685-1696.

Uchida, K., M. Kanematsu, et al. (**1998**). "Acrolein is a product of lipid peroxidation reaction. Formation of free acrolein and its conjugate with lysine residues in oxidized low density lipoproteins." *J. Biol. Chem.* ***273***(26): 16058-16066.

Uchida, K., M. Kanematsu, et al. (**1998**). "Protein-bound acrolein: Potential markers for oxidative stress." *Proc. Natl. Acad. Sci. U S A* ***95***: 4882-4887.

Uchida, K., L. I. Szweda, et al. (**1993**). "Immunochemical detection of 4-hydroxynonenal protein adducts in oxidized hepatocytes." Proc. Natl. Acad. Sci., U S A ***90***(18): 8742-8746.

Varadarajan, S., S. Yatin, et al. (**2000**). "Review: Alzheimer's Amyloid beta-Peptide-Associated Free Radical Oxidative Stress and Neurotoxicity." *J. Struct. Biol.* ***130***: 184-208.

Viney, C. and R. A. Fenton (**1998**). "Physics and gel electrophoresis: using terminal velocity to characterize molecular weight." *Eur. J. Phys.* ***19***: 575-580.

Volmer, D. A. and D. L. Vollmer (**1996**). "Interfacing liquid chromatography with mass spectrometry and tandem mass spectrometry." *LC-GC* ***14***(3): 216-219.

Walker, J. M. (**2002**). *The Protein Protocols Handbook*. Totowa, NJ, Humana Press.

Wang, J., S. Xiong, et al. (**2005**). "Increased oxidative damage in nuclear and mitochondrial DNA in Alzheimer's disease." *J. Neurochem.* ***93***: 953-962.

Wang, J., S. Xiong, et al. (**2005**). "Increased oxidative damage in nuclear and mitochondrial DNA in mild cognitive impairment." *Neurobiol. Aging* ***submitted for publication***.

Washburn, M. P., D. Wolters, et al. (**2001**). "Large-scale analysis of the yeast proteome by multidimensional protein identification technology." *Nat. Biotechnol.* ***19***(3): 242-247.

Wehr, T., R. Rodriguez-Diaz, et al. (1999). Capillary electrophoresis of proteins. New York, NY, Marcel Dekker, Inc.

Wenner, B. R. and B. C. Lynn (**2004**). "Factors that affect ion trap data-dependent MS/MS in proteomics." *J. Am. Soc. Mass Spectrom.* ***15***(2): 150-157.

Whitehouse, C. M., R. N. Dreyer, et al. (1985). "Electrospray Interface for Liquid Chromatographs and Mass Spectrometers." Analytical Chemistry **57**(3): 675-679.

Wiley, W. C. and I. H. Mclaren (**1955**). "Time-of-Flight Mass Spectrometer with Improved Resolution." *Review of Scientific Instruments* ***26***(12): 1150-1157.

Winblad, B., K. Palmer, et al. (**2004**). "Mild cognitive impairment--beyond controversies, towards a consensus: report of the International Working Group on Mild Cognitive Impairment." *J. Intern. Med.* ***256***: 240-246.

Wu, C. C., M. J. MacCoss, et al. (2003). "A method for the comprehensive proteomic analysis of membrane proteins." *Nat. Biotechnol.* ***21***(5): 532-538.

Wu, C. C. and J. R. Yates, 3rd (**2003**). "The application of mass spectrometry to membrane proteomics." *Nat. Biotechnol.* ***21***(3): 262-267.

Yamashita, M. and J. B. Fenn (1984). "Electrospray Ion-Source - Another Variation on the Free-Jet Theme." Journal of Physical Chemistry **88**(20): 4451-4459.

Yan, S. D., X. Chen, et al. (**1994**). "Glycated tau protein in Alzheimer disease: a mechanism for induction of oxidant stress." *Proc. Natl. Acad. Sci. U S A* ***91***: 7787-7791.

Yatin, S., S. Varadarajan, et al. (**2000**). "Vitamin E prevents Alzheimer's amyloid beta-peptide (1-42) induced protein oxidation and ROS formation." *J. Alzheimer's Dis.* ***2***: 123-131.

Yim, S. K., T. Ahn, et al. (**2002**). "Polyacrylamide gel electrophoresis without a stacking gel: application for separation of peptides." *Anal. Biochem.* ***305***(2): 277-279.

Yoshino, K., T. Matzuura, et al. (**1986**). "Fluorometric Liquid Chromatographic Determination of Aliphatic Aldehydes Arising from Lipid Peroxides." *Chem. Pharm. Bull.* ***34***(4): 1694-1700.

Young, C. S. and R. J. Weigand (**2002**). "An Efficient Approach to Column Selection in HPLC Method Development." *LCGC North America* ***20***(5): *465-473*.

Zhu, X., R. J. Castellani, et al. (**2001**). "Differential activation of neuronal ERK, JNK/SAPK and p38 in Alzheimer's disease: the 'two hit' hypothesis." *Mech. Ageing Dev.* ***123***: 39-46.

Zhu, X., H. Lee, et al. (**2002**). "The Role of Mitogen-Activated Protein Kinase Pathways in Alzheimer's Disease." *Neurosignals* ***11***(5): 270-281.

Zhu, X., C. A. Rottkamp, et al. (**2000**). "Activation of p38 Kinase Links Tau Phosphorylation, Oxidative Stress, and Cell Cycle-Related Events in Alzheimer's Disease." *J. Neuropathol. Exp. Neurol.* ***59***(10): 880-888.

Zurek, G. and U. Karst (**1999**). "Liquid chromatography-mass spectrometry method for the determination of aldehydes derivatized by the Hantzsch reaction." *J. Chromatogr. A* ***864***(2): 191-197.

VITA

Taufika Islam Williams
Date of birth: July 3, 1977
Place of birth: Dhaka, Bangladesh

Taufika Islam Williams is a native of Dhaka, Bangladesh. As the daughter of an agricultural scientist who works for the United Nations, she traveled extensively around the world. Taufika lived in Asia, Australia, Africa, Europe and in North and Central America. She met and interacted with people from all backgrounds and is fluent in English and Bengali. She also has a sound knowledge of Spanish and Hindi.

Taufika's elementary education began in Perth, Western Australia and continued in Texcoco, Mexico, followed by a short period in Dhaka, Bangladesh and then Ibadan, Nigeria. She attended middle and high school in Dhaka, Bangladesh and completed the Ordinary and Advanced Level Exams under the University of London Examination and Assessment Council (ULEAC). Upon completing high school, she pursued an undergraduate degree at Transylvania University in Lexington, KY. She graduated magna cum laude with double majors in chemistry and mathematics, following which she enrolled in Purdue University in West Lafayette, IN, for graduate studies. At Purdue, Taufika received one publication and a Master's Degree (cum laude) as a result of her work on thermochemical determinations using the kinetic method with full entropic analysis.

After some time off from academics following her marriage, Taufika returned to Lexington, KY as a graduate student in the Department of Chemistry at the University of Kentucky. In Dr. Bert Lynn's laboratory, she gained experience in mass spectrometric methods development as applicable to small molecule research and proteomics. Most notably, she developed LC-MS techniques for the quantitative analysis of Alzheimer's disease biomarkers and designed two dimensional polyacrylamide gel electrophoresis techniques for the effective analysis of cell membrane proteins. Both methodologies have been successfully applied towards investigations with real biological samples.

Taufika has been the recipient of travel grants to present her research at the annual American Society for Mass Spectrometry (ASMS) Conference in 2004 and 2005. Her work has also been presented at the 2005 American Society for Microbiology (ASM) Conference. Taufika has published two papers during her time at UK, a third manuscript is in press and a fourth manuscript will be submitted shortly. She is a member of ASMS.

Publications:

1. T. Islam Williams, M. A. Lovell and B. C. Lynn, Analysis of Derivatized Biogenic Aldehydes by HPLC Tandem Mass Spectrometry, *Anal. Chem.* 77, (2005) 3383.
2. T. Islam Williams, B. C. Lynn, W. R. Markesbery and M. A. Lovell, Increased levels of 4-hydroxynonenal and acrolein, neurotoxic markers of lipid peroxidation, in the brain in mild cognitive impairment and early Alzheimer's disease, *Neurobiol. Aging*, In press.
3. T. Islam Williams, J. C. Combs, A. P. Thakur, H. J. Strobel and B. C. Lynn, A Novel Bicine Running Buffer System for Sodium Dodecyl Sulfate – Polyacrylamide Gel Electrophoresis of Membrane Proteins, Submitted for publication.
4. T. Islam Williams, J. C. Combs, B. C. Lynn and H. J. Strobel, Proteomic Profile Changes in Membranes of Ethanol-Tolerant *Clostridium thermocellum*, Manuscript in preparation.

Presentations:

1. "The Membrane Proteome of *Clostridium thermocellum* by MALDI-TOF-MS." Taufika Islam Williams, Jennifer C. Combs, Herbert J. Strobel and Bert C. Lynn. 53rd ASMS Conference, June 2005.
2. "Proteomic Profile Changes in Membranes of Ethanol-Tolerant *Clostridium thermocellum*." Taufika Islam Williams, Jennifer C. Combs, Bert C. Lynn and Herbert J. Strobel. 105th ASM Conference, June 2005.
3. "Analysis of Derivatized Biogenic Aldehydes by HPLC Tandem Mass Spectrometry." Taufika Islam Williams, Mark A. Lovell and Bert C. Lynn. 52nd ASMS Conference, May 2004.

4. “Analysis of Aldehydes and Aldehyde-DNA Adducts by HPLC Tandem Mass Spectrometry.” Taufika Islam Williams, Xinli Liu, Mark A. Lovell and Bert C. Lynn. 29th Symposium on Chemistry and Molecular Biology, University of KY, Spring 2003.